

Emergency Communications Node

Group 22- Tutor: Ines Uriol Balbin Coaches: Caroline van Calcar, Yilun Wu
External expert: Stijn Mast

Anujay Singh	4995031	Vatsal Gupta	5104548
Aditya Pati Tripathi	5011442	Giorgio Basile	4998944
Tom Aantjes	5065917	Daan Bolkestein	4451244
Şerban Blaga	4996666	Mateusz Mazurkiewicz	5119189
Aleksandr Pavlov	5003458	Ignacio Quintanilla Rojas	4792122



This page is intentionally left blank.

Preface

The accompanying technical report was composed by the Design Synthesis Exercise Group 22, which consists of ten third year Aerospace Engineering students at the Delft University of Technology completing their bachelor's degree with a final thesis project worth 15 ECTS. The composition of this report consisted of the final design of an emergency communication node for high data transfer rates with Low-Earth Satellites (LEO) and High-Altitude Platform Station (HAPS) through optical laser communication. The objective assigned with this report was to showcase a detailed design of individual ground station subsystems with emphasis on sustainability, a revision of the conducted market analysis, an approach to operations and logistics with RAMS analysis, sensitivity analysis for the design choices undertaken, a production plan, identified risks, compliance with requirements and recommendations.

When writing this report, the supposition was made that the reader has a fundamental comprehension of system engineering concepts within the aerospace industry with relevant technical knowledge. Relevant nomenclature featuring Greek and Latin symbols is included in the report and can be found in the list of symbols. The abbreviations incorporated in the report are compiled in the list of abbreviations.

We extend our gratitude to our tutor *Ms. Ines Uriol Balbin*, who was always available for support, guidance, recommendations and feedback during this project. Our acknowledgements also go to our coaches *Ms. Caroline van Calcar* and *Mr. Yilun Wu* from the Delft University of Technology for their insight, advice and knowledge. We would like to thank *Mr. Stijn Mast* from Airbus Defence and Space Netherlands B.V. for being available as the external expert of the group during this project and providing his technical expertise, support and direction for the design methodology.

Moreover, our acknowledgements also go to *Dr. ir. R. Saathof, S.R. Turteltaub, PhD*, and *C.M. De Servi* working as professors at the Faculty of Aerospace Engineering at the Delft University of Technology for providing technical expertise and consultation for specific design details in the project. Lastly, we would like to thank *Prof. dr Jeannot Trampert* of Utrecht University for guiding and helping us with frequency analysis for earthquakes.

Group 22

<i>Anujay Singh</i>	<i>4995031</i>	<i>Vatsal Gupta</i>	<i>5104548</i>
<i>Aditya Pati Tripathi</i>	<i>5011442</i>	<i>Giorgio Basile</i>	<i>4998944</i>
<i>Tom Aantjes</i>	<i>5065917</i>	<i>Daan Bolkestein</i>	<i>4451244</i>
<i>Șerban Blaga</i>	<i>4996666</i>	<i>Mateusz Mazurkiewicz</i>	<i>5119189</i>
<i>Aleksandr Pavlov</i>	<i>5003458</i>	<i>Ignacio Quintanilla Rojas</i>	<i>4792122</i>

Delft, June 2022

Executive Summary

Maintaining a high speed, secure and robust connection to the world is of paramount importance in modern society. This proved especially true during a recent volcanic eruption in the small island nation of Tonga, where the only optical fibre line to the country was severed due to the cataclysm, completely disconnecting the island from the rest of the world. The lack of communication made the disaster relief to the eruption more complex. The Emergency Communications Node (ECN) can be deployed within 48 hours to enable alternative means of communication that replace damaged communication lines.

Mission Need Statement & Project Objective Statement

A Mission Need Statement has been formulated to drive the design of such an alternative:

Mission Need Statement

Provide a mobile bi-directional air-to-ground optical communication node to be fastly deployed in emergency situations.

To achieve this characteristic link, a series of attributes must be designed, such as the optical sub-system, ease of transportation and structural integrity, among others. As such, a Project Objective Statement has been proposed:

Project Objective Statement

Design a mobile and rugged ground station which communicates with a HAPS (High Altitude Platform Station) using optical communication with 10 students within 10 weeks.

It can thus be established that a solution denominated as the Emergency Communications Node will be designed to fulfill this function and meet this market demand.

Operations and Logistics

One of the fundamental traits of the Emergency Communications Node is its ability to be deployed worldwide within 48 hours. As such, operational characteristics can be explored. Firstly, the transportation analysis assumes that a Node can be found in all NATO countries. By considering a worst case scenario of 14500 [km] air distance, aircraft and helicopter are employed as main vehicles. By taking three refueling stops, loading and unloading and final positioning reference values it was determined that it will take 34 hours to cover this distance. The remaining 14 hours are accounted for the final positioning by means of helicopter. The analysis shows the deployment time requirement is fulfilled and that the Node is sufficiently small so as to be transported by a standard ISO container, that fits into more standard, thus more sustainable transportation solutions.

Furthermore, analysis of the deployment identified three phases: 1. Unloading, 2. Calibration and 3. Establishing Connection. Regarding deployment, Node's operation and Safe Mode were discussed.

Design Overview

After finding the node's limiting dimensions, and its transportation. It is now time to dive deeper into node's specifications.

Optical Communication

To ensure successful link establishment of the node with HAPS or Low Earth Orbit satellite, closer look into modulation, link budget, optical path and sensors was taken.

To guarantee the success of the 16-QAM technique, the Error Correction Coding (ECC) schemes together with interleaving were explored, and the Low Density Parity Check (LDPC) coding scheme has the best performance in turbulent mediums and thus will be used. With the LDPC, the Forward Error Correction (FEC) limit was found to be 10^{-3} , meaning that if Bit Error Rate (BER) is below that value - the signal can be reliably demodulated. Finally, the implications of the revisited modulation technique were investigated. Recommendations on the sensitivity of the receiver are made, given its impact on the BER.

Analysing the link performance for HAPS the uplink margin of 29.2 [dB] and a downlink 4.2 [dB] were achieved for the data rate of 100 [Gbps]. For the LEO a uplink margin of 27.4 [dB] and a downlink margin of 2.5 [dB] are found, with a resulting data rate of 1 [Gbps]. These results mean the link budget closes and communication for HAPS is redundant. The results are found by modelling signal attenuation losses due to effects related to atmospheric phenomena. Static losses such as Cirrus Clouds, Aerosol scattering and Molecular absorption were considered. To consider scintillation effects gamma-gamma and log-normal distribution were performed and attenuation losses were quantified.

Beam Steering

To comply with the link budget margins, the chosen design of EVE has required an increased aperture size of 15 [cm] in diameter from the original 7.5 [cm]. The aperture size larger than 15 [cm] caused concern in the feasibility of the EVE design due to substantial increase in price for a 15 [cm] achromatic lens together with 1550 nm V-coating. To incorporate the larger diameter design, two alternative telescopic design options were considered. The first one was an observatory design which was deemed undesirable due to the high bulkiness and cost. The second option was the coelostat which was too expensive to be incorporated. It was found that the EVE design using the bigger lens was preferred due to significantly lower costs and required volume.

Once the Gimbal is designed, the rest of the optical bench can be devised. A breakdown of the optical path is provided by means of the optical bench. Namely the functionality of the Transceiver, EDFA, Collimator, Point-Ahead mechanism, Beamsplitter, Fibre Coupling, Adaptive Optics and Fast-Steering Mirrors is explained. These are all the elements through which the laser travels before it is emitted.

The section on camera sensing discusses the two roles of the camera sensors: providing feedback to the closed PAT control loop, and performing star tracking for calibration. After a background study and discussion of considerations, image sensor and lenses selection is performed. Pointing, Acquisition and Tracking (PAT) is responsible for actuation of the beam steering subsystem to perform communication, and all routines necessary to establish the connection, such as calibration and acquisition. A full description of the PAT sequence is provided in the section, discussing its performance and routines to be implemented to carry out PAT functions. A flowchart is presented, showing integration of various software components throughout the mission.

Structure

A frequency analysis is done to find a spring-damper system that can cancel out all the external excitation. A spring constant of 250,000 [N/m^2] and a dampening constant of 3000 [Ns/m] are found for the node, and a spring constant of 65,000 [N/m^2] and a dampening constant of 3000 [Ns/m] are found for the optical bench. Based on this, KONI coil over dampers are finalised for both the node as well as for the optical bench.

The frequency analysis of the system explored the response of a simplified two lumped mass model to a sinusoidal excitation with a Peak Ground Amplitude of 14.7 [m/s^2] (1.5 g). Moreover, the system

is capable of withstanding wind speeds of up to 60 [m/s]. Additionally, accidental drops of 5 [m] are considered.

Having quantified several loading cases in the Frequency Analysis and ensuring that the vibration is damped sufficiently fast and to an acceptable extent, it was possible to design the structure that shall withstand these loads. FEM simulations have been performed to preliminary size this structure for the design. The design consisted of a frame structure as well as horizontal and vertical beams that connect these. A trade-off was also performed that selected the optimal material based on mass, cost, sustainability and ease of manufacturing.

Environmental Monitoring

A combination of GNSS for location, LiDAR for detecting laser obstruction, as well as weather sensors for operational envelope monitoring, and particulate matter sensors for predictive maintenance, are some the sensors included in the subsystem. They have been selected to enable the system to monitor its surroundings, and make decisions based on them. They support autonomous operation of the system, contributing to its usability by unqualified personnel.

Thermal Management System

The ECN is thermally managed by two distinct Thermal Management Systems (TMS). The node is managed by a 500 [W] fluid cooling system, and a 500 [W] electric heating system. The battery TMS uses the same cooling system as the node, which is coupled. Furthermore a 180 [W] electric fluid heat pump is used to heat the battery. The goal of the battery TMS is to maintain the battery temperature between 10 [°C] and 30 [°C] at all times, to improve the sustainability of the battery.

Electrical Power System

A battery pack of 9 [kWh] is required to power the node for up to 6 hours. A additional 72 [kWh] battery pack can be added to increase the battery life with 48 hours. Both battery packs are constructed of the LG Chem E66A Lithium-Ion cell. A inverter is used to transform AC from the power grid to the DC supplied by the battery vice versa. All electricity is distributed using automatic circuit breakers.

RAMS Analysis

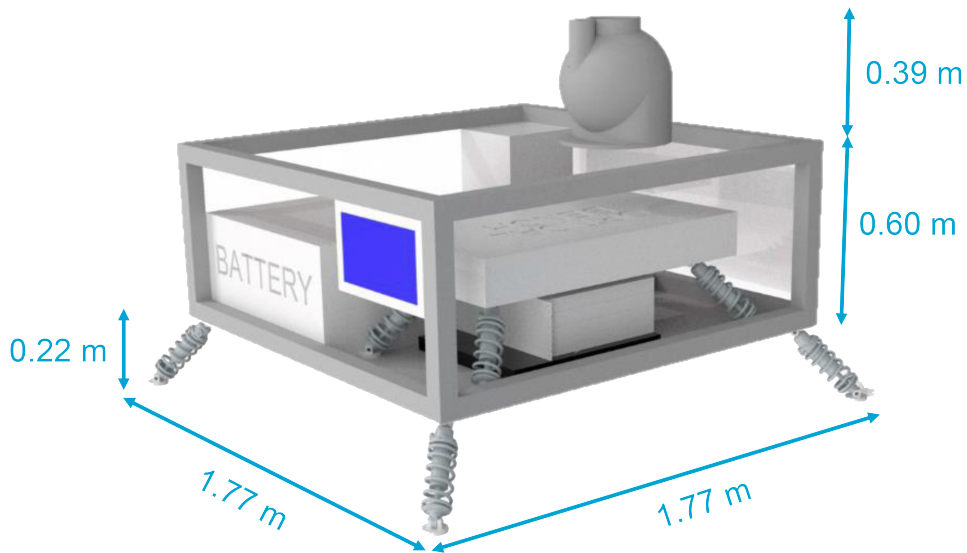
A Reliability Analysis was performed to ensure the functionality of the Node. Moreover, Maintainability and Safety are also considered and explored. Regarding the Reliability, an approach centered around the failure rate is done. The failure rate of individual parts and an aggregate of them is taken to estimate the failure rate for the system. Furthermore, the availability can be estimated. The approach taken consisted of estimating two parameters, the mean time between failure and the time to recovery. Then the time between failure, as a proportion of the total time shall be the availability. Moreover, the maintenance was addressed by taking a predictive maintenance strategy, where an array of sensors is used to feed a model and effectively schedule maintenance events.

Manufacturing, Assembly and Integration

The line manufacturing process has been selected for the node's production, for which a production plan has been constructed incorporating 7 distinct stations, and the connected sub-assemblies to those stations. For each assembly from the production plan, the employee work distribution has been created resulting in 88 Total manhours and the Crew Size of 27 people. For manufacturing, modular design was incorporated to improve the maintainability, upgradeability, reusability and recycling of the node. Finally, the production risks and the sustainability incorporation are discussed.

Sustainability

During the design of each subsystem sustainability has been given priority during design choices. Throughout the report relevant chapters had sustainability sections incorporated into the report. A special focus has been given to modularity allowing the part replacement and prolonging node's service life.



29

Figure 1: Exploded view of node with its dimensions



Key Parameters

Cost	192k EUR
Weight	894 kg
Link margin (Up)	29 dB
Link margin (Down)	4 dB
Power	937 W
Modulation	16-QAM

Figure 2: Key parameters of node with a render of the final product

Contents

Preface	iii
Executive Summary	iv
1 Introduction	1
2 Market Analysis Update	1
2.1 Background Study	1
2.2 Bottom Up Cost Calculations	3
2.3 Updated NPV Break-Even Chart	5
2.4 Further steps	6
3 Sustainable Development	7
3.1 Sustainability Approach	7
3.2 Operations and Logistics	7
3.3 Thermal Management.	7
3.4 Environmental Monitoring.	7
3.5 EPS.	7
3.6 Structure	8
3.7 Manufacturing, Assembly and Integration	8
4 Operations and Logistics	8
4.1 Transportation	8
4.2 Deployment	11
4.3 Operation.	11
4.4 Validation Plan.	12
4.5 Sustainability.	14
5 Detailed Design	14
5.1 Modulation	15
5.2 Link Budget	20
5.3 Telescope Gimbal Design.	35
5.4 Optical Bench	42
5.5 Camera Sensors	48
5.6 Pointing, Acquisition and Tracking.	54
5.7 Frequency Analysis	61
5.8 Structural Design	70
5.9 Thermal Management.	77
5.10 Electrical Power System	82
5.11 Environmental Monitoring.	86
5.12 SWaP and Cost Budgets	92
6 Sensitivity Analysis	93
6.1 Interdependency Matrix	93
6.2 Subsystem Trade-off Sensitivity Analysis	93
6.3 Scenario Analysis	93
7 RAMS Analysis	97
7.1 Reliability.	97
7.2 Availability	99
7.3 Maintenance	100
7.4 Safety	101

8	Risk Assessment	103
9	Manufacturing, Assembly and Integration	108
9.1	Layout	108
9.2	Manufacturing	109
9.3	Assembly	109
9.4	Organization of Production Process	110
9.5	Production Plan	110
9.6	Sustainability	113
10	Requirements and Compliance	114
10.1	Final Requirements	114
10.2	Compliance Matrix	115
10.3	Feasibility Analysis	120
11	Design and Development Logic	121
12	Conclusion and Recommendations	124
12.1	Conclusion	124
12.2	Recommendations	125
	Bibliography	127
A	Work Distribution and flow diagrams	134
A.1	Task Division Final Report	134
B	Detailed Cost Breakdown	137

List of Symbols

			G	Gain	W
			G_R	Receiver Gain	-
λ	Wavelength	m	H	Embodied Energy	J/kg
ρ	Density	kg/m ³	h	Planck's Constant	J-sec
			k	Boltzmann's Constant	m ² kg/sec ² K ¹
α_s	Absorptivity	-	L	Link Communication Range	km
ϵ_{IR}	Emissivity	-	L_0	Initial beam length	m
η_N	Link Spectral Efficiency	-	L_c	Clouds Physical Length	km
λ	Wavelength	m	m	Mass	kg
ρ	Density	kg/m ³	N_0	Some constant	-
σ	Stefan-Boltzmann constant	Wm ² K ⁴	N_b	Receiver sensitivity	photon/bit
σ_I^2	Scintillation Index	-	P_N	Noise Power	W
τ_{opt}	Optical Thickness	-	P_r	Received power	W
A	Area	m ²	P_T	Transmitted power	W
a	Speed of sound	m/s	R	Transfer Data Rate	-
B_N	Equivalent Noise Bandwidth	-	S^*	Stiffness	N/m ²
c	Speed of Light	m/sec	A_i	Surface Area	m ²
C_n^2	Turbulence Strength Profile	-	J_s	Solar Irradiance	W/m ²
D_R	Aperture Diameter	m	k	Conductivity constant	W/mK
E	Young's Modulus	Pa			

List of Abbreviations

		FAA	Federal Aviation Administration
		FEC	Forward Error Correction
		FEM	Finite Element Method
16-QAM	16 Quadrature Amplitude Modulation	FSM	Fast Steering Mirror
ACM	Adaptive Coding and Modulation	FSO	Free Space Optical
AC	Alternating Current	FoV	Field of View
ADCS	Attitude Determination and Control System	GFRP	Glass-fibre-reinforced polymers
APD	Avalanche Photodiode	GNSS	Global Navigation Satellite System
ATC	Air traffic Controller	GPS	Global Positioning System
BER	Bit Error Rate	Gbps	Giga bits per second
BPSK	Binary Phase Shift Keying	HAPS	High Altitude Platform Station
CAN	Controller Area Network	HLAS	High-strength Low Alloy Steel
CDF	Cumulative Distribution function	IR	Infrared
CFRP	Carbon-fibre-reinforced polymers	ISO	International Organization for Standardization
CMOS	Complementary Metal-Oxide Semiconductor	ITWMF	Information Theoretically Weighted Median Filter
COTS	Commercial Off-the-Shelf	LDPC	Low Density Parity Check
C&DH	Command & Data Handling	LEO	Low Earth Orbit
DC	Direct Current	LLGT	Lunar Lasercom Ground Terminal
DEC	Declination	LiDAR	Laser Imaging Detection And Ranging
DLR	Deutsches Zentrum für Luft- und Raumfahrt	MEKF	Multiplicative Extended Kalman Filter
DOF	Degree of Freedom	MEMS	Microelectromechanical system
DPSK	Differential Phase Shift Keying	MIT	Massachusetts Institute of Technology
EASA	European Aviation Safety Agency	MTBF	Mean Time Between Failure
ECC	Error Correction Code	MTTR	Mean Time to Recovery
ECI	Earth Centered Inertial	NASA	National Aeronautics and Space Administration
ECN	Emergency Communications Node	NATO	North Atlantic Treaty Organization
EDFA	Erbium-Doped Fibre Amplifier	NMC	Nickel Manganese Cobalt
EOM	Equations of Motion	NODD	Nominal Ocular Dazzle Distance
EPS	Electrical Power System	NPV	Net Present Value

OCT	Optical Communications Terminal	SDA	Space Development Agency
		SNR	Signal-to-Noise Ratio
ODE	Ordinary Differential Equation	SVD	Singular Value Decomposition
OOK	On-off Keying	SWIR	Short-Wave Infra-Red
OSHA	Occupational Safety and Health Administration	SWaP	Size, Weight and Power
OSNR	Optical Signal-to-Noise Ratio	TAOGS	Transportable Adaptive Optical Ground Station
OSNR	Optical Signal-to-Noise Ratio	TDD	Test-Driven Development
PAT	Pointing, Acquisition, and Tracking	TMS	Thermal Management System
PBS	Polarizing Beam Splitter	TNO	Nederlandse Organisatie voor Toegepast Natuurwetenschappelijk Onderzoek
PDF	Probability Distribution function		
PDU	Power Distribution Unit	TOGS	Transportable Optical Ground Station
PM	Particulate Matter		
PPM	Pulse-position Modulation	TRL	Technology Readiness Level
QPSK	Quadrature Phase Shift Keying	UAV	Unmanned Aerial Vehicle
RAMS	Reliability, Availability, Maintainability, Safety	UV	Ultraviolet
RA	Right Ascension	VOC	Volatile Organic Compounds
RF	Radio frequency	WFoV	Wide Field of View
RMS	Root Mean Square	OSI	Open Systems Interconnection
ROI	Rate of Interest	V&V	Verification & Validation
		FWHM	Full Width at Half-Maximum

Introduction

Since the dawn of time, humanity has strived to build lasting progress for generations to come. Time and time again however, natural disasters have presented obstacles to this. In 79 AD Mount Vesuvius erupted and buried the then bustling city of Pompeii, taking countless lives and leaving an everlasting mark on the place. In 2004 a similar fate befell several cities in South East Asia, when an unprecedented earthquake in the Indian Ocean triggered a tsunami that wiped out entire cities like it was the case in Banda Aceh, Indonesia. More recently, a major volcanic eruption happened in the island nation of Tonga, where a cloud of ash and the severance of the only optical fibre to the island left the community in total blackout from the outside world for 28 days, also taking numerous lives. Nowadays, the effect that these kinds of disasters have can be minimised by implementing a means of communication that is robust to these unpredictable conditions and can offer relief teams uninterrupted communication with the rest of the world. Thorough research and a comprehensive market analysis have indicated that there is indeed a market gap to be filled. The devised solution is denominated as the Emergency Communications Node (ECN).

The aim of the present report is to dive into the particularities of the ECN and make crucial design decisions that will guarantee the correct functioning of the system. Previous design stages have delved into the necessary infrastructure required to establish the optical connection with a HAPS and LEO stationed satellite. This included the Laser source, pre-amplifier, Pointing, Acquisition and Tracking (PAT), Control Algorithm among others. Consequently, subsystems that are significant to the connection yet not directly related are to be designed.

The report will begin with an all-encompassing approach to Sustainability in chapter 3, Sensitivity Analysis in chapter 6, Risk Assessment in chapter 8, as well as Operation, Logistics and Reliability, Availability, Manufacturing and Security (RAMS) analysis in chapter 4 and chapter 7 respectively. These will be followed by an Updated Market Analysis, Modulation, Updated Budget Allocation, Requirement Compliance found in chapter 2, section 5.1, section 5.12, and chapter 10, and an extensive detailing of the design including Structural Design, Frequency Analysis, Environmental Monitoring, Aperture Sizing, Telescope Design, Optical Bench, Sensors, PAT, Thermal Management and EPS found in chapter 5. Finally, a Manufacturing, Assembly and Integration plan will be described in chapter 9.

Market Analysis Update

2.1. Background Study

The market analysis was first conducted in the Baseline Report [1] to investigate a general overview of the market. This section provides a general background summary discussed in the report with some minor updates. Subsequently, the global satellite telecommunications market was valued at USD 71.6 Billion in 2021 and forecasted a growth of 9.8% annually¹. With the ever-growing need for communication, there is a high potential for the application for the laser communication market with

¹<https://www.grandviewresearch.com/industry-analysis/satellite-communication-market>

a forecasted growth-rate of 26.4% ², which is expected to tough up to USD 4,109 Million in the year 2031. With the ability to have superior speeds compared to radio frequency and a narrow bandwidth requirement, laser communication has the ability to disrupt the RF communication market.

Due to climate change, the number of natural disasters is on the rise with an average of 60,000 people dying every year. This identifies a market need for emergency response communication systems for these disaster relief operations. Disasters like Tonga further prove this point. Governments around the world are investing to develop these emergency communication responses in disasters. In military applications, laser communications are identified as a solution to satisfy the need for secure and strong communication in harsh environments. This is supported by NATO and USA alone spending 1.7 billion euros and 10.74 billion USD on satellite communications respectively. Additional need for laser communication was identified for the media and broadcasting segments with high data rates.

The analysis also identified current or potential competitors in the market. The military coalitions already have the assets and are working on developing a similar system. Private big players like NASA, SpaceX and TNO also have shown interest and are considering developing laser communication systems. RedComm and CUBIC GATR ISA are identified as direct competitors developing an emergency response communication system using FSO technology in harsh conditions.

There are several barriers to entry for new competitors, therefore a 7-layered approach based on the Open Systems Interconnection (OSI) model is given to defining a set of general standards. These standards enable interoperability between hardware and different system organisations and reduce the barriers. However, several challenges such as cost in development and operation and diversity of technological maturity within the industry are identified to materialize an interoperable network. NATO countries are assumed to be the main customers, considering every country purchasing 2 stations leads to 60 units sold. However, countries like the USA or other main EU ones might be interested in more than 2 units. Furthermore, there are other countries that this technology would target, mainly countries that are most affected by natural disasters or by threats of war. The estimated unit sold is therefore brought to 100 and for future analysis, it is assumed that a station is present at least in every NATO country.

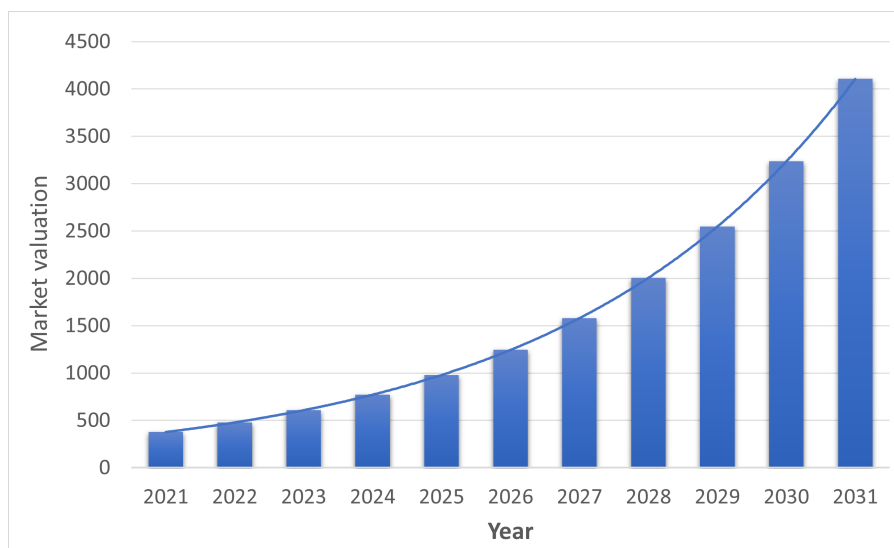


Figure 2.1: Value and growth of the Global Space-based Laser Communication Market

²<https://www.bccresearch.com/partners/bis-market-research/space-based-laser-communication-market.html>

Table 2.1: Cost breakdown structure for different subsystems.

	Subsystem	Cost [€]
1	Command	€ 5,747.82
2	Beam Steering	€ 57,740.50
3	Thermal	€ 1,977.79
4	Electrical	€ 11,878.90
5	Structure	€ 10,000.00
6	Optical	€ 23,500.00
7	I/O	€ 12,968.00
8	Human resources	€ 4,400.00
	Grand total	€ 128,213.01
	Safety factor of 1.5 implemented	€ 192,319.52

2.2. Bottom Up Cost Calculations

The bottom-up costs of all the different subsystems are presented in table 2.1 for which a detailed link to every component at a sub-system level is presented in table B.1 and a detailed analysis can be also found in section 5.12. For the calculations involved in the cost budget further and leading market analysis, a safety factor of 1.5 is taken as shown, because of the bottom approach taken. This is because certain items may have been left out and added later in the development of the project. The costs have been taken from references and external experts in the industry

The costs have been incurred at different times during the duration of the project from 2022 to 2030 and this has to be defined as it affects the discount rate which changes the NPV of the project.

Table 2.2: Costs incurred during the project.

Cost	Time period	Amount	Explanation
Salaries	2022 - 2030	€ 4,696,920.00	Salaries taken and averaged from Airbus NL average rates taken from Glassdoor. ³
Prototyping	2022 - 2023	€ 4,807,988.00	5 prototypes to be built for testing and certification at a cost of 5 times the production cost as advised by industry expert
Lab testing	2023 - 2024	€ 182,175.00	Ref. table 2.3
Field testing	2024 - 2025	€ 481,500.00	Ref. table 2.4
Certification	2025 - 2026	€ 2,000,000.00	The cost of certification is taken as advised by industry expert
Industrialisation	2026 - 2030	€ 5,000,000.00	The cost of setting up a factory and assembly line factory is an estimate by industry expert

Table 2.3: Proposed lab tests to be performed for testing of the ECN

Sl. No.	Testing	Requirement number	Requirement details	How the test is conducted	Cost
1	High temperature	ECN-B-SAR-7	Operational temperature (0 <T <40 [°C])	Testing in an oven/freezer and testing functionality for the given temperature range	€ 7,500.00
2	High temperature	ECN-B-SAR-6	Survival temperature (0 <T <60 [°C])	Testing in oven/ freezer in the given temperature and checking for functionality after the test	€ 4,500.00
3	Wind speed	ECN-B-SAR-5-1	Operational maximum wind speed of 15 [m/s]	Testing in a wind tunnel and testing functionality for the given wind speed from 0 to 15 [m/s] ⁴ .	€ 5,625.00
4	Wind speed	ECN-B-SAR-5-2	Survival maximum wind speed of 55 [m/s]	Testing in a wind tunnel for the given wind speed while not operating from 0 to 55 [m/s] and testing functionality after completion of test ⁵ .	€ 5,625.00
5	Harsh sand and dust	ECN-B-SAR-4-1	Operational IP5#	Testing by putting it into a temperature controlled sand and dust blower for sand for controlled temperatures and testing for functionality during the testing ⁶ .	€ 30,000.00
6	Heavy rain	ECN-B-SAR-4-2	Survival IP#3	Testing by putting it into a water ingestion tester from 5 - 20 [m/s] for controlled temperatures and testing for functionality during the testing.	€ 30,000.00
7	Testing the carbon footprint	ECN-B-SUS-3	less than 500 [g] of carbon footprint	Employ a power cycle and measuring the total carbon footprint by either measuring or simulating it depending on the design decision selected.	€ 12,000.00
8	Pointing accuracy			Testing with various distances from 25 to 150 [m] while testing angular accuracy in a controlled environment and calculating for a longer distance.	€ 15,000.00

⁴<https://www.aa.washington.edu/AERL/KWT/rateguide>⁵<https://www.aa.washington.edu/AERL/KWT/rateguide>⁶<https://www.emitech.fr/en/sand-and-dust-testing>

Table 2.3 continued from previous page

Sl. No.	Testing	Requirement number	Requirement details	How the test is conducted	Cost
9	Vibration			Effects of vibration within the predominant frequency ranges and magnitudes encountered during field service and/or transportation on components ⁷ .	€ 29,925.00
10	Low Temperature + Icing	ECN-B-SAR-7, ECN-B-SAR-6	Operational temperature (-30 <T <0) + Survival (-40<T<0)	Icing along with freezing rain tests at the temperatures specified in requirements ECN-B-SAR-7 and ECN-B-SAR-6 ⁸ .	€ 42,000.00
#				Total cost	€ 182,175.00

Table 2.4: Proposed field tests to be performed for the testing of the ECN

Sl.	Test case	Motivation	Cost
1	Testing in a conventional testing environment for a period of time of 2 months with external power connected	This test is performed so that the pointing system stays aligned with the HAPS UAV for an extended period of time. This will also point out potential failure points if any in the system	€ 30,000.00
2	Testing without an external power source for 1 cycle	This will accurately represent the power cycle life of the system subject to temperature.	€ 1,500.00
3	Testing in high-temperature environment for an extended period of 15 days with external power connected	This test will test the pointing accuracy and thermal subsystems.	€ 90,000.00
4	Testing in low-temperature environment for an extended period of 15 days with external power connected	This test will test the pointing accuracy and thermal subsystems.	€ 90,000.00
5	Testing with different humidity and pressure levels for a period of 15 days	The test will check the effects of different atmospheric parameters with the pointing accuracy and the power subsystems	€ 270,000.00
		Total costs	€ 481,500.00

2.3. Updated NPV Break-Even Chart

To have an accurate representation of the current value of the project, the NPV has been calculated which includes a depreciation discount rate of 10%. This discount rate has been taken in line with

⁷<https://www.generalkinematics.com/international-vibration-analysis-service-rates/>

⁸<https://www.aere.iastate.edu/icing/Laboratory/ISU-IRT/2019-ISU-IRT-Pricing-V100.pdf>

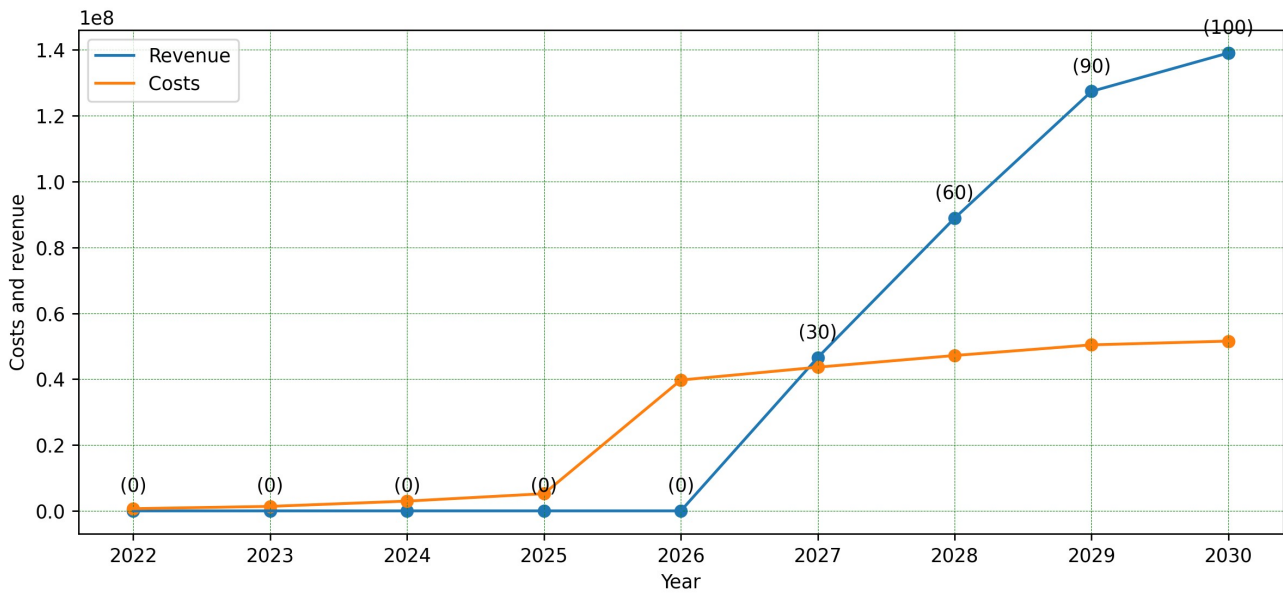


Figure 2.2: Break even analysis with discount rate into account

the industry standards.

The production cost of each unit, as described in section 2.2, has increased from €100,000 to €128,213 as calculated in the base. The development costs and the testing costs have also been changed as described in table 2.3, table 2.4 and table 2.2. This marks a negative impact on the NPV of the project, which has decreased from €92,245,224 to €89,002,820 with the same selling price of €2.5 Million. This is a difference of less than 4% compared to the previous analysis.

With the NPV and costs, a break-even analysis was conducted and it was found that the break-even point is 29 units, this is 1 unit more than the previously calculated BEP of 28 as calculated in the Baseline report [1]. This is because of an increase in the production cost and slight changes in the testing and certification costs.

With the NPV, the Return on investment was calculated. To calculate the NROI (Net Return on Investment), the total costs for development are subtracted from the NPV⁹. The ROI for the project is calculated to be 30.47 %.

2.4. Further steps

Further research into the project can and probably lead to a change in equipment with optimisation. This will lead to a change in the value of components and change the numbers in the analysis conducted. Thus the market analysis needs to be repeatedly conducted and monitored to have an accurate representation of the value of the project at that instance.

⁹<https://www.investopedia.com/articles/basics/10/guide-to-calculating-roi.asp>

Sustainable Development

Sustainability has been an integral part of the design process for the Baseline report [1] and Midterm report[2]. This approach has been continued and improved for this final part of the design. Several common sustainability concepts are discussed in the chapter, whereas the specifics are further integrated in the detailed design sections.

3.1. Sustainability Approach

To make a sustainable product the following approach will be taken. Firstly, in this section subsystems are identified where sustainability will be implemented. In each of these subsystems, goals will be set on how the sustainability will be achieved, and which factors need to be considered. Additionally, each of the goals will be classified by a sustainability category, whether the goal is achieving social, economic, or environmental values. After the goals have been established, a separate section in a corresponding chapter will be written on how the subsystem's sustainability goals were achieved. The main sustainability goals concern the minimisation of raw material waste, material recyclability and prolonging component service life.

3.2. Operations and Logistics

The ECN has been given a volume constraint such that it could fit in the chosen aircraft but most importantly into ISO containers. This approach allows the use of vehicles such as trucks or ships which show much lower fuel consumption, meaning lower emissions. Regarding the environmental monitoring subsystem, the sensors will provide data to ensure the ECN compliance with social and environmental sustainability requirements as explained in section 4.5.

3.3. Thermal Management

For thermal analysis, the main focus lies in reducing the energy usage of the entire system. This would result in a lighter thermal management system with less power required, resulting in less energy usage, which results again in a lighter thermal management system. This effect is called the snowball effect. Furthermore the effect that coolant additives have on health is also discussed. Energy reduction is an example of environmental sustainability since resource depletion is diminished. Ensuring a healthy environment for employees is part of social sustainability.

3.4. Environmental Monitoring

Environmental monitoring concerns environmental sustainability by making sure that the noise pollution, produced by the node, does not exceed allowed noise level limits specified in occupational health and safety regulations. The impact of noise on the environment and compliance with regulations is discussed in subsection 5.11.5.

3.5. EPS

For the electrical power system, the main discussion will concern whether the battery choice was sustainable, and if not what are potential alternative options for sustainability and why those design choices were not made. Secondly, considerations of prolonging the battery's service life were considered. A full discussion can be found in subsection 5.10.4.

3.6. Structure

Considering that the node will need to support the laser subsystem and also have node fixation, a considerable amount of material will be needed to support the node. Therefore, a trade-off on material selection has been done and the importance of sustainability for that choice was described, table 5.21. Furthermore, to minimise the use of raw materials, designs such as gimbals are tried to have minimal volume usage. This sustainability section for structure design can be found in subsection 5.8.6.

3.7. Manufacturing, Assembly and Integration

For Manufacturing, Assembly and Integration the sustainability will mainly concern social and environmental aspects. From social sustainability, main aspects are concerned with workers well being. This will be achieved by ensuring safety during manufacturing, and fair working hours. From environmental standpoint, main considerations concern minimising waste of raw materials, as well as the implementation of the recycling scrap material. More in detail discussion about manufacturing sustainability is provided in section 9.6.

4

Operations and Logistics

In the following chapter the main aspects relative to logistic and operations are analysed. Section 4.1 shows the transportation approach to ensure the deployment is done in under 48 hours as specified in the requirements. Furthermore, section 4.2 and section 4.3 deal with the ECN deployment and its operations during the mission. The validation plan is described in section 4.4 and the sustainability aspects are finally outlined in section 4.5. Regarding the storage and maintenance solutions, the options remain the same as in the previous Midterm report [2] where it was explained that the ECN will be stored in airports and that predictive maintenance is the chosen approach.

4.1. Transportation

To assess whether it is possible to transport the ECN anywhere on Earth within 48 hours, it has been assumed that an ECN is present in every NATO country, specifically in the capital cities. This derives from the market analysis in chapter 2 where those countries are considered to be the main customers. Secondly, the capital cities are chosen because they all have airports and that's the defined storage location. The problem now reduces to transport the station anywhere on Earth starting from any of these capitals. A code has been written [3] to define the furthest point from this set of locations and the result is a distance of 14500 [km] to be covered as worst case scenario. It has to be noted that for the US two cities were considered, namely Washington and Los Angeles, so that the a better coverage of the area is achieved by including locations on the two coasts. Therefore, this analysis defines a worst case scenario where other plausible customers are not considered, but if this conditions can be faced than the 48 hours requirement is considered to be met.

Military cargo aircraft and helicopters have been used for the analysis, as their combination of cargo capacity and velocity is not comparable with other transportation means. Regarding the aircraft, the following three have been selected due to their cargo capacity: the initial ECN's mass estimation was around 1000 [kg] and following iterations brought it to 893.6 [kg].

Table 4.1: Cargo aircraft overview

Vehicle	Payload [kg]	Range [km]	Cross sectional area cargo bay (w X h) [m]
C-130J Super Hercules	18140	4425	3 X 2.7
Alenia C-27J Spartan	4536	5056	2.6 X 3.33
Antonov An-178	8000	4500	2.73 X 2.73

These aircraft have a maximum speed exceeding 600 [km/h], so a common value of 500 [km/h] is used for an averaged approximated cruise speed. The aircraft considered can cover the aforementioned distance with two to three refuelling stops, given their range in table 4.1¹²³. To take a conservative approach, 3 stops are considered. The transportation time can therefore be calculated by taking into account the flight time, the three refuelling stops, the loading and unloading process, and the final positioning of the station by means of other vehicles such as helicopters.

It can be determined that the worst case scenario would require a flight time of 29 hours to travel 14500 [km]. Turnaround times for this particular mission are hard to estimate due to the particularity of the mission and payload. However, for airlines the turnaround time ranges from 30 to 90 minutes⁴. This values include "Re-fueling, inspections, cleaning, baggage handling, cargo handling and passenger boarding", but the cargo aircraft used in the mission do not need to take care of the cleaning, baggage, and passengers steps, thus considerably shortening the overall process. After this considerations, it is assumed that the first and last step of the aerial section of this transportation chain take 90 minutes each. This represents a very conservative approach where the turnaround time for a long haul airlines is used for this quick emergency mission. Further developments and validation processes will refine this time estimations and provide specific results for these scenarios. Furthermore, the aircraft considered have a fuel capacity very similar to a Boeing-737, for which the average refuelling time with one truck and one nozzle is less than 30 minutes⁵. It is therefore safe to assume refuelling stops of 30 minutes for a total of 1.5 hours. Again, a conservative approach is preferred, meaning that the time accounted for the three refuelling stops is considered to be 2 hours. By considering the previously found 29 hours of flight, 3 hours for loading/unloading and 2 hours for refuelling stops, the total aircraft flight time for this worst case scenario adds up to 34 hours, leaving 14 hours for the final positioning.

As previously mentioned, helicopters are the first choice to complete the transportation process. It is therefore important to assess the availability of such vehicles capable of transporting the required payload of the hook. Here some solutions are presented: Bell 412 (cargo hook of 2041 [kg])⁶, Bell Huey-II (cargo hook of 5080 [kg])⁷, Kaman K-MAX (cargo hook of 2722 [kg])⁸, NH90 (cargo hook of 4000 [kg])⁹.

¹https://www.lockheedmartin.com/content/dam/lockheed-martin/aero/documents/C-130J/MG180389_C-130Brochure_NewPurchase_Final_Web.pdf

²https://aircraft.leonardo.com/documents/16114715/17990486/C-27J+Next+Gen_brochure_new_ENG.pdf?t=1647512362260

³<https://antonov.com/en/aircraft/an-178>

⁴<https://www.rtitb-airside.com/decrease-aircraft-turnaround-times/>

⁵<https://pilotteacher.com/how-long-to-refuel-an-airplane-15-most-common-planes/>

⁶<https://www.bellflight.com/products/bell-412>

⁷<https://www.bellflight.com/products/bell-huey-ii>

⁸<https://www.kaman.com/brands/kaman-air-vehicles/k-max/>

⁹https://helicopters.leonardo.com/documents/16114711/18088670/NH90_brochure_NHI_2019.pdf?t=1591609472620

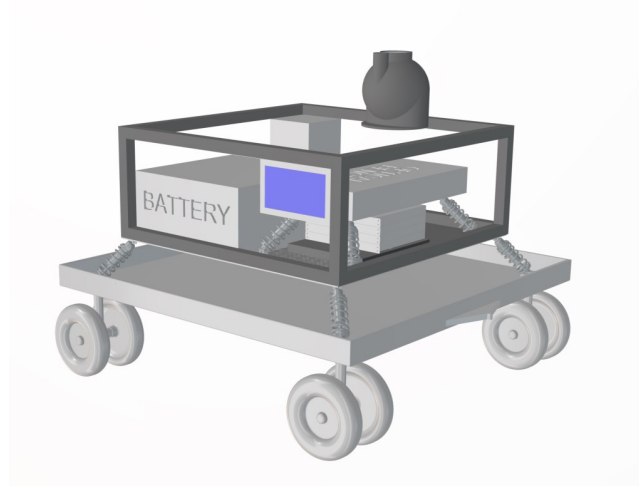


Figure 4.1: *Towing cart initial concept*

The transportation solutions and duration have been taken into account, now the ECN compatibility with these solution has to be considered. In order to allow an easy and quick transport, the container, pallet or box where the ECN will be inserted has to be compatible with all the mentioned vehicles. Meaning that this will pose a first constraint on size. A possible choice would be a standard LD9/AAP container (2.23 x 1.62 x 3.17)¹⁰, all the measures will be in meter and representing (w x h x l). A second solution, is a standard P1P/PAG pallet (2.23 x 3.17)¹¹, which allows for a bigger height of the ECN. This height however is constrained by the smallest cargo bay out of the three aircraft considered, namely 2.7 meters. In order to ease the change of vehicle throughout the process, it is preferred that the ECN fits inside an ISO container. These are the standard containers used for ships, trains and trucks, with an internal size of (2.35 x 2.38 x 5.75)¹². To summarise, to allow the product to be transported by any of the three aircraft listed in table 4.1, the ECN should have a maximum size of (2.23 x 2.7 x 3.17). Furthermore, the station would fit in an ISO container if its height is reduced to 2.38 [m], meaning that the limiting size becomes (2.23 x 2.38 x 3.17).

There might also be the necessity of an always available last mile solution. This aspect is tackled by including a device which introduces the possibility of small distance movements, more precisely it will allow the ECN to be towed by motorized vehicles such as pickup trucks. The solution consists of a 4-wheels towing cart with the size being constrained to a maximum of (2X3) meters due to the container size, and a minimum of (1.8X1.8) meters due to the base dimensions of the ECN. Based on these considerations, figure 4.1 gives an overview of the concept. This concept defines the main characteristics such as the four legs structure, the size and the hook. Further analysis will address aspects like the structural elements to ensure the required stiffness, the detailed features allowing the ECN to be safely mounted on the cart, the wheels size and the final weight. Regarding the weight, the smallest aircraft considered, the Alenia C-27J Spartan, can transport 5 times the ECN mass and therefore it is safe to assume that this towing cart will not pose any issue to the overall transportation process.

¹⁰<https://www.dsv.com/en/our-solutions/modes-of-transport/air-freight/unit-load-devices/ld9-aap-container>

¹¹<https://www.dsv.com/en/our-solutions/modes-of-transport/air-freight/unit-load-devices/p1p-pag-pallet>

¹²<https://blog.intekfreight-logistics.com/iso-container-defined-and-facts>

4.2. Deployment

In this section the three main steps needed to deploy an operational ECN are presented, these include unloading the station, the calibration and connection processes.

4.2.1. Unloading

The loading/unloading process is carried out with the standard protocols of the location in question. In case the ECN has to be unloaded from a truck, a forklift will handle the station¹³.

After the process is completed, the ECN is activated by the operator.

4.2.2. Calibration

Calibration is performed automatically upon activation of the ECN. subsection 5.6.1 covers the detailed design of the attitude determination subsystem, and involves the description of the calibration process. Upon completion, the system can perform pointing, and a connection can be established.

4.2.3. Establishing connection

The airborne or LEO target is selected by the operator from the pre-programmed database of available communication satellites and the list of communication High Altitude Pseudo Satellites, whose telemetry has been intercepted with an RF receiver. Upon selection, the PAT sequence, described in subsection 5.6.5, is performed. Upon successful connection establishment, the product can be operated as a communication node.

4.3. Operation

After the ECN has been deployed and the connection to an airborne or LEO platform established, the ECN can be operated with minimal expert supervision. In case of connection loss, the procedure outlined in subsection 4.2.3 can be repeated. The system performs automatic environmental monitoring and malfunction detection to ensure safe operation. In case of a detected hazard or failure, the station enters safe mode described in subsection 4.3.3.

4.3.1. Connecting to ECN

The ECN is outfitted with interfaces for high-speed cables to connect with other networking infrastructure, as well as an interface for connection with a commercially available laptop.

4.3.2. Automatic malfunction detection

The critical subsystems contain interoceptive sensors: electrical (voltage, current), temperature, battery charge state, and strain gauges. They are summarized in the table 4.2.

Table 4.2: *Interoceptive sensors by subsystem*

Subsystem	Interoceptive sensor
Laser	Current and voltage, temperature.
Thermal management	Current and voltage, temperature.
Electrical power	Current and voltage, temperature, battery charge state.
Environmental monitoring	Current and voltage.
Gimbal	Strain.

When an unusual behavior is detected, the Node enters safe mode. For example, the laser has a maximal temperature at which it can operate, over which it risks significant deterioration of performance and damage to the components.

¹³<https://www.euro1training.com/news/weight-forklift-lift/>

4.3.3. Safe mode

The safe mode is initialized automatically, or manually by an operator. There are three automatic triggers: when constraints of operating envelope are exceeded, when a malfunction is detected, and when weather forecasting software predicts incoming hazardous conditions. Automated malfunction detection is subject of subsection 4.3.2, while operating envelope monitoring and forecasting are both covered in section 5.11. The third trigger is configurable by ECN's operator, who might select different settings for the trigger. High autonomy, long-term operation with limited personnel would benefit from entering safe mode early, while a well-equipped and well-controlled military operation might decide to disable the forecasting trigger altogether and safely operate the ECN with appropriate oversight.

When ECN enters safe mode, the laser is powered off, and the gimbal moves to safe position. Safe position is selected such that the exposure of instrumentation to the environment is minimised. All functions relating to communications are ceased, limiting power use of the system. Powering off the laser also limits the heat produced, working against overheating of the system, as well as limiting the strain on the thermal management subsystem.



Figure 4.2: Military equipment secured with protective cover¹⁴

Furthermore, if possible, the operator should cover the ECN with tarpaulin, and secure it by the designated hooks on the structural frame. The tarpaulin limits exposure to water, dust, sunlight, and partially protects against debris. It is commonly used after disasters to protect damaged structures [4]. Example of a protective cover used to secure equipment is presented in figure 4.2.

Environmental monitoring and automatic malfunction detection continue to monitor the environmental conditions and the state of the system. However, sensing nominal conditions does not automatically trigger exiting the safe mode. Exit must be manually activated by the operator, after verifying that conditions are safe to resume ECN operation.

4.4. Validation Plan

In this section a complete validation plan for the operations and logistic aspects is shown.

¹⁴<https://www.protectivepackaging.net/military-covers>

4.4.1. Transportation

The whole transportation chain needs a validation plan, from the actual sizing issue to the time limit requirement. A validation plan is presented to check whether the ECN can actually fit in the chosen vehicles and ISO container, to check if 14500 [km] can be covered within the time limit and to check how much time usually passes before the chosen vehicles can approach a disaster location.

Regarding the first aspect, a simple demonstration can be performed, meaning that the ECN itself or a sample item with the same dimensions will be loaded onto the various aircraft, the ISO container and the towing cart. In case the communication node appears to be too big for those defined spaces, new transportation means will have to be found. A second option would be an iteration on the re-shaping of the product, considering that this would be more difficult as various subsystems will be affected.

Second, validation is required to assess the feasibility of covering 14500 [km] within 48 hours. Again, a simple demonstration could be carried out, but it would represent an unnecessary expense of money and fuel, making this approach unsustainable and expensive. A better approach consists of analysing previously carried out missions with those vehicles and or with ranges in that order of magnitude. In this analysis special attention has to be given to the load/unload processes of the various vehicles so that the deployment under 48 hours is achieved.

Validating these two aspects shows that the ECN can be loaded and sent to destination in time. However, there is one last aspect that needs to be considered, namely the time that has to pass between a disaster occur and the moment these vehicles can reach its location. This issue might pose new constraints on the transportation technique, depending on the type of emergency and location. The best way to face this analysis is purely analytical, it consists of studying previous emergencies such as the recent Tonga disaster and the 2014 Japan earthquake for example. By doing this, the average response time taken to reach those locations can be assessed. More importantly, it can be determined if there are vehicles which face serious issues in reaching these zones. The transportation approach can be considered validated if a wide enough variety of vehicles can reach all these sites in under 48 hours.

Summarising, the validation for the transportation shall be done by ensuring that the ECN can be loaded into every considered vehicle and sent anywhere within 48 hours, considering also the delay time that might arise due to the impossibility of reaching the wanted location.

4.4.2. Deployment

The procedure for deployment of the station must be validated with an in-house demonstration prior to any deployment in external site. The product must be loaded, secured and unloaded from an airplane transportation container, a truck, and a train wagon, with equipment we know to be available at each site. It is important to validate whether the instructions for deployment are understandable for non-expert personnel, so operators for the validation are not have worked on the ECN development process. This outlines criteria for a collection of validation demonstrations, involving combinations of equipment (for example forklifts) and transportation means.

Upon validating unloading of the product, a test outside must take place, in which operators follow the procedure to initiate calibration and connection to an available platform. If the ECN calibrates and establishes a connection, this part of validation is successful.

4.4.3. Operations

To validate operation of the ECN, the following tests have to be performed. The ECN connection must be used to download a series of large files over a long period, on a personal laptop connected to the node. A series of malfunctions on the node must be simulated, in software and by placing faulty hardware in a controlled manner (such that there is no danger of damage to other components), to make sure an automatic malfunction detection triggers a safe mode. The ECN must be exposed to conditions outside of its operating envelope (in a controlled way), to make sure it enters safe mode. Finally, personnel unfamiliar with the product must follow ECN instructions to secure the product in safe mode with tarpulin, then remove the tarpulin, and activate exit from the safe mode. Such combination of demonstrations and tests validated the operation of the product.

4.4.4. Complete cycle

All the single aspects have been validated separately using ad hoc techniques. As a final step the whole cycle including transportation, deployment and the operations described in section 4.3 will be validated by means of a complete demonstration. This demo mission will be the last validation step to ensure that the product is ready to be deployed. It is assumed that this final step is executed only when all the previous one and the various subsystems have been successfully validated.

4.5. Sustainability

Constraining the ECN size such that it can fit into the aircraft as well as the ISO containers allows for much more sustainable means of transportation. Standard ships, trains and trucks are now viable options, which are cheaper to operate and substantially more fuel efficient when compared to just aircraft and helicopters. These variants are of course feasible for distances shorter than the previously described worst case scenario. Furthermore, its relatively small size allows the ECN to be loaded into commercial aircraft and allows to organise transportation on regular airliner flight when the conditions match the mission needs.

Throughout deployment and operation, the environmental monitoring subsystem, presented in section 5.11, ensures compliance with (social and environmental) sustainability requirements, as well as boasts other sensors, included for reasons other than sustainability, that can be used towards enhancing sustainability of the product. A air quality sensor, used to monitor impact of environment on deterioration of the product, can at the same time be used to monitor pollution from the operation the ECN is a part of. Data from ECN deployment can be used to study the environment, and might be the first extensive source of information about the habitat after a disaster has struck, therefore providing scientific and ecological value.

5

Detailed Design

After analysing how much the node will cost, what will be the sustainability approach, and figuring out the sizing constraints from the operations and logistics, the node's design is elaborated. Firstly, the sections concerning the link establishment will be treated, namely the modulation and link budget. Link establishment will influence the node's aperture sizing, the design of which will be treated in section 5.3. Followed by the optical path the signal will take and the components required to receive the signal, section 5.4. To acquire the signal and maintain the connection, camera sensors will

provide feedback to a multi-stage control sequence. The two elements, cameras and PAT, will be described in section 5.5 and section 5.6 respectively.

After completing the design for the communication link, main structural loads were identified and the frequency analysis was performed to safeguard the node from external vibrations, section 5.7. After identifying the loads, the structural design for supporting the communication subsystem and sustaining the loads will be discussed in section 5.8. Then to make sure that the node's components can operate at the optimal temperatures, a thermal analysis has been performed in section 5.9. To make sure that enough power is provided for the thermal management and other subsystems, an electrical power system design was established in section 5.10. As the finishing touches environmental monitoring was integrated, for the node to be aware of the weather and the surroundings, section 5.11. After the detailed design is complete SWaP budgets regarding mass, costs, power and volume are presented in section 5.12.

5.1. Modulation

While performing verification of the Link Budget presented in the Midterm Report, one of the main aspects missing in the budget was the Signal-to-Noise (SNR) ratio required to establish the successful data communication link. This required SNR ratio comes from the modulation technique chosen. However, the task of finding the SNR becomes complicated since multiple factors play a role, such as Transmission distance, Data Rate, and the acceptable Bit Error Rate (BER).

In this chapter, a discussion regarding 16 - Quadrature Amplitude Modulation (16-QAM) suitability will be performed and assumptions used to make the modulation technique work will be presented. It is followed by the description of the system to achieve 100 [Gbps] data rates with HAPS, and implementation of Forward Error Correction together with multiplexing. Similarly, a system discussion about the 1 [Gbps] LEO satellite communication will be done, together with the choice of appropriate modulation for that case. Finally, the section about the modulation choices and their implications on further design will be presented.

5.1.1. Research on 16-QAM and Assumptions Used

In the midterm report, the trade-off has been performed, and the modulation technique chosen was the 16-QAM due to the possibility of sending high data rates at reasonable power consumption, compared to the other modulation techniques [2]. However, after more in-depth research into the topic of modulation several problematic aspects have been noted, that influence the mission's success. More specifically the high data rate transmission between HAPS and the node. Therefore, this section will introduce and justify the assumptions stated below to be able to establish the data link.

1. Communication happens in the clear sky conditions
2. Clear weather FSO long-haul communication links have been treated as clear-weather altitude-varying communications, without the effect of scintillation included.
3. Scintillation effects included in the Link Budget are not stochastic, and follow Gaussian noise distribution with transmitting distance.

Clear Sky Conditions

To be able to perform the communication with HAPS or LEO, it is essential to assume that the node is communicating in clear sky conditions. Otherwise, any mild weather disturbance such as haze will result in a drastic link range reduction as can be seen in figure 5.1. Weather disturbances such as rain and fog are even more impactful in terms of attenuation loss [5]. The figure is taken from the reference article used for HAPS communication in subsection 5.1.2, and as can be seen even during the low haze link further than 12 [km] would not be established. This would not satisfy the HAPS

requirement, but it is achievable under clear sky conditions, further explanation of why will follow in subsection 5.1.2.

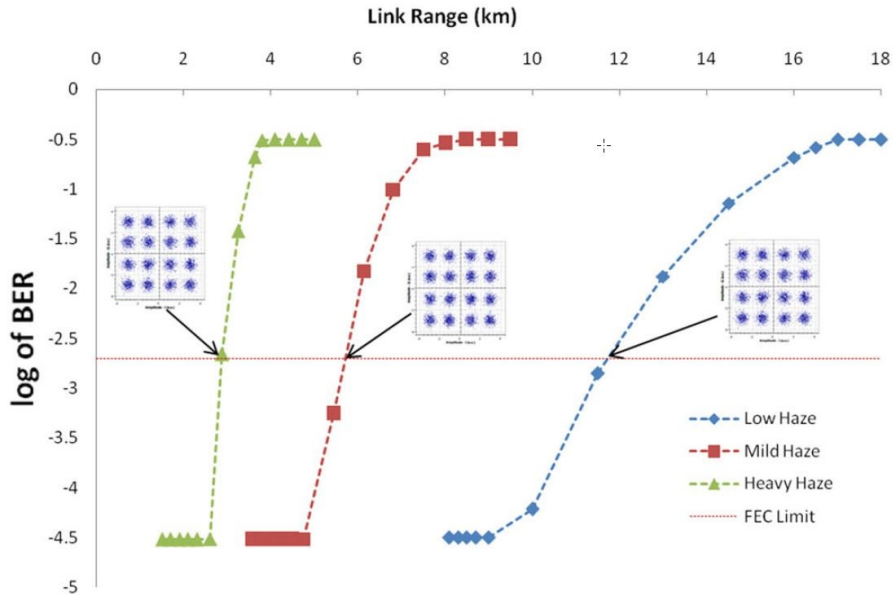


Figure 5.1: Log graphs of BER against link range (km) for the PDM-16-QAM modulation for the long-haul transmission with data rate of 160 Gbit/s [5].

Long-Haul Transmission Links Assumption

One of the major problems with 16-QAM is the performance degradation with distance, meaning that noise gets accumulated producing high Bit Error Rate (BER). The reason for such performance degradation in QAM with distance, is the high bandwidth efficiency. Even though QAM can provide a reduction in power level, the technique is not commonly used for optical communications due to susceptibility to turbulent atmospheric conditions [6]. More about it will be discussed in figure 5.1.3.

For this reason, research articles with comparable communication distances use 16-QAM for long-haul communication. Long-haul communication is used for long physical distances between users, sometimes involving worldwide distances. Compared to conventional communications, long-haul are characterised by administrative or higher command users and higher traffic loads [7]. Such terrestrial communication is not the same as air-to-ground communication. However, it can be argued that the terrestrial results can still be used. Especially considering that certain noise sources, such as aerosol scattering can even be greater at a terrestrial level than air-to-ground [8], more about it in equation 5.2.3.

Furthermore, the air-to-ground communication has been performed by the Facebook mission by using M-QAM modulation with 100 [Gbps] data rate [9]. Meaning it is possible in theory to perform such missions, but the commercial mission does not provide technical graphs for competitive purposes. Therefore, to provide a descriptive modulation system design, the assumption is made that the FSO long-haul transmission links technical graphs can be used for the ground-to-air communication analysis.

Scintillation Susceptibility Assumption

Building upon the topic of signal degradation with distance, the 16-QAM dependence on atmospheric disturbances is non-gaussian, the effect of which can be predicted by using gamma-gamma models [10], creating a highly complex problem to establish the communication link. By using power-efficient modulation schemes such as BPSK or OOK, such problems could have been avoided.

Therefore, in the following modulation analysis, no scintillation in the graphs has been considered. However, scintillation will be included in the link budget, section 5.2, by using simplified lognormal distribution.

5.1.2. Steps To Meet the 100 [Gbps] Requirement

Multiple articles have shown high Bit Error Rate (BER) when 16-QAM was used for distances longer than 1 km [5, 11, 12]. Even in the figure 5.2, at Optical Signal to Noise Ratio (OSNR) of 22 [dB], the BER of only 10^{-3} is achieved. For an uncoded signal, such BER would result in 100 Megabits received in error per second, according to equation 5.1¹.

$$BER = \frac{E(t)}{N(t)} = \frac{\text{number of bits received in error in time } t}{\text{total number of bits transmitted in time } t} \quad [13] \quad (5.1)$$

Such high BER would create a complicated task to demodulate to correctly incoming data rate, not to mention the high OSNR of 22 [dB] which would need to be accounted for in the link budget. However, by including the forward error correction (FEC) and the interleaving the received signal BER rates can theoretically be restored if the BER limit does not exceed the 10^{-3} FEC limit [14]. This would mean that 16-QAM can be used for the mission by including the FEC.

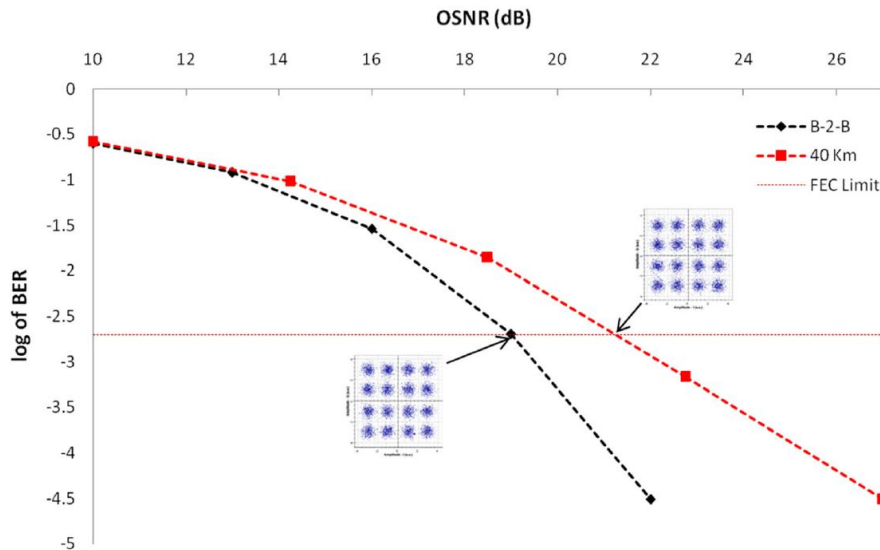


Figure 5.2: Log graphs of BER versus OSNR for the PDM-16-QAM modulation for the long-haul transmission distance of 40 [km] and data rate of 160 [Gbit/s]. [5].

However, including FEC usually comes with a price of fixed overhead, depending on the Error Correction Code (ECC) chosen for the FEC. Overhead is added to the nominal data rate as additional information, to perform the error detection [15]. Meaning that a higher data rate than 100 [Gbps] will need to be sent, to make sure that 100 [Gbps] data can be decoded successfully. Due to the inclusion of overhead, a graph for the 160 [Gbps] uncoded communication link was used, to use it as redundancy and account for the ECC choice.

While choosing the ECC, commonly used codes in Free Space Optical (FSO) communication was researched. From which particular attention was to find the turbulence efficient code, to make sure that the signal is not lost after the scintillation. From these, the low-density parity-check (LDPC) code was the most attractive compared to other turbulence-efficient coding schemes such as Turbo

¹<https://www.fiberoptics4sale.com/blogs/archive-posts/95047174-what-is-ber-bit-error-ratio-and-bert-bit-error-ratio-tester>

or Trellis. Mainly due to the code's usability with high data rates since it has reduced decoding complexity and computational time, compared to the other two techniques [6].

LDPC code is an effective ECC for this mission since it is based on the iterative decoding, allowing near Shannon limit performance [16]. Which in return can make the incoming signal comprehensible. However, based on the simulations LDPC requires 12.59% of the overhead [14], meaning that 112.59 [Gbps] of data will need to be sent. Moreover, other sources of overhead may be applied in the FSO link such as cyclic prefixes, training symbols and the pilot tones [17]. Meaning that the data from the communication link of 160 [Gbps], shown in figure 5.2, will still be used as the reference for the SNR threshold used in the SNR margin.

The final addition to make sure that the 16-QAM is compatible with the HAPS communication requirement is the interleaving. In the communication channels, the errors usually occur in bursts rather than independently. If the number of errors in succession exceeds the ECC's limit, the original code word (within the received data) will not be recovered. Therefore, interleaving shuffles symbols across multiple signals to create a uniform error distribution [18], to ensure the code words in the received data are understandable. Interleaving has been used to improve the performance of the LDPC codes [19]. Therefore, as an additional level of redundancy to establish a successful HAPS link, LDPC will be used with interleaving.

In summary, for the successful 100 [Gbps] data link with HAPS and the use of the 16-QAM. The long-haul data of 160 [Gbps] will be used to account for the overhead sources. From figure 5.2, the OSNR required is 22 [dB] to achieve an acceptable BER of 10^{-3} with use of FEC. Such BER will be demodulated by the inclusion of LDPC together with interleaving. The OSNR of 22 [dB] will be included in the link budget which will serve as a threshold which will need to be exceeded.

5.1.3. LEO Satellite Communication

Now that the HAPS communication is settled, it is time to move to the second communication requirement. More specifically the communication with LEO satellite at 500 [km] altitude in [Gbps] regime, stated in baseline report [1].

ACM Consideration

To the best of author's knowledge, 16-QAM was not found to be used for the FSO ground to LEO communication. More commonly, power-efficient modulation schemes are used, such as the OOK [20]. Therefore, using Adaptive Coding and Modulation (ACM) was considered. ACM is used to match the modulation and coding depending on the conditions of the link². Meaning that if communication with the LEO satellite was found, the modulation and coding will be switched from 16-QAM to OOK.

However, it is complex to implement ACM into the node. Since all of the Forward Error Correction (FEC) should be constant in bits, making a synchronisation a difficult task³, understanding of which is beyond the scope of the project. Therefore, in order not to increase the complexity of the system even further, it was decided not to incorporate ACM into the design. In the literature review performed, no ACM application for the FSO links schemes was found.

Implementing QAM Schemes for the LEO-to-Ground Communication

Coming back to the LEO communication, the closest alternative of communication between Ground to LEO was the use of Quadrature Phase Shift Keying (QPSK or 4-QAM). QPSK modulation, similarly to 16-QAM, has a varying phase angle in 4 different combinations. The only difference between the two modulations is that 16-QAM has also varying amplitude allowing to achieve 16 different

²<https://www.microwave-link.com/microwave/acm-adaptive-coding-modulation/>

³http://www.comtechefdata.com/files/articles_papers/wp-cdm625_acm_white_paper.pdf

combinations of 4 bits [21]. Considering, that there are missions existing with QAM modulation, it has been assumed that the QAM modulation is theoretically possible with such high distances.

The mission using QPSK was the "Shijian-20" satellite to communicate with the LiJiang optical ground station in China, with a data rate of 10 [Gbps] [22]. However, the numerical values, or SNR graphs, were not found from this mission making it difficult to analyse the feasibility of the LEO requirement.

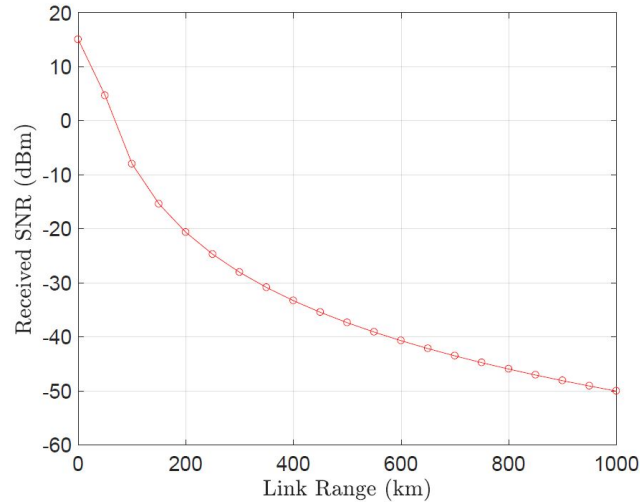


Figure 5.3: SNR against the link distance for the QPSK modulation for 1550 [nm] wavelength FSO link at 128 [Gbps] data rate [23].

There was however a scientific article which has extrapolated a 15 [km] FSO link with QPSK modulation, the graph of which is represented in figure 5.3. From the figure, to reach 500 [km], received SNR was 38 [dB]. Which, if it is decided to be included in the link budget as a threshold, would not result in the unsuccessful communication link. However, the graph is an extrapolation and does not provide information regarding BER achieved at such distance, making it unclear whether such data can still be demodulated at such distance and whether LCPD coding would still suffice. Therefore, considering a lack of data for QAM modulation for long-distance communication, the SNR threshold for the LEO communication link budget was decided to be neglected.

Reason for Lack of Information on QAM

However, why is QAM not used for LEO free space optical communication? As been discussed in the first paragraph of subsection 5.1.3, QAM is heavily based on the phase-angle variation. Those types of modulation schemes are not well suited for space-to-ground links since the phase integrity of the beam is compromised when passing atmospheric turbulence. Consequently, interference contrast in the receiver is deteriorated significantly, making it difficult to achieve reliable decoding [24]. Therefore, for such communications pulse-positioning modulation (PPM) or On-Off Keying (OOK) modulation are more commonly used [6] since they do not involve phase modulation.

5.1.4. Modulation Design Implications

Now after being settled with modulations and the additions in form of FEC, it is now important to discuss how does modulation impact the rest of the node's design. The main implication of modulation is the required OSNR ratio for which the link budget needs to be able to compensate.

Therefore, a low OSNR ratio is preferred which will allow a lower threshold for successful closure of the link budget, which can be seen in table 5.3 and table 5.5. The lower threshold will mean that the aperture size of the node or the transmitting power can be reduced. Consequently, those changes are desirable for the node's design since a smaller aperture size will result in lower component costs,

and lower transmitting power will mean that less energy will be consumed making the node more sustainable.

Another design implication of modulation concerns the receivers. The current design for the HAPS requirement has already involved an increase in system complexity by involving FEC to mitigate the effects of high BER. Therefore, it is undesirable to have new sources of BER, one of which can be the receiver operating at high sensitivity as can be seen in the example presented in figure 5.4. Therefore, it is important to make sure that the receiver produces negligible amounts of BER in order of 10^{-12} or lower.

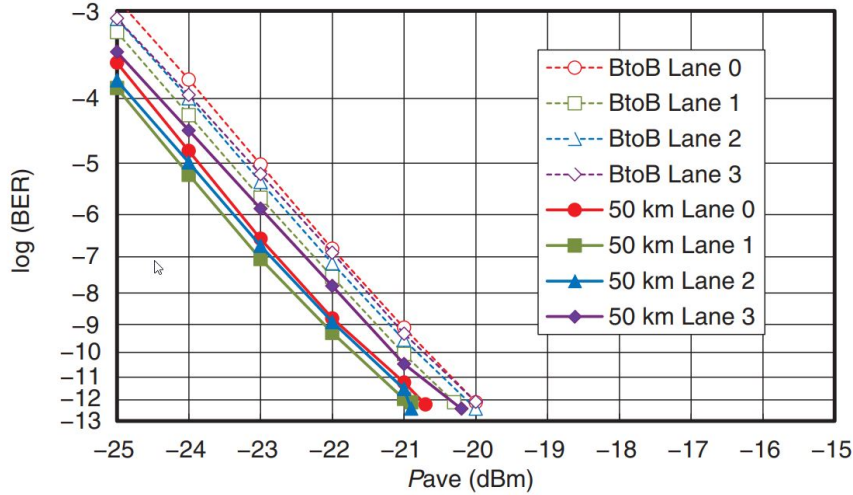


Figure 5.4: Example of BER varying with sensitivity of the APD receiver [25].

The final note about the receiver choice is that not every receiver is sensitive enough for certain modulation formats. For instance, Direct Detection receivers will require delay demodulators for Differential Phase Shift Keying (DPSK). However, in the midterm report, a coherent APD receiver was selected [2], which was a correct choice, reflecting as the design progressed further since such receivers allow to detect the optical field directly, meaning any modulation format can be used without optical pre-processing components [26].

5.2. Link Budget

The link budget was first identified as a technical parameter for performance in the Baseline report. The simplified model for the budget was introduced and explained in the Midterm report. This was done for both the beaconing options and the laser communication where scanning was selected as the beaconing option in the trade-offs.

Some of the aspects missing in the link budget were the downlink budget, the effects of noise in the receiver, the calculation for Optical Signal-to-Noise Ratio (OSNR) and the effects of modulation in the budget. Therefore, the budget is expanded by first including an Erbium-Doped Fibre Amplifier before the laser is collected in the Avalanche Photodiode (APD) detector for both the uplinks and downlinks. This is done to improve the link performance of the received signal by pre-amplifying it and significantly reducing the generated noise. The link model is therefore updated and showcases the link parameters and their sequences below:

$$P_R = P_T G_T L_T L_P L_S L_A L_R G_A G_R \quad (5.2)$$

The received power can then be calculated from the updated link equation in equation 5.2. The most

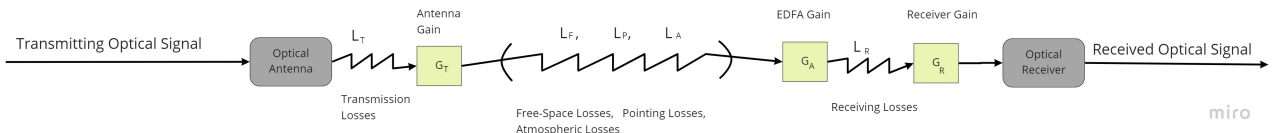


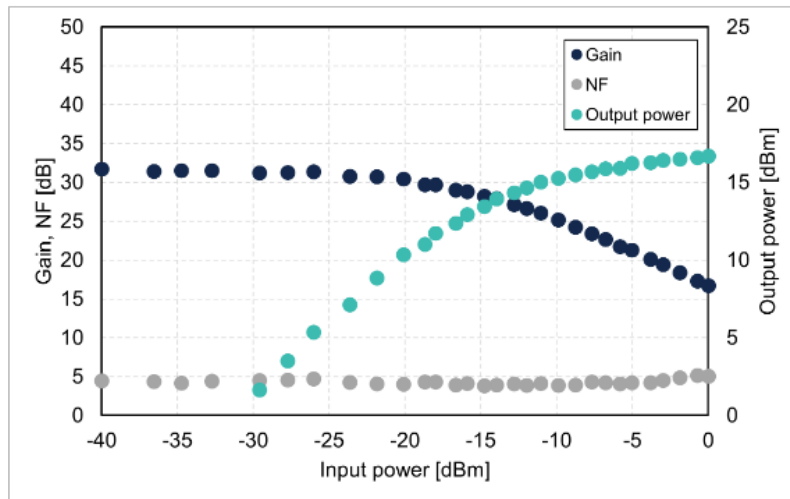
Figure 5.5: Link Model

significant parameters of the link equation are estimated using the relations given in the Midterm report [2]. The inputs affecting the link budget can be derived from these relations and are summarised in table 5.1 below:

Table 5.1: Input Parameters for Link Budget

Input Parameters	Symbol
Transmitting Power	P_T
Transmitting Divergence angle	Θ_T
Altitude	h
Wavelength	λ
Pointing Accuracy	Δ_Θ
Receiver Aperture Diameter	D_R

In the Midterm report, a wavelength of $\lambda = 1550$ [nm] with a pointing accuracy of $\Delta_\Theta = 1$ [μrad] was selected for the communication laser beam. The transmission loss (L_T) was updated as a -2.5 [dB] estimation due to better performing commercial high-end systems utilised by Facebook in minimising Matching losses and Strehl losses [9]. For the EDFA, C-band FiberLabs commercial MP-FL501x-CB component series was selected due to a high gain of $G_A = 30$ [dB] and a low noise Figure of $F_A = 5$ [dB]. The received power will usually be in the -40 to -20 [dBm] and the values are taken to be constant as seen in the figure 5.6:



Gain/NF/output power vs. input power @1550 nm (FL5011-CB-16)

Figure 5.6: Noise Figure and Gain v/s Input Power for C-band EDFA⁴

⁴https://www.fiberlabs.com/products/product_details/c-band-edfa-rack-mount/

System Noise Calculation

The effects of thermal noise contribution to the receiving signal can be estimated by estimating the total noise power generated at the EDFA and the receiver detector at the end of the link. These can be classified as linear devices and can be modelled as internal noise generator devices [27]. For obtaining the noise power, first, the system noise temperature consisting of both the devices needs to be determined. For the InGaAs APD receiver, most literature estimated the noise temperature to be $T_{Noise-APD} = 300[K]$ [28, 29]. For the EDFA, the noise temperature can be calculated by using the Noise Figure value of $F_A = 5[dB]$ from figure 5.6 and can be calculated by equation 5.3 [27]:

$$T_{Noise-EDFA} = (F_A - 1)T_0 \quad (5.3)$$

Here $T_0 = 290[K]$ is the standard room temperature, thus resulting in EDFA noise temperature as $T_{Noise-EDFA} = 627[K]$. The total system equivalent noise temperature could then be obtained as:

$$T_{System-Noise} = T_{Noise-EDFA} + T_{Noise-APD} = 927[K] \quad (5.4)$$

The noise spectral density (N_0) for the system thermal noise can be given by equation 5.5, where ($k = 1.38 * 10^{-23}$) is the Boltzmann's constant:

$$N_0 = kT_{System-Noise} \quad (5.5)$$

The equivalent noise bandwidth (B_N) is the bandwidth of a rectangular filter, which produces the same integrated noise power as that of an actual filter⁵. It is obtained to take account of the contributions of the required data transfer rate, channel bandwidth and the modulation technique incorporated. It is given by equation 5.6, where (R) is the Transfer Data rate and (η_N) is the link spectral efficiency⁶ :

$$B_N = \frac{R}{\eta_N} \quad (5.6)$$

In the above equation, spectral efficiency (η_N) analyses the efficiency with which digital modulation is used to carry the data and is directly a function of modulation technique applied⁷. For HAPS and LEO worst cases, 16-QAM was identified as the optimal modulation technique in subsection 5.1.1 and results to have $\eta_N=4 [bit/Hz]$ ⁸. This results in a value of $B_N = 2.5 [GHz]$ for a transfer data rate of $R=100 [Gbps]$. This matches and is validated with the 16-QAM modulation values used by Facebook using a channel bandwidth of $5 [GHz]$, which is twice the calculated B_N [9]. Finally, the total noise power contribution could be calculated now through equation 5.7, which is used later to obtain the OSNR :

$$P_N = N_0 B_N \quad (5.7)$$

Required Power

The threshold required power determines the worst-case performance of the link by calculating the minimum sensitivity the receiver should be able to detect the signal. The threshold power can be calculated using the Majumdar paper [28] which takes account of the receiver threshold sensitivity, the required data rate and the indirect effect of modulation on the receiver sensitivity.

⁵<https://resources.pcb.cadence.com/blog/2020-equivalent-noise-bandwidth-its-applications-and-how-is-it-calculated>

⁶[https://eng.libretexts.org/Bookshelves/Electrical_Engineering/Electronics/Microwave_and_RF_Design_I_-_Radio_Systems_\(Steer\)/05%3A_RF_Systems/5.05%3A_Spectrum_Efficiency](https://eng.libretexts.org/Bookshelves/Electrical_Engineering/Electronics/Microwave_and_RF_Design_I_-_Radio_Systems_(Steer)/05%3A_RF_Systems/5.05%3A_Spectrum_Efficiency)

⁷<https://www.sciencedirect.com.tudelft.idm.oclc.org/topics/engineering/system-spectral-efficiency>

⁸<https://www.sciencedirect.com/topics/engineering/quadrature-amplitude-modulation>

$$P_{REQ} = N_b R h c / \lambda \quad (5.8)$$

In equation 5.8, Planck's constant is $h = 6.626 * 10^{-34}$ [J - sec], speed of light is $c = 3 * 10^8$ [m/sec], (R) is the data rate [bit/sec] and (N_b) is the receiver sensitivity [photon/bit] taking account of modulation technique. For a 16-QAM modulation scheme, most literature used a threshold sensitivity value of 100 [photon/bit] or its equivalent -30 [dBmW] for required power calculations [28, 30]. However, Facebook is able to demonstrate an optimistic sensitivity value of 4 [photon/bit] for its ground station APD receivers in the HAPS-ground link. Therefore, an assumption is taken that such APD receivers are available in the commercial markets and the value will be used for the required power calculations. This will help in lowering the required power threshold and construct better link margins. However, further evaluation of this assumption for its verification and validity needs to be performed to check whether such a value is achievable in future detailed design stages with budget constraints and availability.

OSNR Calculation and Margin

The contribution of the noise is used to calculate the OSNR achieved before the signal enters the detector. This is given by dividing the received power (P_R) by the noise power (P_N) and is expressed in [dB] by equation 5.9 [27]:

$$OSNR[dB] = P_R[dBW] - P_N[dBW] \quad (5.9)$$

$$OSNR_{Threshold}[dB] = P_{REQ}[dBW] - P_N[dBW] \quad (5.10)$$

Similarly, equation 5.10 derives the threshold OSNR for the worst-case performance that would still establish the link. The link margin could now be derived for both the downlink and uplink budgets. This is done by taking the difference between the achieved OSNR and the threshold SNR as seen in equation 5.11. However, experiments discussed in subsection 5.1.2 point to a higher threshold OSNR to mitigate the risk of large losses of data due to higher BER when propagating through the atmosphere over large link distances. A threshold OSNR of 22 [dB] was presented in figure 5.2 for the 16-QAM modulation scheme for link ranges for HAPS communication. This would result in a BER of 10^{-3} which could then be corrected using FEC scheme. To mitigate this potential risk, the threshold OSNR having a higher value is selected and used to calculate the link margin. This adds redundancy to the budget by taking account of the receiver sensitivity due to noise with data losses due to BER. In subsection 5.1.3, it was showcased that 16-QAM modulation could be used for LEO bi-directional communication. However, a lack of experiments for determining BER means the threshold obtained in equation 5.10 will be used for link margin calculation. Finally, if the link margin is obtained to be more than 3 ([dB]), the requirement (ECN-F-BDG-1) is said to be satisfied.

$$LinkMargin[dB] = OSNR_{Achieved}[dB] - OSNR_{Threshold}[dB] \quad (5.11)$$

5.2.1. Budget for Uplink

For uplink, the transmitted power was updated to be 5 [W] for the optical telescope. Raising the transmitting power will exponentially increase the power consumed for generating the laser and will lead to power budget overruns in section 5.12. This would also increase the cost budget issues and overruns severely. The receiving aperture on the satellite is taken to be 20 [cm]. This is inspired by the receiving detector terminal of the OSIRIS LEO satellite to aid link performance and diminish the potential effects of scintillation [28, 31]. Such aperture values are also available for HAPS through commercial off-the-shelf components⁹. A full-angle full width at half maximum (FWHM) divergence

⁹<https://mynaric.com/products/hawk/>

angle of 15 [μrad] was deemed achievable with advancement in beam steering technologies and is consistent with a selected transmitting diameter of 15 [cm] using relations by Lambert [32]. Using the steps to obtain the OSNR, the uplink budgets for both the worst-case scenarios for HAPS and LEO are constructed. In addition, static losses discussed in subsection 5.2.3 are also included. It was decided not to construct the budget for the beacon since the beacon in itself would be a communication laser beam without high packaged data. The threshold power for uplink communication already accounts for value for those data rates and therefore the beacon is assumed to be taken into account with the uplink budget.

Table 5.2: Uplink Budget for worst case of communication with LEO.

Input Parameters			Link Budget			
Constants			Gains			
Altitude	5.00E+05	m	Tx Power	P_t	dBW	6.99
Elevation	30.0	deg	Tx "Antenna" gain	G_t	dB	109
Link Range (from altitude)	1.00E+06	m	Rx "Antenna" gain	G_r	dB	112
Slant Range	1.11E+06	m	EDFA Gain	G_a	dB	35.0
Wavelength	1.55E-06	m	Losses			
Planks constant	6.63E-34	J/s	Tx Loss	L_t	dB	-2.50
N_b	4.00	photons/bit	Tx Pointing loss	L_p	dB	-0.04
Data rate (R)	1.00E09	bit/s	Free-space loss	L_s	dB	-258
speed of light	3.00E+08	m/s	Atmospheric loss	L_a	dB	-10.0
Boltzmann Constant	1.38E-23	$\text{m}^2\text{kg}/\text{sec}^2\text{K}$	Rx Loss	L_r	dB	-7.40
Transmitter			Noise Figure EDFA	F_a	dB	-5.00
Tx Power	5	W	Static Losses			
Tx Pointing Accuracy	1.00E-06	rad	Cirrus Clouds	L_c	dB	-6.00
Tx Divergence Angle	1.50E-05	rad	Aerosol	L_{abs}	dB	-3.63
Receiver			Molecular	L_{mol}	dB	-0.40
Rx Aperture Diameter	0.20	m	Received Power	P_r	dBW	-65.5
Noise Inputs			Threshold power	P_{req}	dBW	-92.9
T_{noise} receiver	300	K	Noise Budget			
T_{noise} amplifier	627	K	Noise Power	P_n	dBW	-80.0
T_{noise} total	927	K	$OSNR_{achieved}$		dB	49.5
N_0 (spectral density)	1.28E-20	1/Hz	$OSNR_{threshold}$		dB	22.0
	-199	dB/Hz	$OSNR_{threshold}$ QAM		dB	22.0
Spectral Efficiency	4.00	bit/Hz	SNR Margin		dB	27.4
Noise Bandwidth	84.0	dB-Hz				

Table 5.3: Uplink Budget for worst case of communication with HAPS.

Input Parameters			Link Budget			
Constants			Gains			
Altitude	2.80E+04	m	Tx Power	P_t	dBW	6.99
Elevation	20.0	deg	Tx "Antenna" gain	G_t	dB	109
Link Range (from altitude)	8.19E+04	m	Rx "Antenna" gain	G_r	dB	112
Slant Range	1.11E+06	m	EDFA Gain	G_a	dB	35.0
Wavelength	1.55E-06	m	Losses			
Planks constant	6.63E-34	J/s	Tx Loss	L_t	dB	-2.50
N_b	4.00	photons/bit	Tx Pointing loss	L_p	dB	-3.86E-02
Data rate (R)	1.00E+11	bit/s	Free-space loss	L_s	dB	-236
speed of light	3.00E+08	m/s	Atmospheric loss	L_a	dB	-10.0
Boltzmann Constant	1.38E-23	m^2kg/sec^2K	Rx Loss	L_r	dB	-7.40
Transmitter			Noise Figure EDFA	F_a	dB	-5.00
Tx Power	5.00	W	Static Losses			
Tx Pointing Accuracy	1.00E-06	rad	Cirrus Clouds	L_c	dB	-6.00
Tx Divergence Angle	1.50E-05	rad	Aerosol	L_{abs}	dB	-3.63
Receiver			Molecular	L_{mol}	dB	-0.40
Rx Aperture Diameter	0.20	m	Received Power	P_r	dBW	-43.7
Noise Inputs			Threshold power	P_{req}	dBW	-72.9
T_{noise} receiver	300	K	Noise Budget			
T_{noise} amplifier	627	K	Noise Power	P_n	dBW	-60.0
T_{noise} total	927	K	$OSNR_{achieved}$		dB	51.2
N_0 (spectral density)	1.28E-20	1/Hz	$OSNR_{threshold}$		dB	22.0
	-199	dB/Hz	$OSNR_{threshold}$ QAM		dB	22.0
Spectral Efficiency	4.00	bit/Hz	SNR Margin		dB	29.2
Noise Bandwidth	104	dB-Hz				

From table 5.3. the worst case scenario for HAPS uplink well satisfies the requirements for a required link margin of 3 [dBW] (ECN-F-BDG-1), even with the worst case combined effects of static losses. The number of redundancies added ensures that a data rate of 100 [Gbps] would be sent to the HAPS. This holds also true for LEO uplink albeit with a reduced data rate of 1 [Gbps] to close the link margins and take account of high BER. Additional losses due to scintillation are discussed in subsection 5.2.5 but given the vast value of link margin, the budget is able to successfully the worst case of scintillation losses.

5.2.2. Budget for Downlink

For establishing a bidirectional link with HAPS/LEO, the node should be able to receive data from the satellite and therefore a downlink budget is constructed. The link performance indirectly depends on receiver aperture diameter through the receiver antenna gain as seen in equation 5.12 [32].

$$G_R = \left(\frac{\pi D_R}{\lambda} \right)^2 \quad (5.12)$$

Thus, such a budget considerably influences the aperture diameter to be selected for the gimbal and affects its sizing. Therefore, an aperture receiver diameter of 15 [cm] is selected with 30% redundancy to calculate the link performance. This impact is discussed in the detailed design of the telescope in section 5.3. Transmitter power of 5 [W] is chosen due to the availability of commercial components in the market for both HAPS and LEO^{10 11}. A full-angle FWHM divergence angle of 200 [μrad] is identified from OSIRIS v2 satellite [33]. A downlink budget table with static losses is constructed for both HAPS and LEO.

¹⁰<https://mynaric.com/products/space/>

¹¹<https://mynaric.com/products/hawk/>

Table 5.4: Downlink Budget for worst case of communication with LEO.

Input Parameters			Link Budget			
Constants			Gains			
Altitude	5.00E+05	m	Tx Power	P_t	dBW	6.99
Elevation	30.0	deg	Tx "Antenna" gain	G_t	dB	86.0
Link Range (from altitude)	1.00E+06	m	Rx "Antenna" gain	G_r	dB	109
Slant Range	1.11E+06	m	EDFA Gain	G_a	dB	35.0
Wavelength	1.55E-06	m	Losses			
Planks constant	6.63E-34	J/s	Tx Loss	L_t	dB	-2.50
N_b	4.00	photons/bit	Tx Pointing loss	L_p	dB	-2.17E-04
Data rate (R)	1.00E09	bit/s	Free-space loss	L_s	dB	-258
speed of light	3.00E+08	m/s	Atmospheric loss	L_a	dB	-10.0
Boltzmann Constant	1.38E-23	m^2kg/sec^2K	Rx Loss	L_r	dB	-7.40
Transmitter			Noise Figure EDFA	F_a	dB	-5.00
Tx Power	5.00	W	Static Losses			
Tx Pointing Accuracy	1.00E-06	rad	Cirrus Clouds	L_c	dB	-6.00
Tx Divergence Angle	2.00E-04	rad	Aerosol	L_{abs}	dB	-3.63
Receiver			Molecular	L_{mol}	dB	-0.40
Rx Aperture Diameter	0.15	m	Received Power	P_r	dBW	-90.4
Noise Inputs			Threshold power	P_{req}	dBW	-92.9
T_{noise} receiver	300	K	Noise Budget			
T_{noise} amplifier	627	K	Noise Power	P_n	dBW	-80.0
T_{noise} total	927	K	$OSNR_{achieved}$		dB	24.5
N_0 (spectral density)	1.28E-20	1/Hz	$OSNR_{threshold}$		dB	22.0
	-198	dB/Hz	$OSNR_{threshold}$ QAM		dB	22.0
Spectral Efficiency	4.00	bit/Hz	SNR Margin		dB	2.50
Noise Bandwidth	84.0	dB/Hz				

Table 5.5: Downlink Budget for worst case of communication with HAPS.

Input Parameters			Link Budget			
Constants			Gains			
Altitude	2.80E+04	m	Tx Power	P_t	dBW	6.99
Elevation	20.0	deg	Tx "Antenna" gain	G_t	dB	86.0
Link Range (from altitude)	8.19E+04	m	Rx "Antenna" gain	G_r	dB	109
Slant Range	1.11E+06	m	EDFA Gain	G_a	dB	35.0
Wavelength	1.55E-06	m	Losses			
Planks constant	6.63E-34	J/s	Tx Loss	L_t	dB	-2.50
N_b	4.00	photons/bit	Tx Pointing loss	L_p	dB	-2.17E-04
Data rate (R)	1.00E+11	bit/s	Free-space loss	L_s	dB	-236
speed of light	3.00E+08	m/s	Atmospheric loss	L_a	dB	-10.0
Boltzmann Constant	1.38E-23	m^2kg/sec^2K	Rx Loss	L_r	dB	-7.40
Transmitter			Noise Figure EDFA	F_a	dB	-5.00
Tx Power	5.00	W	Static Losses			
Tx Pointing Accuracy	1.00E-06	rad	Cirrus Clouds	L_c	dB	-6.00
Tx Divergence Angle	2.00E-04	rad	Aerosol	L_{abs}	dB	-3.63
Receiver			Molecular	L_{mol}	dB	-0.40
Rx Aperture Diameter	0.15	m	Received Power	P_r	dBW	-68.7
Noise Inputs			Threshold power	P_{req}	dBW	-72.9
T_{noise} receiver	300	K	Noise Budget			
T_{noise} amplifier	627	K	Noise Power	P_n	dBW	-60.0
T_{noise} total	927	K	$OSNR_{achieved}$		dB	26.3
N_0 (spectral density)	1.28 E-20	1/Hz	$OSNR_{threshold}$		dB	22.0
	-199	dB/Hz	$OSNR_{threshold}$ QAM		dB	22.0
Spectral Efficiency	4.00	bit/Hz	SNR Margin		dB	4.20
Noise Bandwidth	104	dB/Hz				

From table 5.5. the worst-case scenario for HAPS downlink is well within the requirements for a required link margin of 3 [dBW] (ECN-F-BDG-1), even with the worst-case combined effects of static losses. The number of redundancies added ensures that a data rate of 100 [Gbps] would be received to the node. However, for LEO downlink in table 5.4, the worst-case scenario fails the required link margin requirements marginally when these static losses are considered. However, it should be noted that the link could still work with the given margin for a data rate of 1 [Gbps]. The data rate is reduced in comparison to HAPS to obtain a positive margin but still complies with the requirements. It should also be considered that these static losses are for the worst conditions and are combined together as an additional redundancy. However, the chances of all of them affecting the link simultaneously in the worst of their respective conditions are highly unlikely. Thus, the link performance is alright in nominal conditions and the link margin requirement is satisfied 99% of the time. Additional losses due to scintillation are discussed in subsection 5.2.5.

5.2.3. Link Budget Static Losses

The static losses in the atmosphere affecting the link performance are due to cirrus clouds, scattering and absorption due to aerosols and molecular absorption. These are discussed below:

Cirrus cloud impact

The full clear sky condition is a rare case. Therefore, short-thickness Cirrus clouds impact has been included in the link-budget. Such clouds are globally distributed, covering 20-30% of Earth's surface, and are typically located at the high altitudes between 10 to 13 [km] [34], which is in the way to communicate with HAPS and LEO. Cirrus clouds contain ice crystals, which will create turbulence for the laser link, and have an effect on attenuation loss [35].

The attenuation effect of the Cirrus cloud depends on the optical thickness parameter [34]. Where the optical thickness of a light-absorbing medium is its geometrical thickness multiplied by the intensity attenuation coefficient. Where optical thickness of 1 implies the transmission power reduction by $1/e$, roughly 37%¹². It has been found that the average scattering distance for Cirrus clouds has an optical thickness (τ_{opt}) in the range of 0.92 to 2.77, for the FSO near-earth and space communications [34]. Consequently, the graph of attenuation loss and the optical thickness for this range has been provided in figure 5.7.

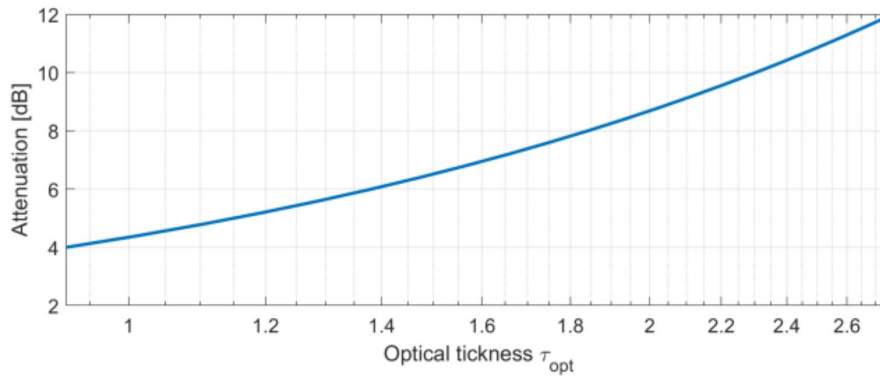


Figure 5.7: Attenuation loss due to Cirrus cloud with change in optical thickness [34]

$$\tau_{opt} = \frac{L_c}{d_{sca}} \quad [34] \quad (5.13)$$

However, to have a fixed attenuation value in the link budget, the mean optical thickness has been computed by using equation 5.13. Where L_c is the clouds physical length [34], which for Cirrus cloud

¹²https://www.rp-photonics.com/optical_thickness.html

average L_c is 1.46 km [36]. The d_{sca} is the average distance between two scattering events, which for Cirrus clouds is 1.08 [km] [34]. This means that the average Optical thickness value is 1.35, which corresponds to an attenuation loss of 6 [dBW] due to Cirrus cloud presence.

Aerosol Scattering/Absorption

Attenuation losses due to aerosol scattering and molecular absorption are altitude related. There are various attenuation coefficients (α), depending on altitude (h), for conversion of those coefficients into attenuation loss in dB, presented in equation 5.14. Finally, T is the total transmission fraction.

$$A[dB] = 10\log_{10}T \approx -4.343 \int_0^L \alpha(h)dz [8] \quad (5.14)$$

Aerosol contributes to the signal's scattering and absorption. Aerosol can be the space particles, ground particles or even created in the atmosphere from gaseous states [8]. Most influential aerosols are ground which affect at lower altitudes (1-2 [km]). Furthermore, in altitudes between 10-14 [km] aerosols from volcanic activities can be present which will have a significant effect on attenuation loss, as can be seen in figure 5.8.

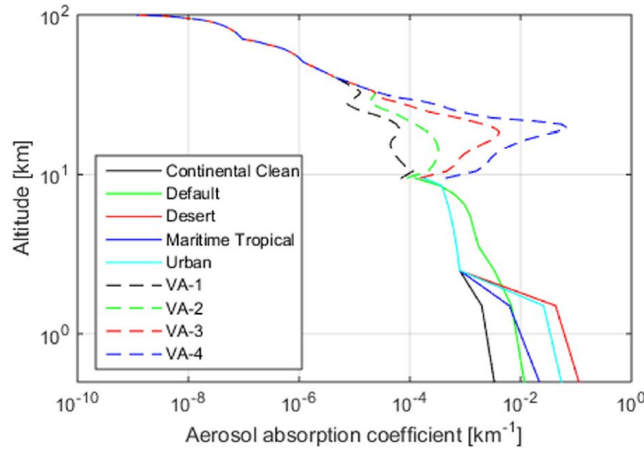


Figure 5.8: Aerosol attenuation coefficient depending on the altitude for the 1550 nm [8].

Considering that ECN has to provide emergency relief in disaster locations, the worst-case volcanic activity scenario (VA-4) has been selected. For redundancy, absorption due to volcanic dust was selected as 0.1 from 10-14 [km] based on the graph above. Also, the aerosol absorption coefficient of the desert has been selected for the link budget, where $\alpha = 0.1 [km]$, for the distance of 3 [km]. After the 30 [km] altitude, the aerosol influence was considered negligible. After adding up values, based on the graph and the equation 5.14, the attenuation loss was found to be 3.6 [dB]. The value was considered as static and was applied for both the LEO and the HAPS communication links.

Molecular Absorption

This type of attenuation loss is highly frequency-dependent, as can be seen from the figure 5.9. The molecular absorption effect is based on the molecule's ability to absorb photons at different energy levels. The most relevant molecules, for the 1550 [nm] wavelength are the H_2O and CO_2 [8]. From the figure 5.9, it can be seen that attenuation is almost negligible compared to other wavelengths. Therefore, a simulation tool Modtran has been used which can be seen in figure 5.10.

For redundancy worst-case tropical atmospheric model was used due to higher abundance of water molecules [8]. After performing the Modtran simulation, the Transmittance ratio at 1550 [nm] was found to be 0.913. To convert the value to decibels, the equation 5.14 was used which has resulted in -0.395 [dB] attenuation loss.

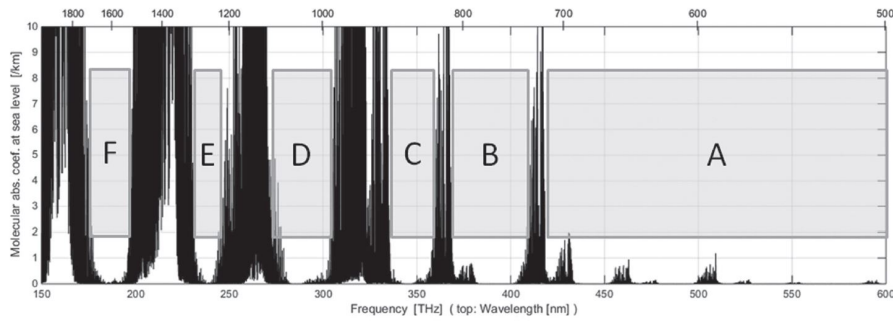


Figure 5.9: Molecular Absorption coefficient depending on the wave's frequency at the sea level [8].

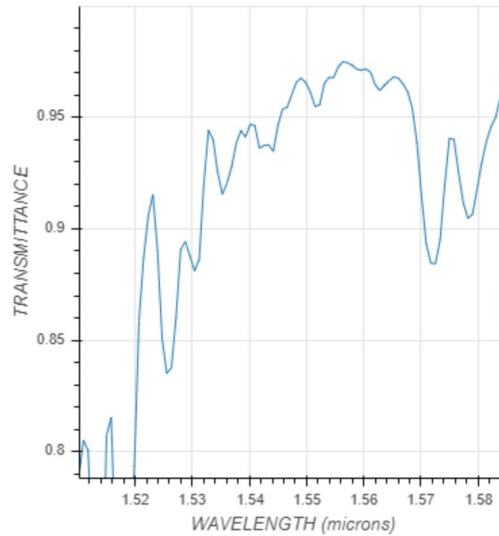


Figure 5.10: Molecular Transmittance depending on the wavelength for tropical atmosphere model at 25 [km] altitude [37].

5.2.4. Effects of Atmospheric Turbulence

Laser signal propagating through atmospheric turbulence develops temporal fluctuations in radiation intensity. The turbulence is caused by atmospheric refraction due to changes in air densities and temperature gradients of atmospheric layers. These effects of fluctuations of irradiance produce large transient dips in the laser signal and are, therefore, termed scintillation [28, 38]. The fading of the received signal is below the threshold margin could deter the overall link performance as seen in figure 5.11. Therefore atmospheric losses due to scintillation for downlink cases for LEO and HAPS are investigated.

Measuring Scintillation

A parameter for the strength of intensity fluctuations is normalised variance of intensity, called scintillation index (σ_I^2) [39]. According to weak fluctuation theory, σ_I^2 depends on the parameter Rytov variance (σ_R^2). It is an analytical measure for the integrated amount of turbulence along the link path, weighted with λ and is given by equation 5.15 [28, 39] :

$$\sigma_R^2 = 1.23 C_n^2 k^{7/6} L^{11/6} \quad (5.15)$$

Here, (L) [km] is the link communication range, ($k = \frac{2\pi}{\lambda}$) [m^{-1}] being the wave-number of the laser beam and (C_n^2) [$m^{-2/3}$] being the turbulence strength profile. Various literature provides different

¹³<https://spie.org/samples/PM99.pdf>

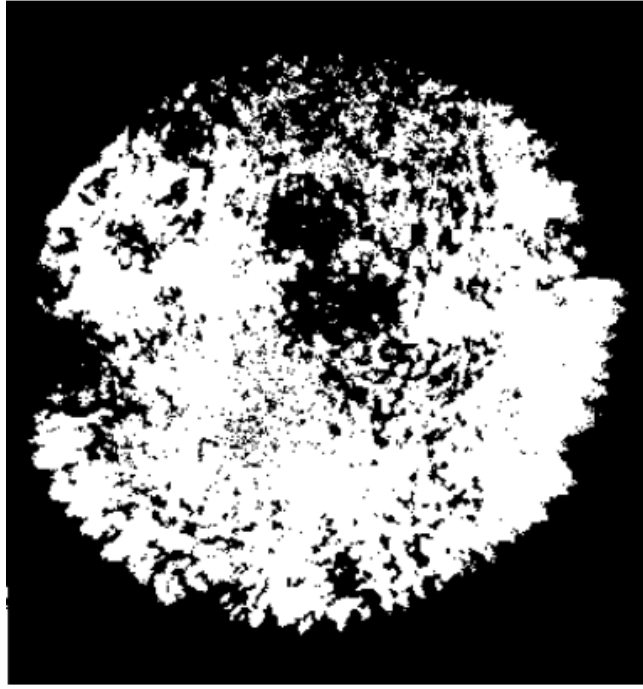


Figure 5.11: Signal Fades in Received Laser Beam due to Scintillation ¹³

estimation methods for describing C_n^2 profile models. However, for practical applications for space-ground communication, the Hufnagel-Valley Model (HV5/7) model is the most common model used for computational purposes. Here C_n^2 is modelled as a function of varying altitude with ranges from 10^{-13} to 10^{-17} [$m^{-2/3}$] [28, 38]. An assumption is made to select a constant value for simplicity with a value of 10^{-13} for strong turbulent profiles for redundancy. For the downlink, the ground-level scintillation near the receiver can be accurately modelled by a plane wave [28]. This adds additional redundancy since planar waves generally produce stronger scintillation than spherical waves [38].

As seen in figure 5.11, the fluctuations of high and low intensity due to scintillation lead to signal fades. These usually stand true for a point receiver. It is found that if the size of the receiver aperture is increased, the signal fluctuations over the aperture size tend to average out. It is called Aperture Sizing and for a normalised irradiance ($\langle I \rangle = 1$) the scintillation index for a planar wave depends on the receiver aperture (D_R) through equation 5.16 [28]:

$$\sigma_I^2(D_R) = \exp \left(\frac{0.49\sigma_R^2}{\left(1 + 0.65d^2 + 1.11\sigma_R^{\frac{12}{5}}\right)^{\frac{7}{6}}} + \frac{0.51\sigma_R^2 \left(1 + 0.69\sigma_R^{\frac{12}{5}}\right)^{-\frac{5}{6}}}{1 + 0.9d^2 + 0.62d^2\sigma_R^{\frac{12}{5}}} \right) - 1 \quad (5.16)$$

where parameter (d) depends on the link range (L) and is defined by:

$$d = \sqrt{\frac{kD_R^2}{4L}}$$

Probability Density Functions

Understanding optical radiation propagation through turbulence is extremely complex because of the complicated scenarios with which turbulence interacts. Therefore, most of the analysis for fluctuations is done stochastically through statistical theory for isotropic and homogeneous turbulence.

Detection and fade probabilities could be determined based on the tails of two probability distribution functions (PDF) discussed :

Log-Normal Distribution

Log-normal PDFs the most widely used model for scintillation modelling. However, it is applicable for weak turbulence regime and underestimates the behaviours in fade in experimental data. The PDF for computational purpose as a function of intensity (for poitive values of I) is given by equation 5.17 [38]:

$$p(I) = \frac{1}{I\sigma_I(d)\sqrt{2\pi}} \cdot \exp\left(-\frac{\left(\ln\left(\frac{I}{\langle I \rangle}\right) + \frac{1}{2}\sigma_I^2(D)\right)^2}{2\sigma_I^2(D)}\right) \quad (5.17)$$

Gamma-Gamma Distribution

Gamma-Gamma PDFs are a two-parameter distribution based on a doubly stochastic theory of scintillation. They are directly related to the atmospheric parameters of the turbulence conditions and are assumed to be valid for both weak and strong turbulence regimes. The Gamma-Gamma PDF can be given by equation 5.18 [28, 38]:

$$p(I) = \frac{2(\alpha\beta)^{\frac{\alpha+\beta}{2}}}{\Gamma(\alpha)\Gamma(\beta)} \cdot I^{\frac{\alpha+\beta}{2}-1} \cdot K_{\alpha-\beta}(2\sqrt{\alpha\beta I}) \quad (5.18)$$

Here, $K_{\alpha-\beta}$ is the modified Bessel function of second kind of order $(\alpha - \beta)$, $\Gamma(\alpha)$ and $\Gamma(\beta)$ are the gamma functions for parameters α and β , which are parameters directly related to atmospheric turbulence conditions and are given by equation 5.19 and equation 5.20 respectively:

$$\alpha = \left(\exp\left(\frac{0.49\sigma_R^2}{\left(1 + 0.65d^2 + 1.11\sigma_R^{\frac{12}{5}}\right)^{\frac{7}{6}}} \right) - 1 \right)^{-1} \quad (5.19)$$

$$\beta = \left(\exp\left(\frac{0.51\sigma_R^2 \left(1 + 0.69\sigma_R^{\frac{12}{5}}\right)^{-\frac{5}{6}}}{1 + 0.90d^2 + 0.62d^2\sigma_R^{\frac{12}{5}}} \right) - 1 \right)^{-1} \quad (5.20)$$

Numerical Model for Scintillation

A Python code was written to simulate a numerical model for the stated PDFs and derive attenuation losses based on fade statistics [3]. Firstly all the input parameters from the Link budget in section 5.2 are used. This includes an aperture receiver diameter of $D_R = 15$ [cm]. Then secondly, the Rytov variances and scintillation indexes through the aforementioned equations are computed for both the LEO and HAPS case using $C_n^2 = 10^{-13}$. Then for constructing the Log-normal and Gamma-Gamma PDFs, the inputs array for the average radiation intensity were taken to be random input arrays for a log-normal distribution, such that the mean intensity of the array $\langle I \rangle = 1$. This mean value was taken to simplify the inputs for the model for computational purposes. After obtaining the PDFs, their Cumulative Distributive Functions (CDFs) are computed and are plotted against the average intensity array[in dB]. They are showcased in figure 5.13 and figure 5.12:

The scintillation losses from the generated CDFs come from the assumption that a certain outage time is defined when during fading the received power in the budget falls below the threshold power and the link fails. This difference must be regarded as a loss in the link calculation. The value of this outage time directly flows from the requirement (ECN-F-SAR-2) where the link should be maintained

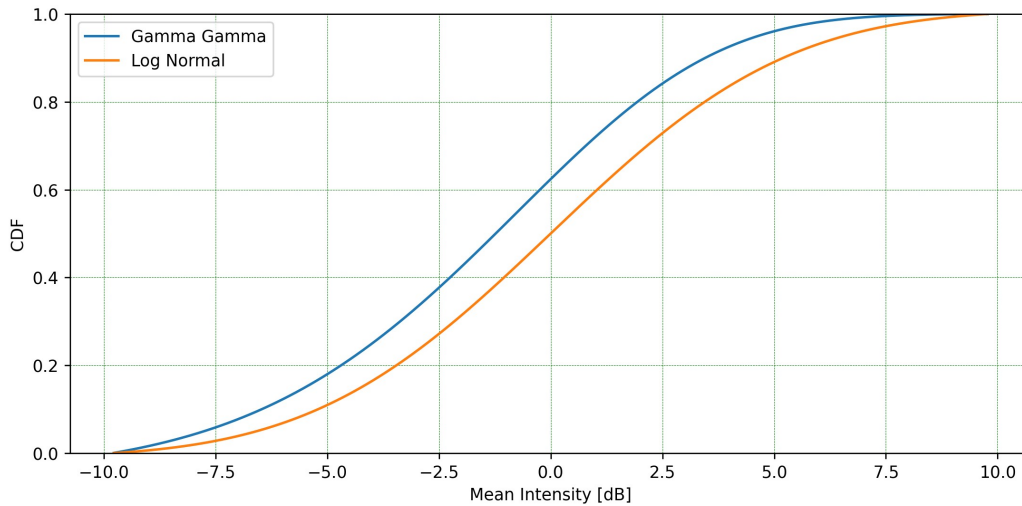


Figure 5.12: Fade level of cumulative distribution function for Gamma gamma and Log normal methods for Low earth orbit satellites

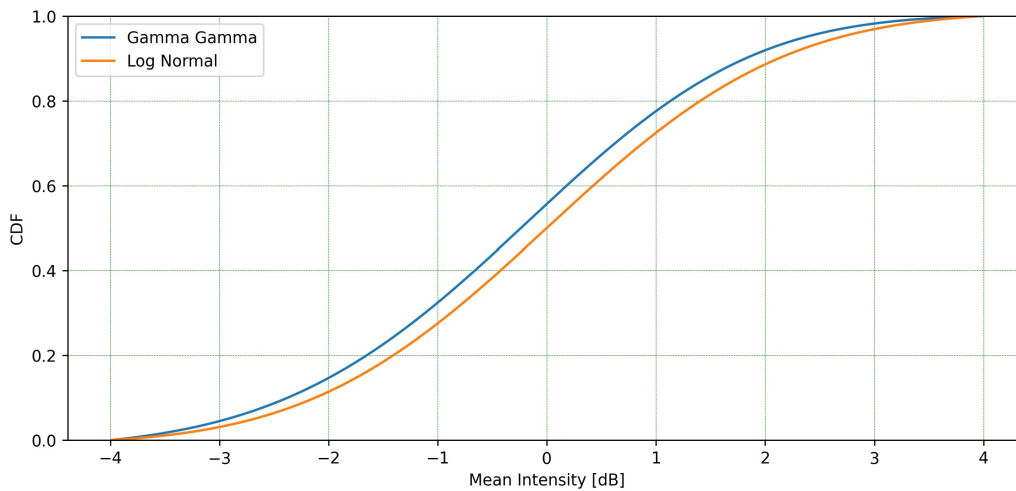


Figure 5.13: Fade level of cumulative distribution function for Gamma gamma and Log normal methods for High Altitude Platform Stations

99% of the time. Thus setting a threshold of 0.01 for both the generated CDFs results in scintillation losses in [dB] in table 5.6 :

Table 5.6: Scintillation Losses for 1% Threshold of outage time

CDF Distribution	Loss for HAPS [in dB]	Loss for LEO [in dB]
Log-Normal	-3.5	-8.6
Gamma-Gamma	-3.9	-9.3

Verification of Numerical Scintillation Model

The numerical model constructed is verified using both code verification and calculation verification. The code verification is performed on the written Python code by adapting various unit tests to check the individual functions for coding bugs and errors. These tests consisted of checking the units and syntax of input parameters, Rytov variance (σ_R), scintillation index (σ_I), Gamma-Gamma and Log-normal CDF plot generation, and identification of 0.01 threshold value. Several functions were found to have unit errors and thus were corrected due to the tests. Calculation verification was performed by testing the functions on Excel and was found to be within 5% margin difference [3].

The model is also verified with other simulation models presented in the literature.

Firstly, the values of obtained for Rytov variance (σ_R) and Scintillation index (σ_I) are verified against each other by being compared to a similar simulation model in figure 5.14b for a link length of 20 [km]. The results and differences are discussed in table 5.7 and are acceptable by being less than 5%:

Table 5.7: Rytov Variance v/s Scintillation Verification

Parameter	Gamma-Gamma PDF	Reference	$\Delta\%$ Gamma gamma
σ_I	0.1911	0.2	4.45
σ_R	0.2334	0.23	1.47826087

Secondly, the parameters α and β in the Gamma-gamma PDF model were functions of the Rytov variance (σ_R). The values are verified against each other by being compared to the graph plotted in figure 5.14c for a similar simulation study for a strong turbulence regime and all the values are within 12% margin of difference. This significant variation could be attributed to a different range of turbulent profiles (C_n^2) in the strong regime and the variations in the diameter and wavelength used. They are showcased in table 5.8 below:

Table 5.8: Rytov Variance v/s α and β Verification

Case	σ_R^2 value	Numerical model		Simulation		Difference in %	
		α	β	α	β	α	β
HAPS	0.202	13.73	11.3	13	10.2	5.615384615	10.78431373
LEO	0.96	4.01	2.19	4.2	2.5	4.523809524	12.4

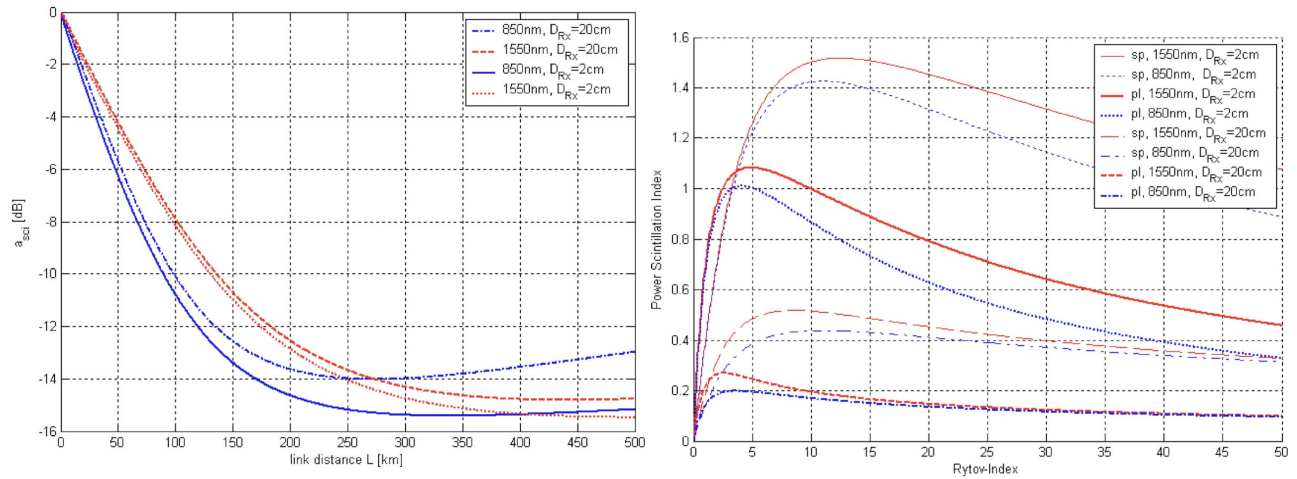
Lastly, the scintillation losses obtained for a link distance of 500 [km] were compared to figure 5.14a for $D_R = 20$ [cm] for a weak turbulence regime ($C_n^2 = 10^{-17}$) with an outage time of 99.9%. However, the model failed to compute the Gamma-Gamma PDF and it is observed that the model fails to compute values for lower turbulence regimes.

Scintillation Numerical Model Evaluation and Discussion

The scintillation numerical model constructed is limited to functioning only in higher turbulence regimes (till= $C_n^2 = 10^{-13}$). This is because for weaker turbulence regimes (i.e. C_n^2 less than 10^{-15} [$m^{-\frac{2}{3}}$]), the Gamma-Gamma PDF shows a computing error for HAPS by reaching extremely high values. The same occurs at a C_n^2 value less than 10^{-17} [$m^{-\frac{2}{3}}$] for LEO satellites. For the case of LEO with a $C_n^2 = 10^{-17}$, the Rytov variance is 0.0001 with α and β being more than 10,000. This renders the value of both the numerator and the denominator in equation 5.18 as infinity. The Value of the Bessel function in the same equation goes to a value below 10^{-300} and is thus rendered as 0 by python. So the equation takes the form of $\frac{\infty}{\infty} \cdot 0$ which generates an overflow error in python. A similar behavior is observed with a C_n^2 of 10^{-15} [$m^{-\frac{2}{3}}$] in the HAPS model.

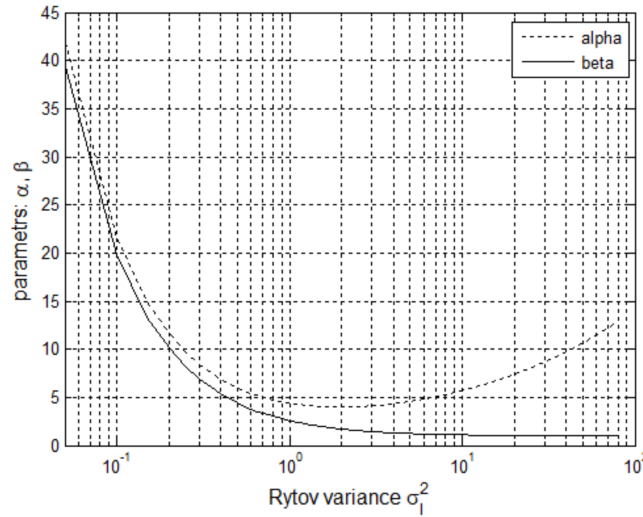
Future Recommendations

It is recommended that the model be adjusted to work for Gamma-Gamma distribution for lower turbulence regimes (i.e. C_n^2 less than 10^{-13} [$m^{-\frac{2}{3}}$]). Additionally, the scintillation effects could be investigated and a model could be constructed for uplink communication. However, this is beyond the scope of the present project phase due to complicated nature for applying spherical wavefront with tip-tilt corrections. Furthermore literature and experiments could be reviewed to compare and aid in verification and validation of the expanded model for Log-normal PDFs.



(a) Scintillation loss a_{sci} depending on link distance L assuming a spherical wave, with the Rx aperture D_{Rx} (2 or 20 cm) and the wavelength of 850 and 1550 [nm] as parameters. Here the IRT strength is given by $10^{-17} [m^{-\frac{2}{3}}]$, as is suitable for strong IRT for altitudes higher than 2000 [m]. The fraction of outage time is rather small with p_{thr} 0.001 [39]

(b) Examples of power scintillation index versus Rytov index for Kolmogorov spectrum with no inner- and outer-scale bounds for spherical (sp) and plane (pl) waves, two different wavelengths, and apertures with a link length of 20 [km] [39]



(c) Values of α and β under different turbulence regimes, viz., weak, moderate to strong and saturation. [40]

Figure 5.14: Literature Simulation used for Verification.

5.2.5. Link Budget Evaluation and Discussion

Verification

Excel was used to do the link budget calculations for the given parameters and inputs and to construct the budget tables. Analytical calculations were employed to verify the verification of functions for received power, noise power, required power and OSNR. The differences were found to be within 5% and the calculations were deemed correct. Additionally, the link budget was constructed with a similar approach utilised by Facebook [9]. Therefore the values used by Facebook were input into the link budget and the results were within 5% of the Facebook results. Sensitivity analysis of link budget impact on aperture, change in power and the overall system is discussed in chapter 6.

Design Implications

During the construction of the link budget, close attention was paid to the aperture diameter for the downlink. The chosen gimbal concept of EVE from the midterm report [2], had included a focusing

lens in the design. It is explained in section 5.3, that the costs of such lens was increasing substantially if the aperture diameter was increased more than 15 [cm]. Considering that it was undesirable to change the gimbal design, the aperture diameter for the downlink communication was not exceeding 15 [cm]. However, parallel to the link budget construction, in case of link budget complications, the backup options of coelostat and observatory design were considered allowing larger aperture diameters. More information about aperture sizing is given in section 5.3.

Impact of Scintillation in Link Budget

The scintillation attenuation losses summarised in table 5.6 take account of the strong turbulence regimes if encountered. The losses are for the downlink scenario and if added to the budget, the link margin requirements for both the HAPS and LEO are not met (ECN-F-BDG-1). However, it should be noted that these losses are for strong turbulent regimes which are very rarely seen phenomena. In addition, these losses are applied to the budget in combination with all the worst-case performance of static losses. It can be inferred that such a worst-case scenario for all losses to occur simultaneously is implausible. Thus the downlink budget would work in nominal conditions for weak turbulence, however, it would need to adjust the model to obtain the losses. In case the link performance is affected, data rates could always be reduced to improve the margins.

Future Recommendations

The numerical model for scintillation could be adjusted to accommodate weaker turbulence regimes and expanded for the uplink budgets. The losses derived from these could be added to the budget and analysed. If the link margin fails then ranges till which the margin is maintained could be obtained. Moreover, the transmit power (P_T) could be reduced to 3 [W] instead of the current value of 5 [W] due to the significant margin for uplink for both HAPS and LEO^{14 15}. This would reduce the cost of the EDFA used by 40% without comprising significant redundancy. The overall reduction in the total cost budget would decrease by 1.8%. Furthermore, 5% of the receiving power could be used by the Fine-tracking camera to improve the control-loop feedback. This is further explained in subsection 5.5.1 and could be visualised in figure 5.21. This reduction in power could be further implemented and analysed in the link budget. Additional models for static losses like clouds and rains could be investigated. The budget could also be verified with additional literature and experimental tests and validated for the optimistic values of the receiver.

5.3. Telescope Gimbal Design

It was found that the required aperture diameter is significantly larger than the size initially reckoned. The original EVE design chosen in the midterm used an aperture of 7.5 [cm] with a refractive lens having a focal ratio of about 4 but the link budget reasonably allowed for a minimum of 15 [cm] [41]. This means that the choices made during the midterm have to be reconsidered which will be done in this section. For this, a scaled-up version of the originally chosen EVE design is proposed in addition to two backup options.

5.3.1. Scaled EVE Design

The design of a telescope is scalable if the focal length of the lens can be kept similar for larger diameters. However, EVE uses a refractive telescope lens and one of the main disadvantages is that manufacturing becomes significantly more expensive above diameters of 15cm [42, 43]. Commercial refractive telescopes with high aperture sizes and short focal lengths do exist such as the Skywatcher AC 150/750¹⁶ which has a 21 [cm] refractive lens at its aperture and a focal ratio of 5. The question becomes whether refractive lenses for laser communication are affordable and producible at this size.

¹⁴[https://www.civillaser.com/index.php?main_page=product_info&products_id=\\$1636](https://www.civillaser.com/index.php?main_page=product_info&products_id=$1636)

¹⁵https://www.civillaser.com/index.php?main_page=product_info&products_id=2962

¹⁶<https://www.astromarket.org/telescopen/skywatcher-telescoop-ac-150-750-startravel-150-eq5/p,20300>

EdmundOptics has been enquired for pricing on 20 [cm] diameter lenses with 1550 [nm] coating at these focal lengths and gave a cost of €2400 without coating and €4000 with coating. Assuming a similar relative price increase for a 15 [cm] lens gives a cost of about €2000¹⁷. This is still deemed reasonable considering that professional telescopes cost in the order of €5000¹⁸. From figure 5.15 it is derived that two mirrors are required to bend the laser towards another two-mirror coude path which bends the laser through the base of the gimbal. Additionally, two direct drive motors are required with an appropriate hole size in the middle. In table 5.9 an overview of these components

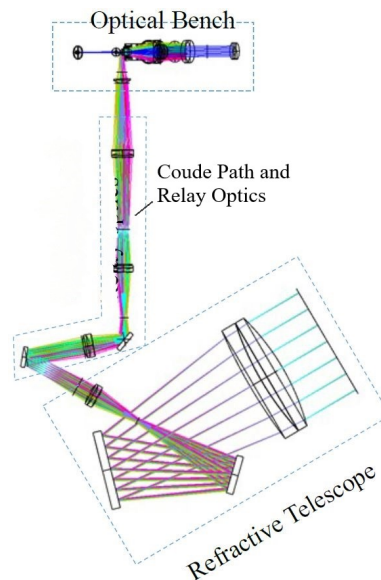


Figure 5.15: EVE optical path layout [41]

and an estimated cost can be found. It can be seen that the total cost is estimated just above €10,000 which is significantly less than the commercial gimbals found such as the Planewave 350-direct-mount which already costs more than €11,000 without the telescope¹⁹. A significant disadvantage

Table 5.9: Estimated cost breakdown for EVE gimbal

Component	Cost
Coated 15cm Lens	€2000
8cm mirror	€674 ²⁰
4cm mirror	€400 ²¹
Coude path	€500 ²²
2x 25cm diameter direct drive motor	2x €910 ²³
Casing and mounting	€5000
Total cost:	€10,394

is that the scaled version of the EVE would have to be developed and produced instead of being bought. But there are many advantages to the EVE design as identified during the midterm. For example, to bend the laser into this Coude path it would be required for the telescope to have a Nasmyth setup as shown in figure 5.16 for which no off-the-shelf telescopes have been found at this aperture size. Consequently, an addition of a third mirror would have to be added to an already

¹⁷<https://www.edmundoptics.eu/f/large-precision-achromatic-lenses/11679/>

¹⁸<https://www.astromarket.org/telescop/en/celestroon-maksutov-telescoop-mc-180-2700-cgx-700-goto/p,61736>

¹⁹<https://planewave.com/product/1-350-direct-drive-mount/>

existing telescope. Moreover, most commercial telescopes are not specifically made for use in the IR range which is most exemplified in the coating, especially at the considered sizes. To gain the best performance telescope mirrors with either gold or silver coating are required which is not used on any commercial telescopes found at this aperture size. The smallest one was the Planewave IRDK14 with a diameter of 35 [cm]²⁴. The commercial telescopes mostly use aluminium coating which has a reflectance of 93% compared to the 98% of gold coating at the 1550 [nm] range²⁵. Using the EVE design the coating can be chosen during the design allowing for optimisation of the receiving path. If these coatings are to be used in a telescope set up they would have to be custom-made at this aperture size. Finally, the compact design means a small volume is extended outside of the housing which is beneficial for environmental protection and the lesser amount of similar components used makes the design overall more sustainable.

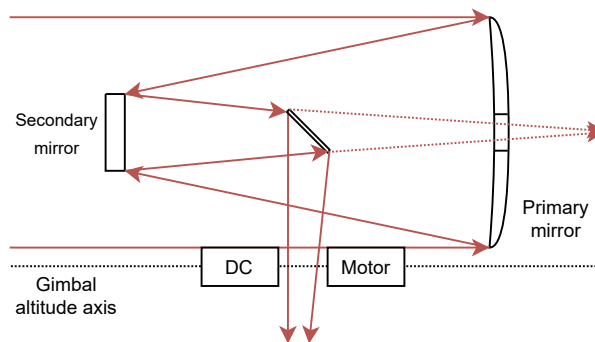


Figure 5.16: Nasmyth telescope setup

Considering the above reasons, the scaled-up EVE gimbal will be considered during the rest of the design while taking into consideration the risk of not being able to develop it. To counter this risk backup solutions are considered which will be explained in the next sections.

5.3.2. Scaled Coelostat Design

To keep the advantage of having limited volume outside of the housing a solution is investigated which uses a 90° version of EVE bending the light towards an internally stored reflective telescope using two mirrors as shown in figure 5.17. This type of gimbal is also referred to as a coelostat and would have to be a scaled design of an existing one shown in figure 5.18 [44].

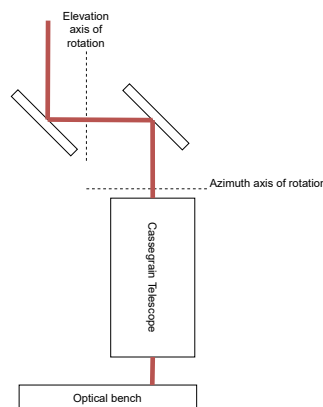


Figure 5.17: Proposed coelostat gimbal

²⁴<https://planewave.com/product/irdk14-infrared-optimized/>

²⁵<https://www.edmundoptics.eu/knowledge-center/application-notes/optics/metallic-mirror-coatings/>

Something to consider when using a reflective telescope is the size. Compact telescopes use a Cassegrain setup which bends the light 180° into a second mirror to reduce the required tube length. A disadvantage of this is that part of the telescope aperture is blocked, for most Cassegrain telescopes the secondary mirror is in the order of 20 – 30% of the aperture diameter. This means that the 15 [cm] aperture would have to increase to $16 \frac{16}{\cos(45^\circ)} = 22$ [cm]. To bend the light at two 45° angles one then needs two

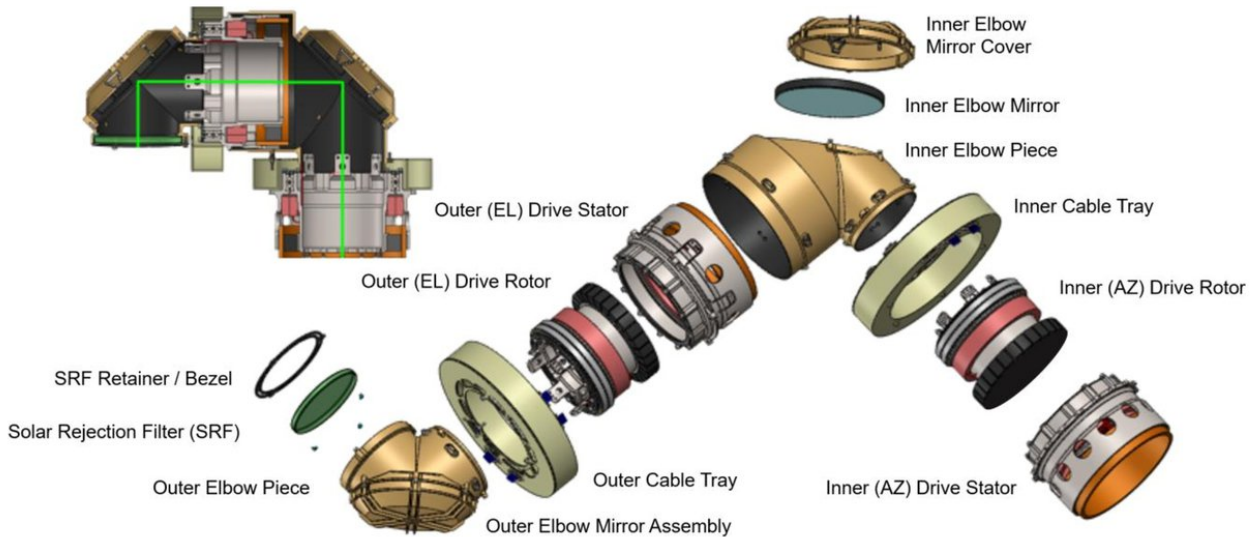


Figure 5.18: Components of the coelostat gimbal developed by Facebook [44]

played in table 5.10. A major consideration would be the requirement of having a direct drive motor with an inner diameter of at least 17 [cm] and the requirement of high diameter mirrors which gets very expensive. The fact that the very sensitive and brittle mirrors now make up more than half of the cost makes this gimbal system unideal. Additionally, the cost of a high-performance telescope and gimbal is very similar at these aperture sizes. It was decided that these reasons outweigh the main advantages which are that no Nasmyth modification is required and that the telescope is protected inside the housing.

Table 5.10: Component list coelostat gimbal

Component	Cost
2x 30cm diameter Direct drive motor	2x€2000 ²⁶
2x 24cm diameter flat mirror	2x€4980 ²⁷
Elbow tubes, casing and mirror mounts	€5000
1x Solar rejection filter (SRF)	€315 ²⁸
Total cost:	€19,295

5.3.3. Observatory Design

If EVE proves unfeasible a final option is the use of an observatory dome such as the 7 [ft] Astro-Haven shown in figure 5.19 with the telescope and gimbal mounted in the middle. A significant disadvantage of this is the bulkiness of using such a dome which for a rugged system will exceed the container size limit of 2.38 [m]. Other, smaller domes have been found in the order of 2 [m] such as the Scopedome 2M however the sturdiness of these in harsh conditions has been doubted due to the small thicknesses and limited supports²⁹. A sturdy observatory such as the Astrohaven excluding

²⁹https://www.scopedome.com/wp-content/uploads/2020/09/ScopeDome_2M_Manual_ver_1_0_EN.pdf

the telescope and gimbal system will cost in the order of €22,000 which is already more than both the coelostat gimbal and EVE design³⁰. This would mean completely off-the-shelf components could be used but the additional costs and transportation issues make it so the scaled EVE design is preferred.

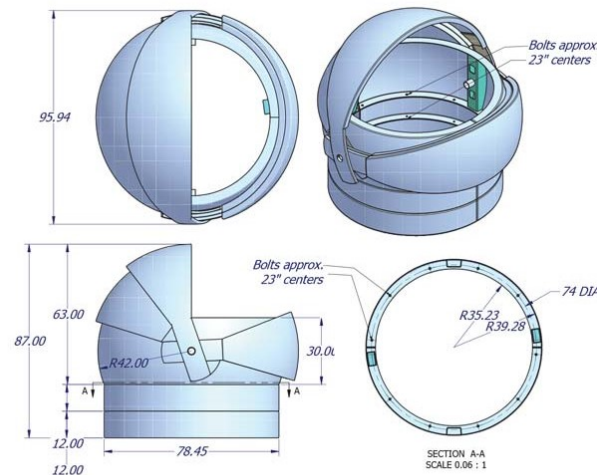


Figure 5.19: Astrohaven observatory technical drawing³¹

5.3.4. EVE Development Plan

Since the development of a telescope design is complex and requires the use of extensive optomechanical and optical considerations it is deemed out of scope for this design. However, in this section, a plan to develop such a system is laid out and recommendations are given. In figure 5.20 the estimated dimensions of the scaled design can be found based on the original layout of EVE. It can be seen that it includes an additional section to mount the tracking camera chosen in subsection 5.5.3. Since the design must be developed it is expected that the target slew rate from ECN-F-PRF-7-3 of $10^\circ/s$ can be met. Other gimbal systems such as the Planewave L-350 can achieve slew rates up to $50^\circ/s$ and is in line with other devices such as the gimbal developed by Facebook which can achieve slew rates of $10^\circ/s$ [44]. This will be a main driver of the design.

Initial Optical Design

To develop the telescope one should start by scaling up the outer dimensions of the current EVE design to find out the location of the different optical mirrors and components. This must be fine-tuned based on the exact focal length provided in the lens by the manufacturer. When this is known software such as OpticsStudio from Zemax³² can be used to model the laser path and assure the angled components and the light beams reach the base of the gimbal.

Motor Sizing

Once the optical path is set an initial estimation can be made on the required direct drive motor to rotate the upper part of the gimbal. Of special consideration is the exact diameter of the hole required in the motor such that the laser can still travel through however, considering the beam size in figure 5.15 this is not expected to become a significant issue. At this point, the expected gimballed mass must be considered to find a motor with the required power and size

³⁰<https://skygazeoptics.com/products/astro-haven-7-ft-dome-wl-ih-e-relaybg-p-d-1ph-nord-abb-0-25-0-5>

³¹<https://astrohaven.com/products/7-foot-domes/>

³²<https://www.zemax.com/pages/opticstudio>

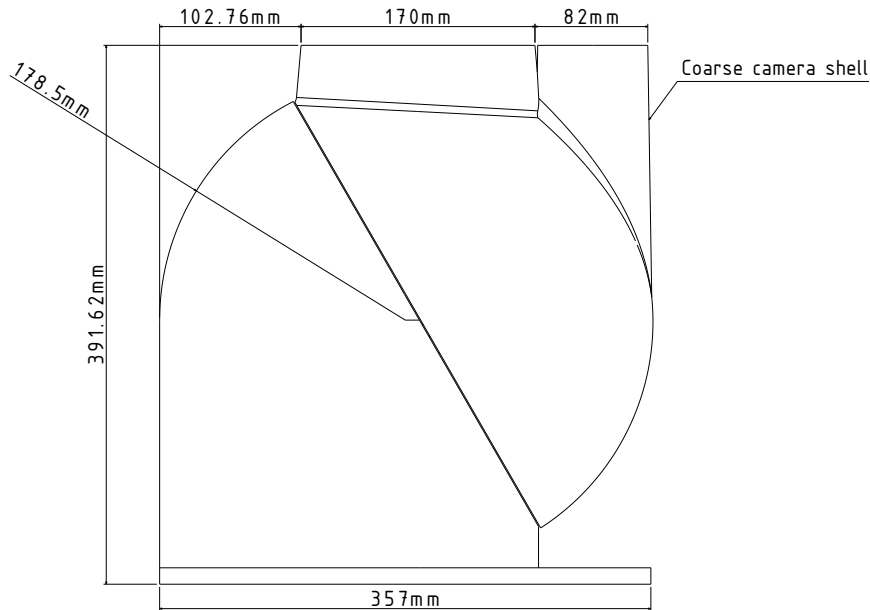


Figure 5.20: Layout and dimensions of the scaled EVE design

Housing and Mounting

At the same time, a structure can be developed enveloping all the optics and motors. This would also include mounting of the mirrors to the housing. For this special attention must be paid to optomechanics to make sure the deformations of the structure do not influence the pointing accuracy to unacceptable extents. This means that the main considerations for material choices will be to prevent strains as much as possible [45]. Mounting materials will have to be chosen which have high stiffness, and very low thermal expansion and to avoid flexure under its own weight, a low-density [45]. The mountings should also be able to withstand vibrations and special care should be taken in the interfacing of the mounting with the housing if different materials are used due to the discrepancy in coefficient of thermal expansion [44]. A choice should also be made about the material of the mirror and its coating, once again taking special consideration to the optomechanical consequences of each choice. Finally, the housing, motors and mirrors would have to be connected. The wiring for both the camera and the motors should also be considered at this point, especially the potential issues due to their rotation [44]. During this process, some iterations would be required mainly due to possible changes in the optical path, performance requirements or optimisations of the housing. During the design at this point thermal and structural models will have to be made both for survivability and the influence their deformation will have on the gimbal performance. Using the Zemax software the optical performance criteria such as the total wavefront error can be assessed to find out the exact performance of the gimbal.

Prototyping

After an initial design is made it should be prototyped for testing. With this prototype, the thermal, structural and optical models can be fully validated and real-life performance testing can be done. The results of this analysis can then also be used to improve the models for further use [44]. It should be tested that the motors are able to provide sufficient torque for the slew rates required. Additionally, since the node will be used in harsh conditions specific scenarios such as extreme heat, cold and earthquake scenarios should be tested to assure structural performance. This entire process must then be iterated to converge to a final gimbal design which can be used in the node.

5.3.5. Sustainability

One of the advantages of developing this gimbal is that sustainability can be taken into consideration while designing the gimbal system. For example, the initial EVE design used a carbon casing mainly for its lightweight properties but since weight is less important for the ECN application other materials can be considered which are more sustainable. Additionally, the compactness of the gimbal means that fewer components and smaller components are required. Having to buy bulky observatories, gimbal and telescope systems would require significantly more material and is thus expected to add more emissions. The small factor also makes sure the ECN can be transported in conventional transportation which is beneficial for sustainability as discussed in chapter 4.

5.3.6. Big Aperture Telescope Issues

As discussed in subsection 5.2.5 there are parts of the link budget which may not work out in reality as currently calculated. Consequently, it is possible the aperture diameter might rise to higher levels than currently anticipated which can cause issues.

Cost of Large Aperture Telescopes

Firstly, the cost of a telescope is highly dependent on the size of the aperture. In table 5.11 an overview of different Planewave telescopes with their prices and mass can be found. At €14,406 the current cost budget of the entire gimbal and telescope system with EVE is already exceeded. At higher apertures of 40 [cm] it starts comprising about one-fourth of the total budget and at apertures higher than 60 [cm] the costs increase to such extent that reaching the budget limit becomes impossible.

Table 5.11: Telescope costs and mass for different aperture sizes

Aperture diameter [cm]	Cost	Mass	Telescope
35	€14,406	22	Planewave IRDK14 ³³
40	€24,970	48	Planewave IRDK17 ³⁴
50	€31,213	63.5	Planewave IRDK20 ³⁵
60	€56,681	108.9	Planewave CDK600 (excluding gimbal) ³⁶
70	€148,936	151	Planewave CDK700 (excluding gimbal) ³⁷
100	€461,116	199	Planewave CDK1000 (excluding gimbal) ³⁸

Structural Considerations

The comparison also shows that the mass of the telescopes starts rising quite significantly, adding concern about structural considerations, at these higher weights the gimbal must become more sturdy increasing cost and the weight even further. For the Planewave gimbals cost increases by about €10,000 for every 45 [kg] which is 10% of the budget.

Nasmyth Addition

As discussed before, commercial Nasmyth telescopes have not been found widely available. This means either a commercial telescope would have to be adapted or a custom one would have to be ordered. The same goes for the gimbal system which must allow the inclusion of a Coude path going to the base of the gimbal.

5.3.7. Higher Aperture Contingency Plans

Considering the above reasons multiple contingency plans have been developed for different aperture sizes based on the expected issues with cost and mass.

Required Aperture Size (less than 20 [cm])

At these aperture sizes, it was established that a scaled EVE design is possible and would be considered. If this is found to not be possible the observatory system with a commercial telescope and

gimbal must be used. No budget problems are expected and the mass is sufficiently small that structural considerations are limited.

Required Aperture Size (between 20 and 30 [cm])

At these aperture sizes, EVE is most definitely becoming infeasible, requiring the need for the observatory system. No cost and structural problems are expected.

Required aperture size between 30 and 40 [cm]

The cost budget is expected to be met. The mass of the telescope is estimated at around 22 [kg] which means relatively small gimbals can be used in combination with the observatory system.

Required Aperture Size(between 40 and 60 [cm])

The cost budget will almost definitely be exceeded. Negotiations will have to be done with the customer for a cost budget increase or the requirements will have to be lowered. Large gimbals in the order of €20000 will be required³⁹. When the telescope is inoperative or being transported, a support structure for protection is desirable and should be investigated.

Required Aperture Size (more than 60 [cm])

At this point, the cost budget will be severely exceeded (orders of 100-500%) and the telescope will weigh in the range of 130-200 [kg]. At these sizes, the size of the telescope will cause issues in transportation (no crate possible due to observatory size) and a structurally sound gimbal is required. If this is caused by the LEO requirement, the design is changed to such an extent that it is deemed justifiable to drop the requirement or lower the data rate to more reasonable data rates. Similarly, for the 100[Gbps] HAPS requirement, it might be more valuable to drop the required data rate in conjunction with the customer as it would reduce the cost and structural requirements significantly.

5.4. Optical Bench

The optical bench is the part of the system after the telescope in which the laser beam performs its receiving and transmission functions. During transmission and receiving the laser must go through multiple phases to be sent through free space. In figure 5.21 an overview of the required path can be found, separating the optical bench into multiple phases.

Transceiver

First, the to-be-sent data has to be modulated in the 16-QAM format which is done in the transceiver. One of the main advantages of choosing coherent detection is that data rates in the orders of 100 [Gbps] can be sent in one data channel as opposed to more commonly used techniques for achieving such high data rates like multiplexing [9, 46]. Multiplexing is a method in which multiple, individually modulated laser signals get combined into one laser, isolating them with for example wavelength or orthogonal isolation [47]. A significant disadvantage of this is that for each channel a separate laser, modulator and demodulator are required, greatly increasing the required number of components and complexity. Because of this, it makes no sense to use 16-QAM with multiplexing, thus using a single transceiver will be the chosen option. An example transceiver that can transmit and receive 100 [Gbps] simultaneously, modulated with 16-QAM modulation is the CFP2-DCO-200g coherent transceiver⁴⁰ which has the best OSNR found of 11 [dB]. However, due to the significant research and improvements in fibre communication, this option will have to be reconsidered in the further design phase, where transceivers with lower OSNR are expected to be available, increasing performance [9]. The transceiver then outputs a fibre cable towards the EDFA where the signal gets amplified so it can be sent through free space.

³⁹<https://planewave.com/product/1-500-direct-drive-mount/>

⁴⁰<https://www.fibermall.com/sale-459142-cfp2-dco-200g-coherent-transceiver.htm>

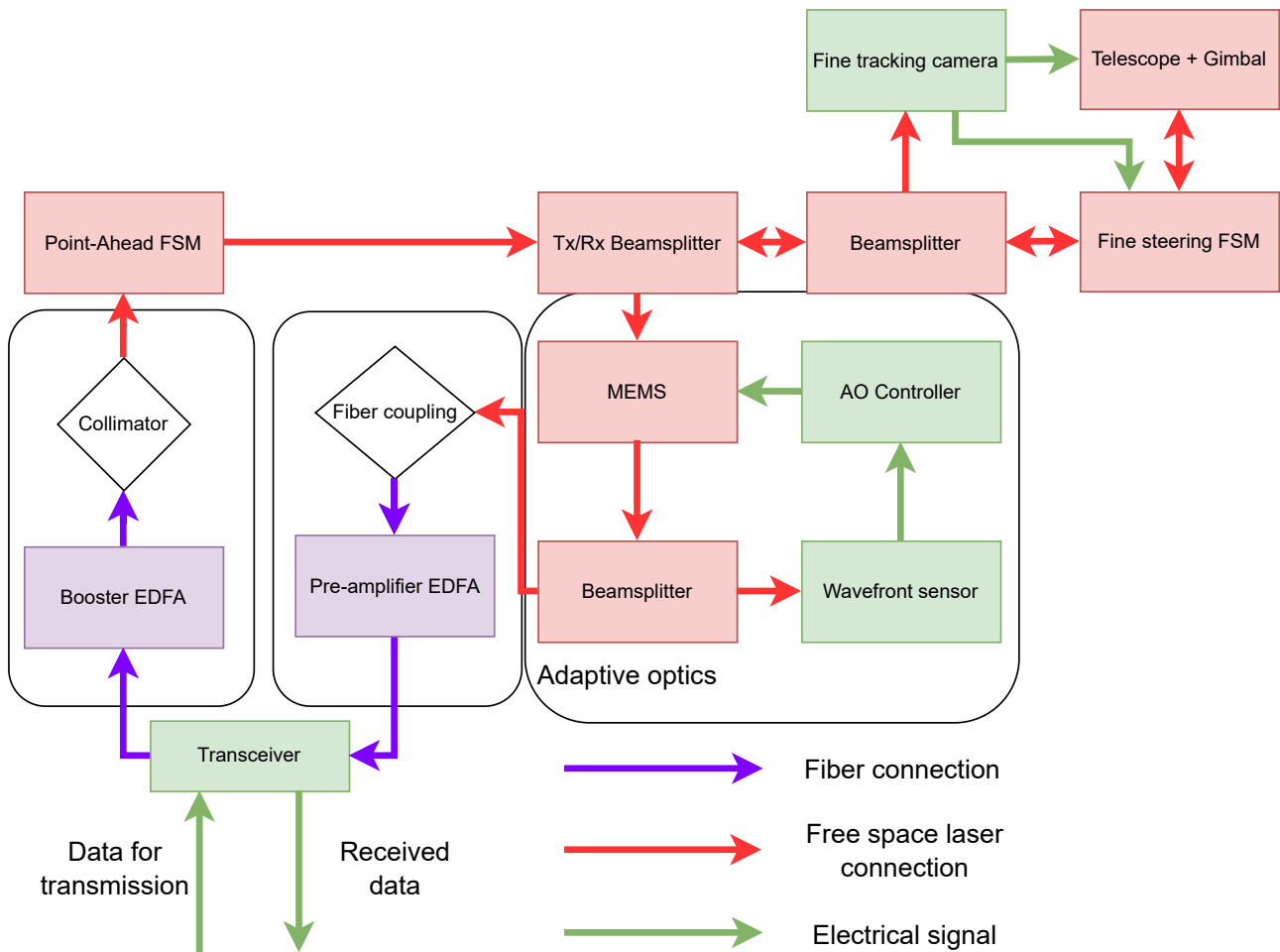


Figure 5.21: Optical bench components and their connection

EDFA

It was found during the midterm trade-off that to gain a high power output of the laser a booster amplifier is required for which an EDFA was chosen [2]. Multiple EDFAs are available for this purpose with similar price and performance parameters. Consequently, the one with the best form factor was chosen which is the Civillaser EYDFA-HP-C-BA-37-Sm⁴¹. This EDFA has a noise level of 5 [dB] as required for the link budget. The EDFA will receive a fibre input from the receiver and have a fibre output which has to be collimated for use in free space.

Collimator

To go from the EDFA fibre output to a free-space signal it is required to collimate the fibre. Two types of collimators have been found; refractive and reflective collimators. Refractive collimators use a lens to collimate the beam while reflective collimators use parabolic mirrors. The main advantage of the use of mirrors is that they have a constant focal length for different wavelengths which means the mirror could for example be used for multiplexed fibres separated by wavelengths⁴². However, since only one wavelength is used this advantage is gone. Two other parameters of interest are the reflectance at 1550 [nm] based on the used coating which influences the collimation losses and the cost. In table 5.12 a comparison of both the cost and reflectance of both methods is provided. It can be seen that a reflective collimator using silver coating has a worse reflectance while being more

⁴¹https://www.civillaser.com/index.php?main_page=product_info&products_id=2966

⁴²https://www.thorlabs.com/navigation.cfm?guide_id=2328

than 4 times as expensive. This makes the choice of collimator clear since for this use case refractive collimators will simply perform better and cost significantly less.

Table 5.12: Cost and reflectance comparison of reflective and refractive collimators

	Reflectance	Cost	Achromatic
Reflective ⁴³	<4%	€900	Yes
Refractive ⁴⁴	<0.5%	€208	No

Point-Ahead Mechanism

Since the satellite or HAPS moves relative to the ground station the required transmission path is not exactly aligned with the receiving path. A simple estimation done with Pythagoras for a satellite at a height 350 [km] with a speed of 7.70 [km/s] [48], and speed of light c of $3.0 \cdot 10^8$ [m/s] [49] yields a required point-ahead angle of 26 [μrad]. Considering the accuracies in the link budget are in the order of 1 [μrad] a constant bias of 26 [μrad] is unacceptable resulting in the need for a point-ahead mechanism [32]. For this an FSM is chosen for similar reasons as the fine steering.

Transmit and Receive Beamsplitter

The purpose of the beamsplitter is to isolate the transmit and receiving signal from each other and send them to different paths. The beamsplitter is an important part of the optical bench, considering that the detector is sensitive to signals smaller than [nW] magnitude and the laser produces a signal of 5 [W], as can be seen in the link budget. The uplink laser signal can saturate the detector [32]. Therefore the isolation technique is required, to protect the detector from the transmitter.

Two main types of isolation techniques were considered; polarization isolation and wavelength isolation. Another third type of isolation, spatial isolation, has been discarded since it is used for the short-range terminals [32].

Polarization Isolation

This isolation technique makes use of quarter-wave plates, or simply $\lambda/4$ wave plate, which is used to switch between polarization states. A quarter-wave plate consists of an adjusted thickness of a birefringent material. The light associated with the larger index of refraction is retarded by 90° in phase with respect to that associated with the smaller index⁴⁵. The polarization state is defined by two parameters, namely the relative phase and relative amplitude of the orthogonal electric-field components of the polarized light wave[50]. The idea behind this isolation is that after the light passes through the transmitting lens, the s-polarized light (i.e. polarized light in which the electric field is oriented perpendicular to the plane⁴⁶) is reflected to the $\lambda/4$ wave plate via a PBS. This light is converted into left circularly polarized light and then transmitted via the telescope. The received polarized light is converted into p-polarized light (i.e. a polarized light that has an electric field direction parallel to the plane of incidence on the given device⁴⁷) via the $\lambda/4$ wave plate, while the stray light is filtered using the PBS and a polarization analyzer. The filtered circularly polarized light eventually reaches the signal capture and communication reception branches[51].

Wavelength Isolation

This technique uses different wavelengths to transmit and receive the wavelengths. Typically for this type of isolation same telescope aperture is used to transmit and receive optical signals, and the narrow receiving beam is used [32]. If two wavelengths are available, this is a preferred isolation approach since it can achieve a greater 120 [dB] of isolation [32], which is enough considering the

⁴⁵<http://hyperphysics.phy-astr.gsu.edu/hbase/phyopt/quarwv.html>

⁴⁶<https://byjus.com/jee-questions/what-is-s-and-p-polarized-light/>

⁴⁷<https://byjus.com/jee-questions/what-is-s-and-p-polarized-light/>

use of a -70 [dB] receiver. However, the use of different wavelengths for transmitting and receiving signals of the 1550 [nm] laser, only complicated systems including multiplexing such as [52], which is not a desired solution as has been explained in figure 5.4. Considering, that the polarization isolation provides 77.8 [dB] [51], and is enough to satisfy -70 [dB] sensitivity. Therefore, the components for the polarization isolation will be searched.

Beamsplitter

The general overview of the polarization isolation can be seen in figure 5.22⁴⁸. In essence, as mentioned before, the light is converted to a p-polarized light and an s-polarized light. The beamsplitter plate has a diameter of 25.4 [mm], with a thickness of 5 [mm]. Moreover, it requires a clear aperture of $\leq 85\%$ of diameter⁴⁹.

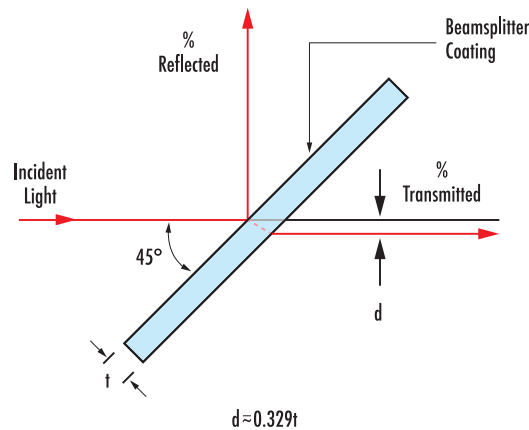


Figure 5.22: Plate beamsplitter⁵⁰

At the same time, the quarter wave plate is used to switch between polarization states, as represented in figure 5.23⁵¹. The quarter wave plate has a diameter of 12.7 [mm], a thickness of 2.5 [mm] and a clear aperture of 11 [mm]⁵².

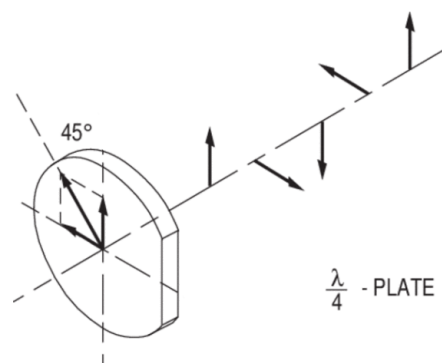


Figure 5.23: Quarter wave plate

The two chosen lenses can be seen in figure 5.24.

⁴⁸<https://www.edmundoptics.eu/knowledge-center/application-notes/optics/what-are-beamsplitters/>

⁴⁹https://www.thorlabs.com/newgrouppage9.cfm?objectgroup_id=6004&pn=PBSW-1550

⁵¹<https://www.edmundoptics.eu/knowledge-center/application-notes/optics/what-are-beamsplitters/>

⁵¹<https://www.edmundoptics.eu/knowledge-center/application-notes/optics/understanding-waveplates/>

⁵²<https://www.meetoptics.com/waveplates/quarter-waveplate/s/eksma-optics/p/460-4401D12>



Figure 5.24: Polarizing beam splitter⁵³(left) and quarter wave plate⁵⁴(right)

Fiber Coupling

Coupling is essentially the reverse process of collimation and the same equipment can be used. Consequently, the same trade-off as for the collimation applies and a refractive coupler will be used.

Adaptive Optics

Since the EDFA requires a fiber input the free-space laser must be coupled with a fiber. A major consideration in this process is the coupling efficiency which is the ratio of the power at the start of coupling and the power reaching the receiver [53]. The coupling efficiency is highly dependent on the quality of the laser wavefront which is quantified using the root mean square (RMS) of the wavefront phase distortion [54]. A significant contributor to this distortion is the turbulence of the air, the effect of which is quantified in figure 5.25 [54]. In this figure the normalised atmospheric turbulence strength, D/r_0 is a measure of the turbulence which for the considered aperture size is about 2 for weak turbulence conditions, 10 for moderate turbulence and 15 for strong turbulence [54]. It can be seen that without the use of adaptive optics the coupling efficiency almost goes to 0 for still relatively weak turbulence conditions of 5. Since the node must still be operable under turbulence conditions the use of adaptive optics is required.

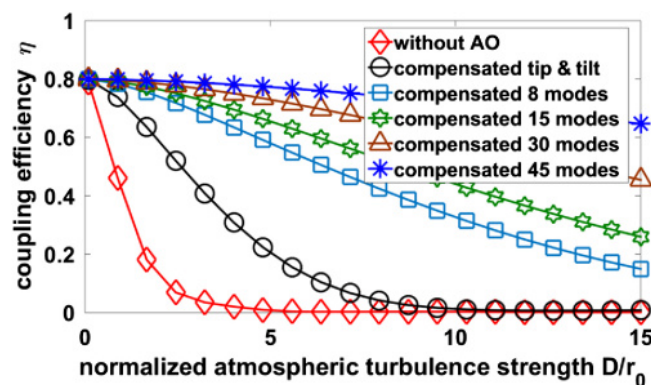


Figure 5.25: Coupling efficiency vs turbulence strength [54]

Adaptive optics (AO) has been the only identified way to deal with these wavefront distortions, a schematic overview of which can be found in figure 5.26 [55]. This system uses a deformable MEMS mirror which corrects for the distortions in the wavefront. Then a small part of the beam gets bent into a wavefront analyser which creates a high-bandwidth closed loop with the MEMS reducing the errors significantly. This means that a MEMS mirror with a wavefront sensor and beamsplitter will have to be added to the receiving path of the optical bench.

⁵²https://www.thorlabs.com/newgrouppage9.cfm?objectgroup_id=6004&pn=PSW-1550

⁵⁴<https://www.meetoptics.com/waveplates/quarter-waveplate/s/eksma-optics/p/460-4401D12>

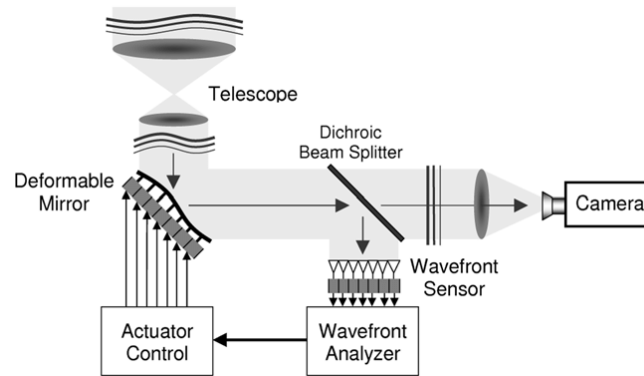


Figure 5.26: Schematic overview of an AO system [55]

EDFA Pre-amplifier

In the midterm, it was chosen to use an EDFA amplified receiver setup [2]. In this setup, the received signal first gets coupled into a fiber after which it gets amplified by the EDFA. It was found in the link budget that a 40 [dB] amplification is required with an input power of -53.67 [dB] which can easily be achieved by currently available EDFA like the one in figure 5.6⁵⁵.

FSM

Fast steering mirrors (FSM) have been used in practice for years, making it easy to find off the shelf components. However, due to the current developments in optical communication FSM development is still going on. For example, TNO has developed a FSM which is operable over a wide range of temperatures (-20° to $+50^{\circ}$) and has high bandwidth of 1 [kHz] [56].

For finding commercially available FSM mirrors, it was complicated to find accuracy specifications for the FSM used in laser communications. Manufacturers could be hiding this information for competitive reasons. Therefore, it was decided to take an FSM Microelectromechanical systems (MEMS) mirror of the same manufacturer, "Mirrorcle", as used in the similar laser communication mission of Facebook [9]. For the Bi-directional dual-axis mirror 7.5 [mm] diameter actuator together with 2.4 [mm] mirror diameter has cumulated in a cost of \$2,050⁵⁶. However, it is worth noting that the price ranges for FSM have a high price variance. Some examples can go up to \$15,000⁵⁷, and still be unclear whether the accuracy is suitable for optical communication. It has been decided that for the current design stage, two FSM will be used (each having cost of \$2,050).

5.4.1. Verification and Validation

At this stage of the design, the optical bench has not yet been modelled but this would be something that has to be done in the next phase of the design to ensure the required performance and proper interfacing of the equipment. For this, a verification and validation procedure is set up which could be used at that point.

Verification

To verify the setup of the optical bench software such as OpticsStudio from Zemax⁵⁸ can be used. This type of software allows for modelling the optical path of the laser against several mirrors to estimate the wavefront errors and the correctness of the optical path. Since flat mirrors are used, the optical path of the software makes sense and should be verified with common-sense and simple calculations

⁵⁵https://www.fiberlabs.com/products/product_details/c-band-edfa-rack-mount/

⁵⁶<https://www.mirrorcletech.com/wp/products/mems-mirrors/>

⁵⁷https://www.opticsinmotion.net/fast_steering_mirrors.html

⁵⁸<https://www.zemax.com/pages/opticstudio>

on the deflection angles based on the angle of incidence. Additionally, the setup and performance of the optical bench can be compared to similar setups such as the one used by Facebook [9].

Validation

The validation of the optical bench would be done by building a breadboard test setup on which the entire optical path can be tested, such as the small example shown in figure 5.27. This setup should be used in combination with an FSM to simulate pointing errors caused by the atmosphere to check the performance under these conditions. Additionally, after the housing exists with the gimbal structure it can be exposed to vibrations to assess performance and survivability under these conditions. Additionally, the performance and survivability when the thermal control system fails can be assessed. The losses between the transceiver and EDFA, fiber coupling and collimating and beamsplitters must also be assessed by checking the strength of the signal between different components.

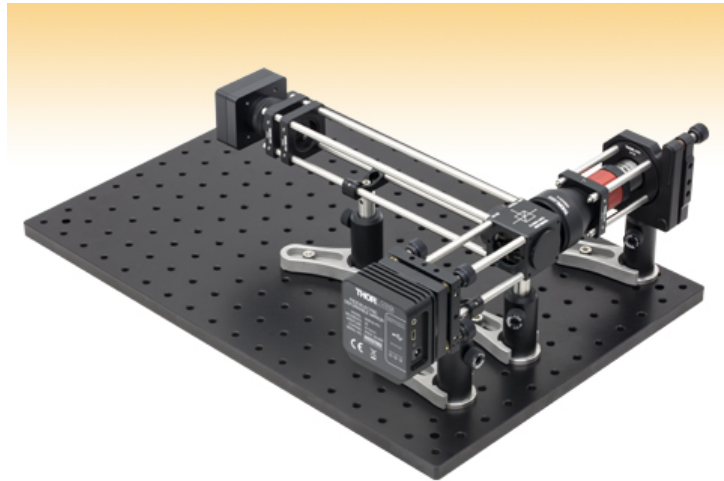


Figure 5.27: Example breadboard setup⁵⁹

5.5. Camera Sensors

The camera sensors address two technical problems identified in the midterm report: providing feedback for the control loop, and determining the attitude of the system [2]. Closed-loop control algorithms for tracking use position-sensitive photodiodes to determine error; the camera is such a sensor, with an incoming beam appearing as a spot on the produced 2D image, with different incident angles corresponding to different pixels. The camera works on the principle of a staring array, with a matrix of light-sensitive pixels placed at the focal plane of the lens. The camera sensor sensitive in the optical C-band is, therefore, a critical part of the tracking sequence. Two cameras can be used for the selected staged control approach (see subsection 5.6.4). The first one is placed in the optical assembly next to the detector for laser communication, and the other wide FOV camera is co-aligned with the main aperture

The other role of the camera sensors is attitude determination. Top scoring design options in the midterm report trade-off included star trackers. Star trackers offer the best performance, being able to achieve orders of magnitude better accuracy than other available alternatives. Since Short-Wave InfraRed (SWIR) star trackers are preferred for ground-based applications [57], there appears an opportunity of using the same imaging sensor for roles of fine tracking feedback and attitude determination. The configuration would leverage powerful optical instruments for laser communication

⁵⁹https://www.thorlabs.com/newgrouppage9.cfm?objectgroup_ID=5056&pn=DMP40-P01

to precisely calibrate the system, even during the daytime, further increasing performance while decreasing cost and mass.

5.5.1. Control Loop Feedback

The staged control sequence for tracking was selected in subsection 5.6.4, with coarse and fine tracking stages. The difference between the sensors for the two is the sensor's field of view: the coarse camera is separate and co-aligned with main aperture, while the fine camera uses the main aperture.

For coarse camera sizing, similar cameras for coarse satellite tracking were reviewed, and findings summarized in table 5.13.

Table 5.13: *Coarse tracking cameras*

Optical ground station	Coarse camera
NASA OCTL	CCD camera with motorized zoom lens, FOV from 34° to 1.7° [58].
DLR OGS-OP	Wide Field of View (WFOV) camera with 165 × 123 mrad FoV and 50 mm focal length [59].
Grasse LLR	Wide field-of-view camera (IR-WFOV) with field of view of 2200×1760 arcsec ² [60].

Converting FoVs of examined cameras to degrees, it is 1.7x1.7 to 34x34 degrees for NASA OCTL, 9.45x7.05 degrees for DLR OGS-OP, and 0.61x0.49 deg for Grasse LLR. Grasse LLR can have very low FoV for their Wide FoV camera because of being a fixed optical ground station: it can reliably be precisely calibrated. ECN, however, is a transportable ground station, with only 2 degrees accuracy of calibration guaranteed in worst case weather conditions (see subsection 5.6.1). The FoV of a coarse tracking camera must be at least 4x4 degrees to reliably acquire a signal from a target with a precisely known location. On the other hand, increasing the Field of View decreases the ability to receive a faint beaconing signal.

For fine tracking camera, similar survey was performed, and presented in table 5.14

Table 5.14: *Fine tracking cameras*

TAOGS	CMOS camera for acquisition and tracking, receiving 5% of RX light, at readout frequency of 25 Hz [61].
PorTeL	InGaAs camera coupled with the telescope, 320×256 pixels, 4.0 × 3.2 mm ² active area, 295×236 arcsec ² FOV, and 0.92 arcsec/pixel plate scale. 60 Hz readout rate [58].
MIT LLGT	InGaAs focal plane with 25 Hz readout rate [58].

The findings will be a relevant reference in component selection in subsection 5.5.3. The value of 5% of RX light being redirected to the fine tracking camera will be used as an estimation for the value for the link budget calculations.

5.5.2. Star Tracking for Attitude Determination

Determining the attitude of the satellite is a complex task which requires an iterative process. It is a critical part of the design as it determines if the communication with the satellite can be actually performed. The choices for the attitude determination methods were narrowed down to the usage of a star tracker. This subsection will provide extensive insight into how the star tracker performs its task and the general algorithms behind it.

The basic idea behind modern tracking systems is to take a photo of a set of stars, detect the stars in the image, determine their position and match them to a pre-processed star database by comparing the position of the stars in the image with the position of the stars in the database. The orientation can then be obtained by using the stars from the image and the matching stars from the database. The star tracker utilises a SWIR camera due to the fact that the transmittance through the atmosphere is higher in the SWIR spectrum. Moreover, the sky background radiation is lower in the SWIR spectrum and the number of stars at a similar intensity level is an order of magnitude greater in the SWIR spectrum, making it possible to have a smaller FOV and still detect the necessary amount of stars [62]. Figure 5.28 provides a representation of the disturbances encountered by the star tracker during operations.

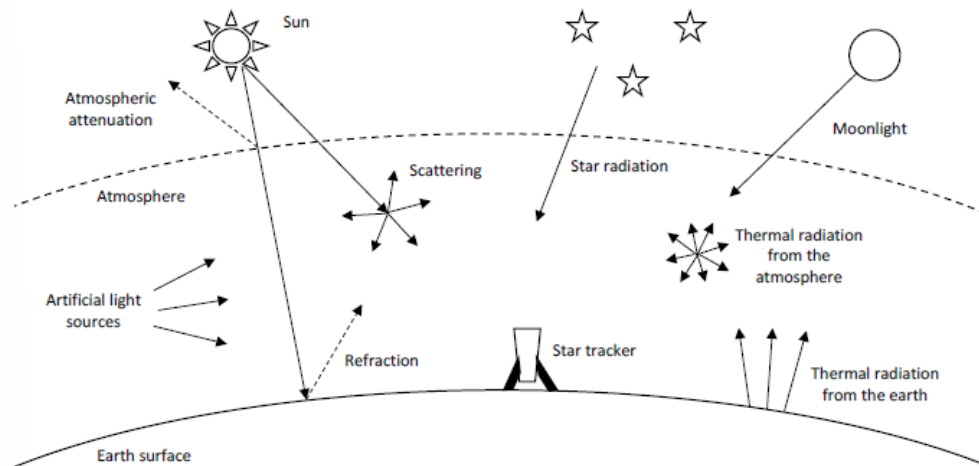


Figure 5.28: Impacts on a star tracker operating inside the atmosphere[63]

The cameras perform better at daytime as the daylight sky background radiation is lower than in the visible waveband, as stated in [62]. At night, however, other light sources dominate. The airglow, a luminescent phenomenon in the upper parts of the atmosphere, becomes larger in the SWIR spectrum compared to the visible one. The thermal radiance from the ground and atmosphere dominate completely at higher wavelengths. Thus, it is assumed that the performance of the SWIR cameras may be worse than for a camera operating in the visible spectrum during the night [63].

Field of View

The field of view is defined in equation 5.21.

$$FOV = 2 \arctan \left(\frac{h}{2f} \right)^{60} \quad (5.21)$$

where f is the focal length and h is the horizontal length. It is desired to use a relatively small FOV to limit the background light, especially during daytime.

Reference Frames

Properly defining the attitude of the tracked object requires a series of reference frames transformation. Commonly used are the inertial frame (usually the Earth Centered Inertial coordinate system - ECI), the body frame and the camera frame. ECI becomes widely attractive as all stars are specified in an ECI frame, represented as Declination (DEC) and Right Ascension (RA) [63], as seen in figure 5.29. One common way to represent the attitude is through the rotation matrix and the quaternion. The

⁶⁰<https://www.edmundoptics.com/knowledge-center/application-notes/imaging/understanding-focal-length-and-field-of-view/>

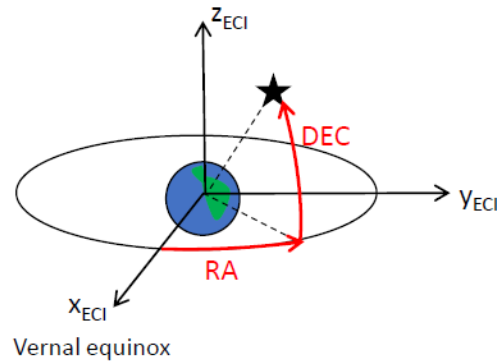


Figure 5.29: ECI reference frame [63]

rotation matrix, constructed in this case by three consecutive rotations around the axes of the coordinate system, defined by the Euler angles of that axis (namely Φ for roll, θ for pitch and ψ for yaw), is defined in equation 5.22,

$$W = AV \quad (5.22)$$

where W is a set of vectors in the body frame, A is the rotation matrix and V is a set of vectors in the reference frame.

Detection

The captured images are dark, so a common way to detect the stars is by using a pre-determined threshold where everything above the threshold is considered to be a star. This threshold can be made adaptive, being determined locally by considering a window around each pixel [63].

Centroiding

Centroiding is a process of calculating the position of every detected star. By intentionally defocusing the image, the accuracy is increased. One simple way to calculate the centroid is by using the Center of Gravity method: by choosing the appropriate pixel in the star area, e.g. the brightest pixel, a window of pixels can be created around this chosen pixel and the centroid is calculated [64].

Star Identification

Highly important is to correctly identify the stars. This is done by matching the detected stars to a star database, which contains the DEC, RA and magnitude of the stars. A common way to identify the stars is by using the Pyramid Star Identification Technique [65].

Attitude Determination

After detecting the stars, what is left is to find the attitude of the system. This boils down to finding A from equation 5.22. Commonly, this is done by Singular Value Determination or the Weighted Triad [63]. Naturally, it is desired to have an estimation as close to reality as possible. Thus, a Kalman filter is used to improve this accuracy, namely, the Multiplicative Extended Kalman Filter [66].

Star Tracking Software

The software used for star tracking is called OpenStarTracker⁶¹. In order to properly recognise the stars, a star database is used, in this case 2MASS⁶² database, which contains 470,992,970 astronomical objects [63], which is then filtered and shrunk to 162,007 stars. The thresholding mechanism used in the software is called the Information Theoretically Weighted Median Filter (ITWMF), which

⁶¹<http://openstartracker.org/>

⁶²<https://irsa.ipac.caltech.edu/Missions/2mass.html>

basically makes a priori assumption that the brightness intensity of the pixels is independently and uniformly distributed. Then, the algorithm is used to maximise the relative entropy of the image histogram, between two-pixel values. Moreover, an adaptive threshold is also evaluated, by computing it locally inside a window [63]. The centroids are then found and transformed to unit vectors. Identifying the stars is done by the previously mentioned Pyramid Star Identification Technique, and determining the attitude is done by solving for A from equation 5.22 using the Singular Value Decomposition (SVD). Finally, a MEKF is used to improve the attitude estimate.

Verification and Validation Procedures

The verification and validation of the algorithm is an important aspect in determining the operational limits of the star tracker and how reliable is for the purposes of the present project. Figure 5.30 presents an overview of the software's architecture which can be used to come up with a verification and validation plan.

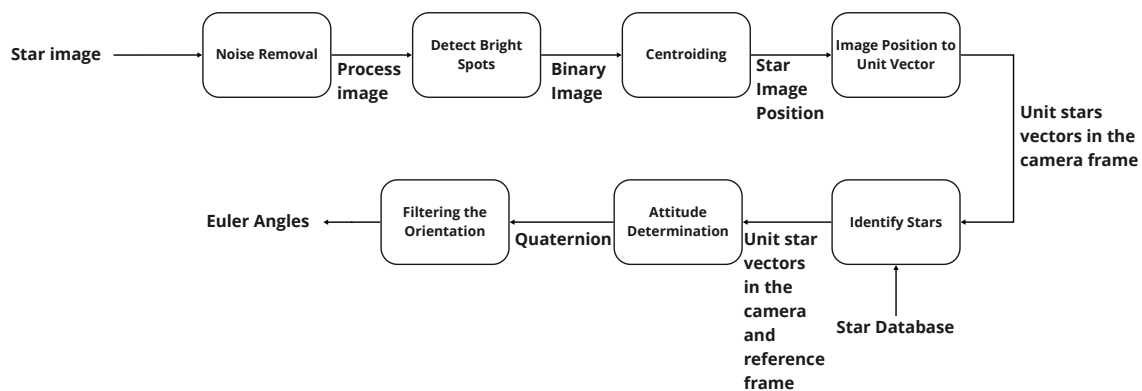


Figure 5.30: Software architecture overview[63]

The verification of the software can be done by analysing the problem numerically. In order to accurately verify the software, a unit test analysis will be performed, as well as a subsystem and system test to verify the functionality of each subsystem and the overall functionality, respectively. By starting with the star image, the first step is to remove the noise. This is done by imposing a threshold. Knowing the threshold and the amount of noise that has to be removed, the noise removal can be done manually. The newly processed image is then further analysed to detect the bright spots and is then transformed into a binary image. All the subsequent steps of the software can be performed manually on a simple sample picture, and the results can be compared to the outcome of the code. If the previously mentioned tests are successfully performed, it can be concluded that the software has been verified.

In order to validate the software, several methods can be used. One common approach is to make use of experimental data and compare the outcomes to the simulated data outcomes. This can be done once the star tracker is put in use and several data points are collected. A simulation can then be performed, and the results can be compared. An alternative for this would be to utilise different star trackers that are already correctly calibrated and compare the results.

5.5.3. Component Selection

This section considers COTS component selection based on criteria introduced in subsection 5.5.2 and subsection 5.5.1. Two selections must be made for a coarse tracking camera: a camera sensor and a lens. The former will determine the resolution, readout speed, and quantum efficiency of the sensor. The latter allows to choose FoV and, optionally, motorized zoom. The fine tracking camera uses a camera sensor and the same telescope as used for optical communication.

Camera Sensor

For the camera sensor, three commercially available sensors have been listed in table 5.15.

Table 5.15: Coarse camera comparison

	Resolution	Readout	Operating temperature	Q.E.	Mass
C12741-03 ⁶³	640×512	60 [Hz]	0°C to 40°C	~65%	520 [g]
C14041-10U ⁶⁴	320×256	216 [Hz]	0°C to 40°C	~ 65%	520 [g]
Zillion Techs 640 ⁶⁵	640×512	240 [Hz]	-20°C to 70°C	>70%	280 [g]
Owl 1280 ⁶⁶	1280×1024	60 Hz	-20°C to 50°C	~85%	247 [g]

Unfortunately, the cost of components is not publicly available, and hence it is not a part of this trade-off. The choice might need to be revised as the cost becomes known. 640 SWIR InGaAs High Cost-Performance Camera offered by Zillion Techs offers the best performance in readout speed and operating temperature range, and it was chosen for coarse tracking based on available information. The sensor boasts 9.6 [mm] × 7.68 [mm] active area, a parameter relevant for the angular field of view calculations. For the fine tracking camera, where resolution is of more importance to maximise the performance, and the sensor is placed on an optical bench in a temperature-controlled environment, Owl 1280 camera was chosen. The model has also been used for daytime star tracking applications, which is the second function of the component [57]. The active area is equal to 12.8 [mm] × 10.24 [mm].

Coarse Camera Lens

For the coarse tracking camera lens, a motorized lens offers a Variable Field of View, solving the problem of a trade-off between signal strength and pointing accuracy required by allowing the lens to actively adapt to whatever is needed. The upper limit on FoV must have a margin above 4x4 degrees required for acquisition (as reasoned in subsection 5.5.1), and the lower limit, the better. Coarse tracking camera being able to maintain good communications link adds to redundancy. Tracking without a fine tracking camera is possible, and employed by for example TOGS, which only has one wide FoV camera and does not use a staged control approach [58].

With this in mind, CVO GAZ1025018M⁶⁷ motorized zoom lens was selected. It has a compatible C mount, and offers 10 - 250 [mm] focal length. This translates to a range of angular FoV from 42° to 1.76°⁶⁸.

The parameters of the entire coarse tracking camera assembly is therefore: 640x512 resolution at 240 [Hz], with 10-250 [mm] focal length corresponding to FoV of 1.76° to 42°, at weight of 1780 [g] (1500 [g] lens, 280 [g] camera), and fitting in bounds of 110x100x265 [mm]. At the highest zoom, 512 pixels for 1.76° results in a resolution of around 12.4 arcseconds per pixel. The coarse camera is therefore easily able to provide sub-arcminute level feedback to the control loop.

Fine Tracking / Star Tracking Camera

Owl 1280 camera is mounted at the optical path through the main telescope. Barlow diverging lens is used to increase the focal length to the desired value of 10,000 [mm]. A motorized adjustable Barlow

⁶³<https://www.hamamatsu.com/eu/en/product/cameras/ingaas-cameras/C12741-03.html>

⁶⁴<https://www.hamamatsu.com/eu/en/product/cameras/ingaas-cameras/C14041-10U.html>

⁶⁵<https://www.zillion-techs.com/products/640-swir-ingaas-high-cost-performance-camera-usb3/>

⁶⁶<https://www.raptorphotonics.com/wp-content/uploads/2022/03/Owl-1280-A4.pdf>

⁶⁷<https://www.stemmer-imaging.com/en-nl/products/cvo-gaz1025018m/>

⁶⁸<https://www.edmundoptics.eu/knowledge-center/application-notes/imaging/understanding-focal-length-and-field-of-view/>

lens is desired, if integration with an optical bench allows—it would allow the tracking camera to adapt to conditions, by starting with low accuracy and signal strength immediately upon acquisition of signal by the camera, and increasing both as the signal is centred. This feature however is not necessary, as an adjustable acquisition / coarse tracking camera is available, using scanning to obtain the signal, and closed-loop feedback to centre it.

A simple calculation, utilizing the focal length and camera detector size, yields a corresponding angular Field of View of 211.2 arcseconds, or 0.206 arcseconds per pixel. Algorithms for a similar application of star tracking are able to centre stars at up to subpixel accuracy [57]. There are, however, some differences between star tracking and lasercom tracking: the following might introduce more angle of incidence jitter, making star tracking level of performance unattainable. It must be considered that the accuracy achieved might be worse than pixel level. In that case, focal length would have to be increased further, or a more powerful imaging sensor would need to be selected. That would result mainly in an increase in cost. The topic must be investigated further, however, due to time and resource constraints, it is out of the scope of this report, and for now, the assumption will be that an appropriate confidence threshold in subpixel accuracy is possible for this application. This is also a level of accuracy expected from literature [31]. The tracking must be performed with an accuracy of 1 [μrad], or 0.21 arcseconds, which, with this assumption, is easily achievable with a margin with the camera sensor.

Finally, coarse camera's 12.4 arcseconds per pixel at minimum Field of View means that signal can be easily acquired in fine tracking camera from the coarse tracking stage, therefore camera performs well enough for integration of and transition between tracking stages.

5.6. Pointing, Acquisition and Tracking

5.6.1. Attitude Determination

Attitude determination sensors are used to calibrate the system, as it is deployed without any prior information about its orientation. The midterm report presented and discussed a trade-off between attitude determination types, the result of which was a combination of daytime-capable star tracker, magnetometer, and a bio-inspired celestial compass [2]. The selection of each type of sensor, and finally the calibration procedure, will be discussed in this subsection.

Star Tracker

The star tracker functionality was successfully integrated into the fine tracking camera, making use of the optical instrumentation for laser communication, reducing cost and complexity of the system. The process of design and component selection for the sensor is contained in section 5.5, and then presented in subsection 5.6.5. The star tracking sensor achieves calibration accuracy much better than 1 arcminute, dictated by the requirement ECN-F-PRF-7-1.

Magnetometer

The COTS high-accuracy electronic compasses were researched, and the suitable options were presented in table 5.16.

Table 5.16: Magnetometer comparison

	Accuracy	Update rate	Cost
ECS eCompass ⁶⁹	$\pm 0.5^\circ$	28 Hz	Not available
HMC5983 ⁷⁰	1 – 2°	220 Hz	€8.50

⁶⁹<https://jewellinstruments.com/product-category/inertial-tilt-sensors/ecompass/>

⁷⁰<https://www.tinytronics.nl/shop/en/sensors/magnetic-field/hmc5983-3-axis-compass-magnetometer-sensor-module>

QMC5883L ⁷¹	1 – 2°	200 Hz	€4.00
HMC6343 ⁷²	2°	10 Hz	€93.93
DFRobot SEN041 ⁷³	2.5°	20 Hz	€8.22
Autonnic A5024 ⁷⁴	0.3° typical, 1° max	Not available	€222.31

Solutions with better than 1 degree accuracy were either expensive or unavailable and had incomplete information available online. The producers of the components were contacted with questions, however, the team did not receive a response. The final choice was to include three QMC5883L magnetometers and three HMC5983 magnetometers, to achieve triple modular redundancy on each sensor type and dissimilar redundancy between sensor types. The two sets of three identical sensors is to be placed in different places on the ECN.

This brings the total cost of the magnetometers to €37.5.

Bio-inspired Celestial Compass

The bioinspired solution exploits the fact that the scattering of sunlight in the atmosphere produces a polarization pattern, which can be used to determine yaw of the sensor to an accuracy of 0.3 to 1.9 degrees (depending on weather conditions). The sensor is robust, excelling in conditions most difficult for the star tracker, and not influenced by presence of an external magnetic field. The bio-inspired celestial compass is very simple in construction, consisting of two SG01D-18 photodiodes, AM0820 stepper motor, two linear UV polarizers, and a 3D-printed small structure holding the components together [67]. The components are presented in table 5.17.

Table 5.17: *Bio-inspired celestial compass components*

	Cost	Operating temperature
2x SG01D-18 ⁷⁵	€98	-55 to 170 °C
Faulhaber AM0820 ⁷⁶	€518	-30 to 70 °C
Linear polarizer ⁷⁷	€37	
Total	€653	

The mass, size, and power consumption of the components is negligible. The mass of components is in the range of 1-100 grams, and the size of the components is up to tens of millimetres.

Calibration Procedure

The calibration starts with magnetometers reading, in case of nighttime deployment, or fusion of magnetometers and bio-inspired celestial compass in daytime deployment. This allows for a robust preliminary calibration with 0.3-2 degree accuracy, depending on conditions. This step boasts multiple levels of redundancy, by using two magnetometer types (each with triple modular redundancy) and a celestial compass. This alone satisfies ECN-F-PRF-7-4 requirement of 2 degree pointing accuracy in any weather condition.

⁷¹<https://www.tinytronics.nl/shop/en/sensors/magnetic-field/qmc5883l-3-axis-compass-magnetometer-sensor-module-3v-5v?sort=p.price&order=DESC>

⁷²<https://www.digikey.com/en/products/detail/honeywell-aerospace/HMC6343/1692480>

⁷³<https://botland.store/magnetometers/20994-fermion-3-axis-magnetometer-bmm150-i2cspi-dfrobot-sen0419.html>

⁷⁴<https://www.mediawinkel.eu/autonnic-a5024-fluxgate-compass.html>

⁷⁵<https://sglux.de/en/produkt/sg01d-18-en/>

⁷⁶<https://nl.rs-online.com/web/p/stepper-motors/9211347>

⁷⁷<https://www.silvestricamerashop.it/shop/en/silvestri-filters/974-linear-polarizer-100x100mm-018mm-thick.html>

Next step is fine calibration, using the star tracker and preliminary calibration described above. The process has been described in detail in subsection 5.5.2. The accuracy of fine calibration easily satisfies ECN-F-PRF-7-1 requirement of 1 arcminute pointing accuracy in clear sky conditions.

Calibration performed on a fixed ground station is very stable, and isn't repeated too often. For this reason, the process is usually quite time-consuming [58]. Transportable ground stations need to be rapidly and often recalibrated, as each time they are moved, information about orientation is lost. However, even if the station is stationary in deployment location for extensive time, factors such as thermal drift, station being jostled, or soil being compacted, can decrease the accuracy of calibration with time. Preliminary calibration sensors can take measurements continuously and detect whenever the Node has experienced sudden movement, and need to be recalibrated. Measuring drift is more difficult on the fine calibration level, since the instrument (fine tracking camera) is used for optical communication, and would need to cease operation to measure the drift. However, it might be advantageous to do that periodically. The characteristic of calibration performance as a function of time will be evaluated on the prototype, and automatic recalibration at optimal time intervals can be implemented, most likely when the station is changing targets, as to not disrupt the communication. This is also supported by the fact that the pointing performance (depending on calibration) is mainly useful during acquisition, while tracking uses Kalman Filter to update trajectory estimation model and account for such errors, including calibration drift.

5.6.2. Pointing

Pointing is achieved with use of calibration, described in subsection 5.6.1, and inverse kinematics. Pointing algorithm takes a unit vector pointing towards a target as an input and calculates pose the mechanical beam steering setup has to achieve to result in LOS with target. Two approaches are possible for following a path: sampling points along it and creating waypoints. Pointing pose is calculated for each waypoint, and the telescope transitions between the discrete positions with pointing. The alternative is to drive gimbal rates directly, by differentiating the model [58].

5.6.3. Acquisition

Trade-off in midterm report [2] identified spoiling (narrow beam scanning) as the preferred option for beaconing. Continuous spiral scanning was selected for the scanning pattern. The pattern is illustrated in figure 5.31. As presented in subsection 5.6.5, this means that during acquisition, gimbals are driven by differentiating the pattern, a better implementation for a step spiral.

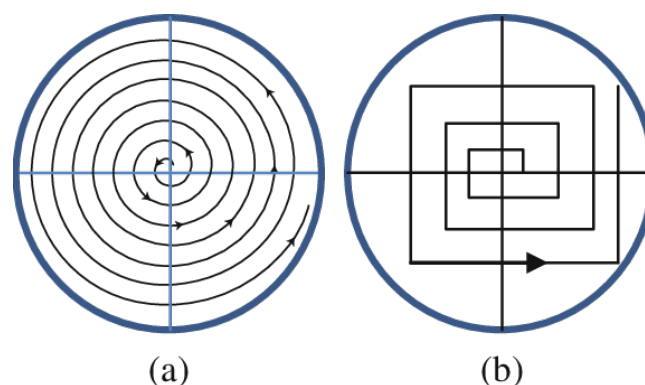


Figure 5.31: Continuous spiral (a) and step spiral (b) scanning patterns

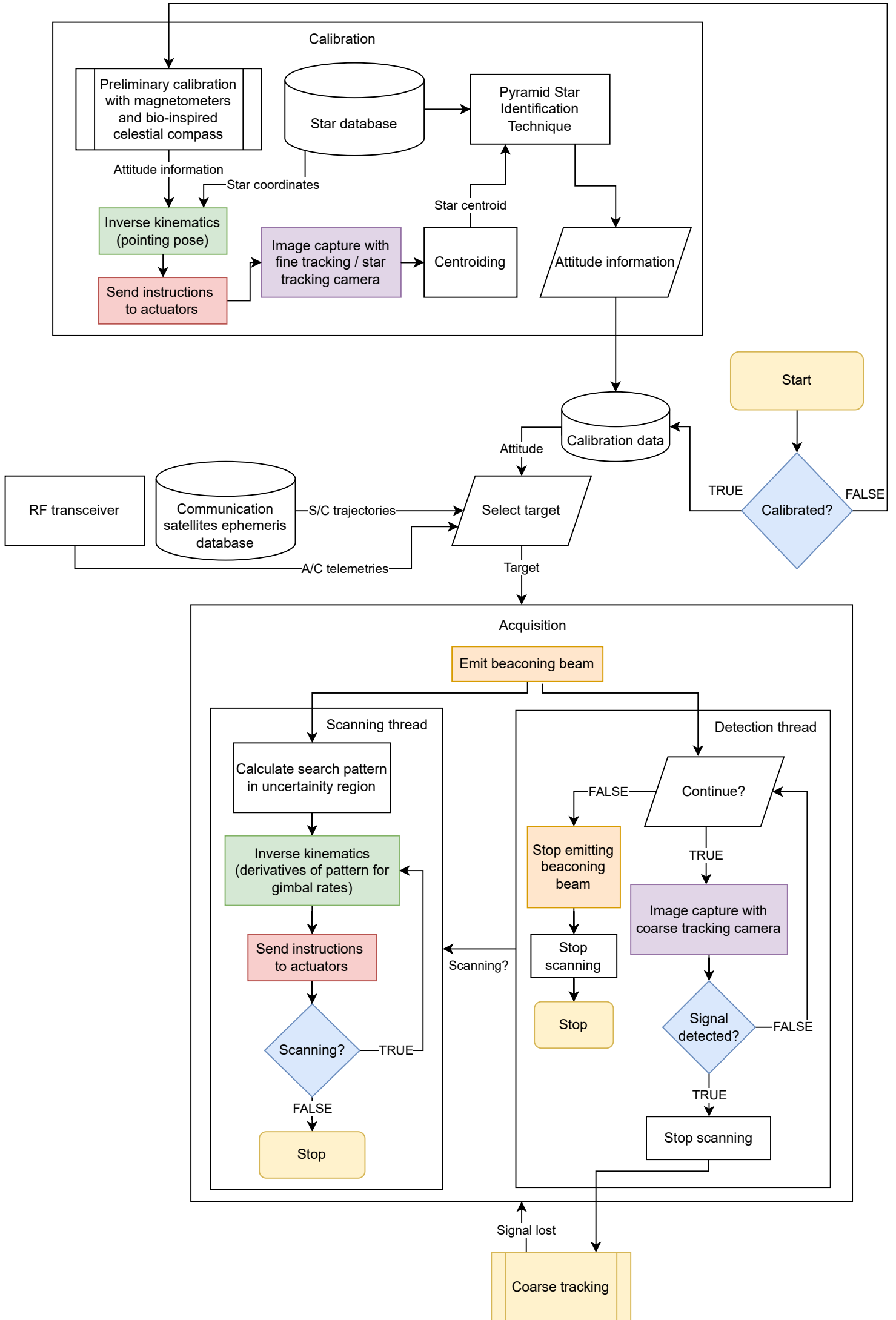
5.6.4. Tracking

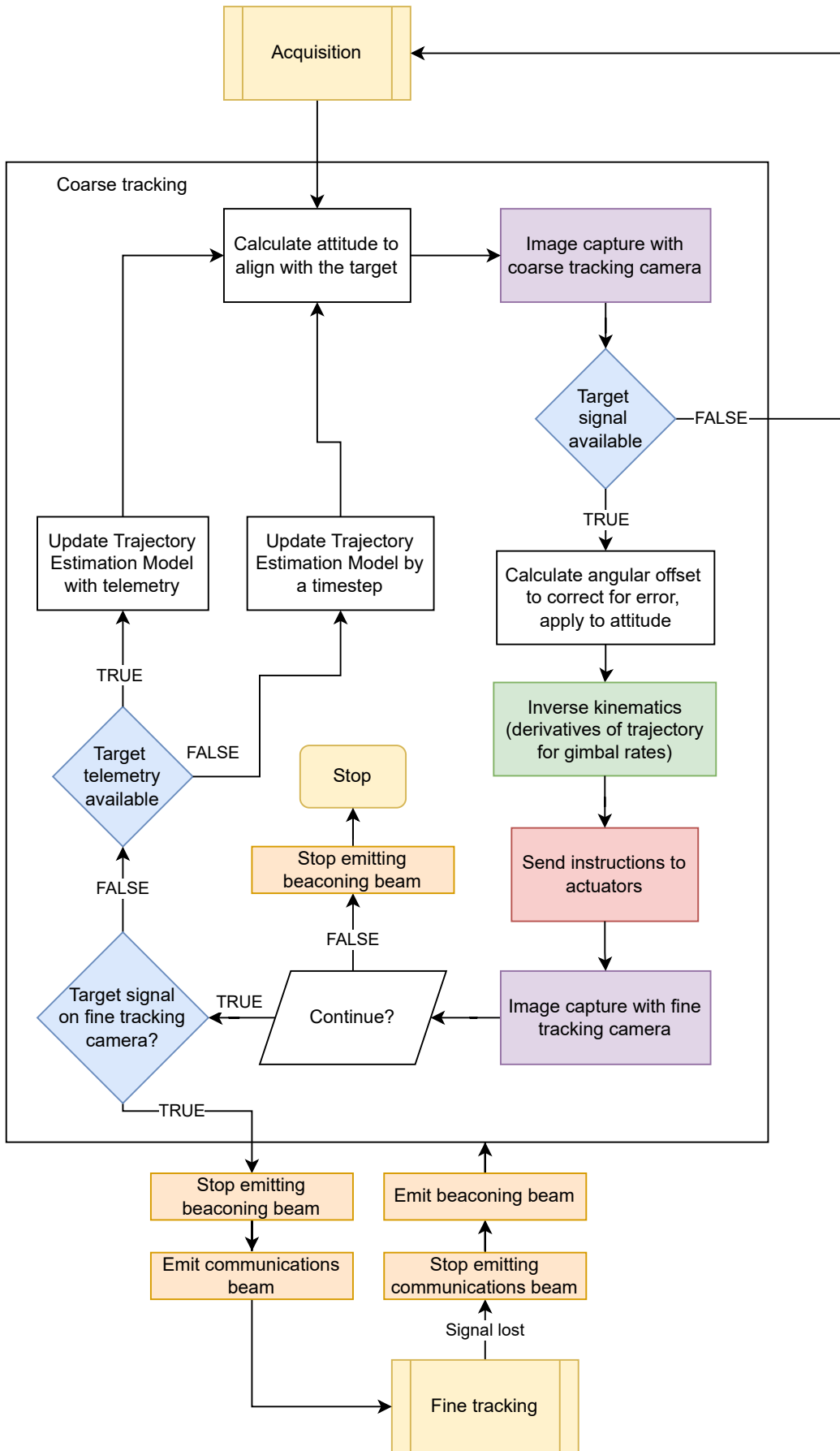
Staged control approach is employed for tracking, with two camera sensors. For discussion on sensors and control loop feedback, refer to section 5.5. Tracking control happens by taking pictures with

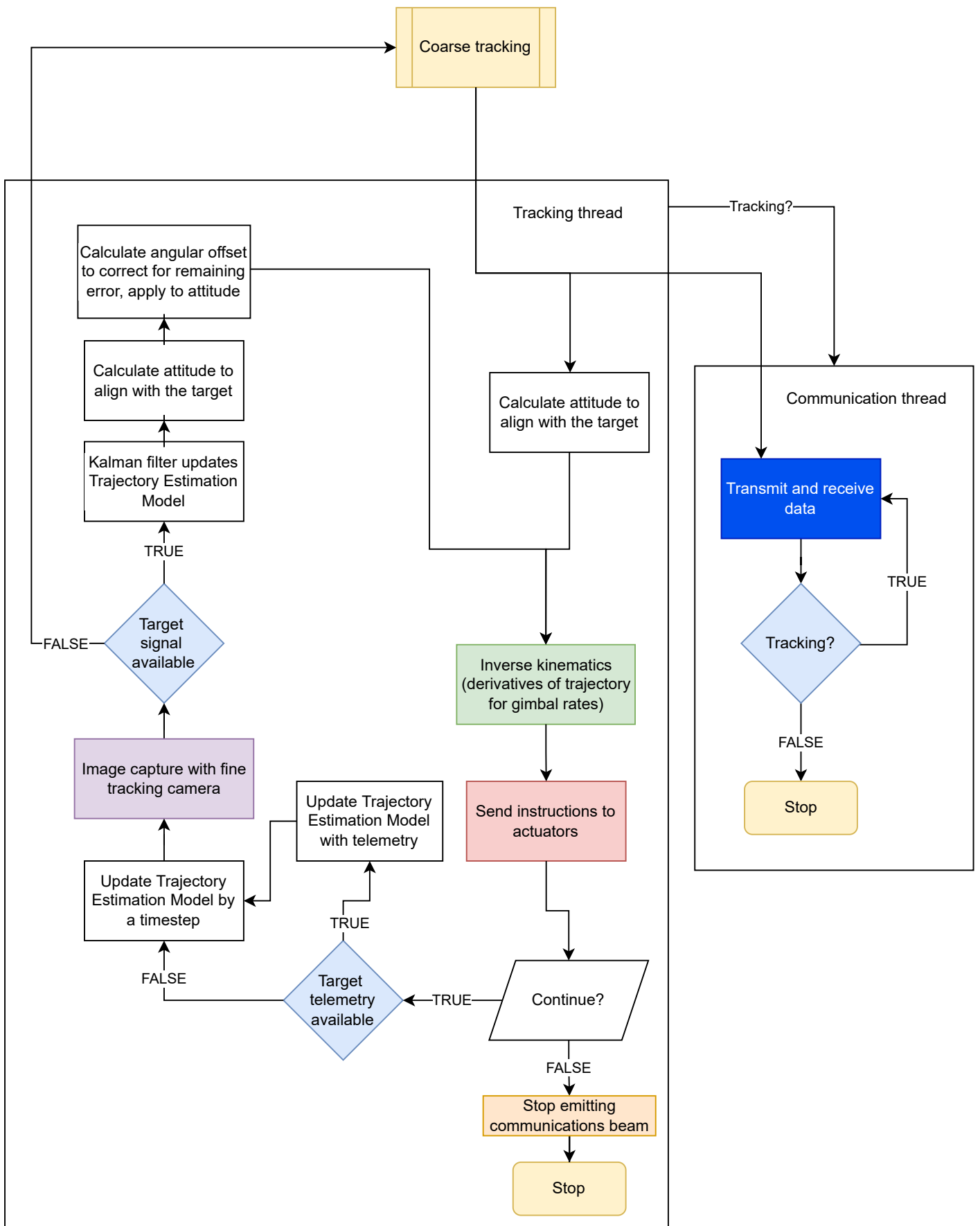
a camera, identifying the brightest object, and error is calculating by finding object's deviation from center of the frame. For coarse control, an angular correction is applied on top of trajectory estimation model prediction. For fine control, Extended Kalman Filter is used to update the model [2]. The camera's accuracy and used algorithm satisfy ECN-F-PRF-7-5 requirement of fine tracking accuracy better than 1 μ rad (see discussion in subsection 5.5.3, and possible steps to be taken if validation shows assumptions taken to be incorrect). The integration of camera into optical bench, with a beam splitter, has been presented in section 5.4.

5.6.5. PAT Sequence

The following pages include a diagram of the Pointing, Acquisition, and Tracking sequence.







5.6.6. Verification and Validation

In chapter 8, risk assessment identified problems with PAT sequence code as risk R18. The efficacy of the product relies on it correctly executing the Pointing, Acquisition, and Tracking sequence. The free space optical connection can only be established with apparatus correctly aligned physically. The control code must be properly verified and validated.

The diagram contained in subsection 5.6.5 suggests a structure for V&V procedure for the software. First off, before the software is developed or integrated, software specifications must be written, specifying the inputs and outputs of each routine. Numerical models applied must be studied and discussed, for future use in verification procedures. Then, the implementation should occur with Test-Driven Development (TDD), with unit tests assuring quality of every function. Code interacting with hardware, such as image capture or controlling actuators, must be tested with selected components. The flowchart divides the code base in several parts: calibration, acquisition, coarse tracking, and tracking. Threads within the parts, and predefined process block used for preliminary calibration within calibration, indicate modules suitable for subsystem tests. Integration testing should be performed, as well as systems tests, ensuring efficacy of the parts of the system working together to perform the mission.

Beyond dynamic code analysis procedures outlined above, static code analysis should be employed. Chosen technologies should make use of static typing, to minimize run-time errors. Code review should be performed on every module.

For validation, two types of procedures must be followed. The first one is testing the product in a simulated environment, using Software-in-the-loop. The other one is within operations validation, as detailed in section 4.4. The calibration procedure must be successfully performed, and connection established. This test is particularly important, as it tests PAT software integration with entirety of the system, in context of active deployment as the product is operated. It also tests the interaction of the software with a human operator.

5.7. Frequency Analysis

As the ECN is meant to achieve very fine accuracy to ensure the link is operational at all times once it is deployed, a subsystem must be designed to safeguard the integrity of the equipment used from external sources of vibrations. That is during all the phases of deployment, such as storage and transport among others. This chapter will dive into the process of such design. The strategy will be as follows: First, a simplified lumped mass model will be developed. Secondly, using the results from the simplified analysis, a more refined model will be developed.

5.7.1. Modal Analysis of the Simplified Model

To do a modal analysis of any structure it is first simplified to a mass-damper-spring model. The ECN is modelled using two mass blocks, one representing the node and the second one above representing the gimbal. Both the blocks of mass are connected by a spring and damper in parallel. The simplified model of the ECN can be seen in figure 5.32.

Once the model is finalised, free body diagrams and kinetic diagrams for both the blocks are made after which the equations of motion (EOM) can be written. Using the EOM, lumped mass matrix (M), Global damping matrix (C) and global stiffness matrix (K) can be formed. Following this modal analysis with Rayleigh damping is used which leads to uncoupled ODEs in principal coordinates. These ODEs can then be transformed to the original degrees of freedom (DOF) which gives the solution as a function of time. Finally, the natural frequency of the system and amplitude of oscillation under the decided forcing functions can be determined and modified using the system parameters.

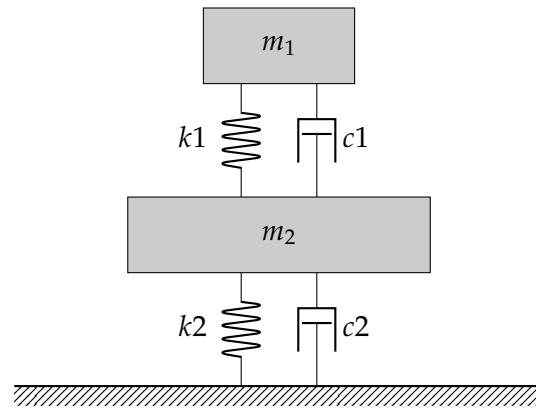


Figure 5.32: Simplified mass-spring-damper model of the ECN.

5.7.2. Earthquake Response

One of the loading cases considered key for analysis was the loading of different earthquakes and the effect it might have on the node. The first step was to determine how to quantify the effect of earthquakes in different areas of the world. This is especially important considering that the node must be deployable anywhere in the world.

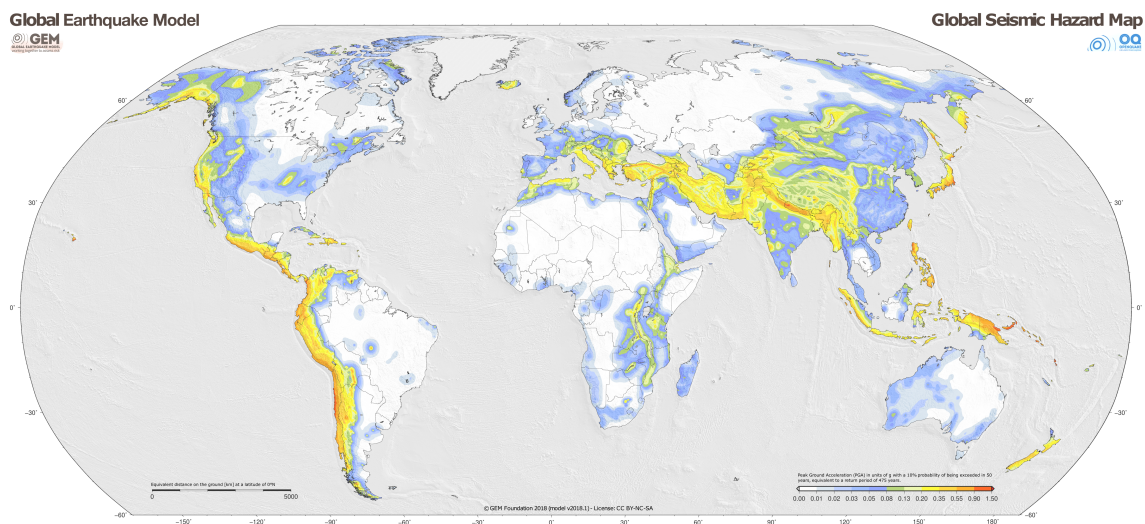


Figure 5.33: Map of Peak Ground Acceleration⁷⁸

Figure 5.33 highlights the areas of the world that are affected by earthquakes of greater magnitude using a heat map. The scale used goes from 0 g's of acceleration in white, to 1.5 g's of acceleration in red, where 1 g is the gravitational acceleration due to gravity; $9.80665 [m/s^2]$. To ensure survivability and deployability anywhere, the most extreme earthquake case was taken.

The next step was to identify the frequency of the forcing function. Consultation with a field expert advised the use of 5 [Hz] as a rule of thumb, however for the sensitivity analysis a range of 0.1-10 [Hz] will be used.

The acceleration of an extreme case earthquake could be modelled into a function as shown in equation 5.23

⁷⁸<https://www.globalquakemodel.org/gem-maps/global-earthquake-hazard-map>

$$a = 1.5g \sin(5t) \quad (5.23)$$

This assumes no phase shift given that for the purpose of applying the loading function, the shift would have little effect on the response. Moreover, the mass of the ECN has been estimated to about 700 [kg]. Then, using Newton's second law the following can be determined.

$$F = ma = 894 \cdot 1.5 \cdot 9.81 \cdot \sin(5t) \quad (5.24)$$

$$F = 13155.21 \cdot \sin(5t)$$

It is now possible to examine the effect of the extreme earthquake loading function on the Node. For this, a Matlab model has been built where different loading functions can be added and the damping required for the system.

5.7.3. Matlab Model

Firstly, a model of the ECN was developed that takes m_1 , k_1 , c_1 , m_2 , k_2 and c_2 as inputs to characterize the model as it was shown in figure 5.32. Furthermore, the extreme earthquake sinusoidal loading was implemented through existing Matlab tools with the addition of a safety factor of 3 to ensure the survival of the node under extreme conditions.

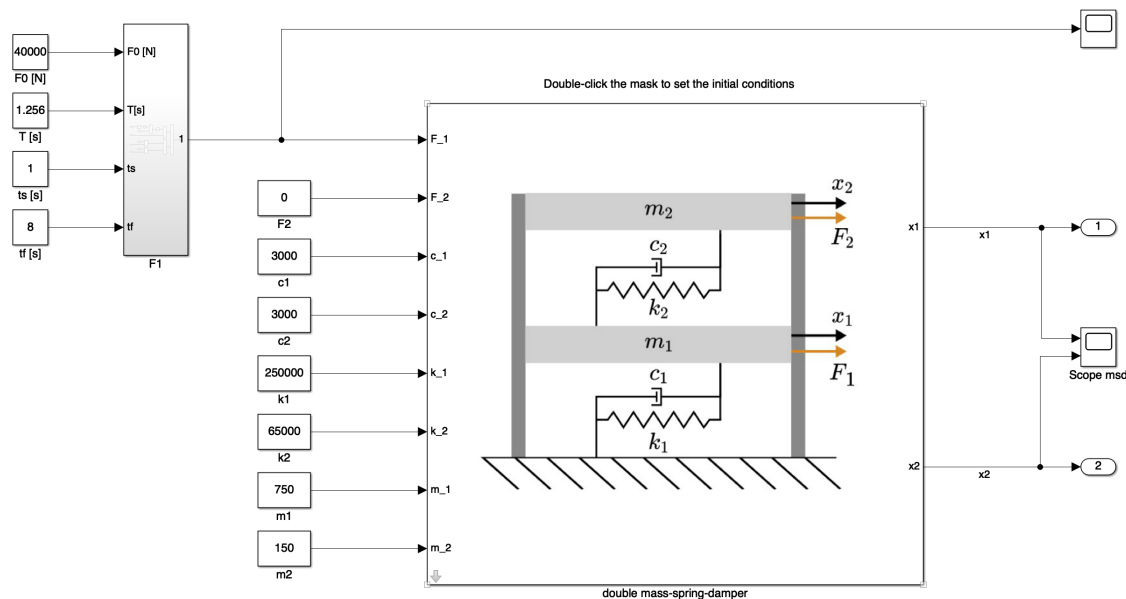


Figure 5.34: Illustration of Simulink model

From the aforementioned it was possible to assess the response of the system under a range of spring constants and dampener ratios. After several iterations, an acceptable response to the earthquake was reached, with displacements that do not exceed 24 [cm] during the earthquake and are negligible to the system 1 second after the earthquake ceases. The response is modelled as follows:

This desired response is achieved by using two springs, of 250 [kN/m] and 65 [kN/m] for k_1 and k_2 respectively and 3000 [Ns/m] for both dampeners. The springs and dampers that will be used for the ECN and the optical bench are both Koni Coil-over suspensions⁷⁹. They have chosen because they are the industry standard. The ECN housing will have a separate kit than the optical bench and both

⁷⁹<https://www.koni.com/en-US/Cars/Products/Sport-Tuning/Coil-Over/>

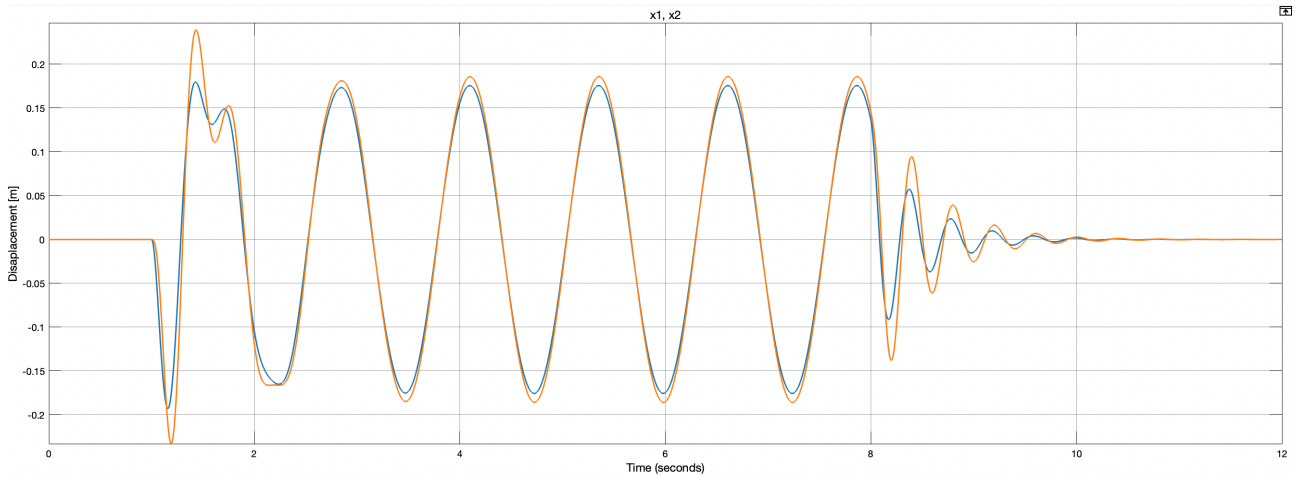


Figure 5.35: Earthquake Response

will tailor made by KONI. Each kit will cost around 2000 Euros⁸⁰. The CAD drawing of the damper system can be seen in figure 5.36.



Figure 5.36: KONI Coil over dampers.

5.7.4. Wind Response

In order to assess the effect of wind loads, an approximation of the wind loads acting on the ECN is approximated. Based on the requirement ECN-B-SAR-5-2, ECN should be able to survive wind speeds of up to 55 [m/s]. Two main categories of wind are analysed in this section. First, a constant wind blowing against the node is analysed and second response to wind gusts is analysed.

Constant Wind

When constant air is blowing against the node, a force acts on the node which the spring-damper system should be able to dampen out. When air with velocity V [m/s], is blowing, the force acting on the node can be calculated by using equation 5.25:

$$F = C_D \frac{1}{2} \rho V^2 S \quad (5.25)$$

where, C_D is the drag coefficient, ρ is the density of air at the current altitude, V is the velocity of flowing air and S is the surface area on which the wind is blowing against. table 5.18 shows the values of all the variables stated above.

⁸⁰<https://www.uspmotorsports.com/Koni-Coil-Over-Suspension-Kit-11505057.html>

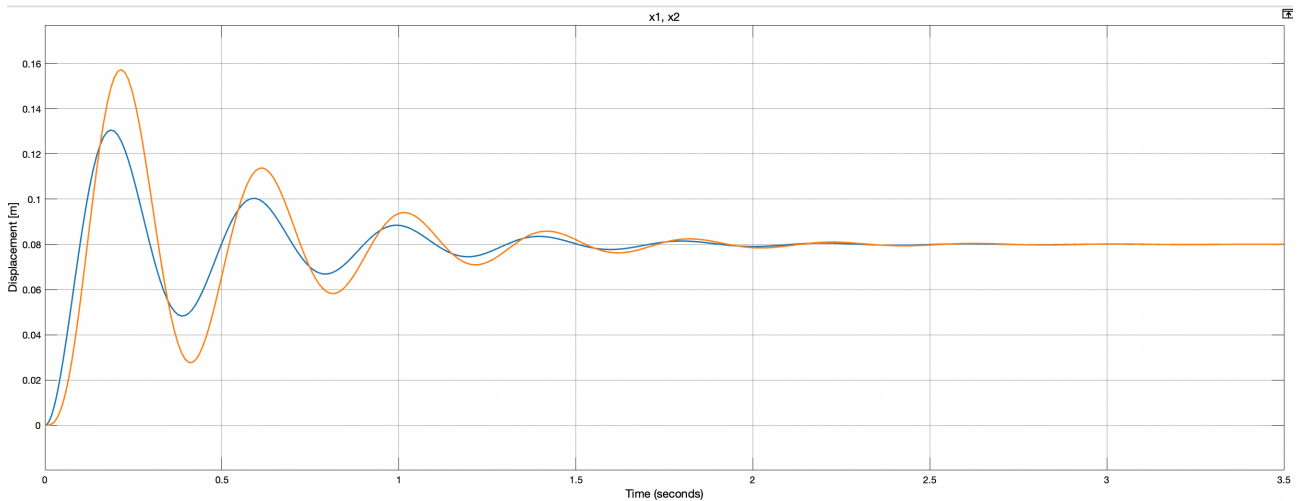


Figure 5.37: Response to constant wind.

Table 5.18: Values of the variables used to calculate the force exerted by wind on the ECN.

Parameter	Value
C_D	0.8 to 1.05 [68]
ρ	1.225 [kg/m^3]
V	55 [m/s]
S	3 [m^2]

Based on the values stated above, F comes out to be 6558 [N]. The value of force is increased by a safety factor of 3 and hence becomes 19676 [N] which is rounded off to 20000 [N] for analysis.

The response of the system is observed with inputs as described in the above paragraph. After several iterations, the response to wind gusts was finalised which can be seen in figure 5.37. As can be seen the displacements do not exceed 18 [cm] after the wind gust. All the vibrations induced due to the gust die out in 4.2 [s]. The system is using two springs, of 250 [kN/m] and 65 [kN/m] for k_1 and k_2 respectively and 3000 [Ns/m] for both dampeners and is discussed in subsection 5.7.3.

Wind Gust

Wind gusts are sudden bursts of wind and are more prone to cause damage as compared to normally normal wind. To be called a wind gust, the brief increase in wind velocity has to be over 18 mph and must be at least 10 mph faster than the average wind speed⁸¹. Based on this, the wind speed on which the calculations for the force imparted by wind is increased to 60 [m/s] from 55 [m/s] which gives a force on 7805 [N] acting on the ECN. In order to analyse the response of this force due to wind gust, it is multiplied by a safety factor of 3 resulting in a force of around 23500 [N]. The time duration for a wind gust is generally 0.5 [s] and hence in order to simulate wind gust on the node, a force of 23500 [N] is input for 0.5 seconds.

The response of the system is observed with inputs as described in the above paragraph. After several iterations, the response to wind gusts was finalised which can be seen in figure 5.38. It can be seen the displacements do not exceed 18 [cm] after the wind gust and all the vibrations induced due to the gust die out in 4.2 [s]. The system is using two springs, of 250 [kN/m] and 65 [kN/m] for k_1 and k_2 respectively and 3000 [Ns/m] for both dampeners and is discussed in subsection 5.7.3.

⁸¹<https://www.ny1.com/nyc/all-boroughs/weather/2020/08/07/all-wind-is-not-created-equal>

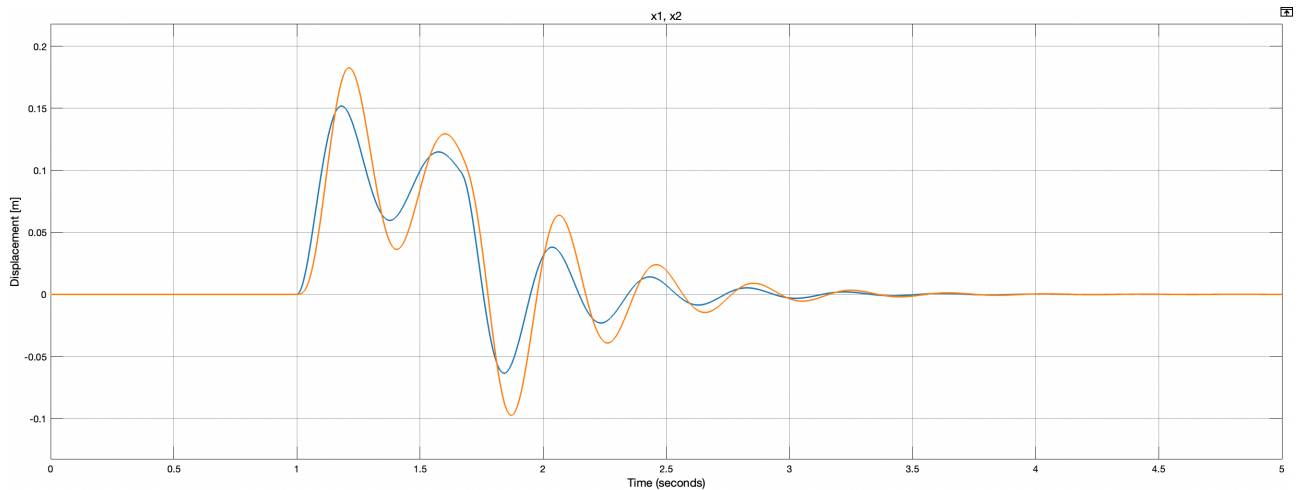


Figure 5.38: Wind Gust response

5.7.5. Accidental Drops

Accidental drops have to be analysed for frequency analysis because they are a risk and the node has to be designed in order to sustain the impact force when dropped accidentally. It is assumed that the node is most susceptible to accidental drops while loading or unloading. As a result of this assumption, the height for the drop is taken to be 5 [m]. This height has been for the worst case scenario in case of loading and unloading in a truck is around 1.75 [m]. This when multiplied by the safety factor leads to 5.25 [m] which is rounded down to 5. The average height figure 5.39 below shows a drawing explaining the drop.

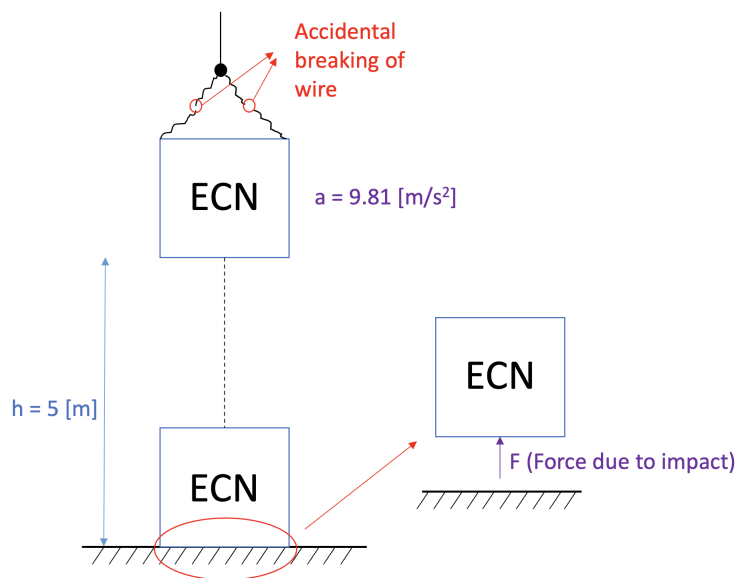


Figure 5.39: Accidental dropping of the ECN

The force acting on the ECN after it hits the ground can be calculated using simple equations from dynamics. Assuming the velocity of the node is zero when it starts falling, the velocity of the block at the end of the fall and just before hitting the ground is calculated using $v = \sqrt{2gh}$. Upon hitting the ground, the block is brought to zero velocity in a very short time which is taken to be 0.5 [s]. Using the second law of motion, the force on imparted on the block is the calculated using equation 5.26 which becomes 19805 [N].

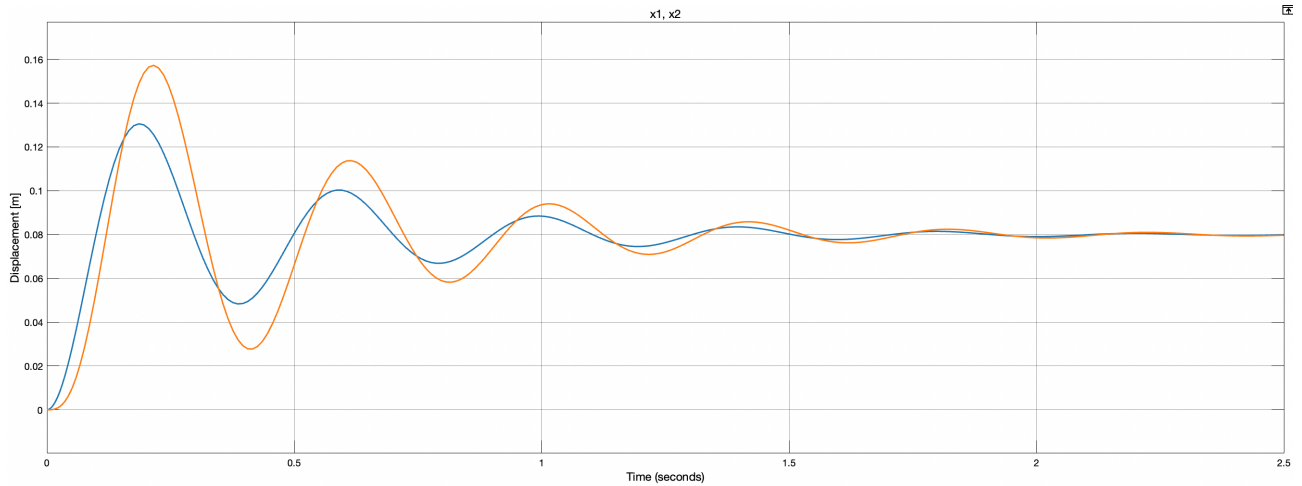


Figure 5.40: Accidental drop response

$$F = \frac{m\Delta v}{\Delta t} \implies \frac{m\sqrt{2gh}}{0.5} \quad (5.26)$$

For frequency analysis, the force on the node is approximated to be 20000 [N]. The response of the system is observed with inputs as described in the above paragraph. After several iterations, the response to wind gusts was finalised and can be found in figure 5.38. As can be seen in figure 5.40 the displacements do not exceed 15 [cm] after the wind gust. All the vibrations induced due to the gust die out in 2.5 [s]. The system is using two springs, of 250 [kN/m] and 65 [kN/m] for k1 and k2 respectively and 3000 [Ns/m] for both dampeners and is discussed in subsection 5.7.3.

5.7.6. Transportation Loads

Transportation loads include all the forces that the ECN will encounter while being transported from one point to another. This includes loads encountered while transport via road, air and water modes. These loads are characterised by periodic functions having low amplitude and high frequency. To analyse the loads faced by the node while transportation, first the different types of road profiles are identified based on ISO 8608.

ISO 8608 mentions fundamental concepts such as spatial frequency, road profile and PSD (Power Spectral Density). Based on these values different road profiles can be modelled with a combination of longer and shorter periodic bumps with different amplitudes. Using this road profiles are classified into different classes based on the maximum height of bumps on the road. The road surface profile can be varied from very good ISO A-B class, with $h_{max}=\pm 15$ [mm]), to good (ISO B-C class, with $h_{max}=\pm 25$ [mm]), average (ISO C-D class, with $h_{max}=\pm 50$ [mm]), and poor (ISO D-E class, with $h_{max}=\pm 100$ [mm]). The generated road profiles can be seen in figure 5.41 and are taken from [69].

Based on the load profiles generated, dynamic loads on different vehicle types are calculated based on which an approximation of the load faced by the ECN can be formulated. The frequency of the loads acting is around 4 [Hz] and the dynamic load acting on the vehicle is around 2500 [N] for the road profile ISO B-C [69]. Based on this the transportation load on the ECN is modelled as equation 5.27.

$$F = 2500\sin(4t) \quad (5.27)$$

Once the force is finalised, it is input into the model and the response of the system is analysed. As can be seen in figure 5.42 the displacements do not exceed 1 [cm] after the loads while transporting

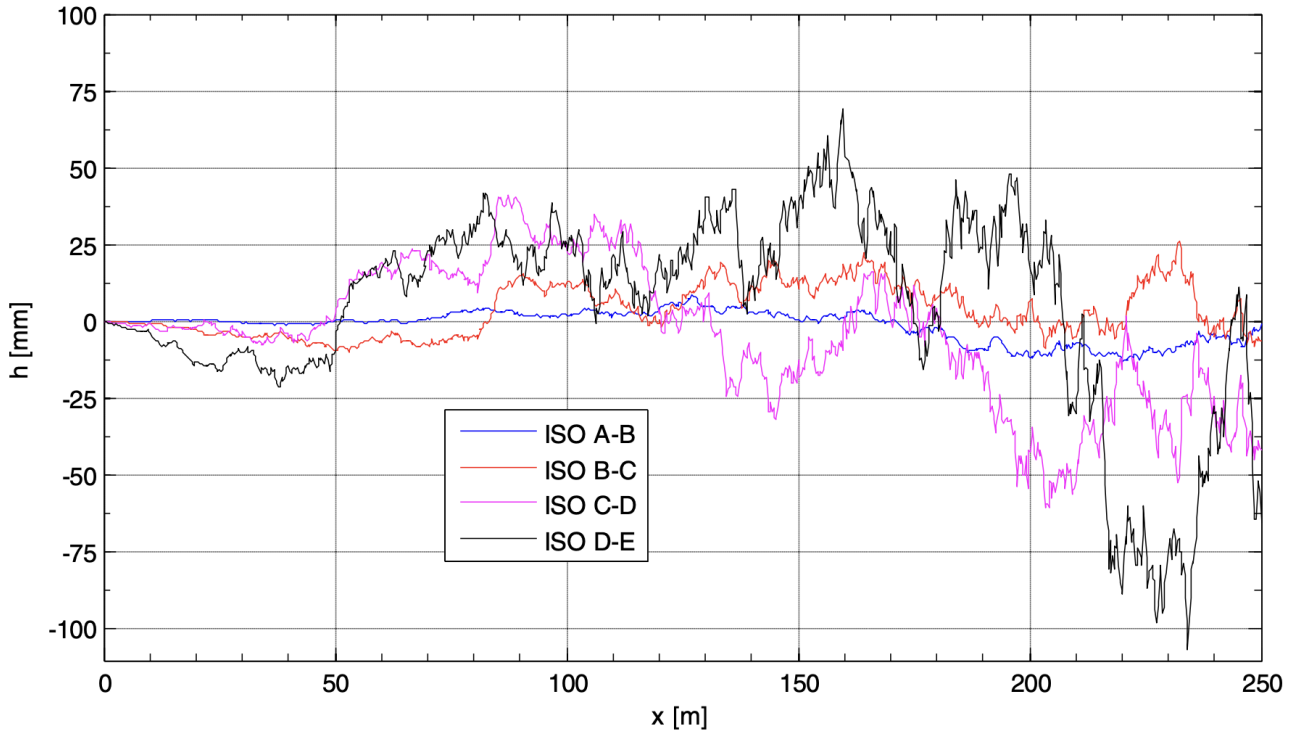


Figure 5.41: Road profiles generated for A-B, B-C, C-D and D-E ISO classes [69].

are applied. All the vibrations induced due to the gust die out within 3 [s] after the load is removed. The system is using two springs, of 250 [kN/m] and 65 [kN/m] for k_1 and k_2 respectively and 3000 [Ns/m] for both dampeners and is discussed in subsection 5.7.3.

5.7.7. Snow

The snow loads are simply modelled as pressure forces on the node. This means that the weight of snow will impart a force directly onto the node in the vertical direction. As only the outer box is exposed, the forces are approximated on the same. Since the majority of the outer surface of the ECN is flat, flat roof snow loads are calculated based on the ASCE 7-10 [70].

Flat snow roof loads is calculated as shown in equation 5.28.

$$p_f = 0.7C_e C_T I_s p_g \quad (5.28)$$

where, p_f is the snow load [kN/m²], C_e is the Exposure factor, C_T is the thermal factor, I_s is the importance factor and p_g is the ground snow load. C_e has values in the range of 0.7 to 0.9 for fully exposed structures. Based on this, C_e is set as 0.8 which is the average of all the values. Since no external restrictions such as keeping the structure below freezing etc. are required, the value of C_T is taken to be 1. The importance factor or the snow importance factor I_s is used to determine all the environmental live loads (i.e., flood, wind, snow, and earthquake). Since the ECN is a structure that will be used in emergency conditions and is essential in times of disaster it comes under category IV based on which the value of I_s can be finalised to 1.2. According to [71], the average ground snow load in Europe is 1.5 [kN/m²]. Using all the values described in this paragraph, the snow load is 1.008 [kN/m²] which becomes 3.024 [kN/m²] using a safety factor of 3.

Assuming that snow will only accumulate on the top of the ECN, the area of the loading is 2.25 [m²]. Hence the total force due to snow becomes 6804 [N]. The response of the system is observed with inputs as described in the above paragraph. After several iterations, the response to snow loads was

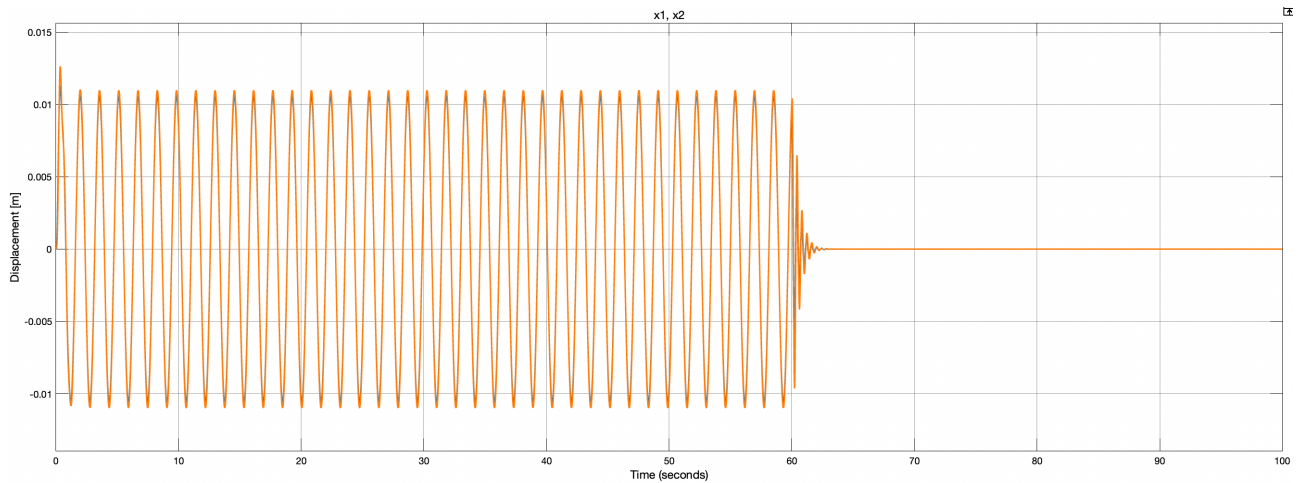


Figure 5.42: Response to transportation loads.

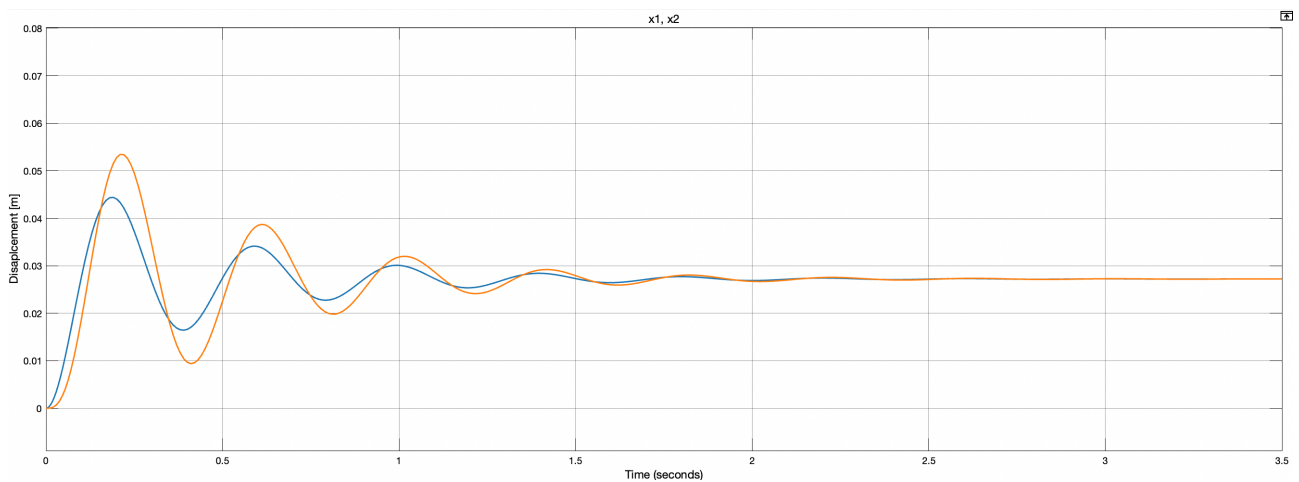


Figure 5.43: Response to snow loads.

finalised which can be seen in figure 5.43. It can be seen the displacements do not exceed 6 [cm] after the wind gust. All the vibrations induced due to the gust die out in 3 [s]. The system is using two springs, of 250 [kN/m] and 65 [kN/m] for k_1 and k_2 respectively and 3000 [Ns/m] for both dampeners and is discussed in subsection 5.7.3.

5.7.8. Further Extensions and Recommendations

The models analysed were 2 DOF systems with the horizontal and vertical systems decoupled and the earthquake modelled as a sine wave. This is just an approximation and brings in errors. A more concrete analysis can be performed with a 6 Degree Of Freedom system. This will give more insight into the rotational part of the movement and movement in the z direction of the node. This will be a better representation of the set of spring and dampener being installed and make the analysis more accurate.

The waves for earthquakes are currently modelled as simple sine waves. More accurate representations of earthquakes can be done with Rayleigh and Love waves as depicted in figure 5.44. Love waves roughly represent the horizontal movement and Rayleigh waves represent the lateral movement. In the current system, Love and Rayleigh waves are dealt independently and it is assumed that the two waves do not interact. Hence the rotational components are also not taken into account. The

accelerations and the movements will change if the system is coupled and is thus proposed to be built. Further improving on the model, a 12 degree of freedom model can be built, taking all the 3 dimensions into account.

The forcing function for the load cases are currently considered as continuous waves of certain frequency for earthquakes and as step function for gust loads. Realistically, the frequency in earthquakes differ and the gusts can act in a different manner bringing inaccuracies in the model. Data from seismographs and real world wind data could be used to further refine the forcing functions to make it more accurate.

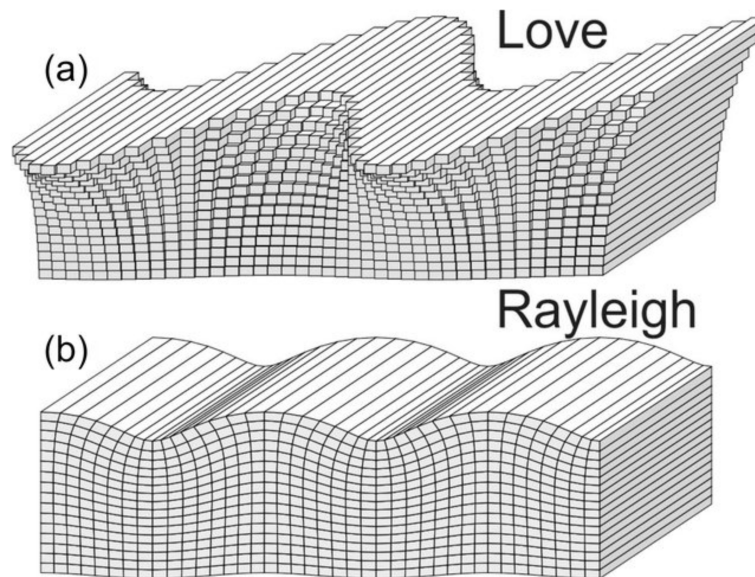


Figure 5.44: Raleigh and Love waves [72]

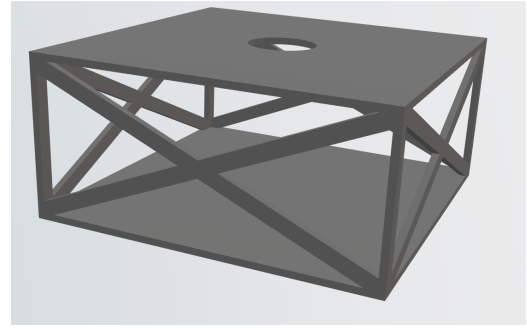
The current approach for reducing the loads into the structure is to dampen it, but technologies related to 'Minus K' may be looked at in the future which uses a pre-stretched spring to make the natural frequency of the system very close to zero such that the system will not vibrate. A major caveat now is that the spring has to be adjusted for specific frequencies and has to be tuned manually for the same as of now. As the current loading scenario takes multiple circumstances, such as transportation, earthquakes, wind etc, the use of 'Minus K' in the current scenario is not feasible but can be used at a later stage if the TRL reaches the required limit and off the shelf components are available.

5.8. Structural Design

For the structure to sustain the loads identified in section 5.7 a load bearing structure will be considered. Two structures are considered; a frame structure and a truss structure as shown in figure 5.45a and figure 5.45b respectively. The frame structure is preferred due to its simplicity and easy access to the inner part of the node. However, if it is found that the loads require the frame structure to become unreasonably big, a truss structure will be considered. To find out the dimensions of such a Finite-Element Analysis will be performed on the frame model. For the analysis, material properties of the beam are needed, which means a material must be selected. Since no major issues with both mass and stiffness requirements have been found up to this point, the material shall first be chosen, after which its performance in the frame structure is assessed.



(a) Simple frame structure



(b) Simple truss structure

Figure 5.45: Considered load bearing structures

5.8.1. Material Choice

With outline of the structural design discussed, a trade-off on material choice for the structure has been performed. There are many properties of materials that need to be weighted against each other. For material trade-off, an assumption is made that the structure must provide certain minimum stiffness S^* in tension and compression, found with the equation

$$S^* = \frac{AE}{L_0} \quad (5.29)$$

where A is cross sectional area of a member, L_0 is its given length, and E the Young modulus. Three objective functions have been selected to be minimized: mass m , cost C , and embodied energy H . The functions can be expressed in equations

$$m = AL_0\rho \quad (5.30)$$

$$C = C_m m = C_m AL_0\rho \quad (5.31)$$

$$H = H_m m = H_m AL_0\rho \quad (5.32)$$

Constraint introduced in equation 5.29 can be used to eliminate unknown variable A from equation 5.30, equation 5.31 and equation 5.32. Substituting $A = \frac{S^* L_0}{E}$

$$m = S^* L_0^2 \left(\frac{\rho}{E} \right) \quad (5.33)$$

$$C = S^* L_0^2 \left(\frac{C_m \rho}{E} \right) \quad (5.34)$$

$$H = S^* L_0^2 \left(\frac{H_m \rho}{E} \right) \quad (5.35)$$

This identifies three metrics that must be maximized for: mass metric $\frac{E}{\rho}$, cost metric $\frac{E}{C_m \rho}$, and sustainability metric $\frac{E}{H_m \rho}$.

Material Selection

Six materials have been selected for comparison: aluminium 5052, aluminium 6061, titanium alloy Ti-6Al-4V, high-strength low alloy steel, used extensively in automotive industry, CFRP, and GFRP.

Mechanical properties were calculated using values from online database of engineering material properties⁸² and Performance Composites⁸³ table (for CFRP and GFRP), unless specified otherwise.

Table 5.19: Material comparison table

Material	Mass metric ($\frac{E}{\rho}$) [MPa m ³ /kg]	Cost metric ($\frac{E}{C_m \rho}$) [MPa m ³ /\\$]	Sustainability metric ($\frac{E}{H_m \rho}$) [MPa m ³ /MJ]
Aluminium 5052	25.2	8.68	0.168
Aluminium 6061	25.6	8.81 ⁸⁴	0.170
Ti-6Al-4V	25.0	5.21 ⁸⁵	0.041
Low Alloy Steel	24.3	22.3	0.870
CFRP	43.8	2.92 [73]	0.187 [74]
GFRP	13.2	3.37 ⁸⁶	0.585 [74]

Thermal Considerations

All structures are subject to alteration of some physical properties, such as volume or shape, under changing temperature, depending on the material choice. The material choice also determine thermal conductivity and influence temperature across the structure. A list of some thermal characteristics has been compiled in table 5.20. The sources are database of engineering material properties⁸² and Massachusetts Institute of Technology Mechanics of Materials⁸⁶, unless indicated otherwise.

Table 5.20: Material thermal properties table

Material	Thermal expansion [$\mu\text{m}/(\text{m K})$]	Thermal conductivity [W/(m K)]
Aluminium 5052	24	140
Aluminium 6061	24	170
Ti-6Al-4V	8.9	6.8
Low Alloy Steel	11	42
CFRP	12	0.65 ⁸⁷
GFRP	19	0.04 ⁸⁸

Thermal conductivity has been deemed of less importance, since an insulation material can be applied to any material performing best as far as structural integrity or sustainability is concerned, easily allowing to tweak the thermal conductivity value of the structure to desired level. It is however preferable to have a material with lower thermal expansion, hence the property will determine thermal score in the trade-off.

Material Trade-off

The materials were evaluated on the following grounds: mass metric, cost metric, sustainability, which compromises of sustainability metric and recyclability considerations, thermal score (explained above), and manufacturability, which scored range of available manufacturing methods and manufacturing cost. The weights assigned were: 10%, 20%, 30%, 10%, and 30%. Sustainability and man-

⁸²<https://www.makeitfrom.com/>

⁸³http://www.performance-composites.com/carbonfibre/mechanicalproperties_2.asp

⁸⁴<https://www.navstarsteel.com/6061-t6-aluminium-plate.html>

⁸⁵<https://www.metalarly.com/titanium-price/>

⁸⁶<https://web.mit.edu/course/3/3.11/www/modules/props.pdf>

⁸⁷https://www.christinedemerchant.com/carbon_characteristics_heat_conductivity.html

⁸⁸<http://hyperphysics.phy-astr.gsu.edu/hbase/Tables/thrcn.html>

ufacturability were the two most important metrics, followed by cost, and finally thermal and mass performance. Outcome of the trade-off was presented in table 5.21.

Table 5.21: Material trade-off

Criteria weight	10%	20%	30%	10%	30%	
Criteria	Mass	Cost	Sustainability	Thermal	Manufacturability	Total Score
Al 5052	3	3	5	2	5	4.10
Al 6061	3	3	5	2	5	4.10
Ti-6Al-4V	3	2.5	1	5	2	2.20
HSLA	2.5	5	4	4	4	4.05
CFRP	5	1	3	4	3	2.90
GFRP	1	2	3	3	3	2.60

Aluminium scored highest on sustainability metric because of its exceptional recyclability. While High-strength Low Alloy steel scored higher on embodied energy comparison, it has a lower sustainability score. The result is Aluminium being the best choice for ECN truss structure. Though the two options, 5052 and 6061, scored the same in trade-off, due to their very similar performance, 6061 had slightly highest score in material property metrics presented in table 5.19. Aluminium 6061 is therefore the selected option.

Sensitivity Analysis

The numerical decision model used in the trade-off was verified using sensitivity analysis, and presented in figure 5.46. It shows HSLA as a highly competitive alternative, and supports the argument for discarding titanium and composites. The fact that HSL comes so close is mostly due to the thermal performance of the material. However, Aluminium, with excellent sustainability and manufacturability performance, is still preferred by the numerical decision model, though the achieved results are almost the same. For the rest of this report, analysis is performed with an assumption of Al 6061 being the primary, and only material used in the structure.

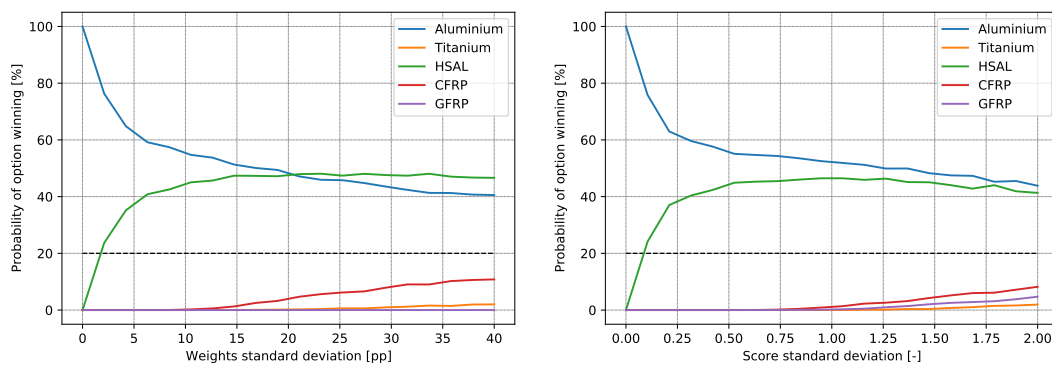


Figure 5.46: Material selection sensitivity analysis

Inclusion of thermal metric makes HSLA an even more appealing choice, however, Aluminium, with excellent sustainability and manufacturability performance, is still preferred by the numerical decision model, though the achieved results are almost the same. For the future work, it is recommended that a combination of Al 6061 and HSAL is considered for the more temperature sensitive sections of the structure which could influence pointing performance such as the area around the gimbal. This needs further consideration and an additional trade-off to be performed, given that mass metric might also be of higher performance. For the rest of this report, analysis is performed with an

assumption of Al 6061 being the primary, and only material used in the structure. A more elaborate analysis including different materials and joint performance of combination of thereof must be considered for the detail design.

5.8.2. Layout

To make the layout of the node Catia models were made of each subsystem with their estimated dimensions, then those were combined to fit into a rectangular box. It was found that a box with $1.5 \times 1.5 \times 0.6 \text{ m}^3$ ($l \times w \times h$) fit the node best. A render of the layout can be found in figure 5.47. As discussed in section 5.7, it was identified that the optical bench and gimbal system should be isolated, so to accomodate for this it is connected to the rest of the box using dampers. Since the batteries take up a lot of space and will require significant thermal management as will be discussed in section 5.9, it was decided to shape the basic battery as a thin layer on the bottom of the node. Above it the main battery for the 48 hour undisturbed functioning of the node is stored. Since the optical bench and gimbal are directly connected they are above for easy access of the optical path. For the power distribution 2 power distribution units (PDU) are stacked together on a rack together with the workbench which will control all the systems. To allow for interaction with the node such as turning it on and off and controlling its settings a screen is added to the side of the box. As discussed in section 5.9 the cooling system will require an extension outside of the box which will have to be considered in the structure.

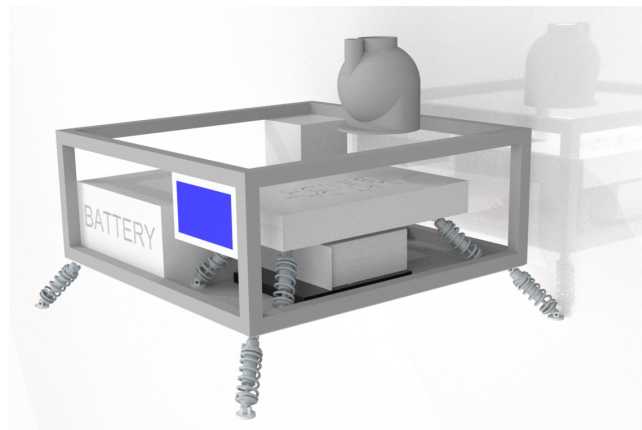


Figure 5.47: Current layout of the ECN

The addition of the gimbal would mean the height is approximately 1 [m] as shown in figure 5.20. The dampeners still have to be fully sized but will definitely keep the total height below the 2 [m] set by the operational limits. The location of the dampening elements might have to be adjusted depending on the width to stay within the 2 [m] but this not expected to be a problem. This means that with the current layout the node is able to fit in the best possible transportation possibilities defined in chapter 4.

5.8.3. Frame Analysis

To analyse the frame structure a FEM analysis was conducted with the Linear Structural Validation module of 3DEXperience. As a first-order estimation, each truss in the frame was modelled as an element. Additionally, the bottom corners of the frame are considered to be simply supported. The two critical forces identified in section 5.7 are the wind load and earthquake load. For the wind load, a static stress simulation will be performed to estimate and find the required thickness.

The wind load will be modelled as if it acts perpendicular to one of the faces of the frame. It is assumed that this is evenly spread over the surface area of the relevant face and that the 4 bottom nodes

of the frame are simply supported. To optimise the required thickness it is varied in the simulation until the maximum stress experienced is at 3 times as low as the yield stress of Aluminium 6061 of 276 [MPa] . In figure 5.48 the results of this analysis can be found after optimisation of the thickness for the wind load of 7000 [N] determined in section 5.7. It should be noted that the deformations are scaled by 9.6 times for clarity. For choosing the thickness a safety factor with the yield stress of 3 is considered. The found optimal thickness is 3 [cm] at which the minimum safety factor in the structure is 3.08 as shown in figure 5.48b.

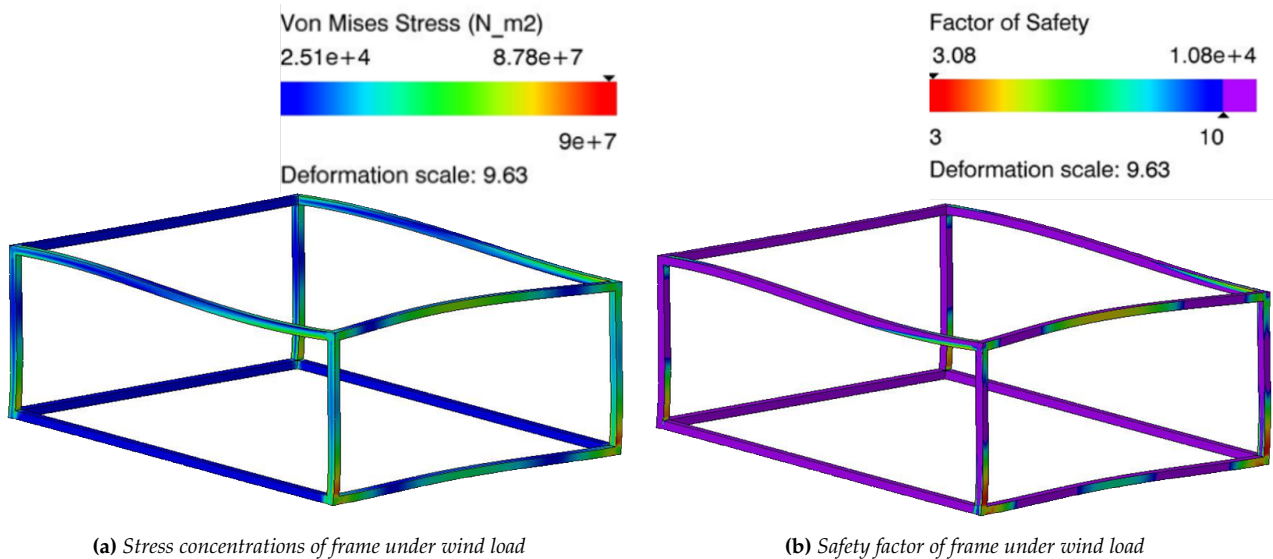


Figure 5.48: Results of the FEM analysis on the frame structure

5.8.4. Discussion

In section 5.7 the earthquake loads were also identified as critical loads, however, since it is a forcing function as shown in equation 5.7.2 it is deemed that it cannot be accurately modelled as a simple point load. The combination of frequency and amplitude greatly influences the structural stability of the node and that cannot be encompassed with point loads.

A vibrational analysis would be one of the first things that have to be done in the future design phase to assure the structure can survive. At this point, the thickness of 3 [cm] is deemed acceptable as it easily fits the structure while providing no issues for the layout shown in figure 5.47. If the vibrational analysis would change the thickness to a more unacceptable extent, the analysis should be reconsidered and it is recommended to investigate the use the more stiff truss structure to optimise the thickness if necessary.

The assumptions made also have an influence on this sizing. For example, in reality the bottom part of the box is not simply supported but connected to dampening legs which are not rigidly connected to the ground. This means that in reality, the deformations at the base of the frame will be less severe since the dampening legs can deform with it. This seems to be supported by figure 5.48 where the highest stresses occur near the simply supported nodes. This means that the sizing currently done is conservative and is a point that can be optimised in the following design phases. Since the corners are still partially supported by the legs it is deemed that there will most likely be a high stress concentration there compared to the rest of the structure. When detailing the design of the connection between the dampers and frame this must be taken into consideration. Another currently missing consideration is the addition of skin. There should be special attention paid to potential buckling or failure occurring in the skin and if required stiffening elements must be added.

5.8.5. Structure Verification and Validation

Verification

To verify the structural model, sanity checks are used to check whether the stresses make sense with the applied forces. Of special interest is the compression and tension of different components which for simple structures and loads are predictable. For instance, the structure shown in figure 5.48a experiences an inward force from the wind, causing the structure to bend inwards, which does make sense logically hence the analysis passes this sanity check. Similar checks were performed for loads from the top, bottom and other sides and were passed. In a similar fashion, the compression and tension modes were verified. The linear structural validation module allows for checking for each stress in the frame whether it is in compression or tension which was done for a variety of forces, confirming it to work. For example, in the wind load case, the beams perpendicular to the face to which the load is applied were in compression as expected. Lastly, the simply supported boundary conditions were checked by analysing the movement of the nodes and attached beams in the model. It was found that the corner nodes do not move, as should be expected and that the connected beams move properly. For example, as shown in figure 5.48a the beams on the face opposite of the wind load do not move which makes sense since the force can never be there since the nodes will not budge. The face of the wind load on the other hand shows that a beam between two bottom nodes can still bend which is precisely the expected behaviour for a simply supported beam.

Validation

More complicated FEM models must be constructed with more accurate loadings in combination with the skin to more accurately model all deformations. Especially a model in which the dampener and structure are combined must be considered to account for the discrepancies discussed above. At the same time, an aerodynamic analysis must also be performed to find out the exact loadings during high wind conditions and loads induced by snow should be considered. To account for worst-case conditions the wind loading, snow loading and vibration loading should be combined to ensure structural safety. For sustainability considerations, the housing should preferably not be produced for testing and FEM models should be mostly used. However, since structural failure means failure of the entire system it is deemed necessary to at some point produce and test a structural model to validate that it can sustain the structural loads, thermal loads and earthquake vibrations. This must occur only after the aerodynamic models, damper integration and skin integration has been concluded with FEM models to avoid making many test frames.

After it has been validated that the skin with the frame can sustain the loads, different subsystem components should be added to assure that the entire structure is able to sustain harsh conditions. Especially the connections to the frame must be assured to work. This would include putting the entire structure on a shaker and exposing it to extreme temperatures.

5.8.6. Sustainability

Due to the limited requirements on mass and volume, more emphasis could be set on the sustainability of the structure. This can be found in the chosen material which had the highest sustainability that could be found. Additionally, the simple box shape of the housing makes the modularity of the subsystems relatively easy. For example, the batteries can easily be replaced when they reach their end of life or better options are developed. Additionally, the entire optical bench can easily be removed due to its modular design in the layout making it easy to replace individual components or upgrade them.

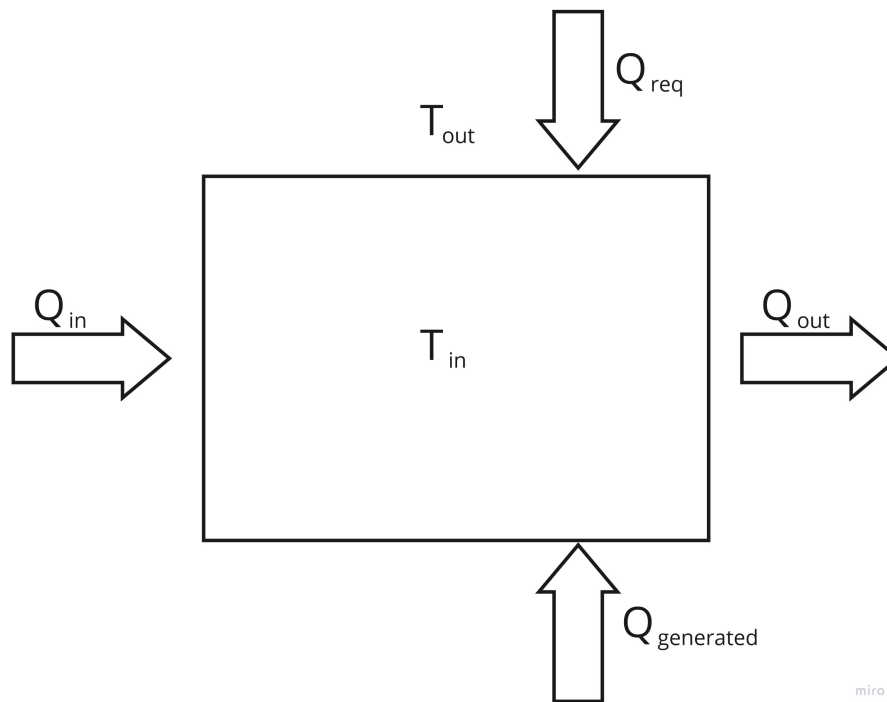


Figure 5.49: Heat balance of system

5.9. Thermal Management

A thermal analysis is relevant for the design of the node since a limiting temperature range is imposed by the use of electronics, which does not align with the operational temperature envelope. Generic electronics have a temperature range of 0 [°C] up unto 70 [°C], while some components impose an even smaller range (40 [°C] as upper bound) [75]. Furthermore batteries are used, which impose an ever smaller temperature range for operations from about 10 [°C] to 30 [°C] [76].

The node temperature envelope for survival conditions ranges from -50 [°C] to 60 [°C], and the operational envelope ranges from -30 [°C] to 40 [°C]. Since the temperature limitations are within the operation envelope, thermal management is required. In addition, some components such as the laser, produce relatively much heat locally, requiring a solution to dispose or distribute this heat.

The goal of the battery TMS is to maintain a temperature range of 10 to 30 [°C] for both operation as well as survival conditions. This achieved by insulating the system and integrating a heating and cooling type of system.

The purpose of the node TMS is to maintain a temperature range of -5 [°C] to 40 [°C] during operations. During survival the inside temperature of the node is of less importance, and the battery TMS is given priority.

5.9.1. Thermodynamic Analysis of Node

To satisfy the temperature needs of all components inside of the node, a simplified thermal analysis of the node and its components is performed. Two systems are considered for the analysis. The entire node, and the battery pack. For both systems a heat balance is evaluated for all heat flowing in and out of the system, as can be seen in figure 5.49. The output of the analysis should be the power required for cooling and heating such that the thermal management system can be sized. Several Assumptions are made to simplify the analysis and listed below.

- Worst case scenario for power consumption inside node (500 [W]). All power is transferred into heat.
- Outer wall is constructed out of aluminium of a thickness in the order of millimeters. It is thus assumed to have negligible contribution to the conductivity of the wall, therefore only isolating material is considered⁸⁴.
- Only sun radiation heat flowing in the system, no albedo and IR radiation.
- The temperature of the system is uniformly distributed and the wall has a temperature equal to the outside temperature.
- Steady-state conditions.
- The outer walls of the node are covered with magnesium oxide paint to minimise the emissivity of the node.
- The solar irradiance is assumed to be 1000 [W/m²].

Methodology of Analysis

For each system, a heat balance is used to calculate the required power input to the system to maintain a set inside temperature for a given outside temperature. The outside temperature is varied from the minimum to the maximum value in steps of 5 [°C]. For each outside temperature an ideal inside temperature is calculated such that equilibrium is reached without adding or subtracting heat. If this obtained required temperature is above or below the temperature limits, the limits are taken. The analysis then proceeds to show the required power. By modifying the input parameters of the program, such as isolation thickness and conduction constant of the isolation material, minimum values for the required power are obtained. For the node analysis both a sunny day as well as night are considered.

Results of Analysis

For the battery TMS, a 30 [W] cooling and heating capacity is required if the node TMS is active and the inside temperature of the node is maintained between 0 and 40 [°C]. When the node TMS is inactive (survival conditions) a 175 [W] heating and 90 [W] cooling capacity is required. For the node TMS, the required capacity is highly dependent on sunlight conditions. Upper bounds for operating conditions are found for no sunlight and -30 [°C] outside temperature, where 250 [W] of heating capacity is required. For 40 [°C] in direct sunlight, a cooling capacity of 280 [W] is required. However, when the outside temperature of the surroundings does not exceed the range of -20 [°C] and 30 [°C], a heating capacity of about 4 [W] is required.

5.9.2. Thermal Management System

With the results of the thermal analysis the components of both TMS's can be selected. Both systems will use a coupled cooling system, where there is one cooling unit which both systems can utilise. The main advantage of coupling the system is the decrease in system complexity and cost. An overview of the both thermal management systems is shown in figure 5.50.

Battery TMS

First of all the battery is packed in between 50 [mm] of ArmaFlex insulation material to provide resistance against heat flow from the battery to the surroundings and the other way around. ArmaFlex is selected for its wide availability, low cost and excellent moisture properties. To thermally manage the battery two cooling plates are added between the battery and the insulation material, where cooling

⁸⁴https://www.engineeringtoolbox.com/thermal-conductivity-metals-d_858.html

Table 5.22: Thermal analysis of the battery

T_{amb} [°C]	T_{bat} [°C]	T_{opt} [°C]	P_{req} [W]
-50	10	10	172.08
-45	30	10	157.68
-40		10	143.28
-35		10	128.88
-30		10	114.48
-25		10	100.08
-20		10	85.68
-15		10	71.28
-10		10	56.88
-5		10	42.48
0		10	28.08
5		10	13.68
10		10	-0.72
15		15	-0.72
20		20	-0.72
25		25	-0.72
30		30	-0.72
35		30	-15.12
40		30	-29.52
45		30	-43.92
50		30	-58.32
55		30	-72.72
60		30	-87.12

Table 5.23: Thermal analysis of the node

Temperature Limits T_{out} [°C]	SUNLIGHT			NO SUNLIGHT		
	T_{amb} [°C] ($P_{req}=0$)	T_{amb} [°C] (Optimum)	P_{req} [W]	T_{amb} [°C] ($P_{req}=0$)	T_{amb} [°C] (optimal)	P_{req} [W]
-50	-31.85	-5.00	1,108.74	-37.21	-5.00	1,333.74
-45	-26.83	-5.00	901.71	-32.21	-5.00	1,126.71
-40	-21.81	-5.00	694.68	-27.21	-5.00	919.68
-35	-16.80	-5.00	487.65	-22.21	-5.00	712.65
-30	-11.79	-5.00	280.62	-17.21	-5.00	505.62
-25	-6.78	-5.00	73.59	-12.21	-5.00	298.59
-20	-1.78	-1.78	-0.08	-7.21	-5.00	91.56
-15	3.22	3.22	-0.03	-2.21	-2.21	0.00
-10	8.22	8.22	0.00	2.79	2.79	0.00
-5	13.22	13.22	0.02	7.79	7.79	0.00
0	18.22	18.22	0.06	12.79	12.79	0.01
5	23.22	23.22	0.15	17.79	17.79	0.05
10	28.22	28.22	0.32	22.79	22.79	0.14
15	33.22	33.22	0.60	27.79	27.79	0.30
20	38.22	38.22	1.01	32.79	32.79	0.59
25	43.22	43.22	1.58	37.79	37.79	1.04
30	48.21	48.21	2.34	42.79	42.79	1.71
35	53.20	53.20	3.32	47.79	47.79	2.66
40	58.19	55.00	-128.77	52.79	52.79	3.96
45	63.17	55.00	-335.80	57.79	55.00	-110.80
50	68.15	55.00	-542.83	62.79	55.00	-317.83
55	73.11	55.00	-749.85	67.79	55.00	-524.85
60	78.06	55.00	-956.88	72.79	55.00	-731.88

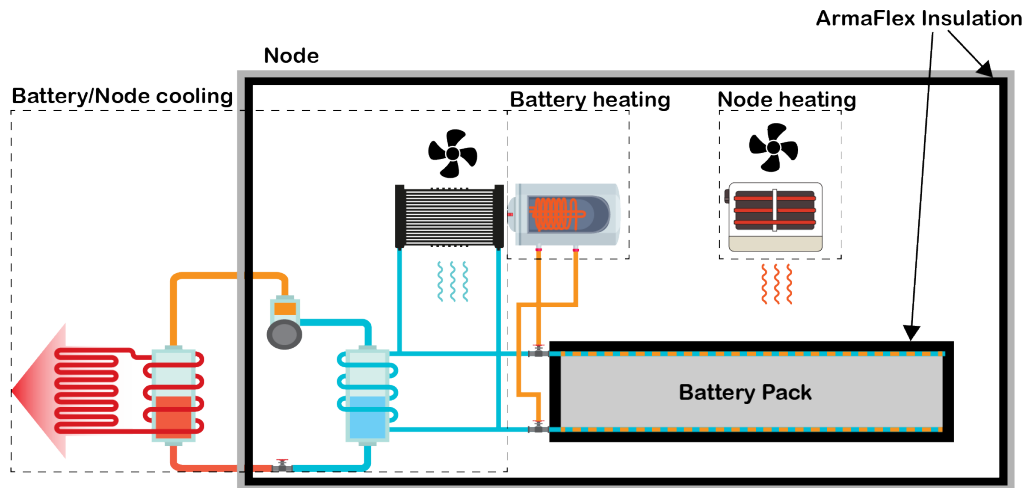


Figure 5.50: Overview of thermal management system

channels are routed along the surface of the cooling plate to cool or heat the battery cells by conduction. In this way all individual cells are managed equally, avoiding large temperature gradients between cells. This method positively influences battery performance and safety [77]. An electric heat pump is added to the system to heat the battery pack when required. This is coupled with the existing system of lines and plates as the cooling system uses.

For the extra battery pack, for the thermal analysis it is assumed to be in the same thermally managed system as the basic battery pack. The additional surface area increases by a small fraction and is thus neglected. The extra heat introduced in the system by the battery is of importance, thus extra cooling capacity is required. However, extra cooling capacity is already available from the over designed cooling unit, which cools both the node as the battery. The extra battery pack can thus be connected to the existing infrastructure.

Node TMS

Similar to the battery TMS the inside of the node is isolated using 9 [mm] ArmaFlex insulation. The node is thermally managed by using convection inside the node. Air is heated or cooled using an electric heater or a heat exchanger, which in turn heats or cools the node and its components. The cooling system is placed outside of the node, which deposits the heat from inside of the node to the surroundings. A fan is used to provide airflow along the heat exchanger and the electric heater for convection heating and cooling.

5.9.3. Verification and Validation

For this stage of the design it is desirable for the thermal simulation to estimate the properties of the TMS within a 50 % to 150% range. The accuracy is thus of less importance, it is merely used as a tool to see the effect of altering certain design parameters such as insulation material, thickness and power input. The required power for the system is thus assumed to be underestimated, and a system with a larger power rating is chosen.

Verification

As stated above the thermal simulation is quite preliminary and lacking in completeness. The relevant assumptions are listed above. A relevant technique to verify the simulation of thermal analysis would be to use an actual numerical model together with thermal analysis software such as Ansys⁸⁵. To be able to perform a unit and subsystem test for the thermal management system, several aspects

⁸⁵<https://www.ansys.com/applications/battery/pack-and-module-thermal-management>

have to be defined. First and foremost, two control temperatures were defined, namely an upper limit of 55 [°C] and a lower limit of -5 [°C]. Using this, two main cases were analysed: when sunlight is present and when it is not.

For the case when sunlight is present, three variables can be calculated and tested one by one to verify that the result is correct, or if it falls within acceptable boundaries. The first aspect that can be unit tested is the ambient temperature when there is no required power, which is calculated using equation 5.36.

$$T_{amb}|_{P_{req}=0} = \frac{t}{k \cdot A} (P_{heat} + a_s \cdot J_s \cdot A_i - e_{IR} \cdot \sigma \cdot A \cdot T_{out}^4) + T_{out} \quad (5.36)$$

Next, the optimal ambient temperature is calculated using equation 5.37.

$$\begin{aligned} T_{amb,optimal} &= -5^\circ, & \text{if } T_{amb}|_{P_{req}=0} &\leq -5^\circ \\ T_{amb,optimal} &= 55^\circ, & \text{if } T_{amb}|_{P_{req}=0} &\geq 55^\circ \\ T_{amb,optimal} &= T_{amb}|_{P_{req}=0}, & \text{if } T_{amb}|_{P_{req}=0} &< 55^\circ \text{ and } T_{amb}|_{P_{req}=0} > -5^\circ \end{aligned} \quad (5.37)$$

Finally, the required power can be calculated using equation 5.38.

$$P_{req} = e_{IR} \cdot \sigma \cdot A \cdot T_{amb,optimal}^4 + k \cdot A \cdot \frac{T_{amb,optimal} - T_{out}}{t} - a_s \cdot J_s \cdot A_i - P_{heat} \quad (5.38)$$

When there is no sunlight, the ambient temperature when there is no power is calculated with equation 5.39.

$$T_{amb}|_{P_{req}=0} = \frac{t}{k \cdot A} \cdot P_{heat} + T_{out} \quad (5.39)$$

The optimal temperature is calculated with equation 5.40.

$$\begin{aligned} T_{amb,optimal} &= -5^\circ, & \text{if } T_{amb}|_{P_{req}=0} &\leq -5^\circ \\ T_{amb,optimal} &= 55^\circ, & \text{if } T_{amb}|_{P_{req}=0} &\geq 55^\circ \\ T_{amb,optimal} &= T_{amb}|_{P_{req}=0}, & \text{if } T_{amb}|_{P_{req}=0} &< 55^\circ \text{ and } T_{amb}|_{P_{req}=0} > -5^\circ \end{aligned} \quad (5.40)$$

Finally, the required power is calculated using equation 5.41.

$$P_{req} = e_{IR} \cdot \sigma \cdot A \cdot T_{amb,optimal}^4 + k \cdot A \cdot \frac{T_{amb,optimal} - T_{out}}{t} - P_{heat} \quad (5.41)$$

For both cases, the maximum power required gives the needed power for heating, while the minimum power required gives the power needed for cooling. All equations used above are taken from [78] and [79] and follow from a generic heat balance.

To properly verify the code, an analytical model should be created using the mentioned formulas. A unit test can then be performed for each calculation separately using the calculated values. This will give an insight into if the outputs of the code are as expected and if the formulas used are indeed correct. Another method to verify the outputs is to choose a temperature interval inside which the outputs should be present. If any of the outputs does not fall inside the interval, the code is then not functioning properly and should be adjusted.

Validation

The validation plan for the thermal analysis is as follows. The node shall be introduced to conditions in a lab setting equal to the conditions that apply outside. The node is left to achieve thermal equilibrium while monitoring and controlling relevant parameters such as temperature, solar flux and power consumed inside the node. This is performed for several ranges of solar intensity, outside

temperature and power consumption (operation or survival mode of the node have different power ratings). The resulting inside ambient temperature at the end of each measurement is used to compare the results to the simulation model. The simulation model is considered "valid" when the results from validation lie within 50% to 150%.

5.9.4. Sustainability of Thermal Management System

To achieve a sustainable design, one would like to reduce energy waste. The goal of the analysis of the thermal system is to find minimum heating or cooling capacity to reduce the size and cost of the thermal system. Using thermal insulation material provides resistance against heat flow, which decreases the energy lost. It is thus favourable to use insulation since it reduces the amount of power required to maintain a certain temperature.

The selection of the coolant and heating system is a different theme where sustainability plays a role. Cooling fluids often are a mix of water and an antifreeze solvent. One of the most commonly used antifreeze solvents is diethylene glycol, which poses a large health hazard. It has a LD50 value of 1 [mL/kg] (50 % of the population who receive this dose will die) [80]. Water has a high heat capacity and is thus an excellent coolant, it is also very sustainable. However, water has a limited temperature range. Using additives can alter the freezing and boiling point to make it more suitable for specific temperatures. The selection of the antifreeze will be left for future work, where a trade-off is to be performed regarding sustainability and performance.

5.9.5. Extensions

For future work, several aspects should be emphasized. For one, the heat generated by the battery is severely underestimated and must be accounted for. Thus research must be conducted to find a proper method to model the heat production of a lithium-ion battery when charging/discharging. The battery thermal analysis can be iterated with the renewed heat power of the battery. Furthermore, the analysis model should be detailed with the actual dimensions and shapes of the final design. The analysis is still preliminary and uses basic shapes and dimensions which allow for simplified calculations, yielding fast but not fully representative results. The influence of the structure of the node was neglected in the analysis due to the high thermal conductivity of aluminium, and should be included in the following analysis. The cut-out for the gimbal construction was also not accounted for. This means the required power calculated was underestimated as well. Also, it is recommended to analyse the final structure on thermal loads using a FEM model. The additional stresses and tolerances have not yet been accounted for and could potentially cause problems regarding the accuracy of the beam steering.

5.10. Electrical Power System

The chapter is about the Electrical Power System (EPS) for the ECN. There are three main components which are included in this chapter; the batteries are discussed in subsection 5.10.1, the voltage conversion is discussed in subsection 5.10.2 with power distribution system is discussed in subsection 5.10.3. The measure to take and taken to make the EPS sustainable is discussed in subsection 5.10.4 and the future prospects are discussed in subsection 5.10.5.

5.10.1. Batteries

The major part of the EPS subsystem will comprise batteries to store the energy needed for the requirement ECN-F-PRF-8-2 of the possibility of 48 hours of operation. Lithium-ion batteries are being used for the ECN as decided in the Midterm report [2] due to their high energy density, TRL and low costs. Four types of Lithium-ion batteries were looked at as stated in figure 5.51.

NMC batteries are chosen from the trade-off because of high scores on all the criteria. The only down-

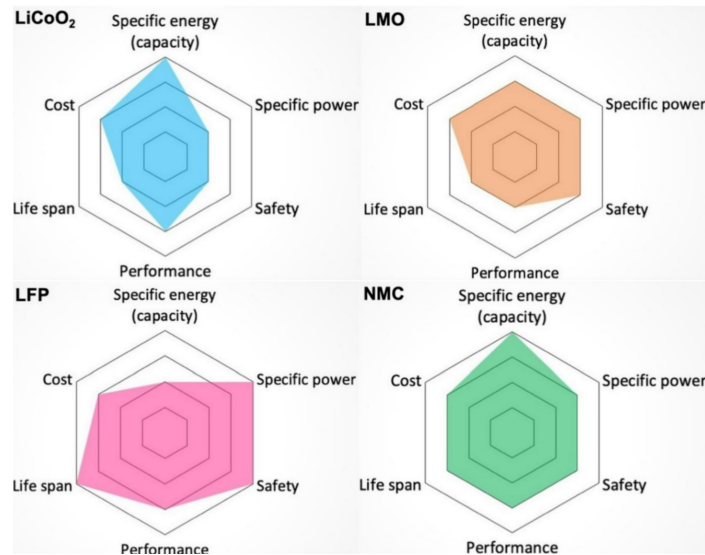


Figure 5.51: Trade-offs for different storage techniques used in Electric Vehicles. Lithium Cobalt Oxide (LiCoO₂), Lithium Nickel Manganese Cobalt Oxide (NMC), Lithium Iron Phosphate (LFP), Lithium Manganese Oxide (LMO) [81]



Figure 5.52: LG E66A battery⁸⁸

side of NMC batteries is that the cycle count on the battery is low. The battery can only sustain 80% of its design capacity after 400 cycles of use, compared to 900 cycles for Lithium Phosphate batteries⁸⁶. But this is not considered in the trade-off as the Node is being designed for emergencies which do not occur at a frequency which will encompass the 400 cycles in the life cycle of the designed ECN.

The NMC Lithium-ion batteries used are also used in cars and laptops⁸⁷, with a high TRL. The ideal choice for the ECN would be NMC 811, but because it is currently not deemed to be stable, an NMC 712 option is used which has a comparatively lower capacity. The LGX E66A battery pack was chosen with a gravimetric power density of 259 [Wh/kg] and a volumetric energy density of 648 [Wh/L]. It being lower, is still the highest capacity for commercially available batteries. The NCM 712 batteries are estimated to cost 80 [EUR/Wh]. The model of cells proposed to be used for the ECN is LG Chem E66A.

Due to the high costs associated with high capacity lithium-ion batteries, the EPS is designed to be modular with two different sections of batteries; One with a battery backup of 6 hours and another

⁸⁶<https://batteryuniversity.com/article/bu-808-how-to-prolong-lithium-based-batteries>

⁸⁷<https://innovationorigins.com/en/batteries-all-around-lets-take-a-good-look-at-the-state-of-battery-technology/>

⁸⁸<https://www.batemo.de/products/batemo-cell-library/e66a/>

with a backup of 48 hours as stated in ECN-F-PRF-8-2. The power consumption of the ECN is estimated to be 1500 [W] continuous which translates to an energy need of 9 [kWh] for the 6-hour version and a 72 [kWh] version.

The 9 [kWh] battery for both of the models will be common and will be built onto the floor bed. The Volume of the battery is calculated to be 13.88 [L]. The dimensions of the base of the battery is 1 x 1 [m²] with a thickness of 6.42 [mm]. This will be cooled by the thermal system designed with a heating plate with a thickness of 5 [cm] as discussed in section 5.9 bringing the total battery thickness to 6.38 [cm]. This battery will not be modular, is not designed to be replaced, and will be present in both models.

The second set of batteries in the more expensive model will have a total volume of 101.77 [L]. The dimensions of the battery will be 0.75 x 0.75 [m²] with a height of 0.18 [m]. The battery itself is proposed to have cooling and heating plates between different layers of cells with a total cooling thickness of 12 [cm] as explained and designed in section 5.9; this brings the total battery thickness to 0.30 [m]. This battery will be modular and can be replaced without minimal effort without disassembling the node.

5.10.2. Voltage Conversion

The 6 kW version will have 42 cells with groups of 7 cells in series and 6 strings in parallel. The voltage of 1 cell is 3.6 [V]⁸⁹. This brings the total voltage to 25.2 [V]DC which can then be used to convert to 110 [V] AC @ 60 [Hz] and 220 [V] @ 50 [Hz] which is used by the off the shelf commercial components used. The inverter and UPS being used for this process is a Helios RM-PSW2KVA⁹⁰ which can output 2000 Watts of continuous power. The power supply can fit into the standard 19" rack and can be connected to the network for monitoring. This will enable real time monitoring of the battery status in the node and enable to accurately predict the remaining battery capacity after use.



(a) Front view of the inverter



(b) Rear view of the inverter

Figure 5.53: Inverter being used

⁸⁹<https://pushevs.com/2021/03/30/ncm-712-by-lg-chem-e66a-and-e78-battery-cells/>

⁹⁰<https://www.heliosps.com/product/rm-psw2kva-series-rack-mount-inverter-2u-2kva/>

5.10.3. Power Distribution

The power has to be distributed after being converted to the required voltage. This can be done by using a power distribution box to allow for real-time monitoring of resources and electronically controlling the circuit breakers. This is important as a short circuit can lead to a failure in other subsystems; circuit breakers will be installed such that they can be electronically deployed to be deployed temporarily automatically in case of a surge and vice versa. The model of circuit breakers proposed to be used is MICO CLASSIC 4⁹¹ for every subsystem and an overall system breaker to protect a possible surge from the EPS.

5.10.4. Sustainability

Lithium ion batteries are ever evolving and widely used everyday but are less sustainable than Zinc batteries. This is because of the distribution and presence of rare earth elements. Zinc is more than 3 times more abundant on the earth's surface and could provide a good alternative to lithium batteries but still are not up to the capacity and TRL required for this project.

A further extension can be the use of Sodium batteries. Sodium batteries, in development, have a similar capacity to lithium batteries but can be manufactured at a much lower cost owing to the low cost of sodium due to its presence in sea salt. This increase in recyclability significantly makes the Li-ion batteries more sustainable. The recyclability though, comes at a very high cost associating to the complex separation of metals required⁹² while Sodium batteries go through a simple 2 step recycling step.

The aspects of the double conversion of the power, explained in subsection 5.10.5, also leads to inefficiencies which leads to loss of energy and faster degradation of batteries which are both not good for the environment. This increases the overall carbon footprint of the ECN while in operation but can be rectified with a future iteration.

The power distribution systems will use off the shelf electrical components made of glass-polyester or thermoset composite resins⁹³ which cannot be recycled. The plastic components in the electrical wires and components can be researched upon to make the EPS system more sustainable.

However, to ensure that the battery choice considers sustainability, the battery life has been prolonged with thermal management consideration. As has been mentioned in section 5.9, the battery has optimal temperature limits obeying which will increase the battery's service life. Consequently, with a longer life span, fewer batteries will need to be used for the node's manufacturing. This is sustainable considering it is a high effort to recycle Lithium-ion batteries [82], and as an alternative approach it is more desirable for sustainability to reuse the batteries.

5.10.5. Extensions

The current model of the EPS focuses on off the shelf components which work on 220 [V] or 110 [V] AC and can be plugged into regular wall outlets. The electronics inside these elements mostly work on DC voltage. So, the power from the battery is first being converted from DC to AC and then back to DC. This is not only introducing extra power draw, but also introducing more components in the system with the conversion also generating more heat. This is making the system larger in order to account for the Inverter/UPS and a larger thermal system which itself is increasing the weight of the

⁹¹<https://shop.murrelektronik.nl/nl/Electronics-in-the-Control-Cabinet/Intelligent-Power-Distribution/Modules/MICO-electronic-circuit-protection-4-CHANNELS-9000-41034-0100600.html>

⁹²<https://cen.acs.org/business/inorganic-chemicals/Sodium-comes-battery-world/100/i19>

⁹³<https://www.galco.com/comp/prod/circ.htm>

structure needed. This will reduce the size of the node considerably.

The battery technology used for the node is NMC712 which has a lower specific capacity than a NMC 811 battery. But the latter is unstable and is not used in commercial components as of now; but this is changing and NCM 811 batteries is extensively being reviewed by LG Chem for their next generation batteries.

Looking further at Sodium batteries as discussed in subsection 5.10.4, the performance at low temperatures is significantly better with it holding more than 90% of its charge at -20 [°C] while a Li-ion battery will lose more than 50 % of its capacity as compared to measurements at 25 [°C]. This will lead to a decrease in the thermal management system to keep the batteries at the optimum temperature at cold environments⁹⁴. This along with the lower cost of Sodium batteries owing to the exponentially lower cost of sodium can significantly bring the battery cost down to half.

5.11. Environmental Monitoring

The node should be aware of the environment surrounding it for several reasons. First of all, the weather must be monitored, since this may influence the link budget significantly. The operational limits must also be checked to see if the node must enter a safe mode for survival. Furthermore, the node should check its surroundings for proper placement. In this way, it is possible to correct ground personnel errors. This follows from the risk mitigation strategies discussed in [2].

Although some, limited, COTS monitoring solutions exist⁹⁵, needs of the ECN, and the potential a tailored solution unlocks, dictated choosing a new design for the subsystem. This way, the environmental monitoring subsystem contributes as much as it can to efficacy of the product, compliance with the requirements, and provides the most value to the stakeholders. This is embodied by the five functions of the subsystem: situational awareness, operational envelope monitoring, weather forecasting, data collection for predictive maintenance, and data collection for sustainability. No COTS solution exists that provides a match for the needs of the system. The design presented in subsequent subsections addresses all of those identified elements in particular context of the product.

5.11.1. Situational Awareness Sensing

Two main drivers behind a surroundings detection system are inexperienced personnel handling the node and laser safety. Therefore several situational awareness sensors are included.

First of all the direct surroundings should be scanned for obstructions. Different types of sensors exist for multiple ranges of distance and applications. First of all the location of the node must be obtained. The placement of the node can be checked using existing maps. A GNSS sensor is the industry standard for this, since it combines GPS, Galileo, BeiDou and GLONASS, and is thus redundant. A combined sensor of GNSS together with 3D inertial measurements and acceleration measurements is chosen, which can be easily connected to the command subsystem using CAN bus⁹⁶

Furthermore the close-range surroundings are to be scanned. Obstructions such as trees, houses and other types of infrastructure must be located outside of the operational "cone" of 20 degrees for the HAPS, and 30 degrees for the LEO satellite. A suitable technique for this is LiDAR, which is a laser-based scanning technique, which maps the surroundings up until 200m [83]. These properties make the LiDAR suitable for a quick surrounding scan. Other techniques, such as radar, have a far larger range which is not required but would increase the mass of the sensor significantly. Since the design of the node includes a gimbal structure on top, it does not allow a FOV of 360 degrees, the most suitable solution would be to include a LiDAR scanner on the outside of the gimbal. In this way,

⁹⁴<https://luciferlights.net/en/li-ion-battery-cold>

⁹⁵<https://www.miratlas.com/>

⁹⁶<https://www.csselectronics.com/products/gps-to-can-bus-gnss-imu>

a relatively low-cost LiDAR with a small FOV can be selected, which is rotated by the gimbal. For example, the Livox Mid-40 sensor, which has a conical VOF of 40 degrees, and costs 600\$⁹⁷. Although use of main laser beam for time-of-flight distance measurement to scan the system's surroundings would allow decreasing number of components, and cost, section 7.4 discusses safety concerns around the laser beam. It was deemed unacceptable to shine laser across a bigger area, with possible presence of untrained personnel, wildlife, etc., even at the reduced power. The lower power LiDAR sensor ensuring no obstructions in the cone around pointing direction assures reliability and safety of the solution.

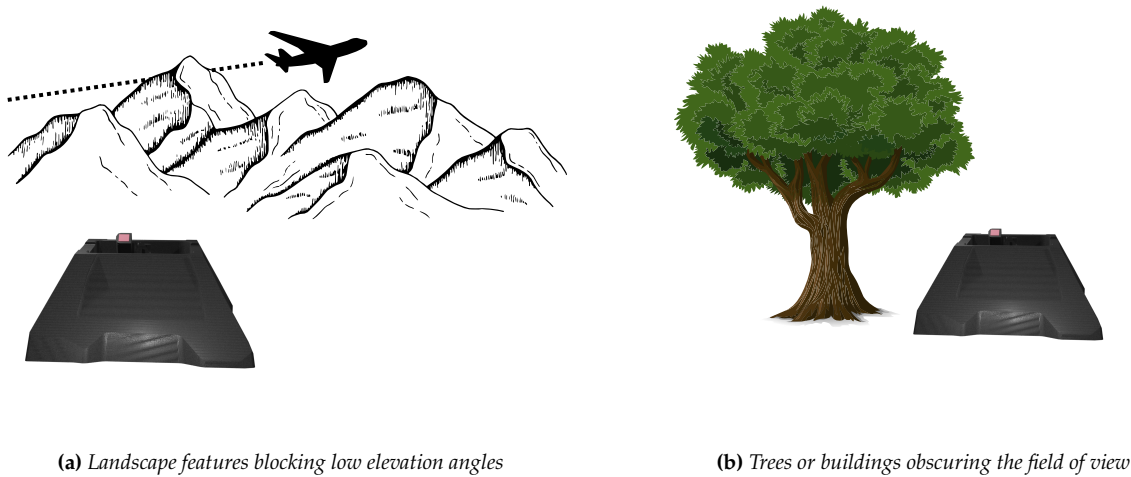


Figure 5.54: Risks dictating a need for situational awareness subsystem

5.11.2. Operating Envelope Monitoring and Weather Forecasting

Operating envelope is a set of constraints within which operation of ECN will result in safe and acceptable performance. It is defined by Safety and Reliability requirements, and defines environmental conditions in which the system must operate and survive. In particular, the requirements of concern are presented in table 5.24.

Table 5.24: Selected Safety and Reliability requirements

Identifier	Requirement
ECN-F-SAR-5-1	The mobile optical ground station shall consider operational wind speeds up to 15 [m/s].
ECN-F-SAR-5-2	The mobile optical ground station shall consider survival wind speeds up to 55 [m/s].
ECN-F-SAR-6	The mobile optical ground station shall be operational in a temperature range from -30 to 40 ° [C].
ECN-F-SAR-7	The mobile optical ground station shall be able to handle a survival temperature range between -50 and 60 ° [C].

The resultant operating envelope is presented in figure 5.55. Green area represents operational conditions, and the red hatched area represents survivability requirements. In the latter regime, the station can enter a safe mode and cease communications. The process is described in subsection 4.3.3. One function of the environmental monitoring subsystem is to detect when conditions exceed the operating envelope, as well as predict when that is to happen. The forecasting element brings utility

⁹⁷<https://www.livoxtech.com/mid-40-and-mid-100>

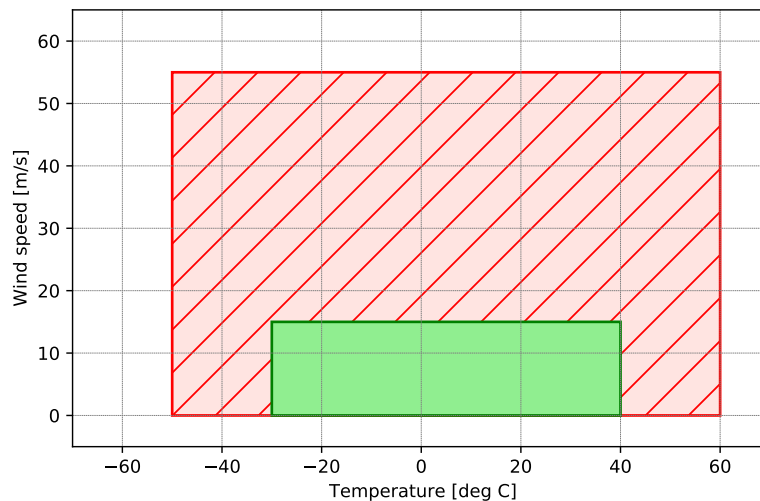


Figure 5.55: Operating envelope

to the operator, who not only understands when the communication will be interrupted and can brace for incoming hazards, but in the absence of dangerous weather events, weather forecasting predicts available link budget and possible data rates.

To this end, nowcasting techniques will be employed. Nowcasting refers to meteorological forecasts with an update frequency of below one hour, on a spatial scale of a few kilometres. It is used to protect people and property in event of incoming extreme weather events, such as severe local storms or flooding. Nowcasting is also used extensively in aviation and maritime sectors [84]. Such forecasts make use of surface weather station data, upper-air observations, meteorological satellites, lightning detection, and radars. The efficacy of each observation type at different phenomena prediction is presented in table 5.25. The sensors potentially available for the environmental monitoring subsystem were marked with grey (surface weather sensors, lightning detection, and radar).

Table 5.25: Efficacy of observation types at nowcasting weather phenomena [85]

Phenomena	Surface stations	Dense network of surface stations	Upper-air observations	Satellite	Lightning detection	Radar
Thunderstorms	2	4	1	5	5	5
Tornado	1	1	1	2	1	5
Strong surface winds	2	4	3	2	1	5
Flash flood	2	5	1	3	1	5
Visibility	4	5	1	2	1	4

Radar is the most important tool for nowcasting, directly observing the precipitation particles in three dimensions over a large area [85]. However, it is very costly and has higher maintenance requirements.

Trade-off

The ECN is assumed to already utilize satellite data since it is readily available at no extra cost or complexity. It also requires a set of weather sensors for detecting present hazardous conditions, setting aside nowcasting capabilities. The following options are therefore considered: satellite + weather

sensors (S+W), satellite + weather sensors + lightning detection (S+W+L), satellite + weather sensors + radar (S+W+R), and, finally, combination of all four (S+W+L+R).

The criteria along which the options are evaluated are: nowcasting capability for thunderstorms (Th), tornadoes (To), strong surface winds (SW), flash floods (FF), visibility (V), and cost (Ct), robustness (R), and complexity (Cm). The criteria are given weights respectively: 10%, 10%, 10%, 5%, 5%, 30%, 15%, and 15%. Visibility and flash floods nowcasting capability was given lower weight, due to the former not endangering the station or operating personnel, and the prediction of the latter not bringing advantage for survivability of the system, since entering safe mode is not helpful for flash floods, and the system is not easily movable after deployment, and can not be moved out of harm's way.

Table 5.26: *Weather sensors trade-off*

Criterion	Th	To	SW	FF	V	Ct	R	Cm	Total
Weight	10%	10%	10%	5%	5%	30%	15%	15%	
S+W	5	2	2	3	4	4	4	4	3.7
S+W+L	5	2	2	3	4	3.5	4.5	3.5	3.5
S+W+R	5	5	5	5	4	1.5	4.5	3	3.5
S+W+L+R	5	5	5	5	4	1	5	2.5	3.4

Lightning detection is a sensor integrated with some available weather sensors, therefore the increase in cost and complexity is smaller (scores lower by 0.5). Each new sensor increases the robustness of the system thanks to redundancy and lowers the complexity and cost scores. Radar is particularly costly. While the evaluation ranks each design option at each metric against each other, the uncertainty about the actual impact of the difference, as well as the weights of the metrics, introduces uncertainty to the model. This can be quantified with sensitivity analysis, presented in figure 5.56.

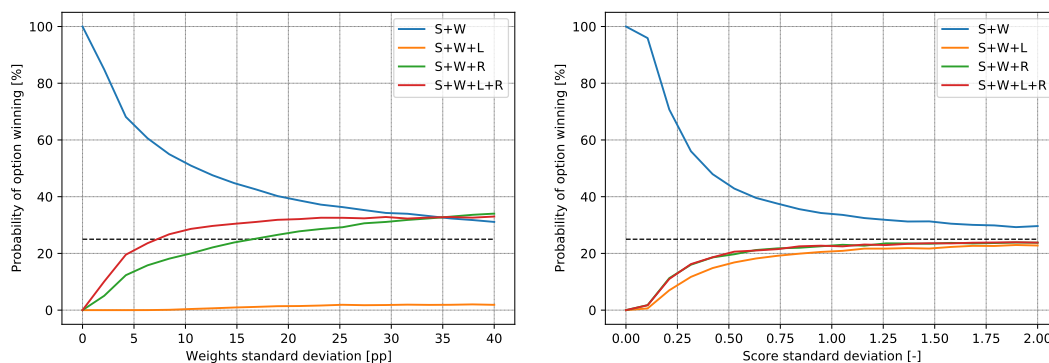


Figure 5.56: *Weather observations sensitivity analysis*

As can be seen, there is high uncertainty about the inclusion of additional devices. The nowcasting performance and robustness can be improved by adding lightning detection or weather radar to the sensors suite, which can be shown as a preferable option by a little altered trade-off. Contingency of higher nowcasting requirements can be accounted for by increasing the cost and complexity. To solve this dichotomy, modular approach was taken. The ECN will be able to interface with a commercially available standalone weather radar, if required by deployment conditions. In case of deployment in the aftermath of a natural disaster, with suspected risk of hazardous weather conditions returning, the product's operator, who is a part of disaster response, is likely to already come with suitable weather sensing equipment.

Component Selection

Two commercial off-the-shelf weather sensors appropriate for the subsystem have been identified. They were compared in table 5.27.

Table 5.27: *Weather sensor comparison*

	ClimaVUE50⁹⁸	WS700-UMB⁹⁹
Sensors	Air temperature, barometric pressure, lightning average distance, lightning strike count, precipitation, relative humidity, solar radiation, tilt, wind direction, and wind speed	Air temperature, relative humidity, precipitation intensity, precipitation type, precipitation quantity, air pressure, wind direction, wind speed and radiation
Temperature measuring range	-50 to 60 deg C	-50 to 60 deg C
Wind speed measuring range	0-30 m/s	0-75 m/s
Size	Diameter 10 cm, height 34 cm	Diameter approx. 150 mm, height approx. 317 mm
Weight	839.15 g	Approx. 1.5 kg
Peak power use	0.4 W	40 W (relies on a heater)
Cost	1730.00 EUR ¹⁰⁰	3866.00 EUR ¹⁰¹

ClimaVUE50 achieves same temperature range while not relying on the heating element, therefore requiring lower power. It also costs half the amount, yet at the lower cost features an additional sensor: lightning detection. The remarkably high price efficiency of this product, when compared to the alternative, goes against predictions of table 5.26. It is therefore selected, though the measurement range of wind speed does not cover the entire survivability range. However, that is not required, since it still covers entire operation range, and can indicate when entering the safe mode is necessary. It measures wind speeds in range of 0-30 [*m/s*], while the operating range for ECN is 0-15 [*m/s*].

5.11.3. Data Collection for Predictive Maintenance

Predictive maintenance is a data-driven process, using empirical data to determine the state of in-service equipment, and use that to schedule inspection and maintenance. The first and most important input to predictive maintenance model are the malfunctions; the ECN uses automatic malfunction detection, based of interoceptive sensors included in subsystems (see subsection 4.3.2). However, to extend the model, it is provided environmental data, the context of the deployment conditions, to analyze environmental factors contributing to deterioration of condition of the node [86]. Finally, collected maintenance and failure history is critical to refine the model over time. This subsection will focus on selection of sensors for the environmental data collection.

Much useful environmental data is already collected by operating envelope monitoring and weather forecasting sensor: among others, temperature contributes to thermal ageing, chemical decomposition, and embrittlement, and humidity influences corrosion, moisture absorption, and penetration of sealing [87].

Atmospheric particles, such as sea salt, wind-blown dust, and volcanic emissions, cause damage to

⁹⁸<https://www.campbellsci.com/climavue-50>

⁹⁹<https://www.lufft.com/products/compact-weather-sensors-293/ws700-umb-smart-weather-sensor-1830/>

¹⁰⁰https://shop.profec-ventus.com/product_info.php?language=en¤cy=EUR&switch_country=DE&info=p520_climavue50-compact-digital-weather-sensor.html

¹⁰¹<https://thomsongroup.com.au/product/lufft-ws700-umb-smart-weather-sensor-temperature-relative-humidity-precipitation-solar-radiation-air-pressure-wind-electronic-compass/>

materials. Dust particles can cause abrasion to materials, and can serve as carriers for aggressive chemicals or chemically active ions. That in turn can cause oxidation on material source [88]. A review of available suitable particulate matter sensors was compiled and presented in table 5.28.

Table 5.28: Air quality sensors comparison

	HPMA115C0-004 ¹⁰²	SEN55-SDN-T ¹⁰³	SN-GCJA5L ¹⁰⁴
Cost	63.78 EUR	32.92 EUR	30.86 EUR
Size	44x36x12 [mm ³]	53x44x23 [mm ³]	37x37x12 [mm ³]
Operating temperature	-20 to 70 [°C]	-20 to 70 [°C]	-10 to 60 [°C]
Sensor	PM1.0, PM2.5, PM4.0, PM10, 0 to 1000 [µg/m ³]	PM1.0, PM2.5, PM4.0, PM10, 0 to 1000 [µg/m ³], Relative Humidity, Temperature, VOC Index, NOx Index	PM2.5, PM10, 0 to 2000 [µg/m ³]

SEN55-SDN-T sensor was chosen for its low cost, high operating temperature range, and additional built-in features (VOC and NOx index sensing, as well as additional redundancy for temperature and humidity).

5.11.4. Animal Deterrence

A problem that would seem non-existent at first glance is that of animal control. From mice in Europe to kangaroos in Australia, if these species are not accounted for, they can have a tremendously detrimental effect on the ECN. Kangaroos in Australia bring up a controversial discussion, especially considering that there are around two times more of them than Australians, and they frequently get in the way of human activities^{105 106}.

In order to manage the threat that kangaroos and other animal species could have on the ECN, the CEX Ultrasonic Pest Control¹⁰⁷ unit has been selected to deter a variety of animals from coming close to the ECN via the use of ultrasonic waves. This way, their life is also safeguarded.

5.11.5. Sustainability and Environmental Sensing

Noise pollution is a serious problem, causing adverse effects on humans and natural environment. Limited, it is unpleasant and straining. Out of control, it can cause hearing loss, stress, and high blood pressure [89], as well as negatively impact ecosystems, threatening certain species and damaging biodiversity [90]. Noise Level Monitoring is implemented to ensure compliance with occupational health and safety regulations. This brings welfare of ECN operators and other third parties (e.g. inhabitants of disaster-stricken area) to light, and is a part of social sustainability. At the same time, it limits potential harm to the natural environment.

PCE-SLD 10-ICA¹⁰⁸ Noise Level Meter was selected for its ISO certificate, wide measuring range (up

¹⁰²<https://eu.mouser.com/ProductDetail/Honeywell/HPMA115C0-004?qs=PzGy0jfpSMv%252BXuZmF5yeTA%3D%3D>

¹⁰³<https://eu.mouser.com/ProductDetail/Sensirion/SEN55-SDN-T?qs=MyNHzdooqQLyWUzejWkZfg%3D%3D>

¹⁰⁴<https://eu.mouser.com/ProductDetail/Panasonic/SN-GCJA5L?qs=XeJtXLi041TxG5n8VEmlSg%3D%3D>

¹⁰⁵https://www.nswfarmers.org.au/NSWFA/Posts/The_Farmer/Community/Kangaroos_decimate_farmers_profits.aspx

¹⁰⁶<https://www.nationalgeographic.com/magazine/article/australia-kangaroo-beloved-symbol-becomes-pest>

¹⁰⁷<https://www.birdgard.com.au/pest-control/cex-ultrasonic-pest-control/>

¹⁰⁸https://www.pce-instruments.com/eu/measuring-instruments/test-meters/noise-meter-sound-meter-pce-instruments-noise-meter-pce-sld-10-ica-incl.-iso-calibration-certificate-det_5973668.htm

to 130 dB), and accessible price when compared with other industrial grade noise sensors¹⁰⁹. It costs €385.90, weights 230 [g], and fits in bounds of 132x90x32 [mm]. Power supply is at 9 [V] and 1 [A], yielding figure of 9 Watts of power consumed. Operating temperature range is 0 to 50 [°C].

5.11.6. Verification and Validation

The environmental monitoring subsystem must be also verified and validated to ensure compliance with requirements and proper, uninterrupted functioning of the integrated subsystem. Operations validation, presented in section 4.4, includes safe mode tests, as triggered by operational envelope monitoring function of the subsystem. Therefore, the tests outlined there also validate environmental monitoring subsystem. A series of lower-level tests must also be performed to verify and validate particular components: a lengthy deployment in any testing location allows to quantify performance of weather forecasting, and the air quality sensors and noise level meters can be tested by exposing the node to air or noise pollution in a controlled manner.

5.12. SWaP and Cost Budgets

This section summarises the mass, cost, power and volume breakdown per subsystem for the ECN as can be seen in figure 5.57 and figure 5.58. table 5.29 quantifies all the different budgets gives an estimate of the mass, power, volume and cost of the ECN.

Table 5.29: Overall budget for the ECN.

Subsystem	Mass [kg]	Power [W]	Volume [m^3]	Cost [€]
Command	4.1	110.0	0.01	€ 5,747.82
Beam Steering	154.3	45.6	0.07	€ 51,840.50
Thermal	37.3	509.0	0.35	€ 1,977.79
Electrical	296.8	0.0	0.62	€ 11,878.90
Structure	380.0	0.0	1.35	€ 16,000.00
Optical	16.1	222.0	0.02	€ 23,534.08
I/O	5.0	50.0	0.01	€ 12,968.00
Human resources				€ 4,400.00
Grand total	893.6 kg	936.6 W	2.42	€ 128,347.09

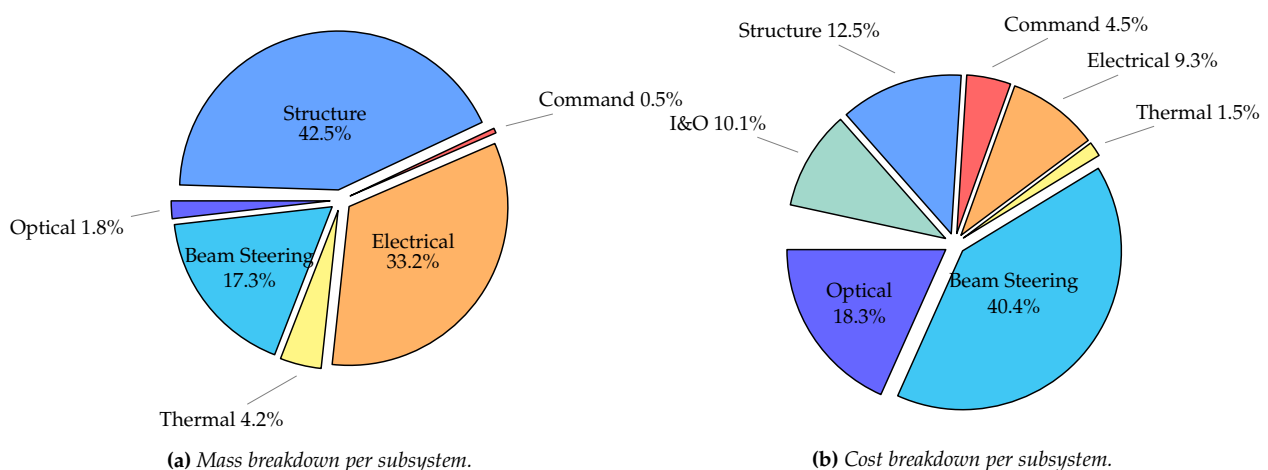
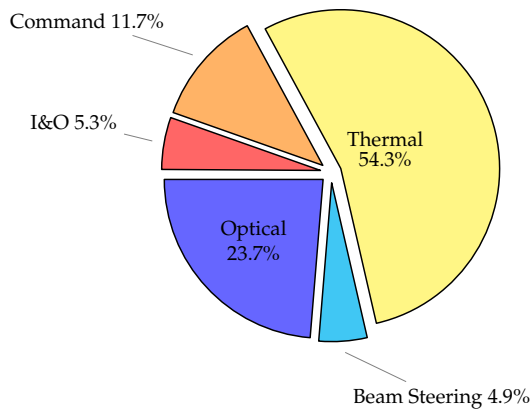
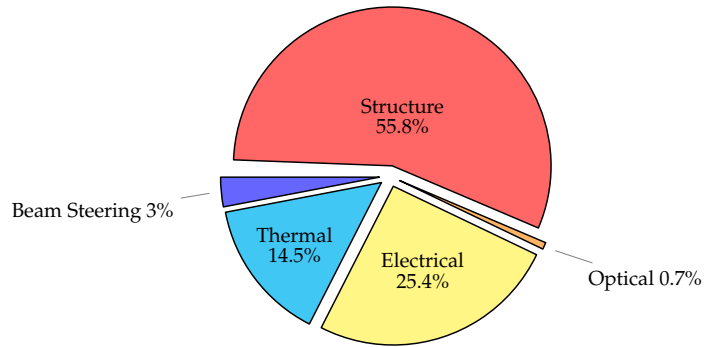


Figure 5.57: Mass and cost breakdown per subsystem.

¹⁰⁹ https://www.pce-instruments.com/eu/measuring-instruments/test-meters/noise-meter-sound-meter-kat_40410.htm



(a) Power breakdown per subsystem.



(b) Volume breakdown per subsystem.

Figure 5.58: Power and volume breakdown per subsystem.

6

Sensitivity Analysis

This chapter will outline the sensitivity analysis strategy undertaken to validate the feasibility of the design choices that are made in this report.

6.1. Interdependency Matrix

To begin with, it is important to identify key subsystem parameters to be varied. For this, a matrix was built that identifies all the parameters to be varied per subsystem and the impact this will have on the rest of the subsystems. It is presented in table 6.1.

The change influencing the most other subsystems is power required in optical subsystem. This suggests exploring the impact of this further, and will be elaborated on in section 6.3. The table is a quick reference for discussion of interrelations in the design, however it is not comprehensive, nor as nuanced as requirement- or subsystem-specific discussions contained in particular subsections.

6.2. Subsystem Trade-off Sensitivity Analysis

Where appropriate, the report included verification of multi-attribute decision models used for design option selection. The verification method was introduced in the midterm report [2], and has been applied to better understand certainty of numerical model used for making design decisions.

6.3. Scenario Analysis

In this section, several scenarios of changes to key parameters have been studied in more detail, to understand their impact on interdependent subsystems. The process verifies sizing methods and decision models, to evaluate robustness and optimality of made design choices. Due to time and resource constraint, the number of considered scenarios is limited. It was decided that the focus will be placed on consequences of changed link budget requirement, since this directly determines the product's ability to establish communication with targets, which is the primary function of the node.

Table 6.1: Subsystem parameters change impact. ↓ marks a decrease, ↑ an increase, and ○ another, for example qualitative, change.

Change in system	C&DH Mass	C&DH Power required	EPS Mass	EPS Power stored	Optical Mass	Optical Power required	Optical Accuracy	Modulation	I/O Mass	I/O Power required	Attitude Accuracy	Structural Mass	Thermal Mass	Thermal Power required	Env. monitoring Mass
C&DH Mass ↑	█											↑			
C&DH Power required ↑	↑	█		↑										↑	
EPS Mass ↑			█									↑			
EPS Power stored ↑			↑	█										↑	
Optical Mass ↑					█	↑						↑			
Optical Power required ↑				↑	↑	█		○						↑	
Optical Accuracy ↓						↑	█	○			↑				
Modulation						○		█							
I/O Mass ↑									█			↑			
I/O Power required ↑				↑					↑	█				↑	
Attitude Accuracy ↓							↓				█				
Structural Mass ↑												█		↑	
Thermal Mass ↑												↑	█		
Thermal Power required ↑				↑									↑	█	
Env. monitoring Mass ↑												↑			█

6.3.1. Impact of Link Budget on Aperture

Risks R10 and R12, presented in chapter 8, concern the link budget lacking. Adverse environmental conditions or subnominal performance of optical assembly components can cause quality of signal to deteriorate, making such scenario important to consider. equation 5.12 introduced in subsection 5.2.2 gives a relation for receiver antenna gain, one of the factors in equation 5.2 for received power. If the received signal power must be increased by ΔP , the receiver aperture diameter (D_R) must increase by ΔD , as described by the following equations:

$$P_R = P_T G_{T,A} L_{T,P,S,A,R} \left(\frac{\pi D_R}{\lambda} \right)^2 \quad (6.1)$$

$$P_R + \Delta P = P_T G_{T,A} L_{T,P,S,A,R} \left(\frac{\pi (D_R + \Delta D)}{\lambda} \right)^2 \quad (6.2)$$

Here, $(D_R + \Delta D)^2$ is equal to $(D_R^2 + 2D_R\Delta D + \Delta D^2) \approx (D_R^2 + 2D_R\Delta D)$ for ΔD significantly smaller than D .

$$P_R + \Delta P = P_T G_{T,A} L_{T,P,S,A,R} \left(\frac{\pi D_R}{\lambda} \right)^2 + P_T G_{T,A} L_{T,P,S,A,R} \left(\frac{\pi}{\lambda} \right)^2 2D_R \Delta D \quad (6.3)$$

Subtracting P_R from both sides, and dividing by ΔD .

$$\frac{\Delta P}{\Delta D} = P_T G_{T,A} L_{T,P,S,A,R} \left(\frac{\pi}{\lambda} \right)^2 2D_R = 2 \frac{P_R}{D_R} \quad (6.4)$$

Or, in other words, partial derivative of D with respect to P , at P_R , is equal to:

$$\frac{\partial D}{\partial P}(P_R) = \frac{1}{2} \frac{D(P_R)}{P_R} \quad (6.5)$$

For the design, final D_R was decided to be equal to 0.26 meters, and P_R was determined to equal to 1.33 [mW]. $\frac{\partial D}{\partial P} = 0.098$ [m / mW]. To obtain a relation between percentage change in diameter of the receiver and change in [dB] of received power, calculated with $L = 10 \log_{10}(\frac{P}{P_R})$, following can be calculated

$$\frac{\partial P}{\partial L} = \frac{\partial(P_R 10^{L/10})}{\partial L} = \frac{\log(10)}{10} P \quad (6.6)$$

Where $\log(10)$ is a natural logarithm of 10.

$$\frac{\partial D}{D_R \partial L}(P_R) = \frac{\partial D}{\partial P}(P_R) \frac{\partial P}{\partial L} \frac{1}{D_R} = \frac{\log(10)}{20} \left[\frac{1}{dB} \right] \quad (6.7)$$

In other words, to increase the signal strength by 1 [dB], aperture must be increased by $5 \log(10) \approx 11.5$ percent. Increasing the area by around 24 percent corresponding to increase of diameter to 11.5 percent, causes an increase in signal strength of 1 dB, or by a factor of $10^{1/10} = 1.26$. The linear relation between area and signal strength verifies the calculation.

Going to the first principles, the weight of an object scales with dimension to the power of 3, $m \propto D^3$. This allows us to estimate influence of link budget on the weight of optical receiver. In reality, the relation will not be exactly like that, but for Sensitivity Analysis, a variable α independent of D_R is assumed such that $m = \alpha D^3$, and therefore $m(D_R) = \alpha D_R^3$.

$$\frac{\partial m}{\partial D}(D_R) = 3\alpha D_R^2 = 3 \frac{m(D_R)}{D_R} \quad (6.8)$$

Two values are of interest: $\partial m / \partial P$ and $\partial m / \partial L$. With gimbal and telescope assembly mass equal to 40 [kg], the estimates of the values are

$$\frac{\partial m}{\partial P}(P_R) = \frac{\partial m}{\partial D}(D_R) \frac{\partial D}{\partial P}(P_R) = \frac{3}{2} \frac{m(P_R)}{P_R} = 45.1 \left[\frac{kg}{mW} \right] \quad (6.9)$$

$$\frac{\partial m}{\partial L}(P_R) = \frac{\partial m}{\partial D}(D_R) \frac{\partial D}{\partial P}(P_R) \frac{\partial P}{\partial L} = \frac{3 \log(10)}{20} m(P_R) = 13.8 \left[\frac{kg}{dB} \right] \quad (6.10)$$

The partial derivative of mass with respect to power received is 45.1 [kg/mW], or 13.8 [kg/dB].

A paper [91] on scaling laws for telescopes classifies costs such as machining of mechanical parts, mirror grinding and polishing, and painting, as scaling with D^2 . Costs scaling with D^3 and D^4 are domes, concrete foundations, and other costs less relevant for the product. Cabling is dependent on D , and computers and similar components are independent of aperture diameter. The relationship between cost C and D is approximated with:

$$C(D) = \beta D^2 \quad (6.11)$$

With $C(D_R) = \beta D_R^2$ equal to 15000 euros. $\partial C / \partial P$ and $\partial C / \partial L$ is calculated similarly to $\partial m / \partial P$ and $\partial m / \partial L$. Since $\partial C / \partial D = 2\beta D = 2C(D) / D$

$$\frac{\partial C}{\partial P}(P_R) = \frac{C(P_R)}{P_R} = 11280 \left[\frac{EUR}{mW} \right] \quad (6.12)$$

$$\frac{\partial C}{\partial L}(P_R) = \frac{\log(10)}{10} C(P_R) = 3454 \left[\frac{EUR}{dB} \right] \quad (6.13)$$

To conclude the analysis of the scenario, equation 6.10 and equation 6.13 give figures of 3454 [EUR/dB] and 13.8 [kg/dB] increase in budgets to achieve stronger received signal.

6.3.2. Impact of Link Budget on Power

The previous scenario analyzed impact of higher requirement on power received on the parameters of optical subsystem - diameter of aperture, and mass and cost. This subsection brings the complimentary problem into focus: deteriorated link causing a need for higher emitted power. In budgets, the transmitter power is $P_T = 5$ [W], with total power consumption of $P_{C,T} = 100$ [W], at a mass of $m_T = 10$ [kg] and cost C_T of 6000 euros.

The first introduced assumption is that the efficiency μ is constant

$$\mu = \frac{P_T}{P_{C,T}} = 0.05 \quad (6.14)$$

Because of the lack of available literature on scaling laws or sizing for laser systems, a linear relations are assumed, $P \propto m$, and $P \propto C$. $\partial P/\partial L = P \log(10)/10$, with derivation same as in equation 6.6.

$$\frac{\partial m}{\partial P} = 2 \left[\frac{\text{kg}}{\text{W}} \right] \quad (6.15) \quad \frac{\partial C}{\partial L} = 1380 \left[\frac{\text{EUR}}{\text{dB}} \right] \quad (6.18)$$

$$\frac{\partial m}{\partial L} = 2.30 \left[\frac{\text{kg}}{\text{dB}} \right] \quad (6.16) \quad \frac{\partial P_C}{\partial P} = \frac{1}{\mu} = 20 [-] \quad (6.19)$$

$$\frac{\partial C}{\partial P} = 1200 \left[\frac{\text{EUR}}{\text{W}} \right] \quad (6.17) \quad \frac{\partial P_C}{\partial L} = 23.0 \left[\frac{\text{W}}{\text{dB}} \right] \quad (6.20)$$

The higher P_C impacts the EPS subsystem, covered in section 5.10. The battery solution chosen has gravimetric density of 259 [Wh/kg], and cost of 80 [euros/kg]. Stored energy E is calculated by multiplying power necessary by 48 hours, which is the time the batteries are designed to power the ECN for, in the more durable of EPS versions (read section 5.10 for more details).

$$\frac{\partial E}{\partial P_C} = 48 [h] \quad (6.21)$$

$$\frac{\partial m_{EPS}}{\partial E} = 0.00386 \left[\frac{\text{kg}}{\text{Wh}} \right] \quad (6.22)$$

$$\frac{\partial C_{EPS}}{\partial E} = \frac{\partial C_{EPS}}{\partial m_{EPS}} \frac{\partial m_{EPS}}{\partial E} = 0.309 \left[\frac{\text{EUR}}{\text{Wh}} \right] \quad (6.23)$$

This is used to calculate the following

$$\frac{\partial m_{EPS}}{\partial P} = \frac{\partial m_{EPS}}{\partial E} \frac{\partial E}{\partial P_C} \frac{\partial P_C}{\partial P} = 3.70 \left[\frac{\text{kg}}{\text{W}} \right] \quad (6.24) \quad \frac{\partial C_{EPS}}{\partial P} = \frac{\partial C_{EPS}}{\partial E} \frac{\partial E}{\partial P_C} \frac{\partial P_C}{\partial P} = 296 \left[\frac{\text{EUR}}{\text{W}} \right] \quad (6.26)$$

$$\frac{\partial m_{EPS}}{\partial L} = \frac{\partial m_{EPS}}{\partial E} \frac{\partial E}{\partial P_C} \frac{\partial P_C}{\partial L} = 4.26 \left[\frac{\text{kg}}{\text{dB}} \right] \quad (6.25) \quad \frac{\partial C_{EPS}}{\partial L} = \frac{\partial C_{EPS}}{\partial E} \frac{\partial E}{\partial P_C} \frac{\partial P_C}{\partial L} = 342 \left[\frac{\text{EUR}}{\text{dB}} \right] \quad (6.27)$$

To summarize impact of increased power requirement on both laser subsystem and EPS, the values can be added

$$\frac{\partial m_{total}}{\partial P} = \frac{\partial m_{EPS}}{\partial P} + \frac{\partial m}{\partial P} = 5.70 \left[\frac{kg}{W} \right] \quad (6.28) \quad \frac{\partial C_{total}}{\partial P} = \frac{\partial C_{EPS}}{\partial P} + \frac{\partial C}{\partial P} = 1496 \left[\frac{EUR}{W} \right] \quad (6.30)$$

$$\frac{\partial m_{total}}{\partial L} = \frac{\partial m_{EPS}}{\partial L} + \frac{\partial m}{\partial L} = 6.56 \left[\frac{kg}{dB} \right] \quad (6.29) \quad \frac{\partial C_{total}}{\partial L} = \frac{\partial C_{EPS}}{\partial L} + \frac{\partial C}{\partial L} = 1722 \left[\frac{EUR}{dB} \right] \quad (6.31)$$

The EPS contribution to weight increase after introducing higher power requirement is substantial: a 65% of total increase traced back to the power subsystem. However, the contribution to price is much smaller, at 20%. This is an important thing to note, as price requirement.

6.3.3. Combined Impact of Link Budget on System

The final scenario is one in which atmospheric conditions impose a signal strength requirement higher by ΔL stronger for both received and emitted beam. The result is combined mass and cost increase from subsection 6.3.1 (A) and subsection 6.3.2 (B).

$$\frac{\partial m}{\partial L} = \frac{\partial m_A}{\partial L} + \frac{\partial m_B}{\partial L} = 13.8 + 6.56 = 20.4 \left[\frac{kg}{dB} \right] \quad (6.32)$$

$$\frac{\partial C}{\partial L} = \frac{\partial C_A}{\partial L} + \frac{\partial C_B}{\partial L} = 3454 + 1722 = 5176 \left[\frac{EUR}{dB} \right] \quad (6.33)$$

This is numerical calculation confirming a qualitative insight from link budget: while emitted beam can be easily made more powerful by including bigger laser and power subsystems, enhancing the incoming signal turns out to be much more difficult, coming at a much greater cost and mass. In as far as linearization is accurate, the model shows the design as robust: aperture, laser system, and EPS are not very sensitive to communication requirements changes. This is however an incomplete picture, taking into account only subsystem sizing. More discussion, including effect of higher size on operations, is contained in chapter 8.

7

RAMS Analysis

Ensuring that a product, process or system fulfils the mission for which it was designed without encountering failures is important for the overall design of the product. To do that, certain analysis can be done that considers reliability, availability, maintainability and safety (RAMS). This chapter considers the reliability and availability of the product and ways to study these.

7.1. Reliability

When considering a product, reliability is defined as the probability that its performance will not deteriorate over time, following a determination of the conditions of use. One particular parameter that determines the reliability of a product is its failure rate. This failure rate is the number of failures that a product undergoes in a set time interval. Forecasting techniques, starting from the failure rates of individual parts, make it possible to gain enough knowledge about the failure rates of the entire product and therefore state its reliability. This process should be carried out during the design phase, making it possible to identify components that are most prone to failure and intervene with

replacements or inclusion of redundancies. Figure 7.1 presents the main sequence for the failure rate and repair analysis.

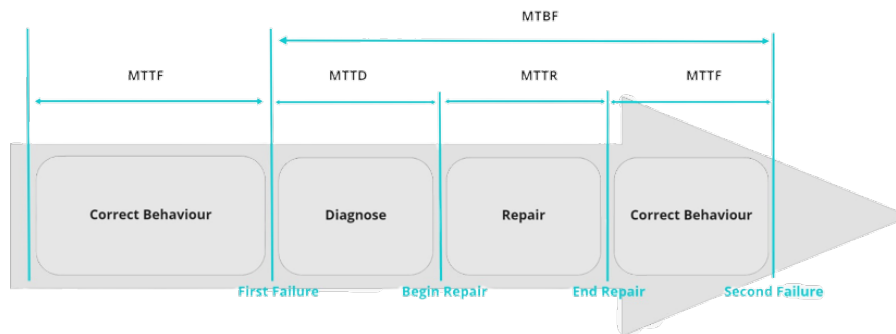


Figure 7.1: Failure sequence

First all the systems are identified which are prone to failure. Following this, failure modes for the particular systems are identified based on which contingencies are made in order to avoid them. The systems susceptible to failure are as follows:

7.1.1. Structure

This system includes all the parts of the nodes which will take up the structural loads including both the static and dynamic loads. Since many assumptions are being used in the simplified model as described in section 5.7, a high safety factor of 3 is used to make sure the structure is able to sustain real world loads. The main loads acting on the node which make it prone to failure are: wind gusts, which are modelled as step inputs, and earthquakes, which are modelled as a periodic loading. Both of the load types are increased by the factor of 3, which in turn will play an important role in the sizing of the support/fixation of the node.

7.1.2. Pointing, Acquisition and Tracking

One of the most important aspects of the communication node is the PAT system. To ensure mission's success, the PAT system is required to be fully functional at all times while the node is operational. Performing the PAT sequence relies on highly sensitive equipment, which can often be damaged or be driven to not function properly anymore. Therefore, a series of redundancies were considered for these subsystems to account for these highly critical risks.

For attitude determination, three systems are to be integrated in the node, namely the star tracker, the magnetometer and the bio-inspired celestial compass. Each of this components can perform the task of determining the attitude. However, it is desired that the star tracker can fulfil this task, since it provides much better accuracy than alternatives. In case it fails, the task will be carried out to a lower, but satisfying degree by the magnetometer or the bio-inspired celestial compass. The magnetometer itself uses both dissimilar redundancy (two types of magnetometer sensors) and triple-modular redundancy (three of each type of sensor).

For tracking, two different cameras will be integrated, namely the coarse tracking camera and the fine tracking and star sensing camera. In case the fine tracking camera fails, the tracking can be carried out in lower accuracy by the other camera. This would still allow the station to establish connection to some targets.

7.1.3. Modulation

Appropriate modulation is required in order to make sure the digital signal is able to reach the receiver. 16-QAM has been chosen as the modulation scheme for communicating with HAPS after doing a trade-off between different modulation schemes. As observed, although 16-QAM has a very high spectral and bandwidth efficiency, it suffers due to atmospheric attenuation and performs worse than simple schemes such as OOK, BPSK and QPSK. In order to make sure that link is established even in worse atmospheric conditions, a good coding technique or FEC (Forward Error Correction) will be used. Using FEC allows communicating with BER values as low as 10^{-3} [17].

7.1.4. Electrical Power Supply

The EPS is required in order to provide sufficient power for the other subsystem to function properly. Thus, due to the importance of this subsystem in relation with the other subsystems, it is important to ensure a backup plan in case of a failure. This has been taken into account in the design by including a backup battery that can last for roughly six hours. Moreover, an additional distribution system is considered for the laser pump with EDFA in order to make sure that the laser is completely functional at all times.

7.1.5. Thermal Management

The battery's performance is dependent on the thermal management system, when it were to fail this could potentially be catastrophic for the battery. A redundant temperature sensor is added to the battery thermal system to allow redundancy for temperature measurements. Freezing temperatures are more destructive than temperatures above 30 degrees, thus heating is deemed more important for survival of the battery pack. The piping network of the heating system of the battery pack is routed in such way that the heating system of the node could heat the battery pack as well.

When using antifreeze solvents it is important to maintain the liquid. The liquid will deteriorate over time, and must be inspected and replaced when required. The placement of the cooling unit is done such that access for maintenance personal is possible, and draining the system of the cooling liquid is easily performed. For sustainability purposes it must be prevented to leak coolant into the environment during maintenance, thus a connection system for a hose is added to change the liquid spill free.

7.1.6. Environmental Monitoring

Environmental monitoring requires sensors in order to detect if the node can operate in the current conditions. As will be seen in subsection 5.11.2, the node will need two sensors to fully monitor the surroundings, a satellite and weather sensor. To take into account the possibility of failure of one of the sensors, additional sensors will be integrated into the system, namely another pair of satellite and weather sensors.

7.2. Availability

Availability is defined as the probability that a product's performance will be unchanged over time, after determining the conditions of use and assuming that any necessary external means are secured. The availability can be calculated using figure 7.1. In general, availability is defined in equation 7.1, where agreed service time is the expected time the service will be in operation, while the downtime is the amount of time during the agreed service time that the service is not available¹.

$$\text{Availability \%} = \frac{\text{Agreed service time} - \text{Downtime}}{\text{Agreed service time}} \quad (7.1)$$

¹<https://www.bmc.com/blogs/service-availability-calculation-metrics/>

As stated in the requirements, the communication node shall be available 99% of the time. Using "The Nines of Availability"² approach, it can be estimated that the downtime per year will be 3.65 days, the downtime per month will be 7.20 hours, while the downtime per week will be 1.68 hours. Availability also determines the instantaneous performance of a component at any given time, usually based on the duration between its failure and recovery³. Thus, it can be calculated using equation 7.2.

$$\text{Availability, } A(t) = \frac{\text{MTBF}}{\text{MTBF} + \text{MTTR}} \tag{7.2}$$

Where MTBF is the Mean time between failures and MTTR is the Mean time to recovery. Using an availability of 99%, it can be calculated that the MTBF has to be 100 times larger than the MTTR, or more accurate, $\frac{\text{MTBF}}{\text{MTTR}} = 100$. This translates to having a time between failures 100 times larger than the time it takes to perform a repair on a subsystem.

For each main subsystem, the availability was calculated using equation 7.2. In each case, the MTTR or the MTBF was found, and the availability was calculated. It was found that all of the subsystems have an availability of 99% or above. This yielded in an overall availability for the node of 96.5%, found by multiplying the availabilities. This is summarized in table 7.1.

Table 7.1: Availabilities of subsystems

System	MTTR (hours)	MTBF (hours)	Availability (%)
EDFA[92]	2	398	99.5
Laser[93]	8	792	99
Modulation	N.A.	N.A.	99
FSM[94]	2	19998	99.99
Transmitter[92]	2	66664	99.997
Receiver[92]	2	199998	99.999
Thermal[95]	16	1660	99
Total			96.5

The availability resulted from table 7.1 is below the 99% required. However, during further stages of the design, this availability can be increased by performing a more detailed analysis and choosing elements with an even higher availability margin.

7.3. Maintenance

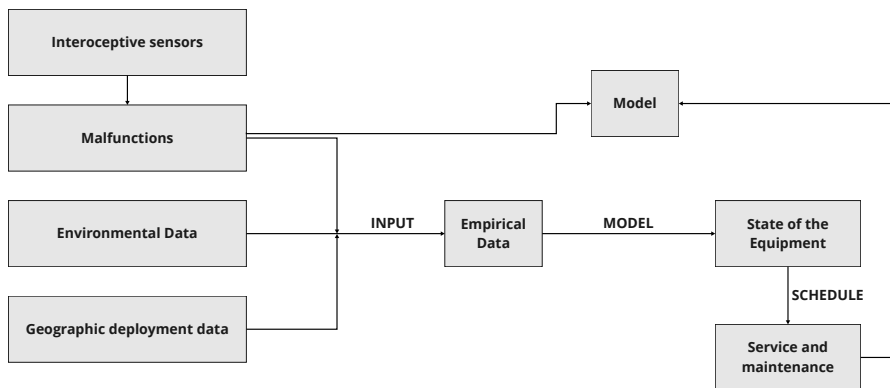


Figure 7.2: Sequence for service and maintenance of the ECN.

²<https://web.archive.org/web/20180728204314/https://www.digitaldaniels.com/availability-service-level-9-s-equate/>

³<https://www.bmc.com/blogs/system-reliability-availability-calculations/>

As stated in subsection 5.11.3, predictive maintenance will be used to schedule events for servicing and maintenance of the node. Different sensors are included in the node. Introspective sensors, which are present in different subsystems, provide information on malfunctions of the respective subsystem and provide empirical data for the predictive maintenance model. This is done by employing a model which assesses the current state of the equipment, taking introspective sensors data as input. Based on the state of the equipment and activities, maintenance of a particular subsystem or the whole node can be scheduled. The model is continuously taking the failures and maintenance activities as input to update the model.

Apart from this, the ECN's optical bench contains all the components for FSO communication, and was designed with modularity in mind. All the components in the optical bench, as described in section 5.4, can be replaced if required, based on the results from sensors which will give an estimate of when a component is prone to failure. Being modular, the optical bench can be simply taken out and a particular system in it can be replaced based on failure.

7.4. Safety

The final part of the RAMS characteristics is the safety which needs to be ensured to avoid harming another human being, the section 7.4 will explain different beam classes and the allowed intensity for the node. Alternatively, safety is important to avoid the undesired events such as interfering in the navigable airspace, which will be further described in subsection 7.4.2.

7.4.1. Laser Wavelength and Intensity

This section has been inspired by the Regulatory Considerations: Laser Safety and the Emerging Technology of Laser Communication⁴. The most important factor in defining the hazard of a laser for an aircraft is the wavelength of the laser. The wavelengths near and above 1400 nm can be seen by human eyes and can be distracting even at low power levels of 1 mW/cm². "The infrared range of wavelengths can be focused by the eye and retina making them especially hazardous". The chosen wavelength, both for the beaconing and transmission is 1550 [nm] and is in the infrared range and is not considered hazardous.

The intensity of a laser beam matters only when a beam is beam looked into. The laser distance which is safe for viewing for a human eye is known as Nominal Ocular Dazzle Distance (NODD), as shown in figure 7.3.

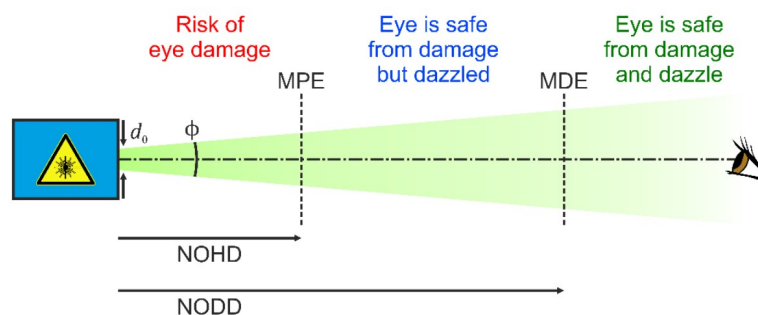


Figure 7.3: Hazard distances for the human eye: Nominal Ocular Hazard Distance (NOHD) and Nominal Ocular Dazzle Distance (NODD). MPE: Maximum Permissible Exposure; MDE: Maximum Dazzle Exposure. [96]

The laser beams can be divided into 4 different classes. Class I lasers are considered safe with no eye damage even after extended exposure of more than 6 to 8 hours. No safety equipment is needed for

⁴https://www.nasa.gov/sites/default/files/atoms/files/17_regulatory_considerations_laser_safety_and_the_emerging_technology_of_laser_communication_b_edwards.pdf

using equipment with a class I rating. Class II lasers are lasers with power below 1 mW in visible range. These laser types can damage eyesight if viewed for extended periods of time. Class III lasers are continuous-wave lasers with power between 1 to 5 mW. These beams should not be looked at directly and should not be viewed with telescopic devices. Class 3B lasers have power between 5 to 500 mW and have an adverse effect when coming in contact with humans⁵. Class IV lasers have power of more than 500 mW and are considered devastating and can cause permanent damage if in contact with any human body part. For Class I, II, III and IV⁶ has been used.

The laser beam used for beaconing and transmission is between 100 [W] as calculated in the section 5.12. This puts it under high power category 4 lasers. This implies that the people working with active laser beams will have to wear protective equipment and untrained personnel would have to be restricted in restricted areas. This also implies that any contact with the laser beam would have irreversible damage to the skin and eyes.

7.4.2. Air Navigation Issues

For laser beams passing through navigable airspace, prior permission from the FAA/ EASA or any government authority has to be taken. The system has to be compatible with guidance and performance criteria as set by AS6029A⁷.

Remote Unmanned Operations

As the ECN being designed has to be operated with limited expertise, and both the node as the HAPS are assumed to be unmanned.

Mitigation in the Current Setup

The ECN would have to be operated without any personnel and thus the only way to educate people about the danger is to stick posters and write warnings outside the ECN in multiple languages and pictures such as figure 7.4. An operation light is also proposed to indicate if the equipment is operational or not.



Figure 7.4: Hazard symbol

The ECN has to be deployed in coordination with the local ATC as the aircraft has to avoid direct contact with the same. A transponder is to be fitted to the ECN along with a GPS device to determine and communicate the location. The pointing device on the ECN can go to a certain angle and will traverse a round cone in the sky. To make sure that the laser does not come in direct contact with an aircraft, two solutions can be approached. First, all aircraft, both commercial and military have to be rerouted around this. However, this process can be complicated and costly. Therefore, the ECN

⁵<https://www.lasersafetyfacts.com/3B/>

⁶<https://www.ehs.iastate.edu/sites/default/files/uploads/publications/factsheets/laserfactsheet.pdf>

⁷<https://www.sae.org/standards/content/as6029a>

pointing range will be restricted to regions without aircraft (i.e. to regions where the laser will not come in the direct contact with a flying aircraft).

8

Risk Assessment

In the following chapter, the risks arising from the various subsystems are analysed and the mitigation strategy is presented. The probability and impact of every risk is considered using methodology introduced in Midterm Report [2]. The probability is rated on the scale: very unlikely, unlikely, likely and very likely, and the impact is rated as: negligible, marginal, critical or catastrophic. The risks in table 8.1 derive from the set previously identified [2]. A mitigation strategy and its results are also included.

Modularity is one of the main feature of the ECN and it can be exploited as a mitigation strategy. Every time a component gets damaged, this can be easily substituted to cope with the damage and the associated risks.

Table 8.1: Updated technical risk probability and impact

Risk ID	Risk	Probability / Impact	Explanation and mitigation strategy	Probability / Impact after mitigation
R1	Spontaneous combustion of lithium batteries	Unlikely / catastrophic	Lithium batteries may overheat and catch fire. The risk is already categorised as unlikely, and as the temperature range will be kept by thermal management subsystem within a defined range (section 5.9), the risk can be neglected.	Risk accepted
R2	Sub-optimal battery performance due to encountered low temperatures	Likely / marginal	In order to prevent malfunction or sub-optimal performance of batteries due to low temperatures, thermal management subsystem maintains suitable temperature range (section 5.9).	Probability: unlikely
R3	EPS failure due to water entering the systems	Unlikely / critical	ECN-F-SAR-4-2 requirement asserts that the product must be IP#3 certified. Suitable steps will be taken, and chapter 2 includes validation plan for watertightness.	Probability: very unlikely
R4	Node is exposed to harsher conditions than assumed in requirements	Unlikely / Critical	The operational envelope is well defined and accounts for a wide range of conditions, it possible anyway that harsher conditions are encountered. In order to cope with this risk, the ECN can enter the so called safe mode as shown in chapter 4	Impact: marginal

Table 8.1 continued from previous page

Risk ID	Risk	Probability / Impact	Explanation and mitigation strategy	Probability / Impact after mitigation
R5	Improper operation of node due to untrained personnel	Likely / Critical	Unavailability of highly trained personnel is the motivation behind requirement ECN-F-PRF-2. Partial autonomy of the system has been implemented, with automatic PAT sequence (section 5.6) and environmental monitoring subsystem including situational awareness element (section 5.11).	Impact: marginal
R6	Damage to telescope during transportation	Unlikely / critical	In order to protect it during transportation, the telescope will be supported structurally, and the aperture will be covered. ECN can be covered with tarpulin to prevent ingress of debris that could damage optics, similarly as with safe mode (subsection 4.3.3). Finally, EVE design already shields sensitive components in the telescope assembly (section 5.3).	Probability: very unlikely
R7	Damage to the station's legs due to severe impacts	Likely / catastrophic	Designing robust legs with damping systems including appropriate safety factors will allow to reduce the impact of such a hazard. The topic has been addressed in section 5.7.	Impact: marginal
R8	Node damaged by atmospheric conditions or environmental hazards, such as falling trees or hail	Unlikely / critical	The system is designed to be rugged, this risk is therefore accepted. However carefully choosing the deployment spot will further reduce the probability of any of these damages.	Probability: very unlikely
R9	Clouds attenuate laser to an unacceptable extent	Likely / catastrophic	This is a danger that cannot be mitigated during deployment, therefore abundant safety margins have been included in the link budget calculations, to account for this risk during design process.	Probability: unlikely
R10	Atmospheric noise making signal impossible to be received	Likely / catastrophic	Forward Error Correction (FEC) will be applied, with redundant data sent so that the target receives uncorrupted data, and operations under reduced data rate is still possible	Probability: very unlikely
R11	Debris deposit on the optical subsystem	Likely / Critical	The chosen gimbal design called EVE shields sensitive components of optical subsystem (section 5.3).	Impact: marginal

Table 8.1 continued from previous page

Risk ID	Risk	Probability / Impact	Explanation and mitigation strategy	Probability / Impact after mitigation
R12	Modulation requiring a SNR ratio higher than the accounted one	Unlikely / critical	Forward Error Correction and high sensitivity receivers are used to account for this risk. Modulation is extensively discussed in section 5.1.	Probability: very unlikely
R13	16-QAM modulation scheme reveals to be unfeasible for LEO	Likely / critical	If problem occurs, change the modulation to one with lower bandwidth efficiency and higher robustness to noise (such as QPSK). Modulation is extensively discussed in section 5.1.	Probability: unlikely
R14	Low frequency external vibrations causing optical difficulties	Likely / Critical	The optical equipment is sensitive and needs to be accurate, and vibrations pose a treat to this accuracy. Damping systems will address the risk. Frequency analysis is adressed in section 5.7.	Impact: marginal
R15	Resonance caused by harmonic excitation	Unlikely / critical	Frequency analysis was performed in section 5.7 to understand the natural frequency of the system and design damping systems accordingly.	Probability: very unlikely
R16	Stars are misidentified during the PAT sequence	Likely / critical	Increasing detection threshold will eliminate more noise and produce more accurate outcomes. The star tracking software will be verified and validated using methods outlined in subsection 5.5.2.	Probability: unlikely
R17	Attitude determination sensors unavailable due to environmental conditions (metal objects for magnetometer, night for celestial compass)	Likely / catastrophic	The system uses three types of attitude determination sensors, each with different strengths. By including this type of redundancy, the probability drops. Discussed in more detail in Midterm Report [2] and subsection 5.6.1.	Probability: unlikely
R18	Bugs in the PAT sequence code or the atmospheric turbulence model	Likely / critical	The risk is tackled by extensively verifying and validating the code. Plan for PAT verification and validation is included in subsection 5.6.6, and for turbulence model in table 5.2.4.	Probability: unlikely
R19	Budget overrun	Very likely / Marginal	Budgets are often overrun, as it is difficult to determine in advance in detail the costs. Continuously updating the various budgets, in consultation with the stakeholders, will allow a more efficient and transparent engineering process.	Probability: Likely

Table 8.1 continued from previous page

Risk ID	Risk	Probability / Impact	Explanation and mitigation strategy	Probability / Impact after mitigation
R20	Price of raw materials rise due to inflation increasing production costs	Very likely / Marginal	With inflation is happening right now, this risk is a near certainty. This must be accounted in the budget analysis. The effect is monitored and accounted for.	Probability: likely
R21	Competitors designing a more competitive station	Likely / Catastrophic	Since FSO is currently undergoing fast development, it is likely that a competitor might come up with a more competitive design. Market analysis must be frequently updated to mitigate this risk. An update has been performed for this report in chapter 2.	Probability: unlikely
R22	Vehicles are unavailable, making it impossible to operate the ECN within 48 hours	Unlikely / Critical	The risk is accepted, as the military vehicles are reliable and nearly always available. Proper logistical planning from side of the operator is nearly certain to prevent this problem.	Risk accepted
R23	The disaster location doesn't allow to be approached within 48 hours	Unlikely / Critical	Extensive verification and validation will be carried out on the transportation chain to make sure that any location can actually be reached in time or within a reasonable time regarding the situation. The V&V plan has been presented in section 4.4.	Impact: marginal
R24	Design iterations increase the ECN size making the current transportation means unfeasible	Likely / critical	Analysis of transportation methods capable of taking care of this bigger station has been added as a recommendation in chapter 12.	Impact: marginal
R25	If the calculated aperture size is too big, the telescope lenses will increase in volume and cost accordingly. This might make telescope design unfeasible.	Likely / critical	Sensitivity analysis of aperture size and its impact has been performed in section 6.3. Alternatives for the telescope design were discussed in subsection 5.3.7.	Impact: marginal

Table 8.1 continued from previous page

Risk ID	Risk	Probability / Impact	Explanation and mitigation strategy	Probability / Impact after mitigation
R26	The ECN does not perform the operations such as entering safe mode as intended	Unlikely / Catastrophic	Verification and validation plan has been created for deployment and operation (section 4.4). Furthermore, there is also the possibility of having a manual override and trigger the safe mode.	Probability: Very unlikely
R27	Underestimation of transmission and receiver losses in link budget	Unlikely / critical	High margins in link budget calculations are considered to compensate for it (section 5.2). Sensitivity analysis has been performed for this scenario in section 6.3.	Impact: marginal
R28	Atmospheric turbulence model uses incorrect assumptions	Unlikely / marginal	Turbulence model already takes very conservative values, has a validation plan, and has been made after an extensive literature review. The risk is therefore accepted.	Risk accepted
R29	Receiver sensitivity values being too optimistic, and not allowing for the desired link	Likely / critical	The risk is monitored and studied, with a worst case scenario of accepting operation at lower data rates as a link.	Impact: marginal

These risks are presented in table 8.2 and table 8.3 where the effect of mitigation clearly shows how the risks have been shifted towards a "safer" area of the graph

Table 8.2: Risk map before mitigation is applied

Catastrophic		R1, R26	R7, R9, R10, R17, R21	
Critical		R3, R4, R6, R8, R12, R15, R22,	R5, R11, R13, R14, R16, R18,	
Marginal		R28	R2	R19, R20
Negligible				
	Very unlikely	Unlikely	Likely	Very likely

Table 8.3: Updated risk map following the mitigation strategy

Catastrophic	R10, R26	R1, R9, R17, R21		
Critical	R3, R6, R8 R12, R15	R13, R16, R18, R22		
Marginal		R2, R4, R5, R23, R27, R28	R7, R11, R14, R19, R20, R24,	
Negligible				
	Very unlikely	Unlikely	Likely	Very likely

9

Manufacturing, Assembly and Integration

9.1. Layout

The components of the system have to be arranged spatially within the casing. The layout of the product is discussed in this section.

9.1.1. Modular Design

Sustainability requirements ECN-F-SUS-1 and ECN-F-SUS-2, and associated subrequirements, introduce a series of assertions about the assembly process of the product. Laser terminal should be removable from the system. The product should be maintainable and able to be refurbished. Finally, it should be possible to replace components with compatible upgraded versions. In other words, the product should be designed for ease of disassembly and reassembly. Modular design is an elemental technique improving maintainability, upgradeability, reusability and recyclability [97].

Optimal modular structure varies according to the goals. Design for recyclability favors placing components with the same constituent materials together in modules. Modular design for maintenance groups components by physical lifetime, while design for upgradeability groups them by value lifetime. Design for reusability takes both into account [97]. Finally, the structure must take into account the required connections between components, manufacturing, and other technical constraints.

The driving criterion for defining the modules was function: modules mostly follow subsystem division in detailed design, with components contributing to same task being placed together in a module. The final modular division is presented in table 9.1

Table 9.1: Modular division

Module	Components
Workstation (Command & Data Handling)	Computer, input/output interfaces

Optical bench	Fine tracking / star tracking camera, detector, adaptive optics, other optical instruments
Thermal (heat pump)	Temperature regulator, sensors, ventilator
Battery	Batteries
Power Distribution Unit	Electrical circuit
Gimbal	Telescope, motors, FSM
WFoV (coarse tracking)	Camera sensor, motorized lens
Display	Screen
Sensors (Attitude Determination and Environmental Monitoring)	Magnetometer, bio-inspired celestial compass, weather sensor, air quality sensor, noise level meter

9.1.2. Other Elements of the System

The modules are placed in the casing, the primary structure, which also includes damping, wiring, and other components necessary for integration of modules into the ECN. Finally, last element is a towing cart, onto which ECN is placed for logistics.

9.2. Manufacturing

The primary truss structure of the ECN is manufactured out of aluminium. Aluminium has excellent machinability. Cutting and chipping aluminium requires less power and less expensive tools than other materials, such as steel¹. The material can be worked and formed using variety of methods, and is one of most popular choices of material for manufacturability. Manufacturing was a part of the trade off for material selected, performed in subsection 5.8.1.

Aluminium is placed at a forefront of innovation in manufacturing thanks to technology enabling producing complicated geometries with the durable and lightweight material with additive manufacturing². Finally, many of other, widely applicable techniques are also viable, such as extrusion to produce long profiles with constant cross-section³. Manufacturing of particular parts is beyond the scope of this report, but a set of manufacturing methods will have to be selected to fit the final detail design once it is arrived at.

To increase the efficiency and the production speed of the node, the structural parts will be produced in batches. This means that the same part will be produced in multiple quantities at once. Such procedure saves the production time since no time is wasted on re-calibrating the machines before the start of the production, and the workers get familiar with repeatability of the same task allowing a faster manufacturing of a part [98]. After the batch has been produced the parts go to storage, parts can be produced again once there starts to be a shortage of those components.

9.3. Assembly

The components are assembled into sections or sub-assemblies, which are then combined into the final assembly. This is done for production efficiency, as to efficiently split work in the production process, as well as to assure the lowest time for delivery of parts. Another reason is operations and maintenance [99]. In this section, the assembly of the ECN components will be discussed.

¹<https://xometry.eu/en/cnc-machining-of-aluminium/>

²<https://www.sculpteo.com/en/materials/slm-material/slm-aluminum-material/>

³<https://www.gabrian.com/what-is-aluminum-extrusion-process/>

9.3.1. Joining

Four main methods of joining components together can be outlined: riveting, bolting, adhesive bonding, and welding.

Adhesive bonding is a proven way to achieve high performance characteristics at minimal weight, and therefore found use in automotive and aerospace applications. It works by placing an adhesive, usually resin, between two joined surfaces. The adhesive solidifies, forming a rigid connection between the components. Though highly performing, adhesive bonding complicates the assembly process, and is not compatible with modularity. Adhesive bonds cannot be open for inspection, maintenance, or upgrade, without destroying the bond [100]. Apart from that, many adhesives emit Volatile Organic Compounds (VOCs) causing, among others, respiratory problems, migraines, and irritation to eyes. Wastewater from adhesive production contains a high levels of pollutants [101]. Adhesive bonding therefore is not suitable to play a big role in assembly of the ECN.

Welding has a unique advantage of mechanical fastening by joining two similar materials into one continuous section. Welded joints are airtight and watertight, however, they are inappropriate for many materials [102]. Welding will be utilized in assembly of sections and sub-assemblies, wherever it is deemed the most efficient or highest performing joint. Assembly of sub-assemblies into a final assembly will be done using another joining methods, more compatible with the modular design.

The modules will be placed within the primary structure of the system, in compatible slots, and secured with bolts. This ensures high accessibility and ease of replacement of the modules. Bolts are very similar to rivets, however with some beneficial differences that the ECN design exploits. Bolts are always used in sections that must be disassembled frequently. Bolted joints are stronger, and can be used at places with large concentrated forces, in shear as well as tension (as compared to rivets, that only tolerate shear) [103]. Bolted joints come at a higher cost, however, are better for structural integrity, manufacturability, and modularity of the product.

9.4. Organization of Production Process

Two very different production approaches are often placed in opposition to each other: mass production, and a dock-like system. Mass production has thousands to millions of components continuously processed by a highly optimized and cost-efficient production facility. It fully leverages economies of scale, to achieve cost reductions at maximal throughput [104]. On the other hand, dock-like system is suited to a production process that must only produce one or a few products [98]. All manufacturing activities are performed on a product resting in one place (the dock).

Aerospace industry, in particular aircraft production, relies on line production. It can be described as an intermediate approach, using parts manufactured in batches supplied to the assembly line, consisting of stations between which the product transitions at time intervals. Each station consists of the same crew, performing the same task on subsequent units. Line production enables efficient organization, minimal transport and a good indication of progress. Sub assemblies are produced in sub-assembly lines, which join the final assembly line. Line production organization can be presented in a schematic assembly lines, a diagram illustrating how inputs and outputs of each station are connected [98].

Line production was chosen for organization of the production process of the ECN.

9.5. Production Plan

Schematic assembly line was constructed for the ECN and presented in figure 9.1.

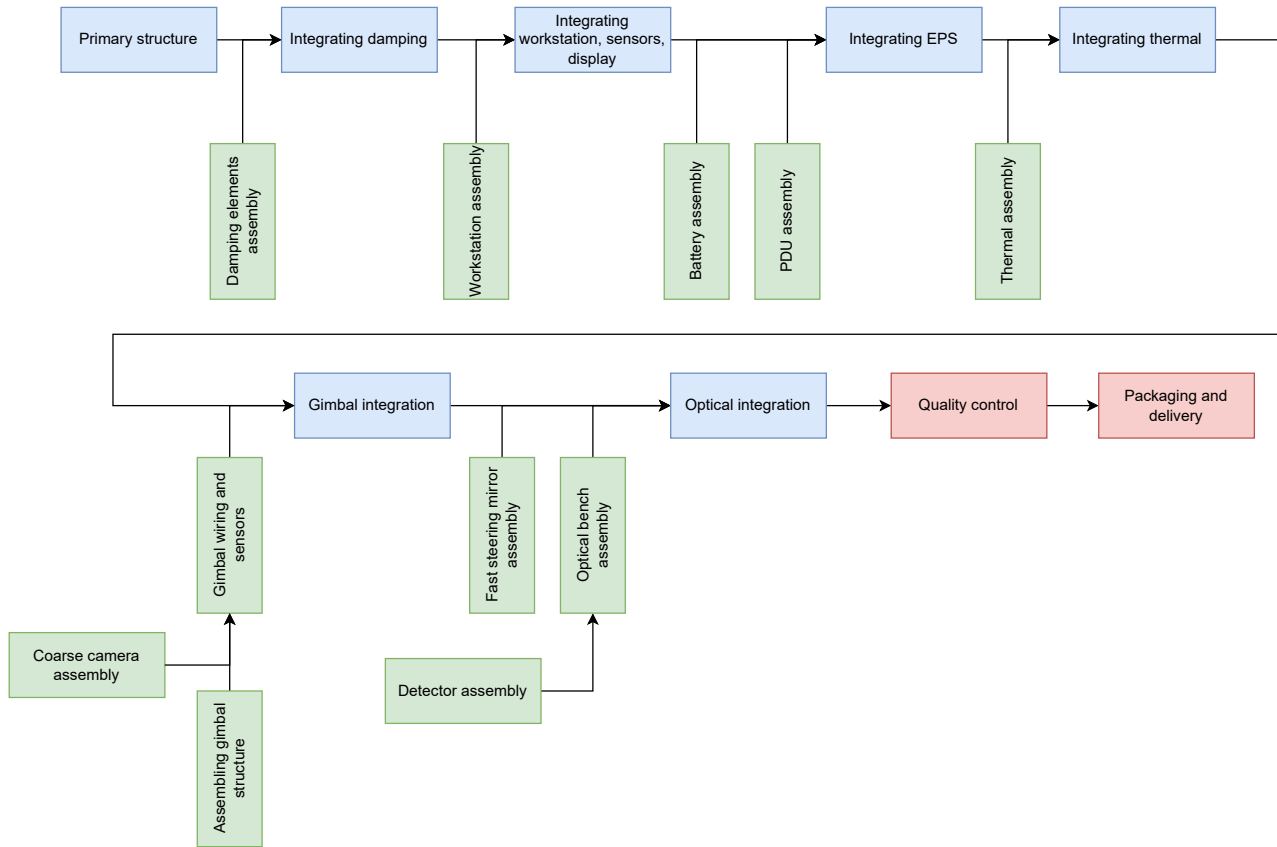


Figure 9.1: Schematic production line of Emergency Communication Node

9.5.1. List of Products

The main assembly line integrates the following modules into the product: damping, workstation assembly (workstation and display modules), sensors suite, battery and PDU assemblies, thermal assembly, gimbal assembly (gimbal and WFoV modules), and optical bench. They are integrated in stations, in the order presented in figure 9.1. The modules are explained in more detail in table 9.1 in subsection 9.1.1. During the work distribution table, it was considered that the workers do not overwork outside of the working hours, and that a sufficient working force is considered.

9.5.2. Production Timeline

Work distribution table, with stations organized as in schematic production line to form a production timeline, is presented in table 9.2. The crew count and time necessary are preliminary estimations. A safety factor of 4 is advised for total manhours required, as predicted in the work distribution table.

Table 9.2: Work distribution

Crew	Part	Task	Time
2	Main assembly	Assemble primary structure	4 hours
1	Damping assembly	Assemble damping elements	3 hours
1	Main assembly	Integrate damping	4 hours
1	Workstation assembly	Assemble workstation	4 hours
3	Main assembly	Integrate workstation, sensors, and display	4 hours
2	Battery assembly	Assemble battery assembly	2 hours

1	Battery assembly	Assemble PDU assembly	1 hour
2	Main assembly	Integrate EPS	8 hours
1	Thermal assembly	Assemble thermal assembly	4 hours
2	Main assembly	Integrate thermal assembly	4 hours
1	Gimbal assembly	Assemble gimbal structure	4 hours
1	Gimbal assembly	Integrate wiring and sensors	2 hours
1	Coarse camera assembly	Assemble coarse camera assembly	2 hours
2	Main assembly	Integrate gimbal	4 hours
1	FSM assembly	Assemble FSM assembly	2 hours
1	Optical bench assembly	Assemble detector assembly	2 hours
2	Optical bench assembly	Assemble optical bench	2 hours
2	Main assembly	Integrate optical bench	4 hours
27		Total manhours	88 hours

9.5.3. Risks

The following risks associated with production have been identified:

Risk 1: Longer main assembly line time interval

Line production has the benefit of specialized crews at each station. The estimations provided are for an experienced crew. It is likely that first prototypes will take orders of magnitude longer times to produce. While integration of wiring and sensors was estimated to reliably only take 2 hours, it might be a multi-day endeavour for the first system produced. This fact must be accounted for by the party responsible for manufacturing of the product.

The provided numbers are also preliminary estimates. As mentioned in subsection 9.5.2, a safety factor of four is advised. It might turn out that tasks must be redistributed between stations, such that the time interval between stations matches for maximum efficiency.

Risk 2: Insufficient quality of components

Since the design uses many COTS components, and design might require outsourcing manufacturing some of the parts, they must be thoroughly inspected. This is true in particular for more complex components, whose efficacy must be confirmed before integrating it with the product. The selected suppliers must be reliable to ensure compliance with technical specification and timely delivery to the production line.

Risk 3: Tools or components missing

An inventory management system must be implemented and kept up to date, to ensure availability of stock and tools, and efficient use of resources. Understanding of production line inventory and demand on it leads to more efficient purchase orders, and ensures no disruptions in production process.

Risk 4: Workers getting injured with the cutting tools

Some of the subtracting manufacturing tools such as lathing or milling, do involve cutting tools which can be dangerous to operate if not handled properly. According to the US database, operating the lathe machine has caused 421 people to suffer severe or fatal injuries⁴. Therefore, for the

⁴https://www.osha.gov/pls/imis/accidentsearch.search?sic=&sicgroup=&naics=&acc_description=&acc_abstr act=&acc_keyword=%22Lathe%22&inspr=&fatal=&officetype=&office=&startmonth=&startday=&startyear=&end month=&endday=&endyear=&keyword_list=on&p_start=&p_finish=0&p_sort=&p_desc=DESC&p_direction=Next&p_s how=20

workers safety and to consider the social sustainability, safety protocols for every scenario need to be established.

To ensure the social sustainability, providing the operating tutorial of the machinery is personnel is important. Though the workers may be familiar with the process, every machine may have its own peculiarities. Secondly, provision safety coat, goggles, gloves and other equipment is necessary to minimise a chance of personnel getting injured. Safety of the workers is important for their own well-being and also it will minimise disruption or delays in the production process, hence chance of getting injuries must be minimised.

9.5.4. Discussion

For the preliminary production plan, each station of the main assembly line was determined to have a time interval of 4 hours. This means that the production plan outputs a complete product every 4 hours, or two products on each workday. There are 7 stations between first and last assembly/integration station, which brings the total time between starting primary structure assembly to finish of optical bench integration to 28 hours. Some of sub-assembly lines take shorter time. If production of optical bench assembly takes 2 hours, 4 assemblies can be produced during a day. Only two optical assemblies can be integrated in the main assembly. That means that the station will produce surplus, which can be stocked, or that the station can operate not every working day.

9.6. Sustainability

Sustainability for the manufacturing, assembly and integration consists of the two main pillars, being the social and the environmental sustainability. One major consideration of social sustainability has already been described in the subsection 9.5.3, talking about worker's safety and injury prevention. Another social sustainability is related to the work distribution, stated in the subsection 9.5.2. It is important that the workers are able to enjoy their own life, therefore it has been considered that no work outside of working hours is required.

Regarding the environmental sustainability, for the subtractive manufacturing the scrap material is being removed in forms of chips. This scrap material is a raw material, therefore for environmental sustainability of the scarcity resources, recycling of the scrap material will be implemented. In case of the node, the material resource is the aluminium, all of the chips from machinery will be collected and sorted together in the recycling container. After which the collected chips, follow the process illustrated in figure 9.2, where the main procedure components are being melting and casting. After this process, the previously collected chips can be used as manufacturing material again.

Another factor regarding environment sustainability considered is the use of different structural parts, rather than having large welded structure. In the modular design section, subsection 9.1.1, parts can be disassembled and provide more room to maintain the node better. Maintenance, allows the node to be operational for the longer periods of time, reducing the urge of constructing a new node and saving the use of raw materials. Maintenance ease also provides economical sustainability of the node since cost per node's operational times is reduced. Second environmental aspect related to the modularity, is that in case a side of the node is damaged, relevant part can be replaced and joined rather than rebuilding the entire node. It is sustainable since the use of raw materials is being minimised.

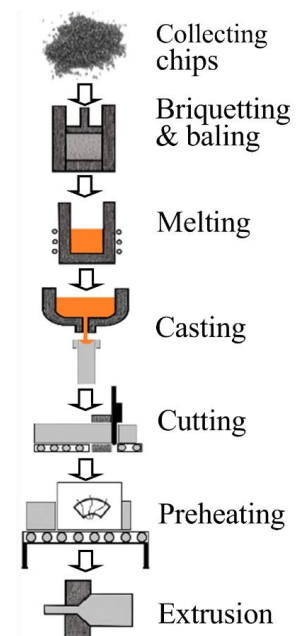


Figure 9.2: Conventional way of recycling the manufacturing chips [105]

Final point regarding the sustainability is for complicated parts, such as the elbow pieces seen in the backup option of coelostat design, subsection 5.3.2. Such parts can be complicated to be mass produced and subtractive manufacturing may be subjected to the human error, and not manufactured properly. Therefore, to reduce the waste of material additive manufacturing for metals such as Selective Laser Melting (SLM) can be implemented [106].

10

Requirements and Compliance

The product addresses the need for a mobile optical communication ground station, rapidly deployable in disaster response scenarios and providing high bandwidth. A compliance matrix was constructed to ensure that the developed product meets stakeholder requirements.

10.1. Final Requirements

Final requirements were inherited from baseline requirements, and affirm to the same designation system. The numbering is consistent across the two sets of requirements, such that the PRF-1 final requirement is inherited from PRF-1 baseline requirement. Following changes were introduced:

Table 10.1: Changes to the requirements

Old identifier	Old requirement	New identifier	New requirement
ECN-B-PRF-7-1	Fine attitude control shall have pointing accuracy less than TBD arcseconds.	ECN-F-PRF-7-1	Attitude control shall have pointing accuracy less than 1 arcminute in clear sky conditions.
ECN-B-PRF-7-2	Fine attitude control shall have stability (peak-peak motion) less than TBD arcseconds.		Merged with ECN-F-PRF-7-5.
ECN-B-PRF-7-3	Fine attitude control shall track objects moving at an angular rate of TBD deg/s.	ECN-F-PRF-7-3	Fine attitude control shall track objects moving at an angular rate of 10 [deg/s].
ECN-B-PRF-8-1	Maximum power output of EPS shall be TBD kW.	ECN-F-PRF-8-1	Maximum power output of EPS shall be 1500 W.
ECN-B-PRF-8-2	EPS shall deliver total energy of TBD kWh.	ECN-F-PRF-8-2	A version of the system with internal power supply for 48 hours of operation shall be available.
		ECN-F-PRF-7-4	Attitude control shall have pointing accuracy less than 2 degrees in any weather condition.
		ECN-F-PRF-7-5	Fine attitude control shall track objects with accuracy better of at least 1 μ rad.

ECN-B-PRF-7-3 corresponds to a slew rate that can manage high slew rates for high target elevation, when the target approaches singularity. Angular rate of 10 [deg/s] allows reliable tracking at elevations lower than 80° [58]. The topic has been discussed in more detail in midterm report [2].

The ECN-F-PRF-7-5 comes from link budget constraint (section 5.2). ECN-F-PRF-7-1 and ECN-F-PRF-7-4 are technical requirements concerning integration of PAT sequences and ability to transition between them, as discussed in section 5.5 and section 5.6. To summarise, multi-stage control approach works as follows. Calibration with attitude determination sensors, determining pointing accuracy (ECN-F-PRF-7-1 and ECN-F-PRF-7-4), must be good enough for efficacy of coarse tracking camera, which in turn must perform well enough to enter fine tracking stage, which then guarantees strong enough link for the communication requirement.

ECN-F-PRF-8-4 was added to satisfy possible operational needs of the product, with another, shorter time version available, as elaborated on in section 5.10. Motivation is as follows: the 48 hours power supply is an advantage in certain conditions, where disruptions to the electrical grid are expected, however it is redundant in others.

10.2. Compliance Matrix

The compliance status is marked with a symbol: + for compliant, +/- for partially compliant, and - for non-compliant. Risk is marked with L for low, M for medium, and H for high.

Table 10.2: Compliance matrix

Identifier	Requirement	Compliance	Risk	Justification
ECN-F-PRF-1	The system must be deployable to any location on Earth (up to 3000 [m] altitudes) within 48 hours.	+	L	See section 4.1.
ECN-F-PRF-2	The station shall be able to be operated by people with limited expertise on the ground.	+	L	See section 4.3. Aspect to be validated, with plan in section 4.4.
ECN-F-PRF-3	The station shall be capable of bi-directional communication (sending and receiving data) with High Altitude Pseudo Satellites.	+	L	See section 5.2.
ECN-F-PRF-3-1	The station shall achieve very high data rate optical communication (> 100 [Gbps] sending and > 100 [Gbps] receiving), to enable short communication 'bursts' between clouds.	+	M	See subsection 5.1.2
ECN-F-PRF-3-2	The station shall establish communication with UAVs at elevation angles $> 20^\circ$.	+	L	This elevation is considered in the link budget found in section 5.2.
ECN-F-PRF-3-3	The station shall establish communication with UAV at altitudes between 18-28 [km].	+	L	See section 5.2.

Table 10.2 continued from previous page

Identifier	Requirement	Compliance	Risk	Justification
ECN-F-PRF-3-4	The station shall establish communication with Airbus Zephyr and Facebook HAPS UAV platforms.	+	M	See section 5.2
ECN-F-PRF-4	Desirable: The station shall be capable of bi-directional communication with LEO satellites.	+	M	Both an uplink and downlink budget are given in section 5.2, and section 5.4 discusses it further.
ECN-F-PRF-4-1	The station shall establish communication with satellites at elevation angles > 30 deg.	+	L	This elevation is considered in the link budget found in section 5.2.
ECN-F-PRF-4-2	The station shall establish communication with LEO satellite at altitudes between 350-500 [km].	+	M	This altitude is considered in the link budget found in section 5.2 and considered in the gamma-gamma model for atmospheric attenuation
ECN-F-PRF-4-3	The station shall achieve high data rate optical communication (Gbps regime).	+	M	See subsection 5.1.3.
ECN-F-PRF-5	The mobile optical ground station shall communicate in the optical spectrum and may use a separate, different beacon signal.	+	L	See midterm report for spectrum discussion [2] and subsection 5.6.3 for acquisition.
ECN-F-PRF-6	The mobile optical ground station shall use trajectory estimation for coarse attitude control to align the optical instruments.	+	M	section 5.5 presents camera sensors used for pointing. section 5.6 covers the multi-stage control sequence.
ECN-F-PRF-7	The mobile optical ground station shall use fine control to maintain alignment of optical instruments.	+	L	See subsection 5.6.4.

Table 10.2 continued from previous page

Identifier	Requirement	Compliance	Risk	Justification
ECN-F-PRF-7-1	Attitude control shall have pointing accuracy less than 1 [<i>arcminute</i>] in clear sky conditions.	+	L	See subsection 5.6.1.
ECN-F-PRF-7-3	Fine attitude control shall track objects moving at an angular rate of 10 [<i>deg/s</i>].	+	L	See subsection 5.3.4.
ECN-F-PRF-7-4	Attitude control shall have pointing accuracy less than 2 degrees in any weather condition.	+	L	See subsection 5.6.1.
ECN-F-PRF-7-5	Fine attitude control shall track objects with accuracy better of at least 1 [<i>μrad</i>].	+	L	See subsection 5.6.4.
ECN-F-PRF-8	The system shall include Electric Power System.	+	M	See section 5.10.
ECN-F-PRF-8-1	Maximum power output of EPS shall be 1500 [<i>W</i>].	+	L	See section 5.10.
ECN-F-PRF-8-2	A version of the system with internal power supply for 48 hours of operation shall be available.	+	L	See section 5.10.
ECN-F-PRF-8-3	EPS shall be interface with most encountered electrical grid infrastructure.	+	L	See section 5.10.
ECN-F-PRF-9	The communication node shall be able to interface with a commercially available laptop	+	L	See section 4.3.
ECN-F-SAR-1	The mobile optical ground station shall operate during day and night.	+	L	subsection 5.6.1 discussed nighttime calibration performance. Does not impact rest of PAT sequence. section 5.9 explores the thermal aspect of operation during the night.
ECN-F-SAR-2	Assuming cloud-free conditions, the mobile optical ground station shall be available 99% of the time when deployed.	+/-		See section 7.2 for discussion.

Table 10.2 continued from previous page

Identifier	Requirement	Compliance	Risk	Justification
ECN-F-SAR-3	The mobile optical ground station shall include precautions to avoid performance degradation due to deposition of sand and/or dust.	+	L	The EVE design isolates optical elements from dust deposition. See section 5.3 and midterm report [2]. Validation in chapter 2.
ECN-F-SAR-4-1	The mobile optical ground station shall be able to survive under harsh sand and dust conditions by being IP5# protected.	+	L	Validation in chapter 2.
ECN-F-SAR-4-2	The mobile optical ground station shall be able to survive under heavy rain conditions by being IP#3 protected.	+	L	Validation in chapter 2.
ECN-F-SAR-5-1	The mobile optical ground station shall consider operational wind speeds up to 15 [<i>m/s</i>].	+	L	subsection 5.7.4 explores the response of the system of 55 m/s winds and explains how to resist them, thus allowing for operation under 15 m/s winds. Validation in chapter 2.
ECN-F-SAR-5-2	The mobile optical ground station shall consider survival wind speeds up to [55 <i>m/s</i>].	+	L	subsection 5.7.4 explores the response of the system of 55 m/s winds and explains how to resist them. Validation in chapter 2.
ECN-F-SAR-6	The mobile optical ground station shall be operational in a temperature range from -30 to 40 [<i>deg</i>].	+	L	See section 5.9. Validation in chapter 2.
ECN-F-SAR-7	The mobile optical ground station shall be able to handle a survival temperature range between -50 and 60 deg C.	+	L	See section 5.9. Validation in chapter 2.

Table 10.2 continued from previous page

Identifier	Requirement	Compliance	Risk	Justification
ECN-F-SAR-8	The mobile optical ground station should comply with the Space Development Agency's Optical Communications Terminal (OCT) Standard.	+/-		Not yet covered.
ECN-F-SAR-9	Laser safety shall be addressed throughout the product life cycle of the mobile optical ground station.	+	L	See section 7.4
ECN-F-SUS-1	It shall be possible to recover and refurbish the laser terminal from the mobile unit.	+	L	See section 9.1.
ECN-F-SUS-1-1	The mobile optical ground station shall have an expected lifetime of at least 50 deployments, assuming it is subject to environmental conditions within specified survival range.	+/-		Not yet covered.
ECN-F-SUS-1-2	The refurbishing cost between missions of mobile optical ground station shall not exceed 15 k€, assuming it is subject to environmental conditions within specified survival range.	+/-		Not yet covered.
ECN-F-SUS-2	It shall be possible to upgrade the mobile optical ground station when new technologies emerge or when a new use case is defined.	+	L	section 9.1 and section 9.3 discuss upgradeability of the Node.
ECN-F-SUS-3	EPS carbon footprint shall not exceed 500 gCO ₂ per kWh.	+	L	Validation in chapter 2.
ECN-F-SUS-4	The mobile optical ground station shall not pose a threat of long-term harm to the environment in case of a leak, a breach, or other loss of structural integrity.	+	L	Environmental sustainability taken into account in chapter 3.
ECN-F-SUS-5	The mobile optical ground station noise pollution shall not require a monitoring program, as regulated by OSHA 1910.95(d)(1) (noise level shall not exceed time-weighted average of 85 decibels).	+	L	Noise meters are included to ensure compliance. See subsection 5.11.5.
ECN-F-SUS-5-1	The mobile optical ground station noise shall never exceed 90 dBA.	+	L	Noise meters are included to ensure compliance. See subsection 5.11.5.

Table 10.2 continued from previous page

Identifier	Requirement	Compliance	Risk	Justification
ECN-F-BDG-1	All link budgets shall consider an implementation margin of at least 3 dB.	+	L	See section 5.2.
ECN-F-CST-1	The recurring cost of a serial produced mobile optical ground station shall be less than 100 [k€].	-		See chapter 2.
ECN-F-OTH-1	A market analysis shall justify the cost targets.	+	M	See chapter 2.
ECN-F-OTH-1-1	A market analysis shall inform an estimated development cost.	+	M	See chapter 2.
ECN-F-OTH-2	Only high TRL technologies (> 4) shall be considered in order to decrease development timeline and non-recurring cost.	+	L	Design options' TRL level was discussed in midterm report [2]. Design decisions were made to conform to the requirement.
ECN-F-OTH-3	The final mobile optical ground station product shall be CE marked.	+/-		Not yet covered.
ECN-F-OTH-4	A first demonstrator of the mobile optical ground station shall be deployed and tested in 2026.	+	M	Covered in: market analysis (chapter 2), TRL levels (midterm [2], chapter 5), and chapter 11.

10.3. Feasibility Analysis

The compliance status of the product is presented in figure 10.1. Vast majority of the requirements have been met, with only 6 requirements not achieving full compliance. Five of those have been not yet solved or covered by the design explicitly due to time constraint, and one of them was deemed impossible to be met.

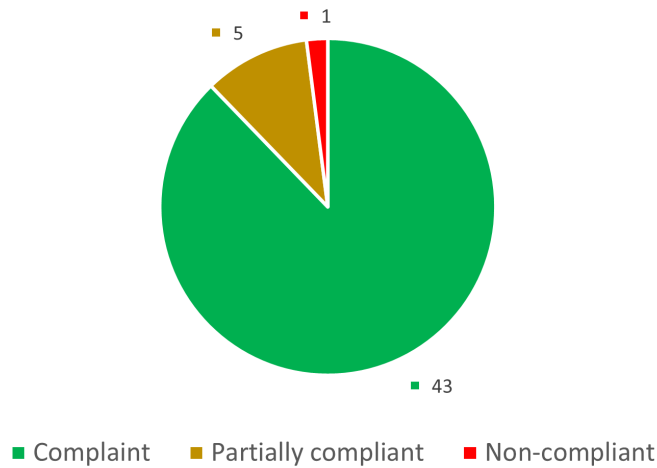


Figure 10.1: Compliance status (number of requirements complied with included)

The design doesn't comply with the ECN-F-CST-1 requirement, as fulfilling it would compromise at least several other driving and key requirements. The bottom up cost calculation, included in section 2.2, points to beam steering and optical subsystems as major contributors to the cost. The total cost estimate is around EUR 130 000, 30% over budget, and cost estimate with chosen safety factor of 1.5 places the estimate at over EUR 190,000, 90% over the budget. Beam steering subsystem is estimated to cost over EUR 50,000, with telescope, gimbal, and adaptive optics costing EUR 45,000. The components are chosen to satisfy crucial requirements ECN-F-PRF-3 and ECN-F-PRF-4. Optical subsystem is estimated to cost around EUR 23,500, with laser pump, transceiver and amplifier being most costly.

To fit within the budget, cost of those two subsystem would have to be substantially reduced. Otherwise, to meet the target with no safety factor, cost of other subsystems would have to be reduced by over 50%, which is very improbable given that safety margin corresponds to expected underestimate of costs. On the other hand, the beam steering and optical components offer the lowest performance to meet the requirements with required margin, and there is no space to compromise performance for cost. The higher cost must be corroborated as feasible with the relevant stakeholders.

11

Design and Development Logic

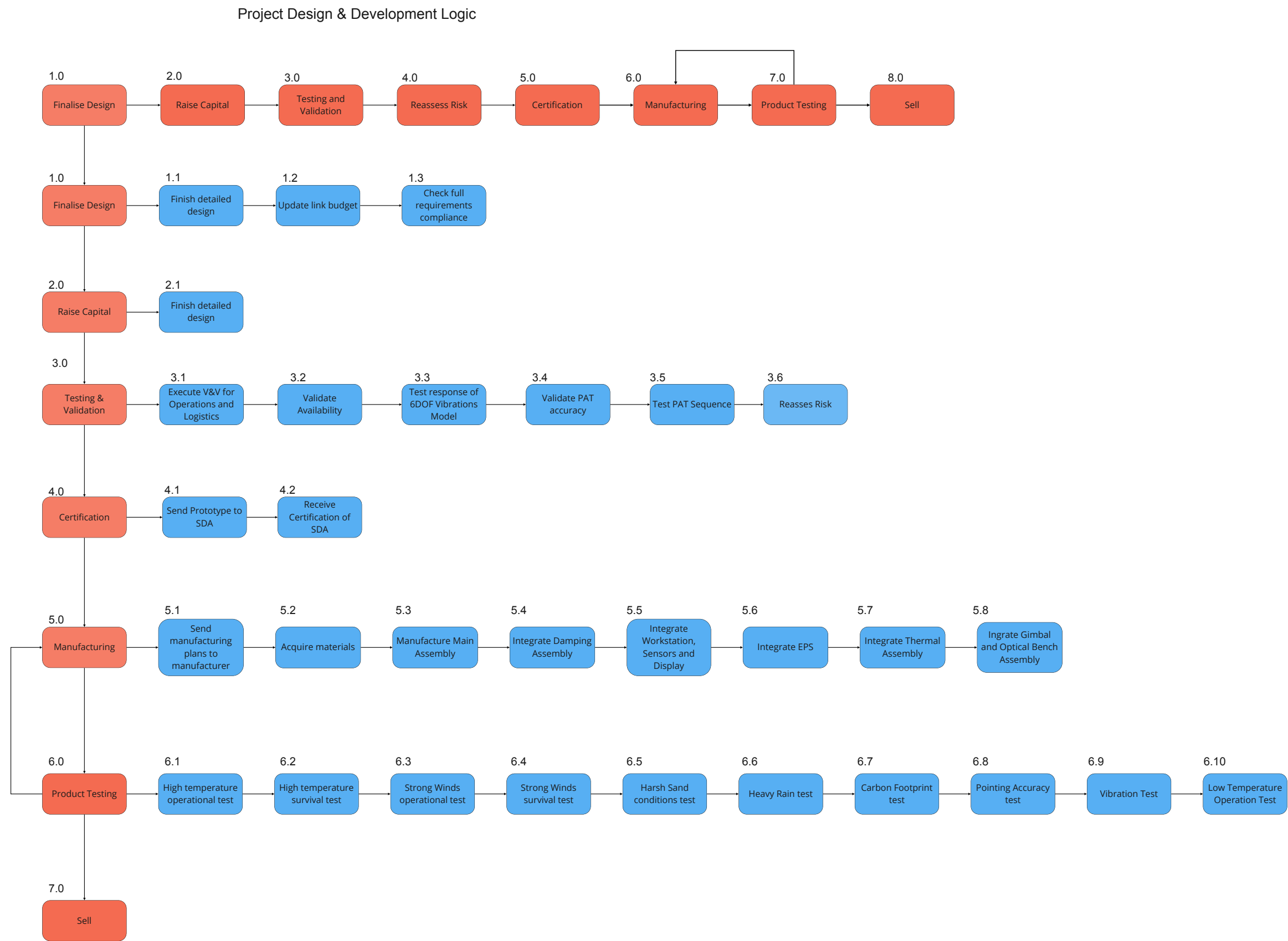
With the design at this stage it is not yet possible to start manufacturing and selling the product. The continuation of the ECN design is thus outlined in this chapter. This accounts for all required to finalize the design, start manufacturing and eventually sell the product. A flow diagram is created of the continuation of the project in figure 11.1. First of all, the design needs refinement for all subsystems. Several more design iterations are required to come to a valid design. According to chapter 2 the majority of the costs are going to be made from 2025 to 2026, thus funds are required to finance the project. After this the system and subsystem risks are evaluated again, and extensive testing and validation is performed on the subsystems. The system is certified after the testing. When certified, it can be manufactured and sold to the customer.

The time allocation for the different phases of the project are shown in table 11.1 using a Gantt chart. Six phases are identified, coming from the project design and development logic diagram.

Table 11.1: Gantt chart of project development

	2022				2023				2024				2025				2026				2027				2028			
	1	2	3	4	1	2	3	4	1	2	3	4	1	2	3	4	1	2	3	4	1	2	3	4	1	2	3	4
Finalise design	■	■	■	■																								
Raise capital				■	■	■	■																					
V&V									■	■	■	■	■	■	■	■												
Certification																	■	■	■	■								
Manufacturing																					■	■	■	■	■	■	■	■
Testing																									■	■	■	■

Figure 11.1: Project design & development logic



Conclusion and Recommendations

12.1. Conclusion

Following the establishment of the stakeholder and system requirements from the Baseline Report [1], trade-offs for the individual subsystems and for the general concepts were performed in the Midterm Report [2]. These cumulated in the final report which dealt with the preliminary design of the subsystems of the emergency communication node. The final product has been designed around the mission need statement, to provide a mobile bi-directional air-to-ground optical communication node to be fastly deployed in emergency situations. Through an iterative process, the mass, power, cost and data budgets were determined. After the design stage, improvement points were considered for further research.

The ECN, short for Emergency Communication Node, is to be produced in 2026. It will be available at a cost of roughly 2.5 million euros, weighing 863.6 [kg], with a power of 936.6 W and a volume of 2.42 [m³], while having a production cost of EUR 128,347.09. It is available 99% of the time, providing high data rate optical communication of 100 Gbps with HAPS UAVs and 1 Gbps with LEO satellites while being able to withstand harsh conditions, such as 60 [m/s] winds, heavy vibrations, and extreme temperatures ranging from -50°C to 60°C. The material used for the node is Aluminium 6061. A dampening mechanism was integrated into the structure of the node which resulted in a small-time to reach an acceptable level of error. It was analysed for 5 different external excitations, namely earthquakes, wind gusts, accidental drops from 5 meters, transportation loads and snow. To account for the large temperature range and the heat produced by the internal systems, a thermal management system was included in the design. The batteries are passively managed by using a 50mm ArmaFlex insulation material and actively by two integrated cooling plates and an electric heat pump. The node itself uses a 9mm ArmaFlex insulation. An electric heater is placed outside the box, while a fan is used to provide airflow for convection heating and cooling. The EPS of the node is designed to be modular, one with a backup NMC Lithium-ion battery of 6 hours and one with a NMC Lithium-ion battery of 48 hours.

Environmental monitoring is taken into account for situational awareness, providing partial autonomy and allowing personnel with limited expertise to operate the node. An operating envelope was constructed to define a set of constraints within which the ECN will result in safe and acceptable performance. To properly monitor the surroundings, the node has weather sensors and is capable of weather forecasting. It has an air quality sensor integrated for predictive maintenance and a noise level meter for sustainability.

The communication is performed by a laser pump with EDFA, which is integrated into a compact telescope system, consisting of an azimuth-altitude gimbal and a fast steering mirror, used for beam steering. A transceiver is used to modulate the data in a 16-QAM format and coherent detection helps in sending data in orders of 100 [Gbps] in only one channel. The modulation technique chosen induces high BER over long-distances, therefore high BER was compensated by using forward error correction (FEC). Furthermore, a polarized beam splitter and a quarter wave plate are used to separate the transmitted data from the received data. A detailed link budget was established, covering sensitivity data rate modulation and noise. Static losses were taken into account, and a Gamma-Gamma and log-normal model were made for scintillation indicating losses of 9.3 [dB] for LEO and 3.9 [dB] for HAPS. Finally, the link budget exhibited an uplink margin of 27.42 [dB] for LEO, 29.16dB for HAPS, and a tight downlink margin of 2.4 [dB] for LEO and 4.2 [dB] for HAPS. This was achieved with an alignment accuracy of 1 [μrad], ensured by a multi-stage control sequence for acquisition and tracking of targets, making use of WFoV and fine tracking cameras, and an Extended Kalman Filter applied to the trajectory estimation model for control. The attitude determination, preceding

acquisition, is performed by a star tracker, backed up by a magnetometer and a bio-inspired celestial compass.

Finally, the ECN can be transported anywhere in the world in up to 48 hours. The case of highly isolated areas has proven that the most efficient and fast way of transportation is performed by an aircraft to reach the closest vicinity of the deployment point, and a helicopter to complete the transportation stage. Moreover, ISO containers are used due to their sustainability advantage.

12.2. Recommendations

Several recommendations and further research points have been identified throughout the project. For each stage of the design, relevant recommendations will be presented in this section.

Operations & Logistics

As mentioned, the transportation of the node can be performed in a variety of ways to meet the 48 hours deployment requirement. The fastest identified mode of transportation to cope with the worst-case scenario consists of aircraft and helicopters. However, a more detailed study should be performed which includes an extended list of available vehicles matching the requirements. An analysis of bigger transportation solutions will also be beneficial due to the risk of an increase in the ECN volume after design iterations. Furthermore, a more precise estimation and calculation of the transportation time is a good starting point for future iterations.

Structure

The structure of the node is designed to withstand extreme cases, such as earthquakes, winds and extreme temperatures. The frequency analysis of the node has taken into account 5 cases. However, a more extensive analysis should be done considering a wider variety of nodes and extreme cases in order to better understand all the response modes.

Considering solely the vibration analysis of the node, a 6 degree of freedom model, as well as the Rayleigh waves, should be considered and analysed, which has not been done due to the limited amount of expertise and time.

Beam Steering

The used gimbal, EVE, is proved to be very suitable for the present design. However, the gimbal itself has not been yet produced. This entails that more research has to be done around this mechanism to justify the choice and provide an extensive report on its reliability and overall performance. Moreover, as the production is to be started in 2026, several components, such as the batteries and the transceiver, will be optimised and improved, an aspect that could improve the performance of the ECN. In further design, this should be considered to ensure the highest performance possible.

During the design of the beam steering mechanism, the concept of opto-mechanics (the manufacture and maintenance of optical parts and devices) has not been taken into account. Incorporating this aspect in the design would yield a more complete product, mainly the pointing errors due to thermal and structural deformations are an important consideration that should be investigated.

Link Budget

It is recommended that the model be adjusted to work for Gamma-Gamma distribution for lower turbulence regimes. Additionally, the scintillation effects could be investigated and a model could be constructed for uplink communication. However, this is beyond the scope of the present project

phase due to the complicated nature of applying a spherical wavefront with tip-tilt corrections. Further- more literature and experiments could be reviewed to compare and aid in the verification and validation of the expanded model.

Pointing, Acquisition, and Tracking

A more robust, accurate way of calibration would enhance ECN's pointing performance. While acquisition and tracking sequence ensure good enough accuracy for optical communication, the signal acquisition would be easier if not for the maximum possible calibration error of 4 degrees. In particular, an overcast night sky is a worst-case scenario, as it severely limits the efficacy of star tracker and bio-inspired celestial compass. Furthermore, a motorized zoom lens offering a higher focal length can be an improvement for a coarse tracking camera. However, during the design process, no good alternative for the selected option was found. Other COTS motorized lenses were much more expensive and heavier. This could create a problem with placement and mounting.

Finally, closed-loop tracking accuracy must be validated and measured, to ensure that the PAT can deliver required performance with necessary availability.

Environmental Monitoring

Expansion of the environmental monitoring subsystem with a modular Doppler weather radar was discussed in subsection 5.11.2. More research can be done on the topic of extending weather forecasting capabilities and integration of ECN with other sensing equipment to enhance the quality of forecasts. The midterm report discussed the inclusion of more types of predictive maintenance and sustainability sensors [2], which were unattainable for this iteration of the design, but could be included if analysis justifies it.

Thermal Management System

For the TMS several recommendations have arisen from the analysis performed in section 5.9. First of all the heat production of the battery, especially during charging/discharging, has been severely underestimated, causing too optimistic results. Furthermore, the final dimensions have not yet been integrated in the simplified thermal analysis. The analysis should be iterated during the next design phase.

Electrical Power System

Regarding the EPS it is advised to enhance more on future battery types that are still being developed. For example, Sodium batteries have excellent thermal properties in comparison to Lithium-ion batteries, and should thus be considered in future design.

Bibliography

- [1] A. Singh, A. P. Tripathi, T. Aantjes, S. Blaga, A. Pavlov, V. Gupta, G. Basile, D. Bolkestein, M. Mazurkiewicz, and I. Q. Rojas, "Emergency communication node: Baseline report," techreport, Delft University of Technology, 2022.
- [2] A. Singh, A. P. Tripathi, T. Aantjes, S. Blaga, A. Pavlov, V. Gupta, G. Basile, D. Bolkestein, M. Mazurkiewicz, and I. Q. Rojas, "Emergency communication node: Midterm report," techreport, Delft University of Technology, 2022.
- [3] A. Singh, A. P. Tripathi, T. Aantjes, S. Blaga, A. Pavlov, V. Gupta, G. Basile, D. Bolkestein, M. Mazurkiewicz, and I. Q. Rojas, "DSE group 22 GitHub repository." <https://github.com/anjaysingh/DSE>.
- [4] M. Thorpe and J. C. Hodge, *Brickwork : for CAA Construction Diploma and NVQs. Level 2*. 2010.
- [5] V. D, M. Singh, and J. Malhotra, "Development of high-speed fso transmission link for the implementation of 5g and internet of things," *Wireless Networks*, vol. 26, 05 2020.
- [6] H. Kaushal and G. Kaddoum, "Free space optical communication: Challenges and mitigation techniques," 06 2015.
- [7] M. H. Weik, *long-haul communications*, pp. 928–928. Boston, MA: Springer US, 2001.
- [8] D. Giggenbach and A. Shrestha, "Atmospheric absorption and scattering impact on optical satellite-ground links," *International Journal of Satellite Communications and Networking*, vol. 40, no. 2, pp. 157–176, 2022.
- [9] C. Chen, A. Grier, M. Malfa, E. Booen, H. Harding, C. Xia, M. Hunwardsen, J. Demers, K. Kudinov, G. Mak, B. Smith, A. Sahasrabudhe, F. Patawaran, T. Wang, A. Wang, C. Zhao, D. Leang, J. Gin, M. Lewis, B. Zhang, D. Nguyen, D. Jandrain, F. Haque, and K. Quirk, "Demonstration of a bidirectional coherent air-to-ground optical link," in *Free-Space Laser Communication and Atmospheric Propagation XXX* (H. Hemmati and D. M. Boroson, eds.), vol. 10524, pp. 120 – 134, International Society for Optics and Photonics, SPIE, 2018.
- [10] B. Vu, N. Dang, T. Cong Thang, and A. Pham, "Bit error rate analysis of rectangular qam/fso systems using an apd receiver over atmospheric turbulence channels," *Optical Communications and Networking, IEEE/OSA Journal of*, vol. 5, pp. 437–446, 05 2013.
- [11] S. Palaniswamy, B. C.s, S. M G, M. Singh, J. Malhotra, and A. Grover, "Ultra-high capacity long-haul pdm-16-qam-based wdm-fso transmission system using coherent detection and digital signal processing," *Optical and Quantum Electronics*, vol. 52, 11 2020.
- [12] T. Gui, T. Chan, C. Lu, A. P. T. Lau, and P. Wai, "Alternative decoding methods for optical communications based on nonlinear fourier transform," *Journal of Lightwave Technology*, vol. PP, pp. 1–1, 01 2017.
- [13] M. Singh, J. Malhotra, S. Mani Rajan, V. D, and M. Aly, "A long-haul 100 gbps hybrid pdm/co-ofdm fso transmission system: Impact of climate conditions and atmospheric turbulence," *Alexandria Engineering Journal*, vol. 60, 10 2020.
- [14] B. Li, *Forward Error Correcting Codes for 100 Gbit/s Optical Communication Systems*. PhD thesis, 2014.
- [15] R. J. Anthony, "Chapter 3 - the communication view," in *Systems Programming* (R. J. Anthony, ed.), pp. 107–201, Boston: Morgan Kaufmann, 2016.

- [16] Sonali, A. Dixit, and V. K. Jain, "Analysis of ldpc codes in fso communication system under fast fading channel conditions," *IEEE Open Journal of the Communications Society*, vol. 2, pp. 1663–1673, 2021.
- [17] J. Karaki, E. Giacomidis, D. Grot, T. Guilloso, C. Gosset, R. L. Bidan, T. L. Gall, Y. Jaouën, and E. Pincemin, "Dual-polarization multi-band ofdm versus single-carrier dp-qpsk for 100 gb/s long-haul wdm transmission over legacy infrastructure," *Opt. Express*, vol. 21, pp. 16982–16991, Jul 2013.
- [18] B. Vucetic and J. Yuan, "Turbo codes: principles and applications.." Springer Verlag. ISBN 978-0-7923-7868-6., 2000.
- [19] M. Baldi, G. Cancellieri, and F. Chiaraluce, "Interleaved product ldpc codes," *IEEE Transactions on Communications - TCOM*, vol. 60, 12 2011.
- [20] D. Giggenbach, A. Shrestha, C. Fuchs, C. Schmidt, and F. Moll, "system aspects of optical LEO-to-ground links," in *International Conference on Space Optics — ICSO 2016* (B. Cugny, N. Karafolas, and Z. Sodnik, eds.), vol. 10562, pp. 1635 – 1643, International Society for Optics and Photonics, SPIE, 2017.
- [21] M. Islam and A. Hossain, "Comparison of traffic performance of qpsk and 16-qam modulation techniques for ofdm system," *Journal of Telecommunications and Information Technology*, vol. 2005, pp. 147–152, 03 2005.
- [22] R. Li, B. Lin, Y. Liu, M. Dong, and S. Zhao, "A survey on laser space network: Terminals, links, and architectures," *IEEE Access*, vol. 10, pp. 34815–34834, 2022.
- [23] M. Adel, H. Seleem, M. Nasr, and H. El-Khobby, "Transmission of 128 gb/s optical QPSK signal over FSO channel under different weather conditions and pointing errors," *Journal of Physics: Conference Series*, vol. 1447, p. 012055, jan 2020.
- [24] Z. Sodnik and M. Sans, "Extending edrs to laser communication from space to ground," 2012.
- [25] F. Nakajima, M. Nada, and T. Yoshimatsu, "High-speed avalanche photodiode and high-sensitivity receiver optical subassembly for 100-gb/s ethernet," *Journal of Lightwave Technology*, vol. 34, no. 2, pp. 243–248, 2016.
- [26] F. Fidler, M. Knapek, J. Horwath, and W. R. Leeb, "Optical communications for high-altitude platforms," *IEEE Journal of Selected Topics in Quantum Electronics*, vol. 16, pp. 1058–1070, 2010.
- [27] L. W. Couch-II, *Digital And Analog Communication Systems*. Pearson Education, Inc, 2013.
- [28] A. Majumdar, "Free-space laser communication performance in the atmospheric channel," *Journal of Optical and Fiber Communications Reports*, vol. 2, pp. 345–396, 2005.
- [29] F. Xu, M.-A. Khalighi, and S. Bourennane, "Impact of different noise sources on the performance of pin- and apd-based fso receivers," *Journal of Optical and Fiber Communications Reports*, vol. UMR CNRS 6133, pp. 211–218, 2011.
- [30] V. Shulyak, M. M. Hayat, and J. S. Ng, "Sensitivity calculations of high-speed optical receivers based on electron-apds," *J. Lightwave Technol.*, vol. 38, pp. 989–995, Feb 2020.
- [31] T. Jono, M. Toyoda, K. Nakagawa, A. Yamamoto, K. Shiratama, T. Kurii, and Y. Koyama, "Acquisition, tracking, and pointing systems of OICETS for free space laser communications," in *Acquisition, Tracking, and Pointing XIII* (M. K. Masten and L. A. Stockum, eds.), vol. 3692, pp. 41 – 50, International Society for Optics and Photonics, SPIE, 1999.

- [32] S. G. Lambert and W. L. Casey, *Laser Communications in Space*. ARTECH HOUSE, INC, 1995.
- [33] D. Giggenbach, F. Moll, C. Schmidt, C. Fuchs, and A. Shrestha, *Satellite Communications in the 5G Era: Optical on-off keying data links for low Earth orbit downlink applications*. Institution of Engineering and Technology, London, United Kingdom, 2018.
- [34] H. Ivanov, P. Pezzei, and E. Leitgeb, "Estimation of cloud-induced optical attenuation over near-earth and deep-space fso communication systems," in *2021 International Conference on Software, Telecommunications and Computer Networks (SoftCOM)*, pp. 1–5, 2021.
- [35] K. N. Liou, Y. Takano, S. C. Ou, and M. W. Johnson, "Laser transmission through thin cirrus clouds," *Appl. Opt.*, vol. 39, pp. 4886–4894, Sep 2000.
- [36] J. Edman, "Deriving characteristics of thin cirrus clouds from observations with the irf lidar", dissertation." urn:nbn:se:ltu:diva-76574, nov 2019.
- [37] A. Berk, P. Conforti, R. Kennett, T. Perkins, F. Hawes, and J. van den Bosch, "MODTRAN6: a major upgrade of the MODTRAN radiative transfer code," in *Algorithms and Technologies for Multispectral, Hyperspectral, and Ultraspectral Imagery XX* (M. Velez-Reyes and F. A. Kruse, eds.), vol. 9088, pp. 113 – 119, International Society for Optics and Photonics, SPIE, 2014.
- [38] L. Andrews and R. Phillips, *Laser Beam Propagation Through Random Media*, pp. 477–531. 01 2005.
- [39] D. Giggenbach and H. Henniger, "Fading-loss assessment in atmospheric free-space optical communication links with on-off keying," *Optical Engineering*, vol. 47, no. 4, pp. 1 – 6, 2008.
- [40] M. Chatterjee and A. Mohamed, "Mitigation of image intensity distortion using chaos-modulated image propagation through gamma-gamma atmospheric turbulence," p. 13, 05 2018.
- [41] A. G. Talmor, H. H. Jr., and C.-C. Chen, "Two-axis gimbal for air-to-air and air-to-ground laser communications," in *Free-Space Laser Communication and Atmospheric Propagation XXVIII* (H. Hemmati and D. M. Boroson, eds.), vol. 9739, pp. 129 – 135, International Society for Optics and Photonics, SPIE, 2016.
- [42] J. Cheng, *The Principles of Astronomical Telescope Design*. Astrophysics and Space Science Library, Springer New York, 2010.
- [43] A. Mackintosh, *Advanced Telescope Making Techniques*, vol. 1. Willmann-Bell, Inc, 1986.
- [44] E. D. Miller, M. DeSpensa, I. Gavriilyuk, G. Nelson, B. Erickson, B. Edwards, E. Davis, and T. Truscott, "A prototype coarse pointing mechanism for laser communication," in *Free-Space Laser Communication and Atmospheric Propagation XXIX* (H. Hemmati and D. M. Boroson, eds.), vol. 10096, pp. 200 – 211, International Society for Optics and Photonics, SPIE, 2017.
- [45] D. Vukobratovich and P. Yoder, *Fundamentals of Optomechanics*. Optical Sciences and Applications of Light, CRC Press, 2018.
- [46] J. C. Geyer, C. Rasmussen, B. Shah, T. Nielsen, and M. Givehchi, "Power efficient coherent transceivers," in *ECOC 2016; 42nd European Conference on Optical Communication*, pp. 1–3, 2016.
- [47] A. E. Willner, H. Huang, Y. Yan, Y. Ren, N. Ahmed, G. Xie, C. Bao, L. Li, Y. Cao, Z. Zhao, J. Wang, M. P. J. Lavery, M. Tur, S. Ramachandran, A. F. Molisch, N. Ashrafi, and S. Ashrafi, "Optical communications using orbital angular momentum beams," *Adv. Opt. Photon.*, vol. 7, pp. 66–106, Mar 2015.

- [48] H. Curtis, *Orbital Mechanics: For Engineering Students*. Aerospace Engineering, Elsevier Science, 2015.
- [49] R. Serway and J. Jewett, *Physics for Scientists and Engineers with Modern Physics*. Cengage Learning, 2013.
- [50] P. M. Fried, T. Lohner, *Handbook of Surfaces and Interfaces of Materials*. Academic Press, 2001.
- [51] F. Xia, J. Yang, Z. Yao, Y. Song, L. Ren, and Q. Tan, "Investigation of isolation for free space laser communication in the mono-wavelength optical t/r channels," *Optik*, vol. 181, 03 2019.
- [52] X. J. Gu, "Wavelength-division multiplexing isolation fiber filter and light source using cascaded long-period fiber gratings," *Opt. Lett.*, vol. 23, pp. 509–510, Apr 1998.
- [53] P. J. Winzer and W. R. Leeb, "Fiber coupling efficiency for random light and its applications to lidar," *Opt. Lett.*, vol. 23, pp. 986–988, Jul 1998.
- [54] M. Chen, C. Liu, and H. Xian, "Experimental demonstration of single-mode fiber coupling over relatively strong turbulence with adaptive optics," *Appl. Opt.*, vol. 54, pp. 8722–8726, Oct 2015.
- [55] G. Zhu, J. Lévine, L. Praly, and Y.-A. Peter, "Flatness-based control of electrostatically actuated mems with application to adaptive optics: A simulation study," *Journal of Microelectromechanical Systems*, vol. 15, 11 2006.
- [56] S. Kuiper, W. Crowcombe, B. Dekker, A. Meskers, G. Witvoet, L. Kramer, M. Lemmen, H. Lagemaat, W. Hoogt, and M. Koppen, "High-bandwidth and compact fine steering mirror development for laser communications," 09 2017.
- [57] K. Gudmundson, *Ground Based Attitude Determination Using a SWIR Star Tracker*. 2019.
- [58] K. M. Riesing, *Portable Optical Ground Stations for satellite communication*. PhD thesis.
- [59] D. Giggenbach, F. Moll, and N. Perlot, "Optical communication experiments at dlr," *Journal of the National Institute of Information and Communications Technology*, vol. Vol. 59, pp. 125–134, 03 2012.
- [60] D. Giggenbach, C. Fuchs, C. Schmidt, B. Rödiger, S. Gaißer, S. Klinkner, D.-H. Phung, J. Chabé, C. Courde, N. Maurice, H. Mariey, E. Samain, and G. Artaud, "Downlink communication experiments with osirisv1 laser terminal onboard flying laptop satellite," *Appl. Opt.*, vol. 61, pp. 1938–1946, Mar 2022.
- [61] E. Fischer, T. Berkefeld, Mikael, M. Feriencik, V. Kaltenbach, D. Soltau, B. Wandernoth, R. Czichy, J. Kunde, K. Saucke, F. Heine, M. Gregory, C. Seiter, and H. Kämpfner, "Development, integration and test of a transportable adaptive optical ground station," *IEEE International Conference on Space Optical Systems and Applications*, 2015.
- [62] Belenkii *et al.*, "Daytime stellar imager," March 2008.
- [63] K. Gudmundson, "Ground based attitude determination using a swir star tracker," 2019.
- [64] R. C. Stone, "A comparison of digital centering algorithms," *The Astronomical Journal*, vol. 97, 1988.
- [65] D. Mortari, M. A. Samaan, and C. Brucoleri, "The pyramid star identification technique," *Navigation*.

- [66] E. J. Lefferts, F. L. Markley, and M. D. Shuster, "Kalman filtering for spacecraft attitude estimation," *Journal of Guidance, Control, and Dynamics*.
- [67] J. Dupeyroux, J. Diperi, M. Boyron, S. Viollet, and J. Serres, "A bio-inspired celestial compass applied to an ant-inspired robot for autonomous navigation," in *2017 European Conference on Mobile Robots (ECMR)*, pp. 1–6, 2017.
- [68] S. F. Hoerner, *Fluid-dynamic drag*. Albuquerque, 1965.
- [69] M. Agostinacchio, D. Ciampa, and S. Olita, "The vibrations induced by surface irregularities in road pavements – a matlab® approach," *European Transport Research Review*, vol. 6, pp. 267–275, 09 2013.
- [70] ASCE, *Minimum Design Loads for Buildings and Other Structures*. American Society of Civil Engineers, asce/sei 7-10 ed., 2013.
- [71] P. Croce, P. Formichi, and F. Landi, "Evaluation of current trends of climatic actions in europe based on observations and regional reanalysis," *Remote Sensing*, vol. 13, p. 2025, 05 2021.
- [72] A. Burtin, N. Hovius, and J. Turowski, "Seismic monitoring of torrential and fluvial processes," *Earth Surface Dynamics*, vol. 4, 04 2016.
- [73] A. Gill, D. Visotsky, L. Mears, and J. Summers, "Cost estimation model for pan based carbon fiber manufacturing process," *Journal of Manufacturing Science and Engineering*, vol. 139, 09 2016.
- [74] J. Howarth, S. S. Mareddy, and P. T. Mativenga, "Energy intensity and environmental analysis of mechanical recycling of carbon fibre composite," *Journal of Cleaner Production*, vol. 81, pp. 46–50, 2014.
- [75] "Commercial and Industrial-Grade Products: White Paper CTWP011," *Cactus Technologies*.
- [76] J. Warner, *The Handbook of Lithium-Ion Battery Pack Design*. Elsevier Science, 2015.
- [77] M. Lu, X. Zhang, J. Ji, X. Xu, and Y. Zhang, "Research progress on power battery cooling technology for electric vehicles," *Journal of Energy Storage*, vol. 27, p. 101155, 2020.
- [78] W. Reynolds and P. Colonna, *Thermodynamics: Fundamentals and Engineering Applications*. Cambridge University Press, 2016.
- [79] A. Cervone, "Adsee ii spacecraft reader," tech. rep., TU Delft, 2021.
- [80] L. J. Schep, R. J. Slaughter, W. A. Temple, and D. M. G. Beasley, "Diethylene glycol poisoning," *Clinical Toxicology*, vol. 47, no. 6, pp. 525–535, 2009. PMID: 19586352.
- [81] Y. Miao, P. Hynan, A. von Jouanne, and A. Yokochi, "Current li-ion battery technologies in electric vehicles and opportunities for advancements," *Energies*, vol. 12, pp. 1074–1094, 03 2019.
- [82] J. F. Peters, M. Baumann, B. Zimmermann, J. Braun, and M. Weil, "The environmental impact of li-ion batteries and the role of key parameters – a review," *Renewable and Sustainable Energy Reviews*, vol. 67, pp. 491–506, 2017.
- [83] S. Thombre, Z. Zhao, H. Ramm-Schmidt, J. M. V. Garcia, T. Malkamäki, S. Nikolskiy, T. Hammarberg, H. Nuortie, M. Zahidul, H. Bhuiyan, and S. Särkkä, "Sensors and ai techniques for situational awareness in autonomous ships: A review," *IEEE TRANSACTIONS ON INTELLIGENT TRANSPORTATION SYSTEMS*, vol. 23, no. 1, 2022.

- [84] J. W. Wilson, Y. Feng, M. Chen, and R. D. Roberts, "Nowcasting challenges during the beijing olympics: Successes, failures, and implications for future nowcasting systems," *Weather Forecast*, vol. 25, 2010.
- [85] F. Schmid, Y. Wang, and A. Harou, "Guidelines for nowcasting techniques," *World Meteorological Organization*, vol. 1198, 2017.
- [86] PwC, "Predictive Maintenance 4.0 Beyond the hype: PdM 4.0 delivers results," 2018.
- [87] S. R. M. Rao, "Influence of environmental factors on component/equipment reliability," *Indian Journal of Engineering and Materials Sciences*, vol. 5, pp. 121–123, 1998.
- [88] A. Moncmanová, "Environmental factors that influence the deterioration of materials," *WIT Transactions on State-of-the-art in Science and Engineering*, vol. 28, 2007.
- [89] R. Vaidya, "A review on noise pollution and its effects on human health," 2020.
- [90] R. Sordello, F. Flamerie De Lachapelle, B. Livoreil, and S. Vanpeene, "Evidence of the environmental impact of noise pollution on biodiversity: A systematic map protocol," *Environmental Evidence*, vol. 8, no. 1, 2019.
- [91] C. Humphries, V. Reddish, and D. Walshaw, "Cost scaling laws and their origin: Design strategy for an optical array telescope," *International Astronomical Union Colloquium*, vol. 79, p. 379–394, 1984.
- [92] C. Y. H. Lee and C. Chou, "Protection scheme for a wavelength-division-multiplexed passive optical network based on reconfigurable optical amplifiers," *Applied Science*, December 2021.
- [93] A. Bayramian, S. Aceves, T. Anklam, K. Baker, E. Bliss, C. Boley, A. Bullington, J. Caird, D. Chen, R. Deri, M. Dunne, A. Erlandson, D. Flowers, M. Henesian, J. Latkowski, K. Manes, W. Molander, E. Moses, T. Piggott, and S. Telford, "Compact, efficient laser systems required for laser inertial fusion energy," *Fusion Science and Technology*, vol. 60, 07 2011.
- [94] M. Sweeney, G. Rynkowski, M. Ketabchi, and R. Crowley, "Design considerations for fast steering mirrors (fsm)," *SPIE*, 2002.
- [95] T. Tanaka, "Investigation on operational reliability of heat pump systems," *Research Fellow*.
- [96] Ritt, "Laser safety calculations for imaging sensors," *Sensors*, vol. 19, p. 3765, 08 2019.
- [97] Y. Umeda, S. Fukushige, K. Tonoike, and S. Kondoh, "Product modularity for life cycle design," *CIRP Annals*, vol. 57, no. 1, pp. 13–16, 2008.
- [98] I. J. Sinke, *AE3211-II Chapter 11 reader: Organization of the production process*. TU Delft, 2022.
- [99] I. J. Sinke, *AE3211-II Chapter 6 reader: Assembly*. TU Delft, 2022.
- [100] V. Burt, "Adhesive bonding," *Aluminum Science and Technology*, 2018.
- [101] M. Łebkowska, M. Załęska-Radziwiłł, and A. Tabernacka, "Adhesives based on formaldehyde– environmental problems," *Biotechnologia. Journal of Biotechnology, Computational Biology and Bionanotechnology*, vol. 98, pp. 53–65, 2017.
- [102] I. J. Sinke, *AE3211-II Chapter 8 reader: Bonding and welding*. TU Delft, 2022.
- [103] I. J. Sinke, *AE3211-II Chapter 7 reader: Riveting and Bolting*. TU Delft, 2022.

- [104] R. Young, *Economies of Scale*, pp. 39–47. London: Macmillan Education UK, 1987.
- [105] A. Wagiman, M. S. Mustapa, R. Asmawi, S. Shamsudin, M. Lajis, and Y. Mutoh, “A review on direct hot extrusion technique in recycling of aluminium chips,” *The International Journal of Advanced Manufacturing Technology*, vol. 106, pp. 1–13, 01 2020.
- [106] D. Herzog, V. Seyda, E. Wycisk, and C. Emmelmann, “Additive manufacturing of metals,” *Acta Materialia*, vol. 117, pp. 371–392, 2016.

Work Distribution and flow diagrams

A.1. Task Division Final Report

	Anujay Singh	Aditya Pati Tripathi	Tom Aantjes	Șerban Blaga	Aleksandr Pavlov	Vatsal Gupta	Giorgio Basile	Daan Bolkestein	Mateusz Mazurkiewicz	Ignacio Quintanilla Rojas
Executive Summary		x			x			x		x
Introduction										x
Market Analysis Update	x					x				
Sustainable Development					x		x	x		
Operations & Logistics							x		x	
Modulation					x					
Link Budget	x	x			x	x				
Telescope			x							
Optical Bench			x	x	x					
Camera				x					x	
PAT									x	
Frequency Analysis	x	x								x
Structural Analysis	x		x						x	
Thermal Management				x				x		
Electrical Power System	x									
Environmental Monitoring								x	x	x
SWAP						x		x		
Sensitivity Analysis									x	x
RAMS Analysis		x		x						
Risk Assessment							x			
Manufacturing, Assembly and Integration			x		x				x	
Requirements & Compliance									x	x
Design & Development Logic								x		x
Conclusion & Recommendations				x						

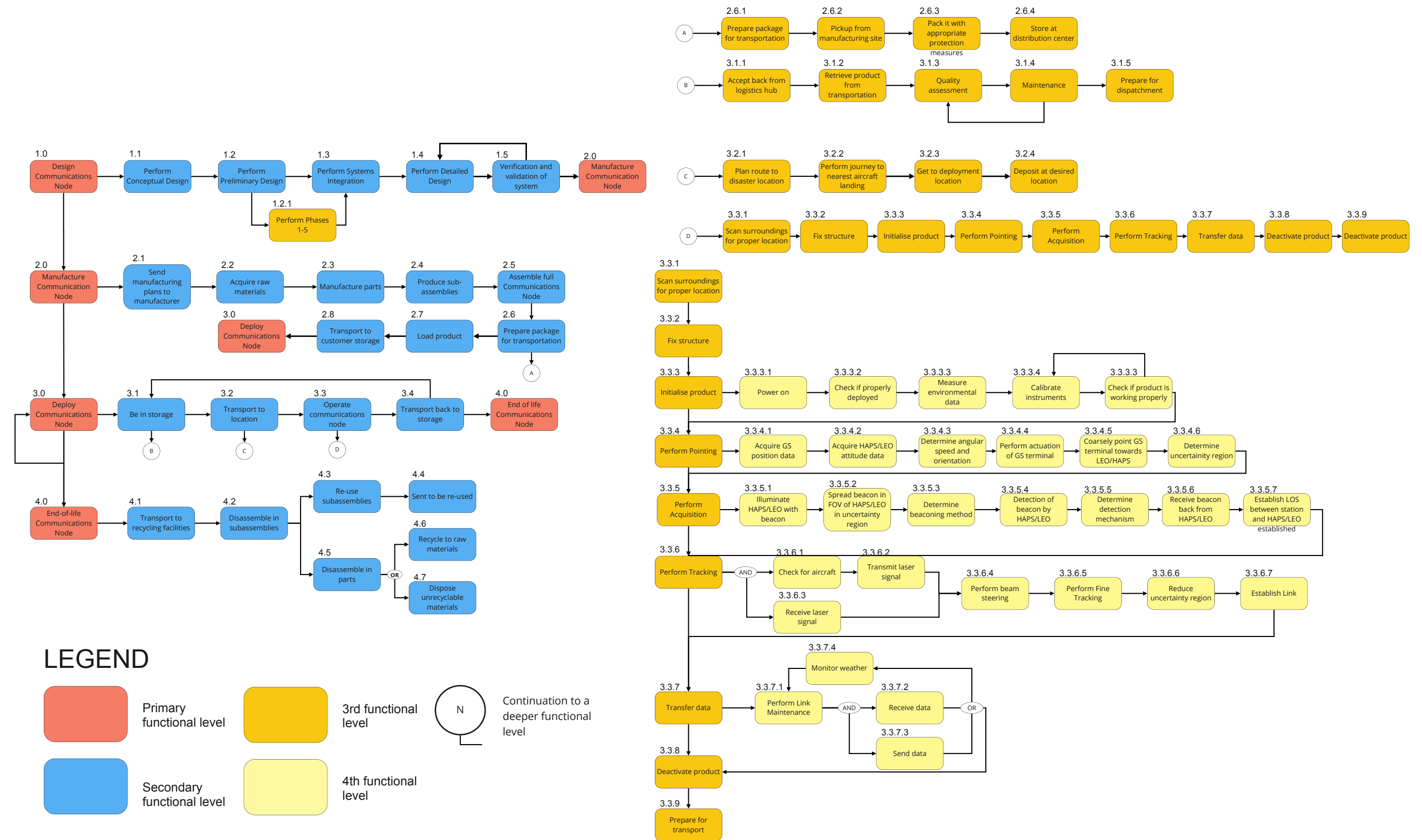


Figure A.1: Functional Flow Diagram for the Emergency Communications Node.

Detailed Cost Breakdown

This appendix shows the components chosen and explains the bottom up approach taken for the calculation of costs.

Table B.1: Cost breakdown of all components to the subsystem level

Component	Cost	Link
<i>Command</i>		
Workstation	€ 3,059.58	https://www.dell.com/nl-nl/shop/alles-weergeven/precision-3930-rack-bouw-je-eigen/spd/precision-3930-r-workstation/xctopr3930emea?configurationid=40067e62-ca6e-4c4b-b9fa-c7afe010d0fa#features_sectionlaptop/xctol542014emea#support_section
Location sensor	€ 229.00	https://www.csselectronics.com/products/gps-to-can-bus-gnss-imu?currency=EUR&utm_medium=cpc&utm_source=google&utm_campaign=Google%20Shopping&gclid=Cj0KCQjw4uaUBhC8ARIsANUuDjWNOB1lYASJ2NQ6IxcgqUJuihLyJf8C-4z1ul2-IWRYHXv163BAtd0aAjzbEALw_wcB#general-tech-specs
Environ. sensor	€ 1,730.00	https://www.campbellsci.com/climavue-50
LiDAR sensor	€ 599.00	https://www.livoxtech.com/mid-40-and-mid-100
PM sensor	€ 32.92	https://eu.mouser.com/ProductDetail/Sensirion/SEN55-SDN-T?qs=MyNHzdoqoQLyWUzejWkZfg%3D%3D
Noise sensor	€ 385.90	https://www.pce-instruments.com/eu/measuring-instruments/test-meters/noise-meter-sound-meter-pce-instruments-noise-meter-pce-sld-10-ica-incl.-iso-calibration-certificate-det_5973668.htm
<i>Beam steering</i>		
Gimbal + Telescope	€ 15,000.00	
FSM+controller	€ 4,100.00	https://www.mirrorcletech.com/pdf/MirrorcleTech_Device_Prices.pdf
Fine/Star Tracker camera	€ 1,000.00	
Coarse Tracker camera	€ 750.00	https://www.zillion-techs.com/products/640-swir-in-gaas-high-cost-performance-camera-usb3/
Coarse Tracker lens	€ 300.00	https://www.stemmer-imaging.com/en-nl/products/cvo-gaz1025018m/
Magnetometer	€ 37.50	See report
Bioinspired celestial compass	€ 653.00	See report
Adaptive optics	€ 30,000.00	https://www.thorlabs.com/thorproduct.cfm?partnumber=A0K5/M
<i>Optical</i>		
EDFA Laser Pump	€ 6,000.00	
Transceiver	€ 10,000.00	https://www.fibermall.com/sale-459142-cfp2-dco-200g-coherent-transceiver.htm
Collimator	€ 300.00	
EDFA Amplifier	€ 6,000.00	

Table B.1 continued from previous page

Component	Cost	Link
Beamsplitter	€ 372.04	https://www.thorlabs.com/newgrouppage9.cfm?objectgroup_id=6004&pn=PSW-1550
Quarter waveplate	€ 245.00	https://www.meetoptics.com/waveplates/quarter-waveplate/s/eksma-optics/p/460-4401
<i>Thermal</i>		
Temperature sensor inside	€ 200.00	https://www.aircraftspruce.com/catalog/inpages/airtempsensor.php?clickkey=9067
Laser Heat Regulator	€ 388.00	https://www.teamwavelength.com/product/ldtc22o-laser-driver-temp-controller/
Insulation	€ 565.92	https://www.buisisolatie.nl/home/121-armaflex-af-plaat-50-mm-op-rol.html
Node heater (500W)	€ 123.87	https://nl.rs-online.com/web/p/heaters-radiators/0172880
Cooling system (500W)		https://lairdthermal.com/products/liquid-cooling-systems/water-heat-exchangers/WL500
Cooling plates		
Pipes et cetera		
<i>Electrical</i>		
Battery	€ 6,750.00	https://www.batemo.de/products/batemo-cell-library/e66a/
Converter DC/AC	€ 2,962.00	https://www.heliosps.com.au/product/rm-psw2kva-series-rack-mount-inverter-1u/
Wiring/Power Distribution	€ 2,066.90	https://www.automation24.biz/electronic-load-circuit-breaker-murrelektronik-mico-classic-4-4-9000-41034-0100400
Wire used	€ 100.00	
<i>Structural</i>		
Dampening	€ 4,000.00	
Frame	€ 4,000.00	
Skin	€ 4,000.00	
Supporting structure	€ 2,000.00	
<i>IO</i>		
Router	€ 12,968.00	https://www.cisco.com/c/en/us/products/routers/asr-1000-series-aggregation-services-routers/index.html